DESIGNING CHEMICAL STRATEGIES TO PROMOTE THERAPEUTIC ACCESS TO RESTRICTED SITES *IN CYTO*

by

Jennifer L. Rowe

A Dissertation

Submitted to the Faculty of Purdue University

In Partial Fulfillment of the Requirements for the degree of

Doctor of Philosophy

Department of Chemistry

West Lafayette, Indiana

December 2019

THE PURDUE UNIVERSITY GRADUATE SCHOOL

STATEMENT OF COMMITTEE APPROVAL

Dr. Jean Chmielewski

Department of Chemistry

Dr. Christine Hrycyna

Department of Chemistry

Dr. David Thompson

Department of Chemistry

Dr. Elizabeth Parkinson

Department of Chemistry

Approved by:

Dr. Christine Hrycyna

Dedicated to my family

ACKNOWLEDGMENTS

First and foremost, I would like to thank Professor Jean Chmielewski for all of the support, guidance, patience and kindness throughout the years. I have learned so much from her, how to be an independent thinker/scientist, a leader in the lab, an efficient worker and an effective communicator. These years have pushed me to be my very best, and I have her to thank for that. Further, I would also like to thank my committee, Professor Christine Hrycyna, Professor David Thompson, and Professor Elizabeth Parkinson. I appreciate your support the last few years and for serving on my defense committee.

I would also like to take a moment to thank my undergraduate research advisor, Professor James Wollack. He was the first person to encourage me to pursue a career in chemistry. After I took his Organic Chemistry I course, he offered me a position researching in his lab, before even Organic Chemistry II. It was his faith in me that helped me to find my true passion in life, chemistry. Thank you for your guidance and support, I would not be where I am today without it.

Thank you to Dr. John Harwood for the help and guidance with my kanamycin and tobramycin NMRs. It is with your expertise that we were able to solve those complex structures. I have learned so much from you about NMR. Thank you to Professor Mohammad Seleem and Hassan Eldesouky for your help testing my tobramycin-P14LRR conjugates. It was always so exciting to receive the activity results, thank you for your time and effort. To Professor Qigui Yu and Jie Lan, for their collaboration and work with my Abacavir-Darunavir conjugate. To Dr. Patricia Bishop, thank you for teaching me how to use various instruments in the instrumentation facility. Further, thank you to Bridget Haley for always maintaining the cell lab so well and for helping to teach me mammalian cell culture.

I would like to thank my past and present labmates. You were the ones I have spent the majority of my time with the past few years. I appreciate the guidance, support and camaraderie. I would particularly like to highlight Dr. Neha Agrawal, Dr. Manish Nepal and Dr. Anna Brezden for training me on all my different projects throughout the years. Neha, your support and friendship helped me to finish my portion of the P-gp project and ultimately led to our joint manuscript. Manish, who taught me CAPHs amino acid and peptide synthesis, knowledge which helped me to finish my tobramycin project. Anna, with your guidance, I was able to crack the kanamycin project. Other past members including Dr. Jerrin Kurkoise, Dr. Jeremy Gleaton, Milata Abraham, and

Kevin Strauss for showing me the ropes of the lab, and especially to Kevin for helping to edit this dissertation. To Dr. Reena Blade and Dr. Monessha Nambiar, who I began graduate school with. I am so glad we began this journey together and we all saw it through to the end! I look forward to a Disney trip, we definitely need to make that happen! To my current labmates, Vallabh Suresh, Moises Morales-Padilla, Samantha Zeiders, Ryan Curtis, Corey Johnson (Corals), Thomas Dietche (Tad), Vinay Menon, and Michael Jorgenson, thank you for always making lab fun. I have enjoyed our coffee runs and our lunch/dinner trips throughout the years. You all know how to make the lab environment lighthearted, which was a wonderful escape. I will miss you all.

To my colleagues in the Lipton and Hrycyna labs, thank you for always being willing to help or talk about synthesis and/or biochemistry. I would especially like to thank Dr. Matthew Hostetler, Miri Neidrauer, Jordan Hunter, Dr. Allison Lange, Jason Goebel and Elias Beretta. Thank you all for the advice and camaraderie over the years.

To my friends and colleagues who have helped me with general joy throughout the years. Whether it was the renaissance faire, our apartment pub crawl, epic Christmas decorating parties, or just a movie night indoors, the camaraderie was always appreciated. Starting with my friends I made my first year, Dr. Keelan Trull, Dr. Anna Ratliff, Jason Goebel, and Katherine Hansen. Our shenanigans our first year will always bring me wonderful memories. To Jordan Hunter, who I met my third year, thank you for your continued friendship and support the last, and most challenging, years of my Ph.D. I also would like to thank my friends from undergrad, Jennifer Miller and Taylor Kloeckl. Although I moved far away from you to Indiana, we have still made a point to see each other in person every year. Thank you for always taking time out of your busy lives to check in on me, it has always meant a lot to me.

Last, but certainly not least, I would like to thank my family, my mother, father, and brother. Michael, for always reminding me to take some time for myself and its okay to treat yourself every once in a while. Dad, for your continuous words of wisdom and support. You always know how to calm me down and to realize what it is really important. Mom, you are a constant beam of love and support. Whenever times got tough, you are the first person I turn to for guidance. Thank you for always helping me, for always supporting me, and for always loving me. Thank you all for always being there for me. Rowes stick together, through thick or thin. I love you all and I wouldn't be where I am today without your love and support.

TABLE OF CONTENTS

LIST OF TABLES 10
LIST OF FIGURES 11
LIST OF SCHEMES 15
LIST OF APPENDIX FIGURES 16
ABSTRACT 19
CHAPTER 1. BIVALENT STRATEGY FOR THE INHIBITION OF THE EFFLUX TRANSPORTER P-GLYCOPROTEIN 20
1.1 P-glycoprotein structure and binding sites 20
1.2 P-gp multivalency and inhibition 22
1.3 Substrate dimerization as a viable inhibition strategy for P-glycoprotein 23
1.4 P-glycoprotein inhibition can reverse multidrug resistance in cancer using quinine dimers 26
1.5 P-glycoprotein inhibition is a viable strategy to target brain disorders 27
1.5.1 Schizophrenia 27
1.5.2 Antiviral dimeric prodrugs as P-gp inhibitors 29
1.6 Tether location and design can confer P-glycoprotein inhibition potency and specificity 32
1.7 Bivalent inhibition strategy beyond P-glycoprotein 34
1.8 Conclusion 35
1.9 References 36
CHAPTER 2. DEVELOPMENT OF A TROJAN HORSE PRODRUG, ABACAVIR-S_2-DARUNAVIR-8, FOR THE INHIBTION OF P-GLYCOPROTEIN WITH ANTI-HIV-1 ACTIVITY 45
2.1 Introduction 45
2.2 Results and Discussion 47
2.2.1 Design 47
2.2.2 Synthesis and characterization of TH dimer Aba-S_2-DRV 47
2.2.3 Inhibition of P-gp efflux with Aba-S_2-DRV8. 52
2.2.4 Probing the reversion of the TH heterodimer into monomers in a reducing environment. 54

2.2.5 The anti-HIV-1 potency of the TH heterodimer as compared to its monomers, alone and combined. 55
2.3 Conclusion 56
2.4 Materials and Methods 56
2.4.1 Materials 56
2.4.2 Methods 57
2.4.2.1 Synthesis of Aba-S_2-COOH 57
2.4.2.2 Synthesis of Aba-S_2-DRV8 58
2.4.2.3 Cell Culture 59
2.4.2.4 Flow Cytometry Assay 59
2.4.2.5 Cell Viability Assay 59
2.4.2.6 Stability of the TH heterodimer with DTT 60
2.4.2.7 Stability of Aba-S_2-DRV8 in cell culture media 60
2.4.2.8 HIV-1 cell inhibition assay 61
2.5 References 61
CHAPTER 3. THE SYNTHESIS OF KANAMYCIN-ARG_8 USING A UV ACTIVE STRATEGY 66
3.1 Introduction 66
3.2 Results and Discussion 70
3.2.1 Design 70
3.2.2 Synthesis 71
3.2.2.1 Kanamycin-2-thiopyrinyl tether isomer 1 characterization 73
3.2.2.2 Kanamycin Boc_4-2-thiopyrinyl tether isomer 2 Characterization 76
3.2.3 Reduction Kinetics of Kanamycin-Arg_8 Isomers 1 and 2 79
3.2.3.1 Kanamycin-Arg_8 isomer 1 80
3.2.3.2 Kanamycin-Arg_8 isomer 2 81
3.3 Conclusions 82
3.4 Materials and Methods 83
3.4.1 Materials 83
3.4.2 Methods 83
3.4.2.1 Synthesis of Kanamycin Boc_4 83

3.4.2.2 Synthesis of 2-mercaptopyridinyl-4-mercaptobutyric acid disulfide (a) 84
3.4.2.3 Synthesis of Kanamycin Boc_4-2-thiopyridinyl tether (isomer 1 and 2) 84
3.4.2.4 Synthesis of Kanamycin-2-thiopyridinyl tether (isomer 1 and 2) 85
3.4.2.5 Synthesis of trityl-4-mercaptobutyric acid (b) 86
3.4.2.6 Synthesis of Arg_8-SH 87
3.4.2.7 Synthesis of Kanamycin-Arg_8 (isomer 1 and 2) 88
3.4.2.8 Reduction of Kanamycin-Arg_8 isomers in the presence of DTT 88
3.5 References 89
CHAPTER 4. A CELL PENETRATING DUAL ANTIBIOTIC CONJUGATE, TOBRAMYCIN-P14LRR 92
4.1 Introduction 92
4.2 Results and Discussion 98
4.2.1 Design 98
4.2.2 Synthesis 100
4.2.2.1 Synthesis of the P14LRR-SH Peptide 100
4.2.2.2 Synthesis of Tobramycin-activated thiol conjugates 103
4.2.2.3 NMR characterization of Tobramycin-2-thiopyridinyl tether-A 104
4.2.2.4 NMR characterization of Tobramycin-2-thiopyridinyl tether-B 106
4.2.2.5 Synthesis of Tobramycin-P14LRR isomers A and B 108
4.2.3 Antibiotic Activity of TobP14 A and B 109
4.2.4 Cell Viability in the presence of TobP14 A and B 111
4.2.5 Kinetics of Release of tobramycin from TobP14 A and B 112
4.2.5.1 Energy minimization of TobP14 A 113
4.2.5.2 Energy minimization of TobP14 B 114
4.2.6 Intracellular antibiotic activity of TobP14 A and B 115
4.3 Conclusions 119
4.4 Future Directions 119
4.5 Materials and Methods 120
4.5.1 Materials 120
4.5.2 Methods 120
4.5.2.1 P14LRR-SH Synthesis 120

4.5.2.2 Tobramycin Boc_5 121
4.5.2.3 Tobramycin Boc_5 2-thiopyridinyl Tether 122
4.5.2.4 Tobramycin-2-thiopyridinyl Tether A 122
4.5.2.5 Tobramycin-2-thiopyridnyl Tether B 123
4.5.2.6 P14LRR-Tobramycin A and B 124
4.5.2.7 Reduction of TobP14 (A and B) isomers in the presence of DTT 124
4.5.2.8 Cell Culture 125
4.5.2.9 *In vitro* cytotoxicity assessment 125
4.5.2.10 TobP14 A and B antibacterial activity assay 125
4.5.2.11 Intracellular *A. baumannii* activity assay 126
4.6 References 127
APPENDIX 130
VITA 173
PUBLICATION 174

LIST OF TABLES

Table 2.1 Inhibition of P-gp mediated efflux of calcein-AM and NBD-Aba in 12D7-MDR and hCMEC/D3 cells[a].....53

Table 4.1 MIC (μM) of TobP14 A and B compared to P14LRR, Tobramycin, a 1:1 mixture of Tobramycin:P14LRR, Gentamicin and Vancomycin against various strains of opportunistic pathogens.....111

LIST OF FIGURES

Figure 1.1 Structure of P-glycoprotein, from Aller *et al.*[4] 20

Figure 1.2 [a] The chemical structure of QZS59-SSS [b] QZS59-SSS associated within mouse P-gp crystal structure. Adapted from Chang *et al.*[22] 22

Figure 1.3 P-glycoprotein inhibition strategy. The dimerization of P-gp substrates should induce stronger affinity for the transmembrane binding domain.....23

Figure 1.4 Stipiamide dimer library with varying tether lengths (n) for P-gp inhibition.[48] 24

Figure 1.5 Emetine dimer library for the inhibition of P-gp.[49].....25

Figure 1.6 Chow/Chan apigenin flavonoid dimer library.[60].....25

Figure 1.7 [a] Quinine and quinidine library of P-gp inhibitors; Q2 reverses multidrug resistance in cancer cell lines.[57] [b] Quinine library of homo- and heterodimers using alkyne-azide click chemistry to generate inhibitiors of P-gp.[58].....27

Figure 1.8 Quetiapine dimers used to inhibit P-gp. [53].....28

Figure 1.9 [a] Library of paliperidone dimers for P-gp inhibitiont[55] [b] Pal-8SSMe reversion to paliperidone in the reducing environment of the cell mechanism.[55] 29

Figure 1.10 Abacavir dimer strategy; dimer will inhibit P-gp, thereby evading the blood brain barrier. When in the reducing environment of the cell, the disulfide will reduce into free thiols which will rearrange to release the active abacavir inside cells. 31

Figure 1.11 [a] Abacavir dimer library using the disulfide tether strategy, with methyl substituents at the α-carbon[51] [b] Abacavir library to probe the most ideal tether length.[52] 32

Figure 1.12 AZT-dimer library for the inhibition of P-gp.[59].....32

Figure 1.13 Flavonoid modification library.[62].....33

Figure 1.14 Flavonoid tether design for specific P-gp inhibition. 34

Figure 1.15 Quinine dimer library for the inhibition of PfCRT and the treatment of malaria.[54] ..35

Figure 2.1 Design of Trojan horse (TH) prodrugs containing a reverse transcriptase inhibitor (RTI), abacavir (Aba), a protease inhibitor (PI), darunavir (DRV), and a disulfide-containing tether. ...46

Figure 2.2 Comparison of ^{1}H NMR from Aba-S_2-DRV8 as compared to ^{1}H from parent darunavir. Proton 8 corresponds with the proton on the methine of the secondary hydroxyl. Note the downfield shift from the parent darunavir. 50

Figure 2.3 Comparison of ^{13}C from Aba-S_2-DRV8 as compared to ^{13}C-DEPT from parent darunavir. Carbon 8 corresponds with the methine of the secondary hydroxyl. Note the downfield shift from the parent darunavir. 51

Figure 2.4 Comparison of ^{1}H from Aba-S_2-DRV8 as compared to ^{1}H from parent darunavir. Protons 14 and 15 corresponds the doublets in the para-aniline in darunavir adjacent. Note there is no shift from the parent darunavir. 51

Figure 2.5 Cell viability of Aba-S_2-DRV8 in the presence of 12D7-MDR cells. 53

Figure 2.6 Abacavir and DRV regeneration with DTT treatment (250 mM) in PBS (pH 7.4). 54

Figure 2.7 (a) Abacavir and (b) DRV regeneration with glutathione treatment (10 mM) in PBS (pH 7.4). 54

Figure 2.8 Anti-HIV-1 activity of individual RTI or PI antivirals, a 1:1 mixture of RTI and PI, and the TH heterodimer in HIV-1_{LAI} infected 12D7 cells. The plotted data is the average of HIV-1 p24 with the standard deviation derived from two independent experiments. 56

Figure 3.1 A selection of aminoglycoside structures. 68

Figure 3.2 P14KanS reversible tether design, which in the reducing environment of the cell may revert to monomeric kanamycin and P14LRR-SH. 69

Figure 3.3 Synthesis of P14KanS[9] 70

Figure 3.4 New synthetic strategy, utilizing a UV active intermediate of kanamycin 71

Figure 3.5 Kanamycin-2-thiopyridinyl tether isomer 1 labeled for NMR analysis purposes. 74

Figure 3.6 The ^{1}H NMR of Kanamycin-2-thiopyridinyl tether isomer 1 in CD_3OD. The peak assignments were made using ^{1}H, ^{13}C, COSY, TOCSY, DEPT-135, HSQC and HMBC NMR techniques. 74

Figure 3.7 [a] The HSQC NMR of Kanamycin -2-thiopyrinyl tether isomer 1 and [b] the HMBC NMR of Kanamycin Boc_4-2-thiopyrinyl tether isomer 1 both in CD_3OD. 75

Figure 3.8 Kanamycin Boc_4-2-thiopyridinyl tether isomer 2 structure, labeled for NMR analysis. 76

Figure 3.9 The ^{1}H NMR of Kanamycin-Boc_4-2-thiopyridinyl tether isomer 2 in d_6-DMSO. The peak assignments were made using ^{1}H, ^{13}C, COSY, TOCSY, DEPT-135, HSQC and HMBC NMR techniques. 77

Figure 3.10 [a] The HSQC Kanamycin Boc_4-2-thiopyridinyl tether isomer 2 [b] The HMBC Kanamycin Boc_4-2-thiopyridinyl tether isomer 2 in d_6-DMSO. 78

Figure 3.11 The release of kanamycin from Kanamycin-Arg_8 isomers 1 and 2 (50 μM) with DTT (10 μM) in ammonium acetate buffer (pH 7.4). 80

Figure 3.12 MM2 energy minimization of fully protonated kanamycin-SH (isomer 1), showing the protonated amine (K) in close proximity to carbonyl (Z) in the inset. 81

Figure 3.13 MM2 energy minimization of fully protonated kanamycin-SH (isomer 2), showing the protonated amines (Y and O) in close proximity to the carbonyl (Z) in the inset 82

Figure 4.1 Polyproline type II helix [a] side view, [b] top down view, [c] CAPHs scaffold (top down) showing the amphipathic faces, with hydrophobic in purple and the cationic groups in blue. 93

Figure 4.2 [a] P11LRR structure and [b] P11LKK structures compared for intracellular accumulation. 93

Figure 4.3 CAPHs library to probe the effects of changing the hydrophobic moieties; [a] the parent P11LRR, and [b] a benzyl substituted P11F/LRR derivative. [c] The parent peptides P11LRR and P14LRR, with 3 and 4 triad repeats, respectively, and [d] the peptide library with hydrophobic modifications, with [e] the different hydrophobic moieties that make up this library. 94

Figure 4.4 CAPHs structures investigating the affect of length on overall intracellular accumulation and antibacterial activity. 96

Figure 4.5 Structures of P14KanC and P14KanS, which were probed for increased intracellular antibiotic efficacy, as compared to the parent peptide P14LRR. 97

Figure 4.6 [a] The Tobramycin-Polymycin B_3 conjugate for enhanced antibiotic efficacy and [b] Pentobra, the cell penetrating peptide with tobramycin conjugate for increased antibiotic efficacy against persister cells. 98

Figure 4.7 Dual TobP14 conjugate for cellular delivery of two antibiotic agents: tobramycin and P14LRR-SH. 99

Figure 4.8 Reversible TobP14 conjugate design that allows for the release of tobramycin and P14LRR-SH in the reducing environment of the cell. 100

Figure 4.9 Tobramycin-2-thiopyridinyl tether isomer A. 104

Figure 4.10 Tobramycin-2-thiopyridinyl tether isomer A ^{1}H NMR in CD_3OD. Each of the peaks were identified by comparison of the ^{1}H, ^{13}C, COSY, TOCSY, DEPT-135, HSQC and HMBC. 105

Figure 4.11 [a] The DEPT-135 -^{1}H HSQC of Tobramycin-2-thiopyridinyl tether A showing the correlation between methine carbon (h) and proton (h). [b] The ^{13}C -^{1}H HMBC of Tobramycin-2-thiopyrdinyl tether A showing the correlation between methine proton (h) and carbonyl carbon (z). 106

Figure 4.12 Tobramycin-2-thiopyridinyl tether isomer B. 107

Figure 4.13 Tobramycin-2-thiopyridinyl tether B ^{1}H NMR in CD_3OD. Each of the peaks were identified by comparison of the ^{1}H, ^{13}C, COSY, TOCSY, DEPT-135, HSQC and HMBC. 107

Figure 4.14 [a] The DEPT-135-^{1}H HSQC of Tobramycin-2-thiopyridinyl tether isomer B showing the correlation between methylene carbon (m) and proton (m). [b] The ^{13}C -^{1}H HMBC of Tobramycin-2-thiopyridinyl tether isomer B showing the correlation between methylene proton (m) and carbonyl carbon (z). 108

Figure 4.15 The cytotoxicity of TobP14 A and B with J774A.1 macrophage cells using an MTT assay after a 9 hour incubation of compounds. 112

Figure 4.16 [a] Tobramycin release from TobP14 A (50 μM) when incubated with DTT (10 mM) in ammonium acetate buffer (pH 7.4). [b] Tobramycin release from TobP14 B 50 μM) when incubated with DTT (10 mM) in ammonium acetate buffer (pH 7.4). 113

Figure 4.17 MM2 energy minimization of fully protonated tobramycin-SH (isomer A), showing protonated amine (i) in close proximity to the alkoxy of the ester (h) in the inset.....114

Figure 4.18 [a] MM2 energy minimization of full protonated tobramycin-SH (isomer B), showing the protonated amines (u and n) in close proximity to the carbonyl (z) in the inset.....115

Figure 4.19 Intracellular *A. baumannii* (strain 19299) clearance using tobramycin, P14LRR. 1:1 tobramycin:P14LRR and TobP14 A and B at concentrations [a] 2.5 μM, [b] 5 μM, and [c]10 μM after 12 hour incubation of treatments with the bacterial infected J774A.1 cells. 116

Figure 4.20 Intracellular *A. baumannii* (19299) treated with ceftazidime, tobramycin, Ac-P14LRR, 1:1 tobramycin:AcP14LRR, TobP14 A and B at 10 μM after 12 hour incubation of treatments with the bacterial infected J774A.1 cells. 117

Figure 4.21 Intracellular *A. baumannii* (19606) treated with ceftazidime, tobramycin, Ac-P14LRR, 1:1 tobramycin:AcP14LRR, TobP14 A and B at 10 μM after 12 hour incubation of treatments with the bacterial infected J774A.1 cells. 118

LIST OF SCHEMES

Scheme 2.1 Synthesis of Aba-S_2-DRV analogs A) PyBOP, DMAP, DIEA, DMF, RT 24 hr, 70% yield; B) EDC, DMAP, DIEA, CH_2Cl_2, 4 Å molecular sieves, 0 ^{o}C for 2 h, RT for 48 h; Aba-S2-DRV8, 27% yield; (Aba-S_2)$_2$-DRV, 21% yield. Atom numbering used for NMR analysis of Aba-S_2-COOH and darunavir derivatives. 48

Scheme 3.1 Synthesis of Kanamycin-Arg_8 utilizing a UV active intermediate. 72

Scheme 3.2 Synthesis of Arg_8-SH. 78

Scheme 3.3 Synthesis of Kanamycin-Arg_8 (isomers 1 and 2). 79

Scheme 4.1 Synthesis of non-natural amino acids, Fmoc-P_L and Fmoc-P_R 101

Scheme 4.2 Synthesis of P14LRR-SH. 102

Scheme 4.3 Synthesis of Tobramycin-2-thiopyridinyl tether isomers A and B. 103

Scheme 4.4 The synthesis of tobramycin-P14LRR, TobP14 (isomers A and B). 109

LIST OF APPENDIX FIGURES

Figure A 1: Analytical purity HPLC of Aba-S_2-DRV8: C18 column, 20-95% acetonitrile with a flow rate of 1.2 mL/min, and visualized at 254 nm. The product is 99% pure. 130

Figure A 2: Analytical purity HPLC of Kanamycin-Arg_8 Isomer 1: C18 column, 5-30% acetonitrile with a flow rate of 1.2 mL/min, and visualized at 254 nm. The product is 99% pure.....130

Figure A 3: Analytical purity HPLC of Kanamycin-Arg_8 Isomer 2: C18 column, 5-30% acetonitrile with a flow rate of 1.2 mL/min, and visualized at 254 nm. The product is 99% pure.....131

Figure A 4: Analytical purity HPLC of P14LRR-SH: C18 column, 25-65% acetonitrile with a flow rate of 1.2 mL/min, and visualized at 214 nm. The product is 99% pure. 131

Figure A 5: Analytical purity chromatogram of TobP14 Isomer A: C18, 10-70% Acetonitrile, 214 nm. Product is 99% pure. 132

Figure A 6: Analytical purity chromatogram of TobP14 Isomer B: C18, 10-70% Acetonitrile, 214 nm. Product is 99% pure. 132

Figure A 7: MALDI mass spectra of Kanamycin-Arg_8 Isomer 1 (Expected Mass: 2010.09, Observed Mass: 2009.94). 133

Figure A 8: MALDI mass spectra of Kanamycin-Arg_8 Isomer 2 (Expected Mass: 2010.09, Observed Mass: 2010.13). 134

Figure A 9: MALDI mass spectra of P14LRR-SH (Expected Mass: 2718, Observed Mass: 2720.0). 135

Figure A 10: MALDI mass spectra of TobP14 Isomer A (Expected Mass: 3285.89, Observed Mass: 3284.9).....136

Figure A 11: MALDI mass spectra of TobP14 Isomer B (Expected Mass: 3285.89, Observed Mass: 3285.9).....137

Figure A 12: Comparison of ^{1}H Aba-S_2-COOH as compared to ^{1}H of parent abacavir. Proton 6 corresponds with the proton off the methylene carbon in abacavir adjacent to the primary hydroxyl. Note the downfield shift in the case of Aba-S_2-COOH. 138

Figure A 13: Comparison of ^{13}C from Aba-S_2-COOH as compared to ^{13}C from parent abacavir. Carbon 6 corresponds to the methylene carbon in abacavir adjacent to the primary hydroxyl. Note the downfield shift in the case of Aba-S_2-COOH. 139

Figure A 14: ^{1}H for Aba-S_2-DRV8 in DMSO-*d6*. Assignments made by ^{1}H, ^{13}C, COSY, TOCSY, HMQC. 140

Figure A 15: ^{13}C for Aba-S_2-DRV8 in in DMSO-*d6*: Assignments made by ^{1}H, ^{13}C, COSY, TOCSY, HMQC. 141

Figure A 16: ^{1}H-^{1}H COSY for Aba-S_2-DRV8. 142

Figure A 17: ^{1}H-^{1}H TOCSY for Aba-S_2-DRV8. 143

Figure A 18: ^{1}H-^{13}C HMQC for Aba-S_2-DRV8 144

Figure A 19: ^{1}H NMR for Kanamycin-2-thiopyridinyl tether (Isomer 1) in CD_3-OD: Assignments made by ^{1}H, ^{13}C, DEPT-135, COSY, TOCSY, HSQC, and HMBC. 145

Figure A 20: ^{13}C NMR for Kanamycin-2-thiopyridinyl tether (Isomer 1) in CD_3-OD: Assignments made by ^{1}H, ^{13}C, DEPT-135, COSY, TOCSY, HSQC, and HMBC. 146

Figure A 21: DEPT-135 for Kanamycin-2-thiopyridinyl tether (Isomer 1). 147

Figure A 22: COSY for Kanamycin-2-thiopyridinyl tether (Isomer 1). 148

Figure A 23: TOCSY for Kanamycin-2-thiopyridinyl tether (Isomer 1). 149

Figure A 24: HSQC for Kanamycin-2-thiopyridinyl tether (Isomer 1). Cross with DEPT-135 and ^{1}H Spectra. 150

Figure A 25: HMBC for Kanamycin-2-thiopyridinyl tether (Isomer 1). Cross with ^{13}C and ^{1}H Spectra. 151

Figure A 26: ^{1}H for Kanamycin Boc_4- 2-thiopyridinyl tether (Isomer 2). in DMSO-d_6: Assignments made by ^{1}H, ^{13}C, DEPT-135, COSY, TOCSY, HSQC, and HMBC. 152

Figure A 27: ^{13}C for Kanamycin Boc_4-2-thiopyridinyl tether (Isomer 2). in DMSO-d_6: Assignments made by ^{1}H, ^{13}C, DEPT-135, COSY, TOCSY, HSQC, and HMBC. 153

Figure A 28: DEPT-135 for Kanamycin Boc_4-2-thiopyridinyl tether (Isomer 2). 154

Figure A 29: COSY for Kanamycin Boc_4-2-thiopyridinyl tether (Isomer 2). 155

Figure A 30: TOCSY for Kanamycin Boc_4-2-thiopyridinyl tether (Isomer 2). 156

Figure A 31: HSQC for Kanamycin Boc_4-2-thiopyridinyl tether (Isomer 2). Cross of ^{13}C and ^{1}H spectra. 157

Figure A 32: HMBC for Kanamycin Boc_4-2-thiopyridinyl tether (Isomer 2). Cross of ^{13}C and ^{1}H spectra. 158

Figure A 33: ^{1}H for Tobramycin-2-thiopyridinyl tether (Isomer A) in CD_3-OD: Assignments made by ^{1}H, ^{13}C, DEPT-135, COSY, TOCSY, HSQC and HMBC. 159

Figure A 34: ^{13}C for Tobramycin-2-thiopyridinyl tether (Isomer A) in CD_3-OD: Assignments made by ^{1}H, ^{13}C, DEPT-135, COSY, TOCSY, HSQC and HMBC. 160

Figure A 35: DEPT 135 for Tobramycin-2-thiopyridinyl tether (Isomer A). 161

Figure A 36: ^{1}H-^{1}H COSY for Tobramycin-2-thiopyridinyl tether (Isomer A). 162

Figure A 37: ^{1}H-^{1}H TOCSY for Tobramycin-2-thiopyridinyl tether (Isomer A) 163

Figure A 38: ^{1}H-^{13}C HSQC for Tobramycin-2-thiopyridinyl tether (Isomer A). 164

Figure A 39: ^{1}H-^{13}C HBMC for Tobramycin-2-thiopyridinyl tether (Isomer A).....165

Figure A 40: ^{1}H for Tobramycin-2-thiopyridinyl tether (Isomer B) in CD_3-OD: Assignments made by ^{1}H, ^{13}C, DEPT-135, COSY, TOCSY, HSQC and HMBC.....166

Figure A 41: ^{13}C for Tobramycin-2-thiopyridinyl tether (Isomer B) in CD_3-OD: Assignments made by ^{1}H, ^{13}C, DEPT-135, COSY, TOCSY, HSQC and HMBC.....167

Figure A 42: DEPT 135 for Tobramycin-2-thiopyridinyl tether (Isomer B). 168

Figure A 43: ^{1}H-^{1}H COSY for Tobramycin-2-thiopyridinyl tether (Isomer B).....169

Figure A 44: ^{1}H-^{1}H TOCSY for Tobramycin-2-thiopyridinyl tether (Isomer B).....170

Figure A 45: ^{1}H-^{13}C HSQC for Tobramycin-2-thiopyridinyl tether (Isomer B).....171

Figure A 46: ^{1}H-^{13}C HMBC for Tobramycin-2-thiopyridinyl tether (Isomer B).....172

ABSTRACT

Therapeutically restricted sites present a formidable barrier in medicine. Herein, chemical strategies to overcome two restricted sites, HIV reservoirs and intracellular bacteria, will be discussed. First, cellular and anatomical HIV reservoirs, such as those in the brain, limit HIV eradication using currently known therapeutic regimes. HIV therapies are unable to localize in the brain, in part, due to high expression of efflux transporters, such as P-glycoprotein (P-gp), at the BBB, because many of these therapies are P-gp substrates. In an effort to overcome therapeutically restricted HIV sanctuaries, a dimerized combination HIV therapy was designed to act two-fold. First, the dimer acts as a P-gp inhibitor allowing therapeutic access to restricted sites. Second, the dimer acts as a prodrug, which once in the reducing environment of the cell, may release monomeric HIV therapies. The dual conjugate, Abacavir-S_2-Darunavir, was shown to potently inhibit P-gp across two separate cell lines, was able to regenerate the component monomers in a reducing environment and contained modest anti-HIV activity.

Further, mammalian cells create sanctuary sites for bacteria to grow and proliferate, because many common antibiotic therapies are unable to cross the mammalian cell membrane. Therefore, these pathogens are able to proliferate without therapeutic constraint. Here, a chemical strategy was developed to deliver a dual antibiotic therapy inside mammalian cells in an effort to clear these intracellular pathogens. First, a new synthetic strategy was developed for facile synthesis of dual conjugates, composed of an aminoglycoside and a cell penetrating peptide (CPP) linked with a reversible disulfide tether, using kanamycin and the known CPP Arg_8 as a model system. Next, this synthetic methodology was expanded for use with the aminoglycoside tobramycin and the known broad-spectrum antibiotic and cell penetrating peptide, P14LRR, once again linked via the reversible disulfide tether (TobP14). Two distinct isomers of TobP14 were synthesized, isolated, and fully characterized by 2D NMR. The TobP14 isomers were shown to be an effective antibiotic across various Gram positive and negative pathogens such as MRSA, *S. epidermidis*, *P. aeruginosa*, and *A. baumannii*. Further, the isomers effectively released the monomeric therapies (tobramycin and P14-SH) in a reducing environment and were nontoxic to mammalian cells up to 16 μM. Finally, the dual conjugate isomers significantly reduce two different strains of intracellular *A. baumannii* within macrophages.

CHAPTER 1. BIVALENT STRATEGY FOR THE INHIBITION OF THE EFFLUX TRANSPORTER P-GLYCOPROTEIN

1.1 P-glycoprotein structure and binding sites

P-glycoprotein (P-gp) is a large transmembrane protein with an overall molecular weight of 170 kDa over a stretch of 1280 amino acid residues.[1] P-gp is a member of the ATP binding cassette superfamily. It contains two homologous halves connected via a 77-amino acid connector sequence. A deeper look at the three-dimensional structure of P-gp has revealed six transmembrane regions and two nucleotide binding domains (Figure 1.1).[2-4]

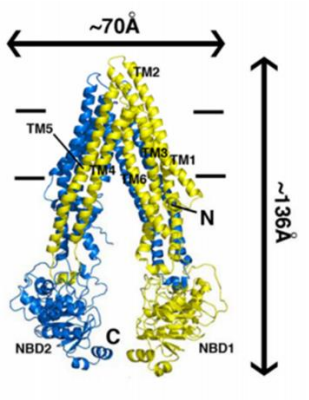

Figure 1.1 Structure of P-glycoprotein, from Aller *et al.*[4]

P-gp is nearly ubiquitous in somatic cells, being expressed in the liver, lungs, colon, jejunum, rectum, prostate, heart, ovary and brain. However, P-gp is most prominently expressed in cancer cells and in many blood-tissue barriers, including the blood brain barrier (BBB) and blood testes barrier (BTB).[5-9] P-gp acts as a defense mechanism for cells, binding to foreign matter as they are entering cells and effluxing them back out. In fact, P-gp overexpression is one of the major causes of multidrug resistance in many cancer cells.[10] Multidrug resistance (MDR) in cancer is a key culprit behind the failure of cancer therapy. Similarly, P-gp expression at the BBB affects the biodistribution and efficacy of therapeutics in the brain.[11] Problematically, many commonly used therapeutics are substrates of P-gp, including anticancer agents, immunosuppressants, and antiretrovirals.[12-14] These are effluxed out of cells by P-gp before they are able to accumulate at

their sites of action. Therefore, P-gp overexpression is a significant therapeutic hurdle that must be overcome for a variety of treatments.

P-gp binds to a wide variety of substrates with a large range in molecular weight (between 100 and 4000 Da).[15] Loo and Clarke have suggested that P-gp does not actually have an active binding site, but more of a large binding pocket, able to fit a wide range of substrates.[16] Most of the substrates are hydrophobic, and as the molecules attempt to diffuse through the plasma membrane to the cytosol, they are taken up and effluxed out of the cell by P-gp. For this reason, P-gp is commonly referred to as a "hydrophobic vacuum cleaner".[17] Due to this diverse substrate pool, researchers have worked extensively on solving the structural basis of P-gp's binding sites.

The number and location of P-gp binding sites has been an area of much empirical focus. Gottesman and coworkers[18] used photoaffinity labeling to determine that the two halves of P-gp can come together to create one common binding pocket. Stein and coworkers[19] hypothesized at least two binding domains based upon a tritium-labeled daunomyocin experiment. These findings were substantiated in 1997 when Shapiro and Ling confirmed at least two distinct binding domains using inside-out plasma membrane vesicles and two fluorescent P-gp substrates, Hoechst 33342 and Rhodamine 123.[20]

There is currently no crystal structure of human P-gp due to the difficulty involved in crystalizing large membrane-bound proteins. However, there are two crystal structures of P-gp in other model organisms, *C. elegans* and mice. *C. elegans*[21] and mouse[4, 22] P-gp are 46% and 87% homologous to human P-gp, respectively. Specifically, with regards to the Chang 2015 experiment,[22] the researchers were successful in crystalizing various macrocycles within the binding domain of P-gp at 3.4 Å resolution. In particular, one of the macrocycles, QZ59-SSS, was seen to associate with more than one location (Figure 1.2). Thus, empirical evidence suggests P-gp has more than one binding site as well as polyspecificity of binding, even within the same substrate.

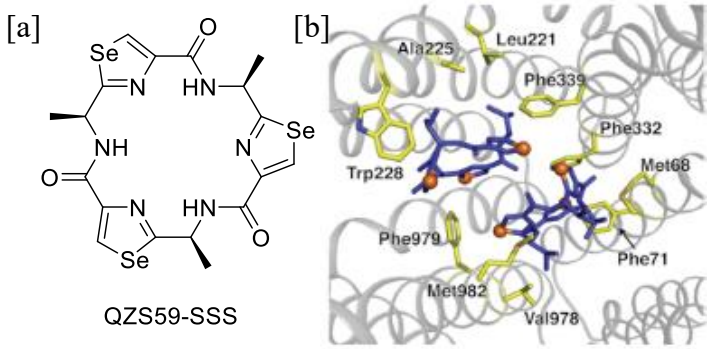

Figure 1.2 [a] The chemical structure of QZS59-SSS [b] QZS59-SSS associated within mouse P-gp crystal structure. Adapted from Chang *et al*.[22]

1.2 P-gp multivalency and inhibition

P-gp inhibition is a possible strategy to overcome multidrug resistance and to target therapeutically restricted locations. There has been a large effort to identify potent P-gp inhibitors. In fact, thus far, three generations of P-gp inhibitor molecules have been developed. The first generation was marked by the development of verapamil, the first P-gp inhibitor.[23] Furthermore, the first generation P-gp inhibitors included drugs such as cyclosporine A[24-27] as well as drug classes such as quinolines,[28] steroids,[29-31] indole alkaloids,[32, 33] calcium channel blockers[34, 35] and calmodulin inhibitors.[36, 37] This work was further refined in the second generation of P-gp inhibitors, such as dexverapamil,[38] valspodar,[30, 39] biricodar[40, 41] and dexniguldipine[42]. Finally, the third generation of inhibitors was developed, including zosuquidar, tariquidar, elacidar, and laniquidar.[43, 44] Each generation was progressively more selective, with fewer off site targets, such as cytochrome P450 and inhibition of other transporters. However, even this generation fell short during clinical trials due to toxicity.[45, 46]

An alternative inhibitor design is one that takes advantage of P-gp's multiple binding sites. This design targets the transmembrane binding domain of P-gp, as it has at least two binding sites where two substrates may simultaneously bind. Multivalent molecules have been shown to cooperatively bind with their target, which accounts for the stronger binding and slower dissociation from the protein/enzyme (Figure 1.3).[47] This approach that exploits P-gp's multivalency can be developed by linking two known P-gp substrates (or modulators) together, thereby allowing cooperative binding within the large substrate binding domain of P-gp. This should increase the overall binding affinity of the bivalent modulator for P-gp, by reducing the

conjugate's off rate as compared to the monomeric agent, thereby producing an inhibitor (Figure 1.3).

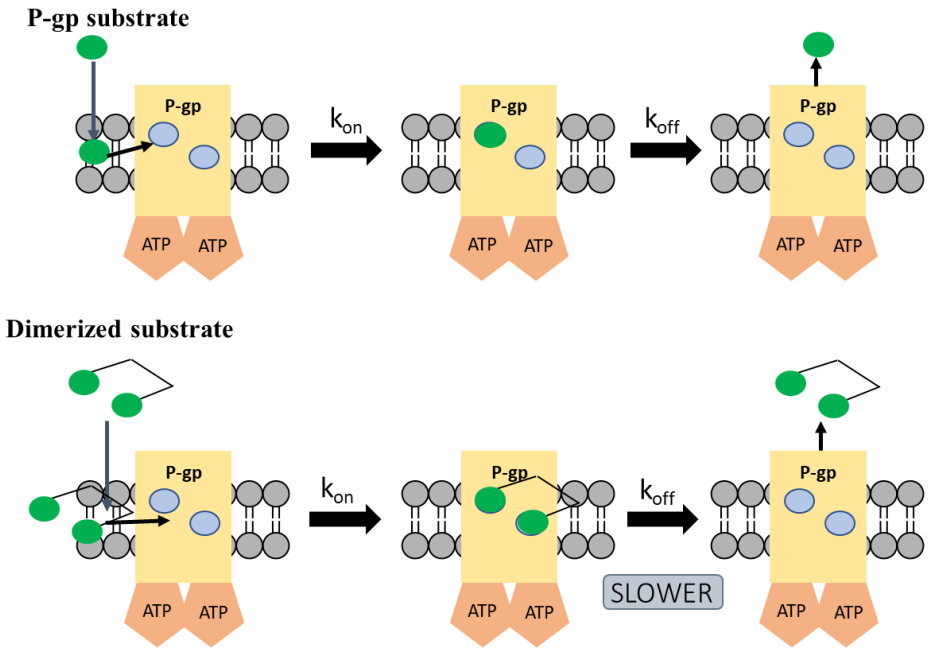

Figure 1.3 P-glycoprotein inhibition strategy. The dimerization of P-gp substrates should induce stronger affinity for the transmembrane binding domain.

Ambudkar *et al*. was the first to utilize this inhibition strategy of dimerized P-gp substrates (or modulators) to inhibit P-gp activity.[48] The Chmielewski/Hrycyna[49-59] and Chow/Chan[60-67] groups have expanded upon this concept, showing that the dimerization of P-gp substrates (or modulators) leads to potent P-gp inhibition. Herein is a summary of the studies using this bivalent approach to generate potent P-gp inhibitors. These groups have investigted libraries of compounds that probe tether design for potent inhibition of P-gp. Maintaining a central focus on tether designs has allowed this methodology to evolve over time into a successful strategy for selective P-gp inhibition and the development of P-gp inhibitors which are also prodrug therapies for the treatment of cancer and brain disorders.

1.3 Substrate dimerization as a viable inhibition strategy for P-glycoprotein

The Ambudkar group was the first to introduce this strategy in 2004.[48] They linked the known P-gp modulator, stipiamide, to make homodimers linked with polyethylene glycol tethers

of varying lengths (N= 0, 2, 5, 8, and 12 ethylene glycol groups) (Figure 1.4). They found that the length of the tether affected the compounds' inhibition capacity. When stipiamide dimers were co-administered with fluorescent P-gp substrates in the presence of cells which overexpress P-gp (NIH-3T3 cells), maximal intracellular fluorescence was observed when the linker contained eight or more ethylene glycol groups. This corresponds to a tether length of 35 Å or longer for maximal P-gp inhibition. This groundbreaking work paved the way for future studies in the field.

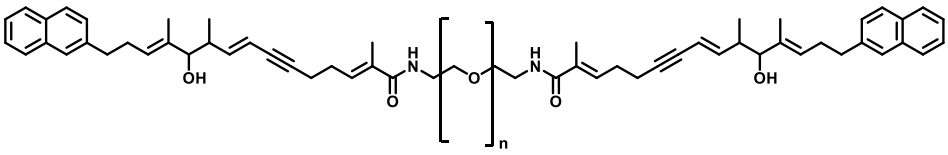

n=0, 2, 5, 8, 12

Figure 1.4 Stipiamide dimer library with varying tether lengths (n) for P-gp inhibition.[48]

In 2006, the Chmielewski/Hrycyna groups used a dimerization strategy with the known P-gp substrate, emetine.[49] They reported a library of emetine dimers constructed with varying tethers. The library probed the importance of length, hydrophobicity and charge, with tethers including polyalkyl (N=4-10), bisamino and a bispolyethylene glycol chains (Figure 1.5). The emetine dimers were co-administered with the P-gp substrate and anticancer drug doxorubicin to cells which highly express P-gp and are resistant to doxorubicin (MCF7-DX1). Based on their results, the C5 alkyl tethered emetine dimer had superior P-gp inhibition with maximal reversion of the multidrug resistant phenotype. The C5 alkyl tether corresponds to a length of approximately 10 Å. Interestingly, this work expands the previously reported results, as the superior tether composition was hydrophobic and significantly shorter than described by Ambudkar.[48]

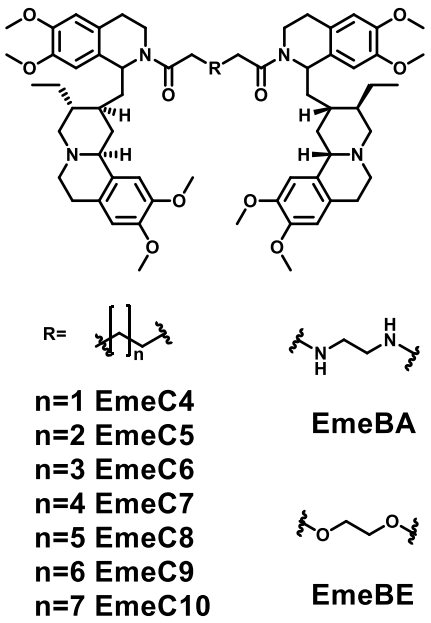

Figure 1.5 Emetine dimer library for the inhibition of P-gp.[49]

The Chow/Chan groups also utilized this bivalent strategy in 2006 with the introduction of their library of flavonoid dimers.[60] The flavonoid, apigenin, is a known P-gp substrate[68] and was used for purposes of this work.[69] They reported a library of apigenin dimers linked together with polyethylene glycol tethers of varying lengths (Figure 1.6). They co-administered their apigenin dimer library with various anticancer drugs, such as paclitaxel (taxol), doxorubicin, daunomycin, vincristine, and vinblastine, using multidrug resistant cell lines which highly express P-gp. The optimal tether length for reversal of the multidrug resistant phenotype by P-gp inhibition was found to contain 2-4 ethylene glycol repeats. Two ethylene glycol units are about 6 Å; therefore, these tethers were approximately 6-12 Å in length.[70] These results were in agreement with the optimal tether lengths reported by the Chmielewski group.[49]

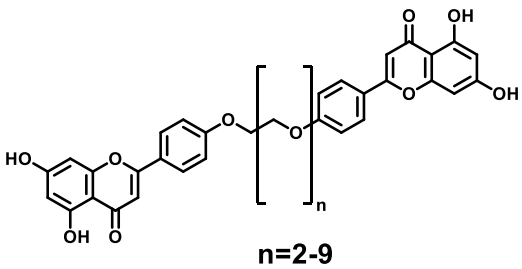

Figure 1.6 Chow/Chan apigenin flavonoid dimer library.[60]

Following these preliminary studies, both the Chmielewski/Hrycyna and Chow/Chan groups continued to work on reversing MDR via inhibition of P-gp with divalent agents. The dimers were formed from two substrates (or modulators) of P-gp and were linked together with various tethers. Alterations in tether design allowed for the release of the unmodified monomers from the dimer molecule, an effective simultaneous P-gp inhibition and drug delivery strategy.[51-53, 55, 56] Further modifications in tether design also conferred specificity for P-gp over other efflux transporters.[65-67]

1.4 P-glycoprotein inhibition can reverse multidrug resistance in cancer using quinine dimers

Having synthesized the first emetine dimer, the Chmielewski/Hrycyna groups honed in on two main areas: treatment of cancer and brain disorders, both of which are detrimentally affected by drug efflux transporters. Multidrug resistance in cancer is known to occur, in part, due to the high concentration of P-gp expressed on the surface of cancer cells. In order to reverse the resistance of cancer cells to various chemotherapeutic agents, quinine dimers were designed.

Quinine and its stereoisomer, quinidine, are inexpensive starting materials, have been deemed safe for human use and are both P-gp substrates. Therefore, quinine and quinidine were dimerized according to the previous strategy to make P-gp inhibitors.[71] A library of quinine homodimers, quinidine homodimers and quinine-quinidine heterodimers was synthesized, therefore, with varying tether lengths and rigidities in order to properly probe the ideal conditions for inhibition of P-gp (Figure 1.7a). The dimer library was co-administered with fluorescent P-gp substrates, such as rhodamine 123, doxorubicin, mitoxantrone and Bodipy-FL-prazosin, using MCF7-DX1 cell lines, which over-express P-gp. The intracellular accumulation of the fluorescent P-gp substrate was directly related to P-gp inhibition of the dimer library. It was evident that the flexible alkyl C8 chain linked quinine dimer (Q2) contained the best tether for P-gp inhibition, with an IC_{50} of 1.7 μM as compared to quinine (103 μM).[57] Further MCF7-DX1 cells were also treated with taxol in the presence of Q_2 and the reversal of the MDR phenotype was observed at 4μM.

This methodology was further expanded by modifying quinine with alkyne and azide functionalities to make use of a copper-assisted alkyne-azide click reaction (Figure 1.7b).[58] A library of clicked quinine homo- and heterodimers with different tether lengths was synthesized.

Inhibition of P-gp in MCF-7-DX1 was assessed with treatment of the library of dimers co-administered with the fluorescent P-gp substrate calcein AM. The maximal intracellular fluorescence was observed with the 6,4', 6,6' and 4,6' lengths (Figure 1.7b) with IC_{50} values of ~3 μM. Therefore, in the case of the clicked quinine dimers, a tether length of 10 or 12 methylene units with a central triazole ring confers the most potent P-gp inhibition.

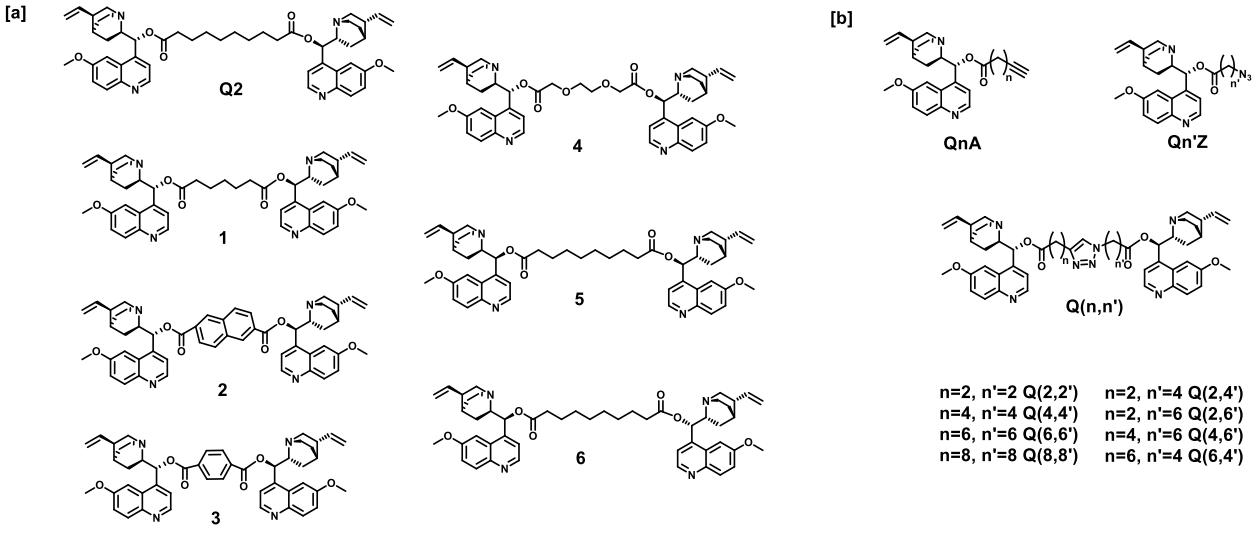

Figure 1.7 [a] Quinine and quinidine library of P-gp inhibitors; Q2 reverses multidrug resistance in cancer cell lines.[57] [b] Quinine library of homo- and heterodimers using alkyne-azide click chemistry to generate inhibitiors of P-gp.[58]

1.5 P-glycoprotein inhibition is a viable strategy to target brain disorders

1.5.1 Schizophrenia

Two common schizophrenia medications, quetiapine[72, 73] and paliperidone[74-76], are both substrates of P-gp, which likely accounts for their limited bioavailability in the brain. In order to circumvent this issue, the Chmielewski/Hrycyna groups used the bivalent approach to develop P-gp inhibitors. This work started in 2013,when Emmert *et al.* synthesized a library of quetiapine dimers esterified with varying length dicarboxylic acids (Figure 1.8).[53] These dimers were co-administered with fluorescent P-gp substrates, such as rhodamine 123, calcein-AM, BODIPY-FL-verapamil, doxorubicin and [^{3}H]-daunorubicin, using an immortalized blood brain barrier model cell line, hCMEC/D3,[77] which expresses an endogenous level of P-gp. Based on the intracellular accumulation of the fluorescent substrates, the most potent member of the library, QT_2C_2, inhibited

P-gp 80-fold more potently than quetiapine alone. A lack of plasma stability of QT_2C_2 (half-life 3 hours) led to the development of new agent, $QT_2C_2Me_2$, with methyl substituents α to the carbonyl of the ester. The more sterically bulky compound ($QT_2C_2Me_2$) exhibited an increased half-life (38 hrs) and maintained potent P-gp inhibition. This design of reversible schizophrenia prodrugs that also inhibit P-gp is a promising strategy to potentially deliver schizophrenia medications to the brain.

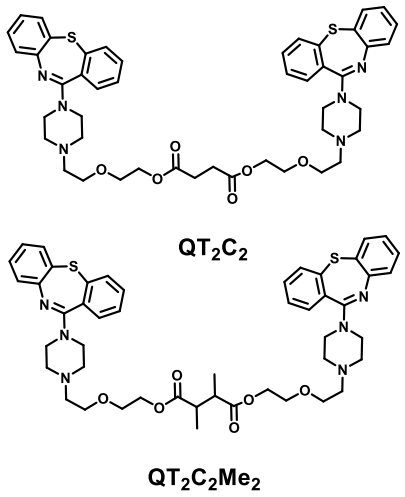

Figure 1.8 Quetiapine dimers used to inhibit P-gp. [53]

This design was further expanded in 2017 with the generation of paliperidone dimers.[55] Paliperidone, a known P-gp substrate[74-76] and schizophrenia medication, was dimerized using a library tether approach. The library contained tethers using various dicarboxylic acids of differing lengths, with and without a disulfide moiety and added methyl groups or a carbamate based (C6) tether, (Figure 1.9a). The inclusion of the disulfide was for enhanced drug delivery purposes. In the reducing environment of the cell, this disulfide moiety reduces and the resulting thiol may then intramolecularly attack the carbonyl of the ester, releasing paliperidone inside the cell (Figure 1.9b).

The library was co-administered with the fluorescent P-gp substrates, calcein-AM, rhodamine 123, and mitoxantrone, using the MCF7-DX1 cell line, which overly expresses P-gp.[78] The increased intracellular accumulation of fluorescence confirmed that Pal-8SS was the superior dimer of the library with an IC_{50} of 2-3 μM for P-gp inhibition with calcein AM, rhodamine 123 and mitoxantrone. However, the dimer was again susceptible to esterases. Therefore, methyl

groups α to the carbonyl were added to Pal-8SS. This extra steric bulk increased the half-life of the conjugate in human plasma from 0.5 hours (Pal-8SS) to 11.4 hours, a greater than 20-fold increase. Pal-8SSMe was incubated with human blood brain barrier endothelial cells (hCMEC) and its intracellular accumulation was monitored over time. Pal-8SSMe reached a maximal intracellular concentration after 8 hours with the maximal release of paliperidone observed after 24 hours. Therefore, this strategy for P-gp inhibition and intracellular accumulation of schizophrenia drug seems to be effective. Further, this disulfide delivery methodology enhances the dual design of the conjugates, a P-gp inhibitor and an active prodrug, for a particular disease of interest.

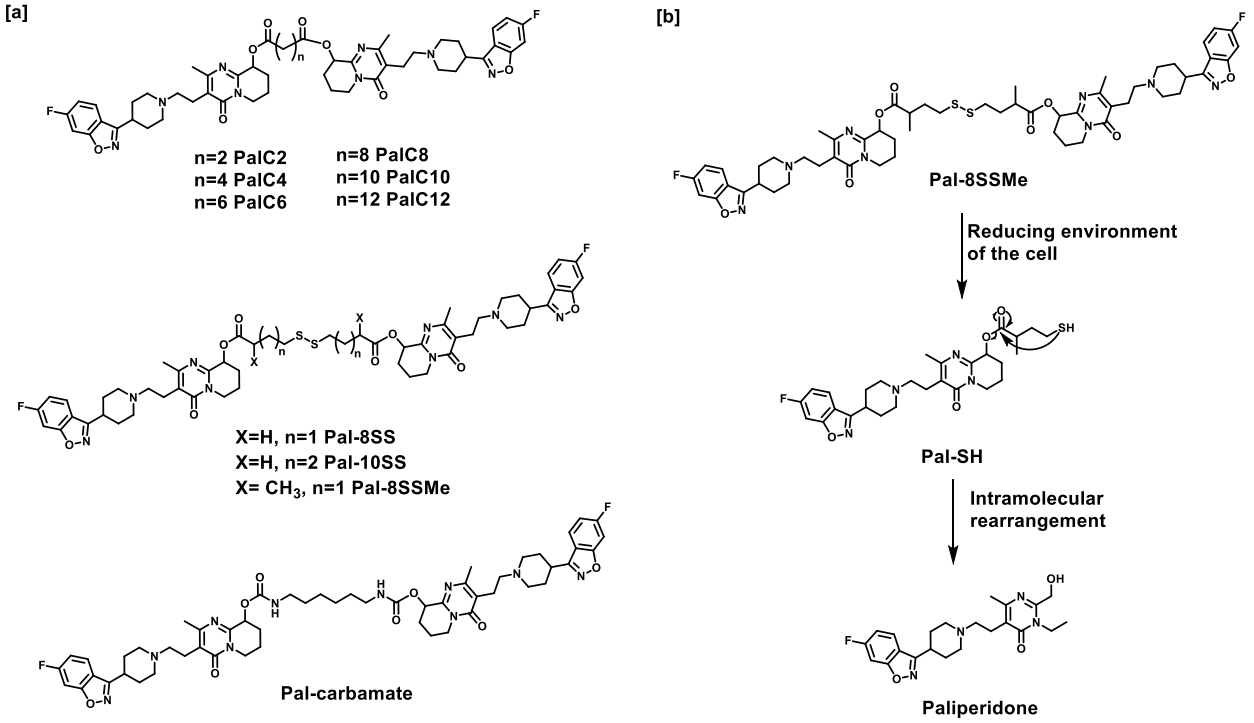

Figure 1.9 [a] Library of paliperidone dimers for P-gp inhibition[55] [b] Pal-8SSMe reversion to paliperidone in the reducing environment of the cell mechanism.[55]

1.5.2 Antiviral dimeric prodrugs as P-gp inhibitors

This bivalent methodology for the design of P-gp inhibitors was further expanded in 2011 and 2013 when Namanja *et al*. used this approach with antivirals targeting HIV.[51, 52] HIV treatment has progressed substantially using treatment regimes such as highly active antiretroviral therapy (HAART).[79, 80] On this therapeutic regime, the patient's HIV viral plasma levels may reduce below

a detectable limit. However, when the therapies are stopped, viral resurgence occurs.[81, 82] This viral resurgence is due, in part, to cellular and anatomical HIV reservoirs. These reservoirs are located in macrophages, lymphocytes, and the central nervous system, to name a few. In the brain, these reservoirs proliferate due to limited therapeutic access. Many HAART drugs are unable to accumulate in the brain due to tight junctions, the physiochemical properties of the drugs and the high prevalence of efflux transporters at the BBB.[83-85] One such efflux transporter highly expressed at the blood brain barrier is P-glycoprotein (P-gp). Many of these HAART drugs are substrates of P-gp, thus accounting, in part, for their limited bioavailability in the brain.[84, 86-92]

Although the accumulation of HAART therapeutics in the brain is limited in part due to P-gp, HIV can accumulate inside the brain via various mechanisms, such as paracellular or transcellular diapedesis.[93] Therefore, HIV is able to proliferate in the brain with limited therapeutic constraint. Thus, inhibiting P-gp would likely be very beneficial in targeting HIV reservoirs in the brain. Using known P-gp substrates, which are also HIV therapeutics, dimer libraries were designed to assist with these challenges.

This work began with a library of abacavir dimers for the inhibition of P-gp and the treatment of HIV.[51] Abacavir is a reverse transcriptase inhibitor for the treatment of HIV infections. *In vitro* studies have confirmed that abacavir is a substrate of P-gp.[86] These results were further substantiated with *in vivo* studies, where abacavir was able to accumulate in the brains of P-gp null mice 20-fold more than in wild type mice.[86]

The abacavir dimers were designed for a two-fold purpose: (1) to inhibit P-gp at the BBB and (2) to release the monomeric abacavir therapy in cells (Figure 1.10). A library of dimeric abacavir compounds was designed for this study, using tethers containing a disulfide moiety in the center with and without additional methyl groups α to the carbonyl (Figure 1.11a). In fact, the introduction of methyl substituents resulted in an overall longer half-life in human plasma, with $AbaS_2Me_4$ displaying an impressive half-life of >100 hours. Further, $AbaS_2Me_4$ was co-administered with calcein-AM and NBD-abacavir using 12D7-MDR cells, $CD4^+$ T-cells that over-express P-gp. $AbaS_2Me_4$ was found to have an IC_{50} value of 0.7 μM as compared to abacavir with an IC_{50} of greater than 500 μM. Using a DTT release study, which mimics the intracellular reducing environment, $AbaS_2Me_4$ released abacavir with a half-life of approximately 17 hours. $AbaS_2Me_4$ was further tested against HIV-1 in a 12D7 (T-cell) model. The compound displayed moderate dose-dependent anti-HIV activity, similar to the monomer, abacavir. Thus, this model

further substantiated the prodrug design since the dimer must break down into the abacavir monomer in order to confer anti-HIV activity. Taken in tandem, these results confirm the effectiveness of the overall abacavir dimer design for targeting HIV.

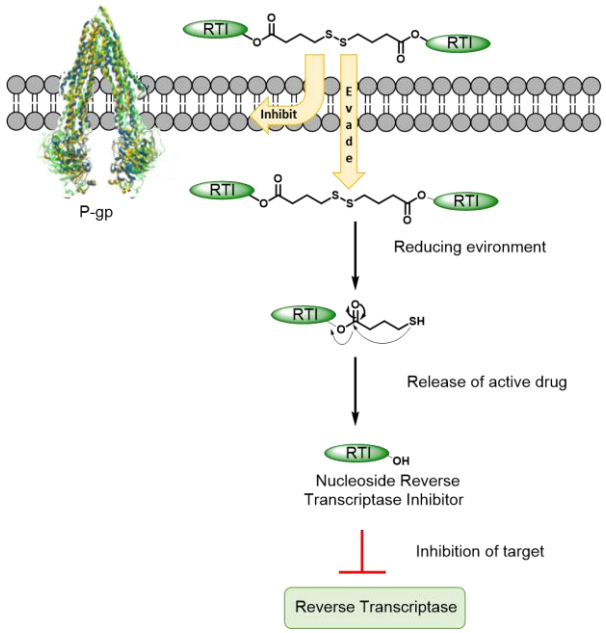

Figure 1.10 Abacavir dimer strategy; dimer will inhibit P-gp, thereby evading the blood brain barrier. When in the reducing environment of the cell, the disulfide will reduce into free thiols which will rearrange to release the active abacavir inside cells.

Additionally, abacavir was linked with dicarboxylic acids of various lengths via an ester bond (Figure 1.11b).[52] The library was co-administered with a wide variety of fluorescent P-gp substrates (including BODIPY-prazosin, doxorubicin, NBD-abacavir, and calcein AM) in 12D7-MDR cells[94] (CD4+ T cells) and hCMEC/D3 cells[77] (immortalized blood brain barrier endothelial cells). The library displayed an increase in intracellular fluorescence, corresponding with P-gp inhibition, with the best library member being the C8 tether with an IC_{50} of 2.3 μM as compared to abacavir alone (>500 μM). Together, these abacavir dimer libraries paved the way for other bivalent HIV therapeutics for the goal of P-gp inhibition and eradication of viral reservoirs of P-gp in the brain (Chapter 2).

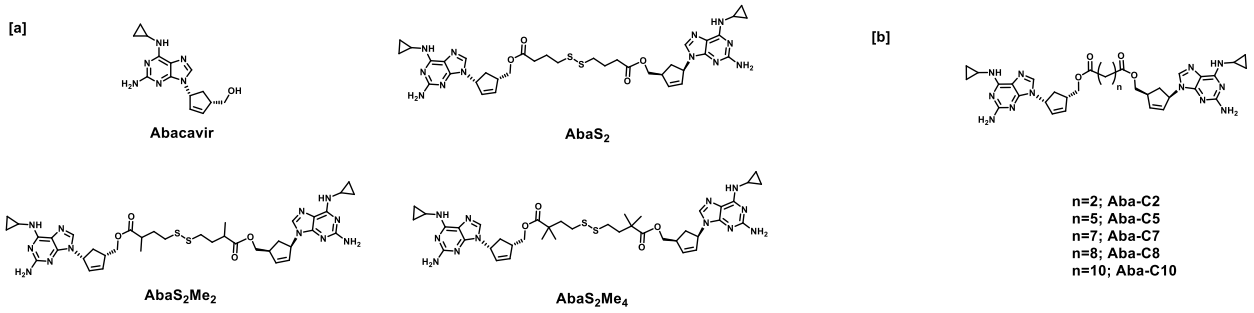

Figure 1.11 [a] Abacavir dimer library using the disulfide tether strategy, with methyl substituents at the α-carbon[51] [b] Abacavir library to probe the most ideal tether length.[52]

In 2017, Namanja *et al.* expanded the repertoire of bivalent P-gp inhibitor designs by using zidovudine (AZT), a known P-gp substrate and reverse transcriptase inhibitor for the treatment of HIV-1.[59] In this study, AZT was dimerized using a library of dicarboxylic acids generating reversible ester linkages (Figure 1.12). The library of AZT dimers was co-administered with the P-gp fluorescent substrate calcein AM, using the MCF7-DX1 cell line. In this study, the increased intracellular fluorescence was observed with the longer tethers, C10 and C12, which corresponds to potent inhibition of P-gp, with >200-fold enhanced P-gp inhibition as compared to AZT alone.

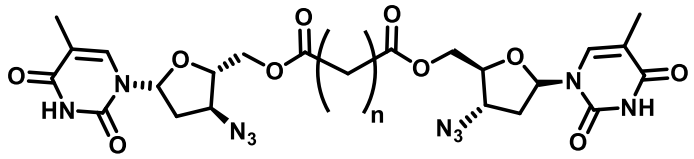

n=2; AZT-C2
n=5; AZT-C5
n=8; AZT-C8
n=10; AZT-C10
n=12; AZT-C12

Figure 1.12 AZT-dimer library for the inhibition of P-gp.[59]

1.6 Tether location and design can confer P-glycoprotein inhibition potency and specificity

The Chan/Chow group made a library of structurally diverse flavonoids with modifications along the core apigenin structure (1-81) as well as altering their conjugation location (2', 3' or 4')

(Figure 1.13).[62] The dimers were synthesized with four repeats of polyethylene glycol as the tethers for all members of the library. The library was co-administered with taxol using the P-gp over-expressing breast cancer cell line MDA435/LCC6MDR, and was assessed based on their effectiveness in reversing cellular resistance to taxol. Based on their findings, the structure activity relationship suggests that flavonoid substituents with more non-polar and hydrophobic substituents at positions C3, C6 and C7 conferred superior resistance reversing activity, as compared to more polar or hydrophilic substituents. Further, the most superior resistance reversing activity seen in the library (IC_{50}=9 nM) was with the flavonoid monomers conjugated to the tether at the para position (4') (Figure 1.13). Therefore, structural modification and tether positioning along a monomer does affect the resultant dimer's P-gp inhibition potency.

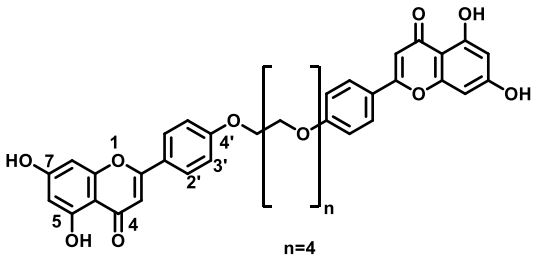

Compound	R=
1, 21	H
2, 22	4-F
3, 23	5-F
4, 24	5-Cl
5, 25	5-Br
6, 26	3,5-diCl
7, 27	3,5-diBr
8, 28	4-Me
9, 29	5-Me
10, 30	4-MeO

Compound	R=
11, 31	5-MeO
12, 32	6-MeO
13, 33	4,5-diMeO
14, 34	4-BnO
15, 35	5-BnO
16, 36	6-BnO
17, 37	4, 6-diMeO
18, 38	4,6-diBnO
19, 39	5-Et
20, 40	3-NO_2, 5-Me_2

Compound	R=
41, 61	H
42, 62	7-F
43, 63	6-F
44, 64	6-Cl
45, 65	6-Br
46, 66	6,8-diCl
47, 67	6,8-diBr
48, 68	7-Me
49, 69	6-Me
50, 70	7-MeO

Compound	R=
51, 71	6-MeO
52, 72	5-MeO
53, 73	6,7-diMeO
54, 74	7-BnO
55, 75	6-BnO
56, 76	5-BnO
57, 77	5, 7-diMeO
58, 78	5,7-DiBnO
59, 79	6-Et
60, 80	6-Me, 8-NO_2
81	5-OH

Figure 1.13 Flavonoid modification library.[62]

Further improvements to the flavonoid dimers for reversal of resistance in cancer was seen when modifying the tether. Originally, the flavonoid dimers contained polyethylene glycol tethers. In a 2012 study, Chan *et al.* included an amine functionality in the center of the polyethylene glycol tether.[63] The secondary amine was further substituted with a library of different moieties. This library of apigenin, conjugated with various tether substituents, was co-administered with taxol and doxorubin using LCC6MDR cells. P-gp inhibition was assessed based on the reversal of

cellular resistance to taxol or doxorubicin. These modifications led to high potencies in reversing P-gp mediated resistance in LCC6MDR cells, which corresponds to greater P-gp inhibition. These compounds were found to have overall low cellular toxicity. The most potent compound in the library was substituted with a benzyl moiety off the amine in the tether with an IC_{50} of 2.6 μM (Figure 1.14). Further, this tether modification (benzyl substituted amine) conferred preferential inhibition of P-gp over other efflux transporters, such as MRP-1 and BCRP (IC_{50} of 192 and 147 μM, respectively). This specificity enhancement is an interesting design feature, which they have further utilized for other studies in combating drug resistance.

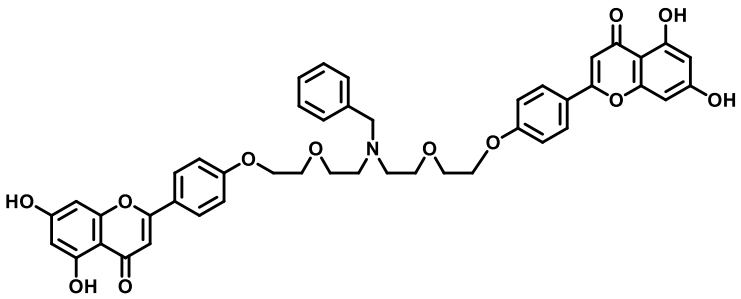

Figure 1.14 Flavonoid tether design for specific P-gp inhibition.

1.7 Bivalent inhibition strategy beyond P-glycoprotein

This bivalent P-glycoprotein inhibition strategy has been further expanded to other drug resistance efflux transporters. The Chmielewski/Hrycyna groups synthesized a potent and reversible quinine dimer library for inhibition of *P. falciparum* chloroquine resistance transporter PfCRT (Figure 1.15).[54] Their most potent library members, Q2 and Q_2C, exhibited antiparasiticidal activity against *in vitro* drug resistant *P. falciparum*, and Q2 demonstrated potent activity in an *in vivo P. berghei* infection model in mice.

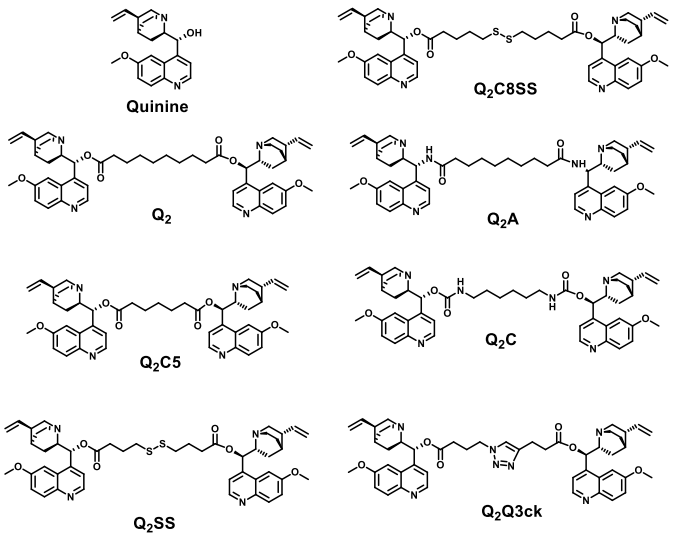

Figure 1.15 Quinine dimer library for the inhibition of PfCRT and the treatment of malaria.[54]

Furthermore, the bivalent strategy to target the ATP binding cassette efflux transporters has also been used for ABCG2 and MRP-1, also with much success.[55, 59, 65-67] For instance, the paliperidone and AZT dimers served a dual purpose for both P-gp and ABCG2 inhibition.[55, 59] Flavonoid dimers have also demonstrated inhibition of MRP1 and ABCG2.[65-67]

1.8 Conclusion

Overall, this bivalent approach to efflux transporter inhibition is a very promising strategy to overcome multidrug resistance and treat diseases ranging from cancer, malaria, and brain disorders. By modifying the length of the tether, P-gp substrates can become potent P-gp inhibitors. Tether design can also determine the dimer's target. Altering the polyethylene glycol tether to an amino substituted version transforms the flavonoid dimer into a specific P-gp inhibitor. Connecting the target drugs with an ester functionality and/or including a disulfide within the tether transforms the P-gp inhibitor into a multipurpose therapeutic, both a P-gp inhibitor and a prodrug. Changing the site of connectivity of the monomer to the tether can alter the resulting dimer's P-gp inhibitory effectiveness and/or prodrug efficacy. These powerful chemical tools within the bivalent strategy may hold the key to overcoming multidrug resistance and many notoriously difficult to treat disorders.

1.9 References

1. Ambudkar, S. V.; Dey, S.; Hrycyna, C. A.; Ramachandra, M.; Pastan, I.; Gottesman, M. M., Biochemical, cellular, and pharmacological aspects of the multidrug transporter. *Annu. Rev. Pharmacol. Toxicol.* **1999,** *39*, 361-398.

2. Hrycyna, C. A.; Ramachandra, M.; Germann, U. A.; Cheng, P. W.; Pastan, I.; Gottesman, M. M., Both ATP sites of human P-glycoprotein are essential but not symmetric. *Biochemistry* **1999,** *38* (42), 13887-13899.

3. Gottesman, M. M.; Pastan, I., The multidrug transporter, a double-edged sword. *J. Biol. Chem.* **1988,** *263* (25), 12163-6.

4. Aller, S. G.; Yu, J.; Ward, A.; Weng, Y.; Chittaboina, S.; Zhuo, R.; Harrell, P. M.; Trinh, Y. T.; Zhang, Q.; Urbatsch, I. L.; Chang, G., Structure of P-glycoprotein reveals a molecular basis for poly-specific drug binding. *Science* **2009,** *323* (5922), 1718-1722.

5. Fojo, A. T.; Ueda, K.; Slamon, D. J.; Poplack, D. G.; Gottesman, M. M.; Pastan, I., Expression of a multidrug-resistance gene in human tumors and tissues. *Proc. Natl. Acad. Sci. U. S. A.* **1987,** *84* (1), 265-9.

6. Cordon-Cardo, C.; O'Brien, J. P.; Casals, D.; Rittman-Grauer, L.; Biedler, J. L.; Melamed, M. R.; Bertino, J. R., Multidrug-resistance gene (P-glycoprotein) is expressed by endothelial cells at blood-brain barrier sites. *Proc. Natl. Acad. Sci. U. S. A.* **1989,** *86* (2), 695-8.

7. Jette, L.; Tetu, B.; Beliveau, R., High levels of P-glycoprotein detected in isolated brain capillaries. *Biochim. Biophys. Acta, Biomembr.* **1993,** *1150* (2), 147-54.

8. Croop, J. M.; Raymond, M.; Haber, D.; Devault, A.; Arceci, R. J.; Gros, P.; Housman, D. E., The three mouse multidrug resistance (mdr) genes are expressed in a tissue-specific manner in normal mouse tissues. *Mol. Cell. Biol.* **1989,** *9* (3), 1346-50.

9. Chin, J. E.; Soffir, R.; Noonan, K. E.; Choi, K.; Roninson, I. B., Structure and expression of the human MDR (P-glycoprotein) gene family. *Mol. Cell. Biol.* **1989,** *9* (9), 3808-20.

10. Breier, A.; Gibalova, L.; Seres, M.; Barancik, M.; Sulova, Z., New insight into P-glycoprotein as a drug target. *Anti-Cancer Agents Med. Chem.* **2013,** *13* (1), 159-170.

11. Eyal, S.; Ke, B.; Muzi, M.; Link, J. M.; Mankoff, D. A.; Collier, A. C.; Unadkat, J. D., Regional P-glycoprotein activity and inhibition at the human blood-brain barrier as imaged by positron emission tomography. *Clin. Pharmacol. Ther.* **2010,** *87* (5), 579-585.

12. Sallustio, B. C.; Noll, B. D.; Coller, J. K.; Tuke, J.; Russ, G.; Somogyi, A. A., Relationship between allograft cyclosporin concentrations and P-glycoprotein expression in the 1st month following renal transplantation. *Br. J. Clin. Pharmacol.* **2019,** *85* (5), 1015-1020.

13. Kobori, T.; Harada, S.; Nakamoto, K.; Tokuyama, S., Mechanisms of P-glycoprotein alteration during anticancer treatment: role in the pharmacokinetic and pharmacological effects of various substrate drugs. *J. Pharmacol. Sci. (Tokyo, Jpn.)* **2014,** *125* (3), 242-254.

14. Chandler, B.; Almond, L.; Ford, J.; Owen, A.; Hoggard, P.; Khoo, S.; Back, D., The effects of protease inhibitors and nonnucleoside reverse transcriptase inhibitors on P-glycoprotein expression in peripheral blood mononuclear cells in vitro. *JAIDS, J. Acquired Immune Defic. Syndr.* **2003,** *33* (5), 551-556.

15. Ward, A. B.; Szewczyk, P.; Grimard, V.; Lee, C.-W.; Martinez, L.; Doshi, R.; Caya, A.; Villaluz, M.; Pardon, E.; Cregger, C.; Swartz, D. J.; Falson, P. G.; Urbatsch, I. L.; Govaerts, C.; Steyaert, J.; Chang, G., Structures of P-glycoprotein reveal its conformational flexibility and an epitope on the nucleotide-binding domain. *Proc. Natl. Acad. Sci. U. S. A.* **2013,** *110* (33), 13386-13391.

16. Loo, T. W.; Bartlett, M. C.; Clarke, D. M., Methanethiosulfonate derivatives of rhodamine and verapamil activate human P-glycoprotein at different sites. *J. Biol. Chem.* **2003,** *278* (50), 50136-50141.

17. Higgins, C. F.; Gottesman, M. M., Is the multidrug transporter a flippase? *Trends Biochem. Sci.* **1992,** *17* (1), 18-21.

18. Bruggemann, E. P.; Currier, S. J.; Gottesman, M. M.; Pastan, I., Characterization of the azidopine and vinblastine binding site of P-glycoprotein. *J. Biol. Chem.* **1992,** *267* (29), 21020-6.

19. Ayesh, S.; Shao, Y.-M.; Stein, W. D., Co-operative, competitive and non-competitive interactions between modulators of P-glycoprotein. *Biochim. Biophys. Acta, Mol. Basis Dis.* **1996,** *1316* (1), 8-18.

20. Shapiro, A. B.; Ling, V., Positively cooperative sites for drug transport by P-glycoprotein with distinct drug specificities. *Eur. J. Biochem.* **1997,** *250* (1), 130-137.

21. Jin, M. S.; Oldham, M. L.; Zhang, Q.; Chen, J., Crystal structure of the multidrug transporter P-glycoprotein from Caenorhabditis elegans. *Nature* **2012,** *490* (7421), 566-569.

22. Szewczyk, P.; Tao, H.; McGrath, A. P.; Villaluz, M.; Rees, S. D.; Lee, S. C.; Doshi, R.; Urbatsch, I. L.; Zhang, Q.; Chang, G., Snapshots of ligand entry, malleable binding and induced helical movement in P-glycoprotein. *Acta Crystallogr., Sect. D Biol. Crystallogr.* **2015,** *71* (3), 732-741.

23. Tsuruo, T.; Iida, H.; Tsukagoshi, S.; Sakurai, Y., Overcoming of vincristine resistance in P388 leukemia in vivo and in vitro through enhanced cytotoxicity of vincristine and vinblastine by verapamil. *Cancer Res.* **1981,** *41* (5), 1967-72.

24. Chao, N. J.; Aihara, M.; Blume, K. G.; Sikic, B. I., Modulation of etoposide (VP-16) cytotoxicity by verapamil or cyclosporine in multidrug-resistant human leukemic cell lines and normal bone marrow. *Exp. Hematol.* **1990,** *18* (11), 1193-8.

25. Slater, L. M.; Sweet, P.; Stupecky, M.; Gupta, S., Cyclosporin A reverses vincristine and daunorubicin resistance in acute lymphatic leukemia in vitro. *J. Clin. Invest.* **1986,** *77* (4), 1405-8.

26. Slater, L. M.; Sweet, P.; Stupecky, M.; Wetzel, M. W.; Gupta, S., Cyclosporin A corrects daunorubicin resistance in Ehrlich ascites carcinoma. *Br. J. Cancer* **1986,** *54* (2), 235-8.

27. Twentyman, P. R.; Fox, N. E.; White, D. J. G., Cyclosporin A and its analogs as modifiers of adriamycin and vincristine resistance in a multi-drug resistant human lung cancer cell line. *Br. J. Cancer* **1987,** *56* (1), 55-7.

28. Solary, E.; Velay, I.; Chauffert, B.; Bidan, J. M.; Caillot, D.; Dumas, M.; Guy, H., Sufficient levels of quinine in the serum circumvent the multidrug resistance of the human leukemic cell line K562/ADM. *Cancer* **1991,** *68* (8), 1714-9.

29. Barnes, K. M.; Dickstein, B.; Cutler, G. B., Jr.; Fojo, A. T.; Bates, S. E., Steroid transport, accumulation, and antagonism of P-glycoprotein in multidrug-resistant cells. *Biochemistry* **1996,** *35* (15), 4820-7.

30. Gruol, D. J.; Zee, M. C.; Trotter, J.; Bourgeois, S., Reversal of multidrug resistance by RU 486. *Cancer Res.* **1994,** *54* (12), 3088-91.

31. Ueda, K.; Okamura, N.; Hirai, M.; Tanigawara, Y.; Saeki, T.; Kioka, N.; Komano, T.; Hori, R., Human P-glycoprotein transports cortisol, aldosterone, and dexamethasone, but not progesterone. *J. Biol. Chem.* **1992,** *267* (34), 24248-52.

32. Beck, W. T.; Cirtain, M. C.; Glover, C. J.; Felsted, R. L.; Safa, A. R., Effects of indole alkaloids on multidrug resistance and labeling of P-glycoprotein by a photoaffinity analog of vinblastine. *Biochem. Biophys. Res. Commun.* **1988,** *153* (3), 959-66.

33. Tsuruo, T.; Iida, H.; Kitatani, Y.; Yokota, K.; Tsukagoshi, S.; Sakurai, Y., Effects of quinidine and related compounds on cytotoxicity and cellular accumulation of vincristine and adriamycin in drug-resistant tumor cells. *Cancer Res.* **1984,** *44* (10), 4303-7.

34. Hoellt, V.; Kouba, M.; Dietel, M.; Vogt, G., Stereoisomers of calcium antagonists which differ markedly in their potencies as calcium blockers are equally effective in modulating drug transport by P-glycoprotein. *Biochem. Pharmacol.* **1992,** *43* (12), 2601-8.

35. Tsuruo, T.; Iida, H.; Nojiri, M.; Tsukagoshi, S.; Sakurai, Y., Circumvention of vincristine and adriamycin resistance in vitro and in vivo by calcium influx blockers. *Cancer Res.* **1983,** *43* (6), 2905-10.

36. Ganapathi, R.; Grabowski, D.; Turinic, R.; Valenzuela, R., Correlation between potency of calmodulin inhibitors and effects on cellular levels and cytotoxic activity of doxorubicin (adriamycin) in resistant P388 mouse leukemia cells. *Eur. J. Cancer Clin. Oncol.* **1984,** *20* (6), 799-806.

37. Tsuruo, T.; Iida, H.; Tsukagoshi, S.; Sakurai, Y., Increased accumulation of vincristine and adriamycin in drug-resistant P388 tumor cells following incubation with calcium antagonists and calmodulin inhibitors. *Cancer Res.* **1982,** *42* (11), 4730-3.

38. Pirker, R.; FitzGerald, D. J. P.; Raschack, M.; Frank, Z.; Willingham, M. C.; Pastan, I., Enhancement of the activity of immunotoxins by analogs of verapamil. *Cancer Res.* **1989,** *49* (17), 4791-5.

39. Twentyman, P. R.; Bleehen, N. M., Resistance modification by PSC-833, a novel non-immunosuppressive cyclosporin A. *Eur. J. Cancer* **1991,** *27* (12), 1639-42.

40. Germann, U. A.; Ford, P. J.; Shlyakhter, D.; Mason, V. S.; Harding, M. W., Chemosensitization and drug accumulation effects of VX-710, verapamil, cyclosporin A, MS-209 and GF120918 in multidrug resistant HL60/ADR cells expressing the multidrug resistance-associated protein MRP. *Anti-Cancer Drugs* **1997,** *8* (2), 141-155.

41. Germann, U. A.; Shlyakhter, D.; Mason, V. S.; Zelle, R. E.; Duffy, J. P.; Galullo, V.; Armistead, D. M.; Saunders, J. O.; Boger, J.; Harding, M. W., Cellular and biochemical characterization of VX-710 as a chemosensitizer: reversal of P-glycoprotein-mediated multidrug resistance in vitro. *Anti-Cancer Drugs* **1997,** *8* (2), 125-140.

42. Hofmann, J.; Wolf, A.; Spitaler, M.; Boeck, G.; Drach, J.; Ludescher, C.; Grunicke, H., Reversal of multidrug resistance by B859-35, a metabolite of B859-35, niguldipine, verapamil and nitrendipine. *J. Cancer Res. Clin. Oncol.* **1992,** *118* (5), 361-6.

43. Krishna, R.; Mayer, L. D., Multidrug resistance (MDR) in cancer. Mechanisms, reversal using modulators of MDR and the role of MDR modulators in influencing the pharmacokinetics of anticancer drugs. *Eur. J. Pharm. Sci.* **2000,** *11* (4), 265-283.

44. Thomas, H.; Coley Helen, M., Overcoming multidrug resistance in cancer: an update on the clinical strategy of inhibiting p-glycoprotein. *Cancer Control* **2003,** *10* (2), 159-65.

45. Yde Christina, W.; Clausen Mathias, P.; Bennetzen Martin, V.; Lykkesfeldt Anne, E.; Mouritsen Ole, G.; Guerra, B., The antipsychotic drug chlorpromazine enhances the cytotoxic effect of tamoxifen in tamoxifen-sensitive and tamoxifen-resistant human breast cancer cells. *Anticancer Drugs* **2009,** *20* (8), 723-35.

46. Wesolowska, O.; Paprocka, M.; Kozlak, J.; Motohashi, N.; Dus, D.; Michalak, K., Human sarcoma cell lines MES-SA and MES-SA/Dx5 as a model for multidrug resistance modulators screening. *Anticancer Res.* **2005,** *25* (1A), 383-389.

47. Mammen, M.; Chio, S.-K.; Whitesides, G. M., Polyvalent interactions in biological systems: implications for design and use of multivalent ligands and inhibitors. *Angew. Chem., Int. Ed.* **1998,** *37* (20), 2755-2794.

48. Sauna, Z. E.; Andrus, M. B.; Turner, T. M.; Ambudkar, S. V., Biochemical basis of polyvalency as a strategy for enhancing the efficacy of P-glycoprotein (ABCB1) modulators: stipiamide homodimers separated with defined-length spacers reverse drug efflux with greater efficacy. *Biochemistry* **2004,** *43* (8), 2262-2271.

49. Pires, M. M.; Hrycyna, C. A.; Chmielewski, J., Bivalent probes of the human multidrug transporter P-glycoprotein. *Biochemistry* **2006,** *45* (38), 11695-11702.

50. Namanja, H. A.; Emmert, D.; Pires, M. M.; Hrycyna, C. A.; Chmielewski, J., Inhibition of human P-glycoprotein transport and substrate binding using a galantamine dimer. *Biochem. Biophys. Res. Commun.* **2009,** *388* (4), 672-676.

51. Namanja, H. A.; Emmert, D.; Davis, D. A.; Campos, C.; Miller, D. S.; Hrycyna, C. A.; Chmielewski, J., Toward Eradicating HIV Reservoirs in the Brain: Inhibiting P-glycoprotein at the blood-brain barrier with prodrug abacavir dimers. *J. Am. Chem. Soc.* **2012,** *134* (6), 2976-2980.

52. Namanja, H. A.; Emmert, D.; Hrycyna, C. A.; Chmielewski, J., Homodimers of the antiviral abacavir as modulators of P-glycoprotein transport in cell culture: probing tether length. *MedChemComm* **2013,** *4* (10), 1344-1349.

53. Emmert, D.; Campos, C. R.; Ward, D.; Lu, P.; Namanja, H. A.; Bohn, K.; Miller, D. S.; Sharom, F. J.; Chmielewski, J.; Hrycyna, C. A., Reversible dimers of the atypical antipsychotic quetiapine inhibit P-glycoprotein-mediated efflux in vitro with increased binding affinity and in situ at the blood-brain barrier. *ACS Chem. Neurosci.* **2014,** *5* (4), 305-317.

54. Hrycyna, C. A.; Summers, R. L.; Lehane, A. M.; Pires, M. M.; Namanja, H.; Bohn, K.; Kuriakose, J.; Ferdig, M.; Henrich, P. P.; Fidock, D. A.; Kirk, K.; Chmielewski, J.; Martin, R. E., Quinine dimers are potent inhibitors of the Plasmodium falciparum chloroquine resistance transporter and are active against quinoline-resistant P. falciparum. *ACS Chem. Biol.* **2014,** *9* (3), 722-730.

55. Bohn, K.; Lange, A.; Chmielewski, J.; Hrycyna, C. A., Dual modulation of human P-glycoprotein and ABCG2 with prodrug dimers of the atypical antipsychotic agent paliperidone in a model of the blood-brain barrier. *Mol. Pharmaceutics* **2017,** *14* (4), 1107-1119.

56. Agrawal, N.; Rowe, J.; Lan, J.; Yu, Q.; Hrycyna, C. A.; Chmielewski, J., Potential tools for eradicating HIV reservoirs in the brain: development of trojan horse prodrugs for the inhibition of P-glycoprotein with anti-HIV-1 activity. *J. Med. Chem.* **2019**, DOI: 10.1021/acs.jmedchem.9b00779.

57. Pires, M. M.; Emmert, D.; Hrycyna, C. A.; Chmielewski, J., Inhibition of P-glycoprotein-mediated paclitaxel resistance by reversibly linked quinine homodimers. *Mol. Pharmacol.* **2009,** *75* (1), 92-100.

58. Kuriakose, J.; Hrycyna, C. A.; Chmielewski, J., Click chemistry-derived bivalent quinine inhibitors of P-glycoprotein-mediated cellular efflux. *Bioorg. Med. Chem. Lett.* **2012,** *22* (13), 4410-4412.

59. Namanja-Magliano, H. A.; Bohn, K.; Agrawal, N.; Willoughby, M. E.; Hrycyna, C. A.; Chmielewski, J., Dual inhibitors of the human blood-brain barrier drug efflux transporters P-glycoprotein and ABCG2 based on the antiviral azidothymidine. *Bioorg. Med. Chem.* **2017,** *25* (19), 5128-5132.

60. Chan, K.-F.; Zhao, Y.; Burkett, B. A.; Wong, I. L. K.; Chow, L. M. C.; Chan, T. H., Flavonoid dimers as bivalent modulators for P-glycoprotein-based multidrug resistance: synthetic apigenin homodimers linked with defined-length poly(ethylene glycol) spacers increase drug retention and enhance chemosensitivity in resistant cancer cells. *J. Med. Chem.* **2006,** *49* (23), 6742-6759.

61. Wong, I. L. K.; Chan, K.-F.; Burkett, B. A.; Zhao, Y.; Chai, Y.; Sun, H.; Chan, T. H.; Chow, L. M. C., Flavonoid dimers as bivalent modulators for pentamidine and sodium stibogluconate resistance in Leishmania. *Antimicrob. Agents Chemother.* **2007,** *51* (3), 930-940.

62. Chan, K.-F.; Zhao, Y.; Chow, T. W. S.; Yan, C. S. W.; Ma, D. L.; Burkett, B. A.; Wong, I. L. K.; Chow, L. M. C.; Chan, T. H., Flavonoid dimers as bivalent modulators for P-glycoprotein-based multidrug resistance: structure-activity relationships. *ChemMedChem* **2009,** *4* (4), 594-614.

63. Chan, K.-F.; Wong, I. L. K.; Kan, J. W. Y.; Yan, C. S. W.; Chow, L. M. C.; Chan, T. H., Amine linked flavonoid dimers as modulators for P-glycoprotein-based multidrug resistance: structure-activity relationship and mechanism of modulation. *J. Med. Chem.* **2012,** *55* (5), 1999-2014.

64. Wong, I. L. K.; Chan, K.-F.; Chan, T. H.; Chow, L. M. C., Flavonoid dimers as novel, potent antileishmanial Agents. *J. Med. Chem.* **2012,** *55* (20), 8891-8902.

65. Dury, L.; Nasr, R.; Lorendeau, D.; Comsa, E.; Wong, I.; Zhu, X.; Chan, K.-F.; Chan, T.-H.; Chow, L.; Falson, P.; Di Pietro, A.; Baubichon-Cortay, H., Flavonoid dimers are highly potent killers of multidrug resistant cancer cells overexpressing MRP1. *Biochem. Pharmacol.* **2017,** *124*, 10-18.

66. Wong, I. L. K.; Zhu, X.; Chan, K.-F.; Law, M. C.; Lo, A. M. Y.; Hu, X.; Chow, L. M. C.; Chan, T. H., Discovery of novel flavonoid dimers to reverse multidrug resistance protein 1 (MRP1, ABCC1) mediated drug resistance in cancers using a high throughput platform with "click chemistry". *J. Med. Chem.* **2018,** *61* (22), 9931-9951.

67. Zhu, X.; Wong, I. L. K.; Chan, K.-F.; Cui, J.; Law, M. C.; Chong, T. C.; Hu, X.; Chow, L. M. C.; Chan, T. H., Triazole bridged flavonoid dimers as potent, nontoxic, and highly selective breast cancer resistance protein (BCRP/ABCG2) inhibitors. *J. Med. Chem.* **2019,** *62* (18), 8578-8608.

68. Fang, Y.; Xia, M.; Liang, F.; Cao, W.; Pan, S.; Xu, X., Establishment and use of human mouth epidermal carcinoma (KB) cells overexpressing P-glycoprotein to characterize structure requirements for flavonoids transported by the efflux transporter. *J. Agric. Food Chem.* **2019,** *67* (8), 2350-2360.

69. Hadjeri, M.; Barbier, M.; Ronot, X.; Mariotte, A.-M.; Boumendjel, A.; Boutonnat, J., Modulation of P-glycoprotein-mediated multidrug resistance by flavonoid derivatives and analogues. *J. Med. Chem.* **2003,** *46* (11), 2125-2131.

70. Ma, Z.; LeBard, D. N.; Loverde, S. M.; Sharp, K. A.; Klein, M. L.; Discher, D. E.; Finkel, T. H., TCR triggering by pMHC ligands tethered on surfaces via poly(ethylene glycol) depends on polymer length. *PLoS One* **2014,** *9* (11), e112292/1-e112292/10, 10 pp.

71. Pussard, E.; Merzouk, M.; Barennes, H., Increased uptake of quinine into the brain by inhibition of P-glycoprotein. *Eur. J. Pharm. Sci.* **2007,** *32* (2), 123-127.

72. Boulton, D. W.; DeVane, C. L.; Liston, H. L.; Markowitz, J. S., In vitro P-glycoprotein affinity for atypical and conventional antipsychotics. *Life Sci.* **2002,** *71* (2), 163-169.

73. Schmitt, U.; Kirschbaum, K. M.; Poller, B.; Kusch-Poddar, M.; Drewe, J.; Hiemke, C.; Gutmann, H., In vitro P-glycoprotein efflux inhibition by atypical antipsychotics is in vivo nicely reflected by pharmacodynamic but less by pharmacokinetic changes. *Pharmacol., Biochem. Behav.* **2012,** *102* (2), 312-320.

74. Feng, B.; Mills Jessica, B.; Davidson Ralph, E.; Mireles Rouchelle, J.; Janiszewski John, S.; Troutman Matthew, D.; de Morais Sonia, M., In vitro P-glycoprotein assays to predict the in vivo interactions of P-glycoprotein with drugs in the central nervous system. *Drug Metab Dispos* **2008,** *36* (2), 268-75.

75. Doran, A.; Obach, R. S.; Smith, B. J.; Hosea, N. A.; Becker, S.; Callegari, E.; Chen, C.; Chen, X.; Choo, E.; Cianfrogna, J.; Cox, L. M.; Gibbs, J. P.; Gibbs, M. A.; Hatch, H.; Hop, C. E. C. A.; Kasman, I. N.; LaPerle, J.; Liu, J.; Liu, X.; Logman, M.; Maclin, D.; Nedza, F. M.; Nelson, F.; Olson, E.; Rahematpura, S.; Raunig, D.; Rogers, S.; Schmidt, K.; Spracklin, D. K.; Szewc, M.; Troutman, M.; Tseng, E.; Tu, M.; Van Deusen, J. W.; Venkatakrishnan, K.; Walens, G.; Wang, E. Q.; Wong, D.; Yasgar, A. S.; Zhang, C., The impact of P-glycoprotein on the disposition of drugs targeted for indications of the central nervous system: Evaluation using the MDR1A/1B knockout mouse model. *Drug Metab. Dispos.* **2005,** *33* (1), 165-174.

76. Wang, J.-S.; Ruan, Y.; Taylor, R. M.; Donovan, J. L.; Markowitz, J. S.; DeVane, C. L., The brain entry of risperidone and 9-hydroxyrisperidone is greatly limited by P-glycoprotein. *Int. J. Neuropsychopharmacol.* **2004,** *7* (4), 415-419.

77. Weksler, B. B.; Subileau, E. A.; Perriere, N.; Charneau, P.; Holloway, K.; Leveque, M.; Tricoire-Leignel, H.; Nicotra, A.; Bourdoulous, S.; Turowski, P.; Male, D. K.; Roux, F.; Greenwood, J.; Romero, I. A.; Couraud, P. O., Blood-brain barrier-specific properties of a human adult brain endothelial cell line. *Faseb J.* **2005,** *19* (13), 1872-1874, 10 1096/fj 04-3458fje.

78. Ejendal, K. F. K.; Hrycyna, C. A., Differential sensitivities of the human ATP-binding cassette transporters ABCG2 and P-glycoprotein to cyclosporin A. *Mol. Pharmacol.* **2005,** *67* (3), 902-911.

79. Autran, B.; Carcelain, G.; Li, T. S.; Blanc, C.; Mathez, D.; Tubiana, R.; Katlama, C.; Debre, P.; Leibowitch, J., Positive effects of combined antiretroviral therapy on CD4+ T cell homeostasis and function in advanced HIV disease. *Science* **1997,** *277* (5322), 112-116.

80. Nath, A., Eradication of human immunodeficiency virus from brain reservoirs. *J. NeuroVirol.* **2015,** *21* (3), 227-234.

81. Lambotte, O.; Deiva, K.; Tardieu, M., HIV-1 persistence, viral reservoir, and the central nervous system in the HAART era. *Brain Pathol* **2003,** *13* (1), 95-103.

82. Pierson, T.; McArthur, J.; Siliciano, R. F., Reservoirs for HIV-1: Mechanisms for viral persistence in the presence of antiviral immune responses and antiretroviral therapy. *Annu. Rev. Immunol.* **2000,** *18*, 665-708.

83. Thomas, S. A., Anti-HIV drug distribution to the central nervous system. *Curr. Pharm. Des.* **2004,** *10* (12), 1313-1324.

84. Varatharajan, L.; Thomas, S. A., The transport of anti-HIV drugs across blood-CNS interfaces: summary of current knowledge and recommendations for further research. *Antiviral Res.* **2009,** *82* (2), A99-A109.

85. Kandanearatchi, A.; Williams, B.; Everall, I. P., Assessing the efficacy of highly active antiretroviral therapy in the brain. *Brain Pathol.* **2003,** *13* (1), 104-110.

86. Shaik, N.; Giri, N.; Pan, G.; Elmquist, W. F., P-glycoprotein-mediated active efflux of the anti-HIV1 nucleoside abacavir limits cellular accumulation and brain distribution. *Drug Metab. Dispos.* **2007,** *35* (11), 2076-2085.

87. de Souza, J.; Benet, L. Z.; Huang, Y.; Storpirtis, S., Comparison of bidirectional lamivudine and zidovudine transport using MDCK, MDCK-MDR1, and Caco-2 cell monolayers. *J. Pharm. Sci.* **2009,** *98* (11), 4413-4419.

88. Lee, C. G. L.; Gottesman, M. M.; Cardarelli, C. O.; Ramachandra, M.; Jeang, K.-T.; Ambudkar, S. V.; Pastan, I.; Dey, S., HIV-1 protease inhibitors are substrates for the MDR1 multidrug transporter. *Biochemistry* **1998,** *37* (11), 3594-3601.

89. Bousquet, L.; Roucairol, C.; Hembury, A.; Nevers, M.-C.; Creminon, C.; Farinotti, R.; Mabondzo, A., Comparison of ABC transporter modulation by atazanavir in lymphocytes and human brain endothelial cells: ABC transporters are involved in the atazanavir-limited passage across an in vitro human model of the blood-brain barrier. *AIDS Res. Hum. Retroviruses* **2008,** *24* (9), 1147-1154.

90. Fujimoto, H.; Higuchi, M.; Watanabe, H.; Koh, Y.; Ghosh, A. K.; Mitsuya, H.; Tanoue, N.; Hamada, A.; Saito, H., P-glycoprotein mediates efflux transport of darunavir in human intestinal Caco-2 and ABCB1 gene-transfected renal LLC-PK1 cell lines. *Biol. Pharm. Bull.* **2009,** *32* (9), 1588-1593.

91. Gimenez, F.; Fernandez, C.; Mabondzo, A., Transport of HIV protease inhibitors through the blood-brain barrier and interactions with the efflux proteins, P-glycoprotein and multidrug resistance proteins. *JAIDS, J. Acquired Immune Defic. Syndr.* **2004,** *36* (2), 649-658.

92. Hashiguchi, Y.; Hamada, A.; Shinohara, T.; Tsuchiya, K.; Jono, H.; Saito, H., Role of P-glycoprotein in the efflux of raltegravir from human intestinal cells and CD4+ T-cells as an interaction target for anti-HIV agents. *Biochem. Biophys. Res. Commun.* **2013,** *439* (2), 221-227.

93. Ivey Nathan, S.; MacLean Andrew, G.; Lackner Andrew, A., Acquired immunodeficiency syndrome and the blood-brain barrier. *J Neurovirol* **2009,** *15* (2), 111-22.

94. Lee, C. G. L.; Pastan, I.; Gottesman, M. M., Retroviral transfer of human MDR1 gene into human T lymphocytes. *Methods Enzymol.* **1998,** *292* (ABC Transporters: Biochemical, Cellular, and Molecular Aspects), 557-572.

CHAPTER 2. DEVELOPMENT OF A TROJAN HORSE PRODRUG, ABACAVIR-S_2-DARUNAVIR-8, FOR THE INHIBTION OF P-GLYCOPROTEIN WITH ANTI-HIV-1 ACTIVITY

2.1 Introduction

HIV treatment has progressed substantially since the first documented case, with combination antiretroviral therapies (cART) successfully reducing plasma viral levels below the detectable limit.[1] Although cART has been a significant advancement in HIV treatment, HIV has not been eradicated due, in part, to viral reservoirs.[2-3] These viral reservoirs exist in a number of cellular and anatomical locations, including the central nervous system (CNS), macrophages and lymphocytes. Viral accumulation in the brain, for instance, has been proposed to mainly proceed through paracellular or transcellular diapedesis.[4] While HIV is able to enter the brain through these mechanisms, numerous cART treatments do not accumulate well in the brain due to the physiochemical properties of the drugs, the presence of tight junctions, and the high concentration of efflux transporters at the blood brain barrier (BBB).[5-7] One of the well studied efflux transporter, P-glycoprotein (P-gp), resides in the apical membrane of brain capillary endothelial cells where it is known to efflux many therapies.[8-9]

P-gp has many substrates, including various cART drugs targeting HIV-1 protease (PR), reverse transcriptase (RT), and integrase (IN). *In vitro* and *in vivo* experiments confirm that RT inhibitor drugs, such as abacavir and didanosine, PR inhibitors, such as nelfinavir and darunavir, and IN inhibitor drugs, such as raltegravir, for instance, are P-gp substrates.[6,10-16] Notably, in P-gp null mice studies, abacavir and nelfinavir accumulated in the brain at increased levels as compared to wild-type mice (20-fold and 36-fold, respectively).[10,17] Further, chemical inhibition of P-gp efflux with a known inhibitor, LY-335979, was shown to increase the brain accumulation of four different PR inhibitors (PI) *in-vitro* and *in-vivo*.[18] Such studies strongly support the hypothesis that P-gp efflux limits the accumulation of cART drugs in the brain, leaving viral replication unchecked.

An x-ray structure of P-gp has shown a large binding site region that can accommodate the binding of two cyclic peptides.[19-20] To block P-gp efflux, we wished to take advantage of this multiplicity of binding sites within the transmembrane domain of P-gp.[19-26] In this way, we envisioned that taking two antiviral agents that are substrates of P-gp and combining them into the

same molecule with a linker would allow the heterodimeric compounds to occupy the multiple binding sites within P-gp. This process would turn two substrates into one inhibitor. Dimerizing a P-gp substrate has been demonstrated to be an effective means to inhibit P-gp efflux in cells and *in situ* at the BBB.[27-36] Using this concept for antiviral substrates, reversibly linked homodimeric prodrugs of abacavir demonstrated potent P-gp inhibition with cellular anti-HIV-1 activity.[32] This proof of concept study paved the way for the current Trojan horse (TH) design (Figure 2.1), a reversible combination therapy in one molecule that also may act as a P-gp inhibitor to improve cell accumulation. Specifically, agents were designed as a cART prodrug containing the RT inhibitor (RTI) abacavir (Aba) and the protease inhibitor (PI) darunavir (DRV), linked via a disulfide-containing tether. Such compounds were designed to inhibit P-gp efflux and, in the reducing environment of an HIV infected cell, release two monomeric therapies within the cell. Herein, we discuss the successful synthesis and application of a cART heterodimer, Abacavir-S_2-Darunavir (Aba-S_2-DRV8), as a P-gp inhibitor and antiviral prodrug.

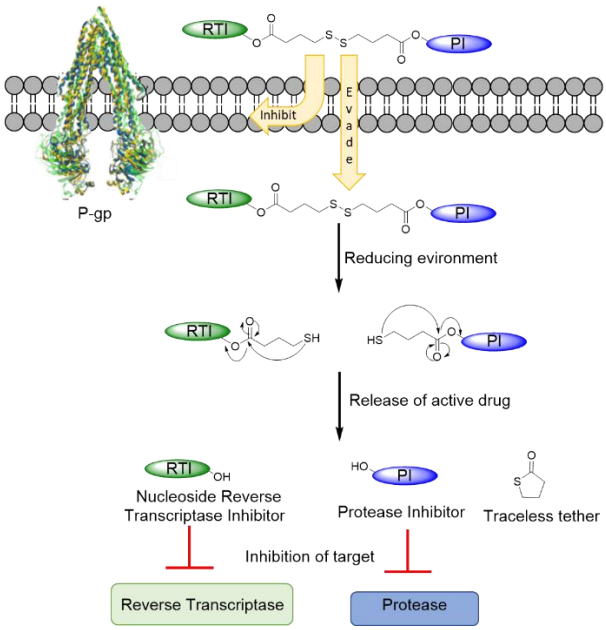

Figure 2.1 Design of Trojan horse (TH) prodrugs containing a reverse transcriptase inhibitor (RTI), abacavir (Aba), a protease inhibitor (PI), darunavir (DRV), and a disulfide-containing tether.

2.2 Results and Discussion

2.2.1 Design

The TH combination cART prodrug was designed to provide two functions (1) inhibit P-gp efflux in brain endothelial cells and T-cells and (2) in the reducing environment of cells, release the monomeric therapies for interaction with target enzymes (Figure 2.1). This was accomplished by conjugating two classes of known FDA approved HIV-1 drugs, a RTI (Aba) and PI (DRV) connected by ester linkages via a disulfide-containing tether. This tether contains a central disulfide moiety that is reduced in the reducing environment of the cell. The thiols that are generated can then rearrange to release the monomeric drugs of interest within the cell. Thus, the design creates a TH heterodimer that may be useful tools in the treatment of cellular and anatomical reservoirs of HIV-1.

2.2.2 Synthesis and characterization of TH dimer Aba-S_2-DRV

The TH heterodimer was synthesized over two steps. The presence of an alcohol functional group within Aba and DRV (C8) allowed us to introduce ester linkages to generate Aba-S_2-DRV analogs (Scheme 2.1).

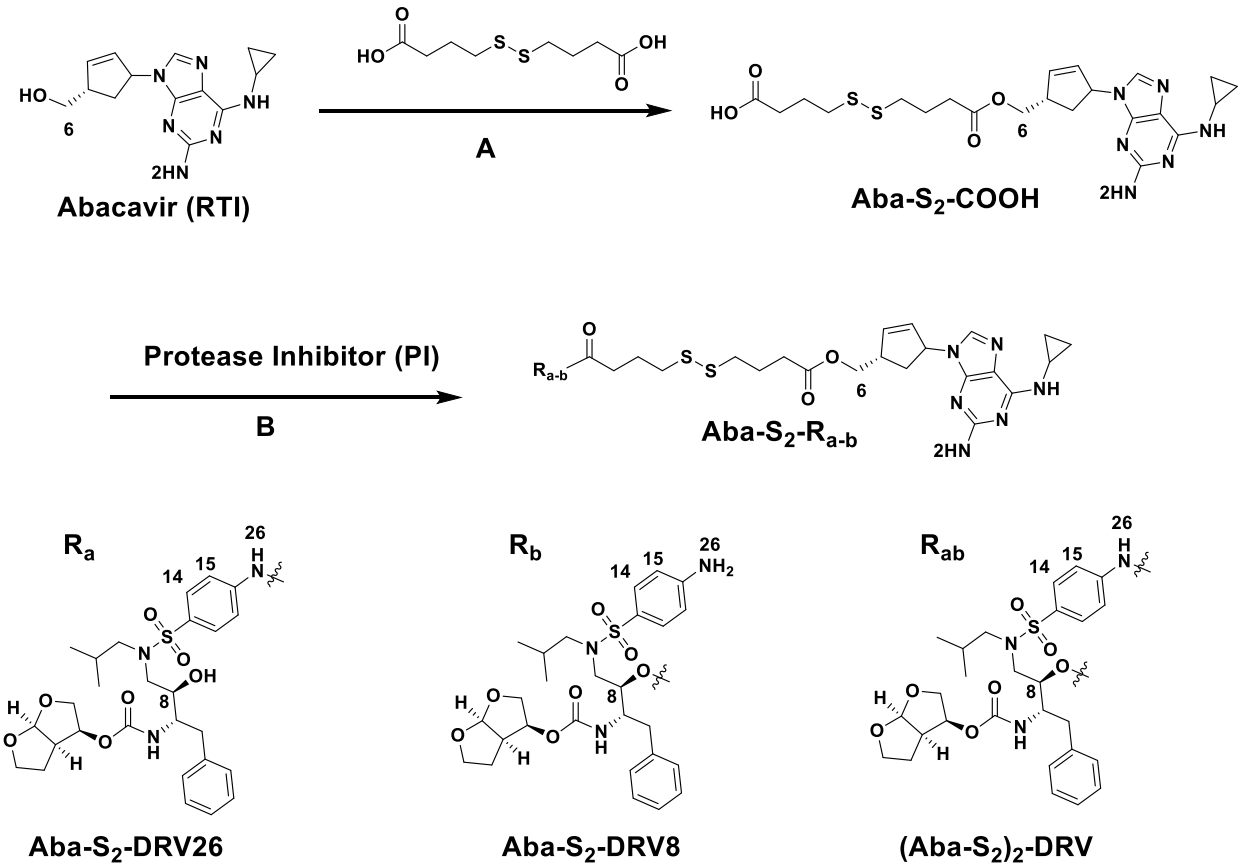

Scheme 2.1 Synthesis of Aba-S_2-DRV analogs A) PyBOP, DMAP, DIEA, DMF, RT 24 hr, 70% yield; B) EDC, DMAP, DIEA, CH_2Cl_2, 4 Å molecular sieves, 0 ^{o}C for 2 h, RT for 48 h; Aba-S2-DRV8, 27% yield; (Aba-S_2)$_2$-DRV, 21% yield. Atom numbering used for NMR analysis of Aba-S_2-COOH and darunavir derivatives.

In the first step of the synthesis of the heterodimer, Aba was treated with PyBOP-activated 4,4′-dithiodibutyric acid in the presence of DMAP and DIEA to produce Aba-S_2-COOH (Scheme 2.1) in 70% yield after purification by reverse phase HPLC (RP-HPLC). The selective acylation of the primary alcohol in Aba was established based on the resonances corresponding to the H-6 proton and the C-6 carbon of Aba-S_2-COOH, that were shifted downfield from the corresponding proton H-6 and carbon C-6 signals in Aba by 0.7 ppm (4.1 ppm from 3.4 ppm) and 2.7 ppm (66.9 ppm from 64.2 ppm), respectively (Figures A12 and A13).

The acylation of DRV with Aba-S_2-COOH was accomplished using the PI and Aba-S_2-COOH in the presence of EDC/DMAP (Scheme 2.1). DRV has two possible conjugation locations, the secondary alcohol on C8 (Aba-S-DRV8) or the aniline N26, with the possible acylation at both

sites ((Aba-S_2)$_2$-DRV). Upon RP-HPLC separation of the reaction mixture, Aba-S_2-DRV8 was obtained in 27% yield with the diacylated product ((Aba-S_2)$_2$-DRV) in 21% yield. The structure of Aba-S_2-DRV8 was also elucidated by ^{1}H and ^{13}C NMR spectroscopy using COSY, TOCSY and HMQC NMR. The acylation of the secondary alcohol of darunavir in Aba-S_2-DRV8 was confirmed by the observed deshielding of the proton H-8 by 1.5 ppm, as compared to the parent darunavir (Figure 2.2). The formation of the secondary ester was further confirmed by ^{13}C NMR with the deshielding of the C-8 signal by 2.3 ppm in Aba-S_2-DRV8 as compared to DRV (Figure 2.3). Furthermore, ^{1}H and ^{13}C NMR resonances in the vicinity of the aniline nitrogen (H-14/C-14 and H-15/C-15) showed no significant change in Aba-S_2-DRV8 as compared to DRV (Figure 2.4). These NMR data taken together confirmed that acylation proceeded on the secondary alcohol of darunavir. (Data for diacylated darunavir not shown). In all, this synthetic method allowed the preparation of the TH heterodimer, Aba-S_2-DRV8, for biological analysis.

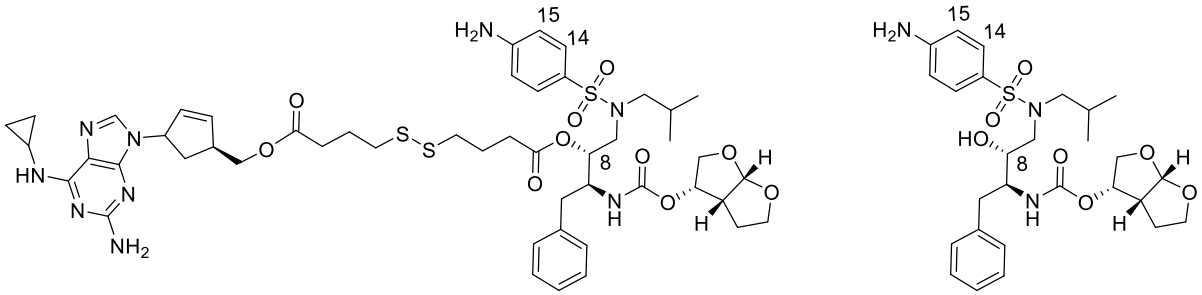

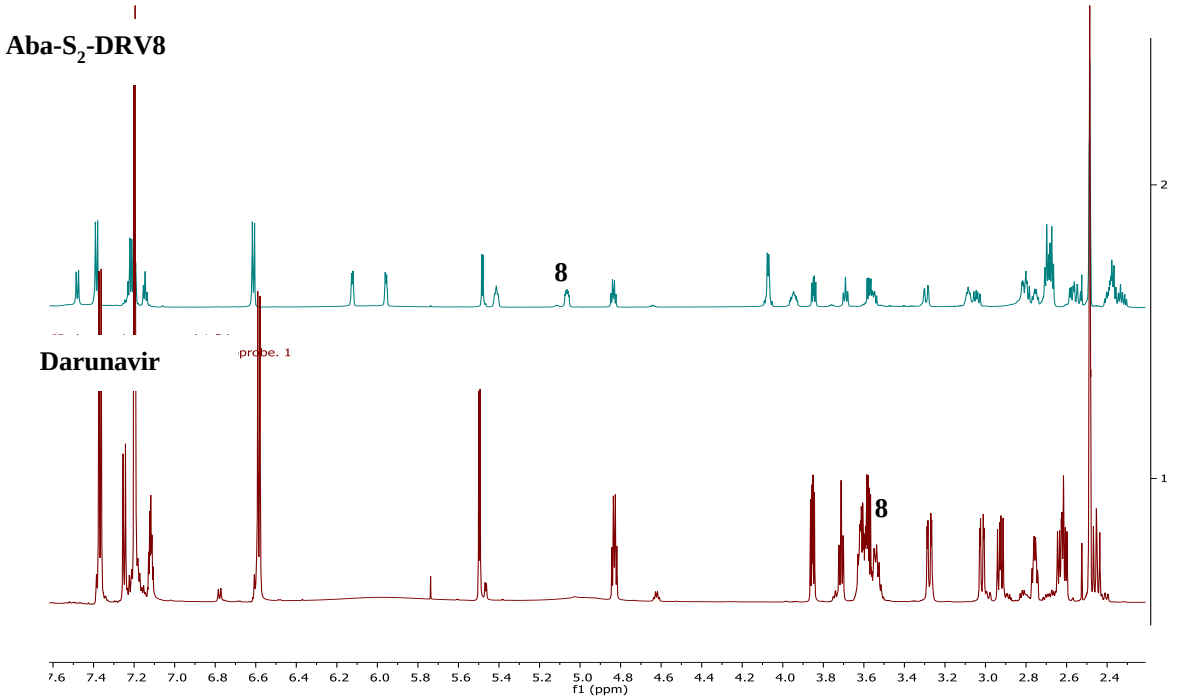

Figure 2.2 Comparison of ^{1}H NMR from Aba-S_2-DRV8 as compared to ^{1}H from parent darunavir. Proton 8 corresponds with the proton on the methine of the secondary hydroxyl. Note the downfield shift from the parent darunavir.

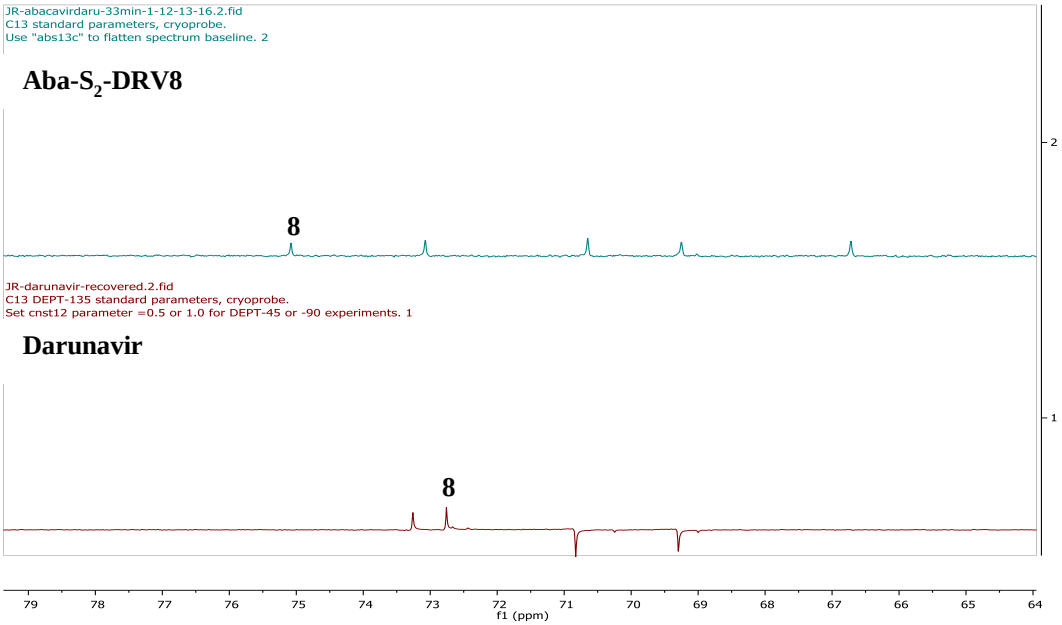

Figure 2.3 Comparison of ^{13}C from Aba-S_2-DRV8 as compared to ^{13}C-DEPT from parent darunavir. Carbon 8 corresponds with the methine of the secondary hydroxyl. Note the downfield shift from the parent darunavir.

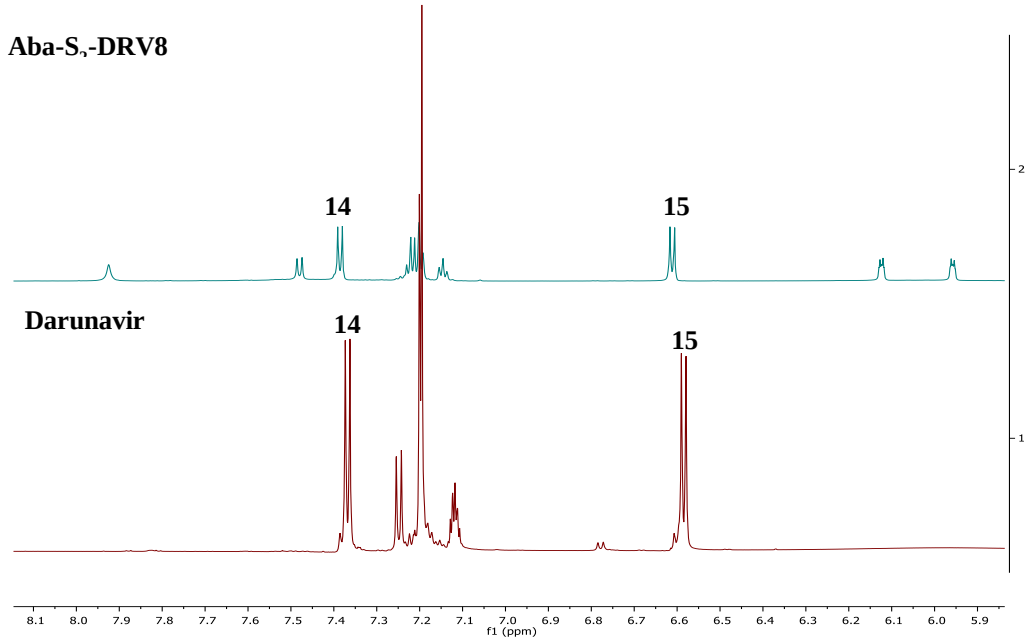

Figure 2.4 Comparison of ^{1}H from Aba-S_2-DRV8 as compared to ^{1}H from parent darunavir. Protons 14 and 15 corresponds the doublets in the para-aniline in darunavir adjacent. Note there is no shift from the parent darunavir.

2.2.3 Inhibition of P-gp efflux with Aba-S_2-DRV8.

One of the goals of the designed TH heterodimer is to inhibit P-gp-mediated efflux. A substrate accumulation assay was used to evaluate the potency of Aba-S_2-DRV8 as a P-gp inhibitor using the P-gp substrates calcein-AM and NBD-Aba.[38-39] Two cell lines were used to monitor the accumulation of these fluorescent P-gp substrates: 12D7-MDR cells which are CD4+ T lymphocytes with overexpression of P-gp,[40] and hCMEC/D3 cells as an *in vitro* BBB model cell line.[41] hCMEC/D3 cells are an immortalized human brain capillary endothelial cell line that expresses endogenous levels of P-gp.[42-43] Inhibition of P-gp efflux was measured by monitoring the increase in cellular fluorescence with added heterodimer by flow cytometry. While the dimeric prodrugs have limited water solubility, they were fully soluble in 1% DMSO up to 100 μM, Therefore, the cell-based P-gp experiments used 1% DMSO with no observed cytotoxicity.

With the 12D7-MDR and hCMEC/D3 cell lines, Aba-S_2-DRV8 demonstrated dose-dependent, potent inhibition of P-gp efflux of calcein-AM and NBD-Aba with sub-micromolar IC_{50} values (Table 1). Interestingly, the IC_{50} values obtained with the hCMEC/D3 cells are lower than 12D7-MDR cells, likely due to the lower expression of P-gp in the brain capillary endothelial cells. Analogous experiments were performed with monomeric DRV using the fluorescent substrates. A striking 66- to 118-fold increase in inhibition of P-gp was found for Aba-S_2-DRV8 with respect to DRV alone (Table 1). Abacavir has been shown to minimally inhibit (<10%) P-gp in 12D7-MDR in cells up to 500 μM in these assays, whereas the known P-gp inhibitor verapamil had an IC_{50} value of 1.2 ± 0.4 μM in 12D7-MDR cells with the calcein-AM substrate.[32] These data substantiate that the TH heterodimer is an inhibitor of P-gp efflux in both T-cells and in a BBB cell model. Together, these IC_{50} data confirm that the dimerization of two antivirals that are P-gp substrates – Aba and DRV– into one molecule successfully led to the generation of a potent P-gp inhibitor.

Table 2.1 Inhibition of P-gp mediated efflux of calcein-AM and NBD-Aba in 12D7-MDR and hCMEC/D3 cells[a]

	IC_{50} (μM)			
	12D7-MDR cells		hCMEC/D3 cells	
Compound	calcein-AM	NBD-Aba	calcein-AM	NBD-Aba
DRV	33.2 ± 6.5	60 ± 9.4	6.6 ± 1.9	15.4 ± 3.2
Aba-S_2-DRV8	0.50 ± 0.04	0.51 ± 0.08	0.08 ± 0.02	0.09 ± 0.02

[a] Cells were treated with calcein-AM (0.25 μM) or NBD-Aba (5 μM) with different concentrations of compound. The accumulated fluorescence was analyzed using flow cytometery.

An MTT assay was used to determine the cell toxicity of Aba-S_2-DRV8 in the 12D7-MDR cell line after 24 hours (Figure 2.5).[44] In this assay, Aba-S-DRV8 maintained 70% cell viability at 10 μM, which is 20 times its IC_{50} for inhibition of P-gp. These data suggest that the TH heterodimer is minimally cytotoxic to 12D7-MDR cells at bioactive concentrations and can be used for further biological assays without detrimental effect on cell growth.

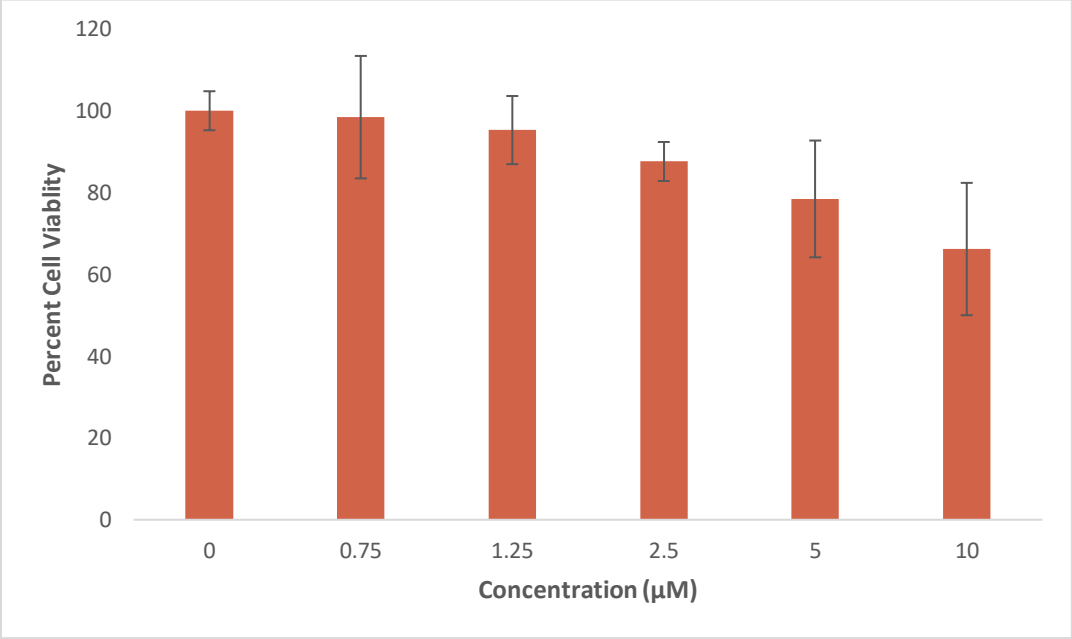

Figure 2.5 Cell viability of Aba-S_2-DRV8 in the presence of 12D7-MDR cells.

2.2.4 Probing the reversion of the TH heterodimer into monomers in a reducing environment.

In a reducing environment the disulfide bonds within the TH heterodimer would yield 2 thiols (Figure 1a) that may rearrange to produce monomeric drugs (Aba and DRV). The breakdown of the TH heterodimer with DTT and glutathione (GSH), and the release of monomers was monitored using UPLC-MS at various timepoints. The reduction of the heterodimer to free thiols occurs rapidly, with full reduction observed within 1 hour. Upon appearance of free thiols, the subsequent rearrangement led to the generation of the component monomeric drugs. Aba regeneration from the TH heterodimer (Aba-S_2-DRV8) displayed a half-life ($t_{1/2}$) of 34.5 ± 1.5 hours with DTT, and 21.6 ± 2 hours with GSH. DRV was regenerated with a $t_{1/2}$ of 21.3 ± 0.8 hours with DTT and 36.3 ± 4 hours with GSH, respectively (Figures 2.6 and 2.7).

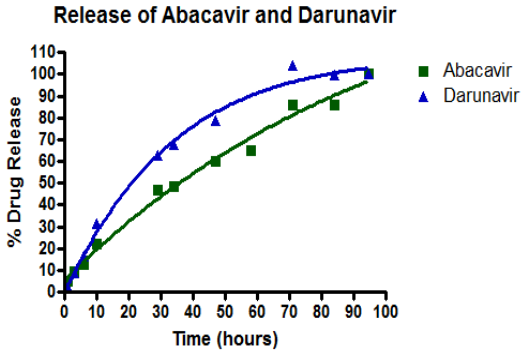

Figure 2.6 Abacavir and DRV regeneration with DTT treatment (250 mM) in PBS (pH 7.4).

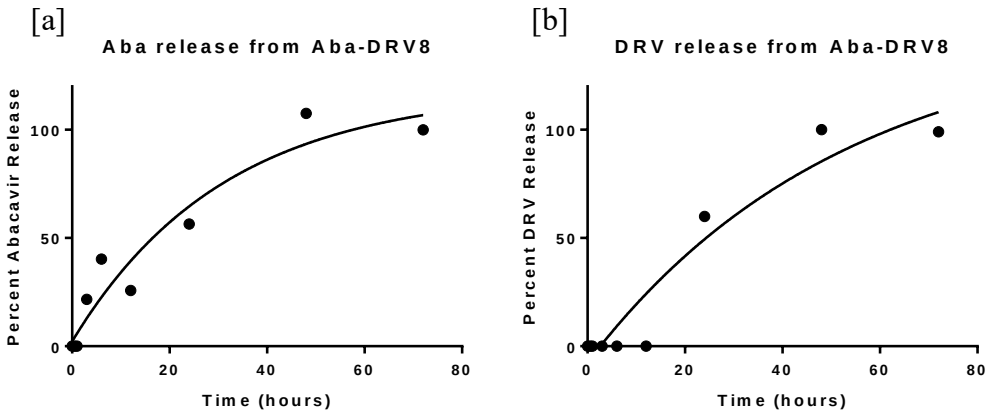

Figure 2.7 (a) Abacavir and (b) DRV regeneration with glutathione treatment (10 mM) in PBS (pH 7.4).

2.2.5 The anti-HIV-1 potency of the TH heterodimer as compared to its monomers, alone and combined.

To investigate if Aba-S_2-DRV8 is effective against HIV-1 in cells, an *in vitro* HIV-1 titer assay was performed using the 12D7 cell line. 12D7 cells were infected with HIV-1_{LAI} and anti-HIV-1 activity was measured by monitoring p24 protein levels as previously described.[45-46] First the stability of the prodrugs was monitored in PBS and cell culture media using UPLC-MS. Aba-S_2-DRV8 was greater than 95% intact after 3 days under both conditions, but with 20% decomposition observed after day 4. Therefore, for the cell-based anti-HIV-1 experiments, the media, with drugs, was changed every 3 days. The anti-HIV-1 activity of different concentrations of monomeric drugs alone (Aba or DRV), a 1:1 combination of Aba and DRV, or the TH heterodimer was determined after 6 days. All drugs and drug combinations demonstrated a decrease in p24 levels as compared to the control, which corresponds to an increase in anti-HIV-1 activity. The PI used is known to be the superior antiviral as compared to the RTI Aba,[47] and this was also observed (Figure 2.8). Therefore, the antiretroviral activity of the 1:1 mix of Aba with DRV was dominated by the PI potency. Aba-S_2-DRV8 was less potent than the 1:1 mixture of Aba and DRV, but still displayed a concentration dependent decrease in p24 levels.

This demonstrated dose dependent decrease in the p24 levels of Aba-S_2-DRV8 further corroborates the overall goal of the study. In order for darunavir to display anti-HIV-1 activity, the secondary hydroxyl (8) must be unmodified. Aba-S_2-DRV8 is conjugated at darunavir's secondary hydroxyl (8), as previously discussed. Therefore, in the reducing environment of the cell, the prodrug was able to release its individual therapies (Aba and DRV) and induce anti-HIV-1 activity, as observed by the decrease in p24. The release of Aba and DRV from Aba-S_2-DRV takes some time, therefore, it is not surprising that the overall anti-HIV-1 activity is less than that of the 1:1 mixture of Aba and DRV. Overall, the Aba-S_2-DRV8 displayed a dose dependent decrease in p24 levels, which also suggests that Aba-S_2-DRV8 was able to release active monomer inside of a cell.

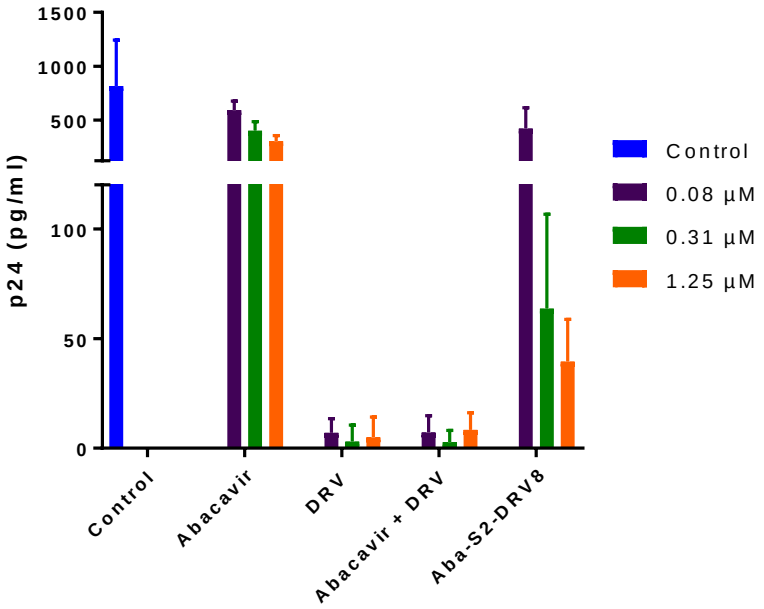

Figure 2.8 Anti-HIV-1 activity of individual RTI or PI antivirals, a 1:1 mixture of RTI and PI, and the TH heterodimer in HIV-1_{LAI} infected 12D7 cells. The plotted data is the average of HIV-1 p24 with the standard deviation derived from two independent experiments.

2.3 Conclusion

Herein, the successful synthesis and application of the TH heterodimer, Aba-S_2-DRV8, as a P-gp inhibitor and antiviral prodrug is discussed. The heterodimer was synthesized and the connectivity points within the monomers was fully characterized by NMR. The TH heterodimer is a potent P-gp inhibitor with activity in T-cells and endothelial cells from the BBB. The dimer was found to revert to their component monomers (Aba and DRV) in a reducing environment. The TH heterodimer displayed modest anti-HIV-1 activity in T cells.

2.4 Materials and Methods

2.4.1 Materials.

Abacavir and darunavir were provided by the NIH AIDS Reagent Program (Germantown, MD). 1-(3-Dimethylaminoproyl)-3-ethylcarbodiimide hydrochloride (EDC) was purchased fom AK Scientific (Union City, CA). 4,4′-Dithiodibutyric acid,N,N-dimethylpyridin-4-amine (DMAP) and N-ethyl-N-isopropylpropan-2-amine (DIEA) were purchased from Sigma-Aldrich (St. Louis,

MO).((1H-benzo[d][1,2,3]triazol-1-yl)oxy)tri(pyrrolidin-1-yl)phosphonium hexafluorophosphate (PyBOP) was bought from GenScript Corporation (Piscataway, NJ). DTT was purchased from Roche (Indianapolis, IN). hCMEC/D3 cells were donated from Institut National de la Sante et de la Recherche Medicale (INSERM, Paris, France). Rat tail collagen I was purchased from BD Biosciences (San Jose, CA). EBM-2 growth medium was purchased from Lonza (Basel, Switzerland). Calcein-AM was bought from Invitrogen (Carlsbad, CA), All other reagents were either purchased from Sigma Aldrich (St. Louis, MO). or Invitrogen (Carlsbad, CA) and used without further purification.^{1}H, ^{13}C, and 2D NMR spectra were recorded with a Bruker AC 800 and Bruker AC 500 MHz. DMSO-*d6* was used to prepare NMR samples.

2.4.2 Methods

2.4.2.1 Synthesis of Aba-S_2-COOH

To a solution of 4,4′-dithiodibutyric acid (400 mg, 1.7 mmol) was added PyBOP (114 mg, 0.22 mmol), DIEA (0.20 ml, 0.75 mmol) and DMAP (2.6 mg, 0.022 mmol) under nitrogen atmosphere at room temperature in dry DMF (2 ml). After 20 min, abacavir sulfate (50 mg, 0.15 mmol) was added. The mixture was left to stir at room temperature for 24 hours. The resulting reaction mixture was dissolved in DMSO and purified using RP-HPLC. The RP-HPLC solvent consisted of acetonitrile with 0.1 % TFA (solvent A) and water with 0.1 % TFA (solvent B). A gradient of 20–70% of solvent A with the flow rate of 12.0 mL/min and UV detection at 214 nm and 280 nm with a C8 column (Phenomenex, USA) was used for purification. Purity of the product (~99%) was estimated by C8 analytical RP-HPLC using a flow rate of 1.2 mL/min and UV detection at 214 and 280 nm and a gradient from 20-70% (solvent A) over 30 mins. The retention time for Aba-S_2-COOH was found to be 16.2 mins. The yield for this reaction was calculated to be 70%. Calculated mass for Aba-S_2-COOH 506.18, observed mass by ESI-MS 507.2 $[M+H]^+$.

Aba-S_2-COOH: ^{1}H NMR (500 MHz, DMSO-*d6*) δ 12.18 (s, 2H), 9.77 (s, 1H), 7.93 (s, 1H), 7.45 (s, 2H), 6.13 (dd, J = 5.3, 2.5 Hz, 1H), 5.98 (dt, J = 5.1, 2.2 Hz, 1H), 5.43 (ddd, J = 8.6, 6.1, 2.4 Hz, 1H), 4.09 (d, J = 6.1 Hz, 2H), 3.11 (ddt, J = 12.0, 8.5, 4.1 Hz, 1H), 2.85 (s, 1H), 2.68 (qd, J = 8.1, 7.2, 4.4 Hz, 5H), 2.38 (td, J = 7.3, 4.4 Hz, 2H), 2.29 (t, J = 7.2 Hz, 2H), 1.82 (dp, J = 11.4, 7.2 Hz, 4H), 1.62 (dt, J = 13.8, 5.9 Hz, 1H), 0.88 (s, 2H), 0.74 (s, 2H); ^{13}C NMR (126 MHz, DMSO-*d6*) δ 174.34, 172.85, 159.09, 158.84, 158.59, 137.79, 130.49, 118.60, 116.23, 66.72, 59.61, 45.70,

44.48, 40.48, 40.32, 40.15, 39.98, 39.82, 39.65, 39.48, 37.28, 37.10, 34.71, 32.54, 32.34, 26.07, 24.43, 24.40, 7.39.

2.4.2.2 Synthesis of Aba-S_2-DRV8

To a flame dried round bottom flask under nitrogen, was added DRV (20 mg, 36µmol), Aba-S_2-COOH (21.5 mg, 34.8 µmol), EDC (10 mg, 52.2 µmol), DMAP (8.5 mg, 69.7 µmol), DIEA (60µl, 348 µmol) and 4 Å powdered molecular sieves followed by dry DCM (1 ml) at 0 °C. The reaction mixture was stirred at room temperature for 72 hours, and the progress of the reaction was monitored by RP-HPLC. The reaction mixture was diluted with DMSO and components separated by RP-HPLC on a C18 column (Phenomenex, USA) with a flow rate of 12 ml/min, a gradient of 20–95% solvent A over 60 min and UV detection at 214 nm and 254 nm. Aba-S_2-DRV was obtained (27% yield, major product) with (Aba-S_2)$_2$-DRV (21% yield, minor product). The retention time of Aba-S_2-DRV8 (major product) had a purity of 99% , and the compound was fully characterized by NMR. ESI-MS: calculated mass: 1036.4, observed mass: 1036.8; high resolution MS: calculated mass: 1036.4089, observed mass: 1036.4106. (Analytical purity trace: Figure A1, 1 and 2 D NMR spectra: Figures A14-A18)

Aba-S_2-DRV8: ^{1}H NMR (800 MHz, DMSO-d_6) δ 7.48 (d, *J* = 9.4 Hz, 1H), 7.39 (d, *J* = 8.7 Hz, 1H), 7.21 (dt, *J* = 15.3, 7.1 Hz, 3H), 7.16 – 7.13 (m, 1H), 6.61 (d, *J* = 8.7 Hz, 1H), 6.12 (dt, *J* = 5.6, 2.1 Hz, 1H), 5.96 (dt, *J* = 5.6, 2.2 Hz, 1H), 5.48 (d, *J* = 5.2 Hz, 1H), 5.41 (ddq, *J* = 8.2, 6.2, 2.1 Hz, 1H), 5.06 (ddd, *J* = 9.0, 4.5, 2.8 Hz, 1H), 4.84 (dt, *J* = 8.0, 5.8 Hz, 1H), 4.07 (dd, *J* = 6.2, 2.1 Hz, 2H), 3.95 (ddd, *J* = 14.9, 9.1, 4.1 Hz, 1H), 3.85 (dd, *J* = 9.6, 6.0 Hz, 1H), 3.69 (td, *J* = 8.2, 1.9 Hz, 1H), 3.56 (ddt, *J* = 16.4, 8.3, 5.6 Hz, 2H), 3.29 (dd, *J* = 15.4, 2.9 Hz, 1H), 3.08 (ddp, *J* = 8.3, 6.2, 2.0 Hz, 1H), 3.04 (dd, *J* = 15.3, 9.0 Hz, 1H), 2.81 (dt, *J* = 13.4, 3.8 Hz, 2H), 2.78 – 2.72 (m, 1H), 2.69 (dt, *J* = 18.8, 7.1 Hz, 4H), 2.60 – 2.51 (m, 1H), 2.50 – 2.47 (m, 3H), 2.42 – 2.38 (m, 1H), 2.38 – 2.30 (m, 3H), 2.06 (s, 0H), 1.91 – 1.85 (m, 2H), 1.83 (q, *J* = 7.3 Hz, 2H), 1.78 (ddt, *J* = 13.1, 9.0, 6.5 Hz, 1H), 1.61 (dt, *J* = 13.8, 5.9 Hz, 1H), 1.39 – 1.30 (m, 1H), 1.17 – 1.11 (m, 1H), 0.77 (dd, *J* = 6.6, 4.5 Hz, 5H). ^{13}C NMR (800 MHz, DMSO-d_6) δ 172.82, 172.35, 155.81, 153.44, 138.77, 137.77, 130.46, 129.56, 129.52, 128.48, 126.54, 123.29, 113.18, 109.22, 109.20, 75.08, 73.07, 70.65, 69.25, 66.72, 59.60, 57.73, 53.72, 49.50, 45.47, 44.45, 40.29, 40.18, 40.08, 39.97,

39.87, 39.77, 39.66, 37.08, 37.05, 35.56, 34.68, 32.51, 32.30, 26.82, 25.89, 24.34, 24.07, 23.56, 20.37, 20.21.

2.4.2.3 Cell Culture

12D7-MDR cells were grown in complete RPMI 1640 media with vincristine (0.5 ng/mL), 50 units/mL of penicillin and 50µg/mL streptomycin, 5 mM of L-glutamine and 10 % FBS. The growth of cells was maintained at 37 ^{o} C in 5% CO_2. hCMEC/D3 cells were cultured according to literature protocols with minor modifications.[41] The media used for growth consisted of endothelial growth medium-2 (EGM-2) supplemented with 5% fetal bovine serum, 1 % penicillin-streptomycin, 0.5% human basic fibroblast growth factor (hbFGF), 1.4 µM hydrocortisone, 5 µg/mL ascorbic acid, 1% (10 mM) HEPES and 1% lipid concentrate.

2.4.2.4 Flow Cytometry Assay

Flow cytometry was used to estimate P-gp inhibition using a substrate accumulation assay as described previously with some minor changes.[38] BME media (with fluorescent P-gp substrate) along with the compound of interest in DMSO (1%) was added to 125,000 cells in suspension and stored in a CO_2 incubator at 37 °C for 30 mins. The cells were harvested by centrifugation at 300 x g at 4 °C for 7 mins. The supernatant was carefully removed, and 400 µl of cold, sterile PBS was added to the cell pellet. The accumulation of calcein-AM or NBD-Aba was measured using a FACSCalibur flow cytometer (BD Biosciences) with an excitation wavelength of 488 nm argon laser and an emission 530 nm bandpass filter (FL1). The mean fluorescence value for each concentration corresponded to 10,000 cells. Each sample was run in duplicate and all the experiments were run in duplicates on two different days. The average fluorescence accumulated in the cells for samples was used to plot the mean fluorescence vs. concentration, and the IC_{50} values were estimated using the Graph Pad Prism.

2.4.2.5 Cell Viability Assay

The viability of 12D7-MDR cells in the presence of the TH heterodimer (Aba-S_2-DRV8) was measured using the standard MTT assay.[44] 20,000 12D7-MDR cells were plated in 96-well plate in 100 µL of cell media. After 12 hours, the TH heterodimer in media was added to each well to

give a final concentration of 5, 10 and 20 µM (1% DMSO). After 24 hours 20 µl of MTT in PBS (5 mg/mL) was added to all the wells and incubated for 2.5 hours. The 96 well plates were centrifuged at 300 x g for 7 mins, followed by careful removal of supernatant. 100 µl of DMSO was added to dissolve the formazan. The absorbance of the DMSO solution was read using plate reader at 590 nm. Cell viability was reported as the ratio of absorbance of cells treated with TH heterodimer relative to cells treated with DMSO.

2.4.2.6 Stability of the TH heterodimer with DTT

Stability studies with DTT and GSH were adapted from a previously published protocol with some changes.[32] Aba-S_2-DRV8 (4 µM) was incubated at 37 °C with 250 mM DTT or 10 mM GSH in degassed 30% methanol/ PBS (pH ~7.4) containing 5 µM quinine as the internal standard. When monitoring DRV release, an aliquot of the reaction mixture was taken at different time points and directly analyzed by UPLC-MS. For analysis of Aba release, an aliquot of reaction mixture was taken and stored at -80 °C before analysis. The time points were analyzed using RP-UPLC with a C18 column consisting of solvent A (water and 0.1% formic acid) and solvent B (acetonitrile and 0.1% formic acid), a gradient of 5-95% of solvent B over 10 mins and a flow rate of 0.5 ml/min. The peaks corresponding to m/z for quinine (325.4), Aba-S_2-DRV8 (1036.5), Aba-SH (389.4), Aba (287.4), and DRV (548.4) were detected and extracted using MassLynx software. The experiments were run in duplicate, and the average percentage of release vs time was fitted using Graph Pad Prism 7 to generate $t_{1/2}$'s.

2.4.2.7 Stability of Aba-S_2-DRV8 in cell culture media

The cell media stability studies for the TH heterodimer (Aba-S_2-DRV8) was carried out following a previously published protocol with some modifications.[32] The heterodimer (100 µM) was incubated at 37 °C in the cell media used for 12D7 cells (complete RPMI 1640 media with 50 units/mL of penicillin and 50µg/mL streptomycin, 5 mM of L-glutamine and 10 % FBS) with 1% DMSO. Every 24 hours ice-cold acetonitrile with 4-methoxybenzyl alcohol (1.0 mM) was added to an aliquot of the reaction mixture (1:1). The resultant solution was vortexed for 1 min, sonicated for 10 mins and centrifuged twice at 10000 x g for 10 mins each. The supernatant was stored at -80 °C. All samples were analyzed using a C8 analytical column (Phenomenex, USA) on RP-HPLC

with eluent consisting of solvent A (water and 0.05% TFA) and solvent B (acetonitrile and 0.05% TFA). A gradient of 15-75% solvent B over 30 min with a flow rate of 1.2 ml/min and UV detection at 254 nm was used. The assays were performed in duplicate.

2.4.2.8 HIV-1 cell inhibition assay

12D7 cells were grown in the identical media for the cell culture media stability studies. The cells in log-phase were pelleted and resuspended at 1 million cells per ml. 500 $TCID_{50}$ HIV-1_{LAI} was used to infect cells for 4 hours using a known procedure.[45] These infected cells were plated at a density of 75,000 cells per ml in 48-well plates after three washes with the media. Different concentrations of the compound of interest were added keeping the DMSO concentration at 0.05%. After three days, the media was replaced with fresh media containing the same concentration of the compound of interest. On the 6^{th} day, the supernatant was analyzed using ELISA to quantify the amount of HIV-1 p24 (gag) protein generated in each sample.[46] All assays were run in duplicate.

2.5 References

1. Autran, B.; Carcelain, G.; Li, T. S.; Blanc, C.; Mathez, D.; Tubiana, R.; Katlama, C.; Debré, P.; Leibowitch, J. Positive effects of combined antiretroviral therapy on CD4+ T cell homeostasis and function in advanced HIV disease. *Science* **1997**, *277* (5322), 112–116.

2. Lambotte, O.; Deiva, K.; Tardieu, M. HIV-1 Persistence, viral reservoir, and the central nervous system in the HAART era. *Brain Pathol.* **2003**, *13* (1), 95–103.

3. Pierson, T.; McArthur, J.; Siliciano, R. F. Reservoirs for HIV-1: mechanisms for viral persistence in the presence of antiviral immune responses and antiretroviral therapy. *Annu. Rev. Immunol.* **2000**, *18*, 665–708.

4. Ivey, N. S.; MacLean, A. G.; Lackner, A. A. Acquired immunodeficiency syndrome and the blood-brain barrier. *J. Neurovirol.* **2009**, *15* (2), 111–122.

5. Thomas, S. A. Anti-HIV drug distribution to the central nervous system. *Curr. Pharm. Des.* **2004**, *10* (12), 1313–1324.

6. Varatharajan, L.; Thomas, S. A. The transport of anti-HIV drugs across blood-CNS interfaces: summary of current knowledge and recommendations for further research. *Antiviral Res.* **2009**, *82* (2), A99-109.

7. Kandanearatchi, A.; Williams, B.; Everall, I. P. Assessing the efficacy of highly active antiretroviral therapy in the brain. *Brain Pathol.* **2003**, *13* (1), 104–110.

8. Schinkel, A. H. P-glycoprotein, a gatekeeper in the blood-brain barrier. *Adv. Drug Deliv. Rev.* **1999**, *36* (2–3), 179–194.

9. Saidijam, M.; Karimi Dermani, F.; Sohrabi, S.; Patching, S. G. Efflux proteins at the blood-brain barrier: review and bioinformatics analysis. *Xenobiotica.* **2018**, *48* (5), 506–532.

10. Shaik, N.; Giri, N.; Pan, G.; Elmquist, W. F. P-glycoprotein-mediated active efflux of the anti-HIV1 nucleoside abacavir limits cellular accumulation and brain distribution. *Drug Metab. Dispos.* **2007**, *35* (11), 2076–2085.

11. de Souza, J.; Benet, L. Z.; Huang, Y.; Storpirtis, S. Comparison of bidirectional lamivudine and zidovudine transport using MDCK, MDCK-MDR1, and Caco-2 cell monolayers. *J. Pharm. Sci.* **2009**, *98* (11), 4413–4419.

12. Lee, C. G.; Gottesman, M. M.; Cardarelli, C. O.; Ramachandra, M.; Jeang, K. T.; Ambudkar, S. V.; Pastan, I; Dey, S. HIV-1 protease inhibitors are substrates for the MDR1 multidrug transporter. *Biochemistry* **1998**, *37*(11), 3594-3601.

13. Bousquet, L.; Roucairol, C.; Hembury, A.; Nevers, M. C.; Creminon, C.; Farinotti, R.; Mabondzo, A. Comparison of ABC transporter modulation by atazanavir in lymphocytes and human brain endothelial cells: ABC transporters are involved in the atazanavir-limited passage across an in vitro human model of the blood-brain barrier. *AIDS Res. Hum. Retroviruses* **2008**, *24*(9), 1147-1154.

14. Fujimoto, H; Higuchi, M.; Watanabe, H.; Koh, Y.; Ghosh, A. K.; Mitsuya, H.; Tanoue, N.; Hamada, A.; Saito, H. P-glycoprotein mediates efflux transport of darunavir in human intestinal Caco-2 and ABCB1 gene-transfected renal LLC-PK1 cell lines. *Biol. Pharm. Bull.* **2009,** *32*(9), 1588-1593.

15. Gimenez, F.; Fernandez, C.; Mabondzo, A. Transport of HIV protease inhibitors through the blood brain barrier and interactions with the efflux proteins, P-glycoprotein and multidrug resistance proteins. *J. Acquir. Immune Defic. Syndr.***2004**, *36*(2), 649-658.

16. Hashiguchi, Y.; Hamada, A.; Shinohara, T.; Tsuchiya, K.; Jono, H.; Saito, H. Role of P-Glycoprotein in the Efflux of raltegravir from human intestinal cells and CD4+ T-Cells as an interaction target for anti-HIV agents. *Biochem. Biophys. Res. Commun.* **2013**, *439* (2), 221-227.

17. Kim, R. B.; Fromm, M. F.; Wandel, C.; Leake, B.; Wood, A. J.; Roden, D. M.; Wilkinson, G. R. The drug transporter P-glycoprotein limits oral absorption and brain entry of HIV-1 protease inhibitors. *J. Clin. Invest.* **1998**, *101* (2), 289–294.

18. Choo, E. F.; Leake, B.; Wandel, C.; Imamura, H.; Wood, A. J.; Wilkinson, G. R.; Kim, R. B. Pharmacological inhibition of P-glycoprotein transport enhances the distribution of HIV-1 protease inhibitors into brain and testes. *Drug Metab. Dispos. Biol.* **2000**, *28* (6), 655–660.

19. Aller, S. G.; Yu, J.; Ward, A.; Weng, Y.; Chittaboina, S.; Zhuo, R.; Harrell, P. M.; Trinh, Y. T.; Zhang, Q.; Urbatsch, I. L.; Chang, G. Structure of P-glycoprotein reveals a molecular basis for poly-specific drug binding. *Science* **2009**, *323* (5922), 1718–1722.

20. Jin, M. S.; Oldham, M. L.; Zhang, Q.; Chen, J. Crystal Structure of the multidrug transporter P-glycoprotein from Caenorhabditis elegans. *Nature* **2012**, *490* (7421), 566–569.

21. Kim, Y.; Chen, J. Molecular structure of human P-glycoprotein in the ATP-bound, outward-facing conformation. *Science* **2018**, *359* (6378), 915–919.

22. Bruggemann, E. P.; Currier, S. J.; Gottesman, M. M.; Pastan, I. Characterization of the azidopine and vinblastine binding site of P-glycoprotein. *J. Biol. Chem.* **1992**, *267* (29), 21020–21026.

23. Shapiro, A. B.; Ling, V. Positively cooperative sites for drug transport by P-glycoprotein with distinct drug specificities. *Eur. J. Biochem.* **1997**, *250* (1), 130–137.

24. Dey, S.; Ramachandra, M.; Pastan, I.; Gottesman, M. M.; Ambudkar, S. V. Evidence for two nonidentical drug-interaction sites in the human P-glycoprotein. *Proc. Natl. Acad. Sci.* **1997**, *94* (20), 10594–10599.

25. Loo, T. W.; Bartlett, M. C.; Clarke, D. M. Methanethiosulfonate derivatives of rhodamine and verapamil activate human P-glycoprotein at different sites. *J. Biol. Chem.* **2003**, *278* (50), 50136–50141.

26. Chufan, E. E.; Sim, H. M.; Ambudkar, S. V. Molecular basis of the polyspecificity of P-glycoprotein (ABCB1): recent biochemical and structural studies. *Adv. Cancer Res.* **2015**, *125*, 71–96.

27. Sauna, Z. E.; Andrus, M. B.; Turner, T. M.; Ambudkar, S. V. Biochemical basis of polyvalency as a strategy for enhancing the efficacy of P-glycoprotein (ABCB1) modulators: stipiamide homodimers separated with defined-length spacers reverse drug efflux with greater efficacy. *Biochemistry* **2004**, *43* (8), 2262–2271.

28. Pires, M. M.; Hrycyna, C. A.; Chmielewski, J. Bivalent probes of the human multidrug transporter P-glycoprotein. *Biochemistry* **2006**, *45* (38), 11695–11702.

29. Chan, K. F.; Zhao, Y.; Burkett, B. A.; Wong, I. L.; Chow, L. M.; Chan, T. H. Flavonoid dimers as bivalent modulators for P-glycoprotein-based multidrug resistance: synthetic apigenin homodimers linked with defined-length poly(ethylene glycol) spacers increase drug retention and enhance chemosensitivity in resistant cancer cells. *Med. Chem.* **2006**, *49* (23), 6742–6759.

30. Pires, M. M.; Emmert, D.; Hrycyna, C. A.; Chmielewski, J. Inhibition of P-glycoprotein-mediated paclitaxel resistance by reversibly linked quinine homodimers. *Mol. Pharmacol.* **2009**, *75* (1), 92–100.

31. Kuriakose, J.; Hrycyna, C. A.; Chmielewski, J. Click chemistry-derived bivalent quinine inhibitors of P-glycoprotein-mediated cellular efflux. *Bioorg. Med. Chem. Lett.* **2012**, *22* (13), 4410–4412.

32. Namanja, H. A.; Emmert, D.; Davis, D. A.; Campos, C.; Miller, D. S.; Hrycyna, C. A.; Chmielewski, J. Toward eradicating HIV reservoirs in the brain: inhibiting P-glycoprotein at the blood–brain barrier with prodrug abacavir dimers. *J. Am. Chem. Soc.* **2012**, *134* (6), 2976–2980.

33. Namanja, H. A.; Emmert, D.; Hrycyna, C. A.; Chmielewski, J. Homodimers of the antiviral abacavir as modulators of P-glycoprotein transport in cell culture: probing tether length. *MedChemComm* **2013**, *4* (10), 1344–1349.

34. Emmert, D. ; Campos, C. R.; Ward, D.; Lu, P.; Namanja, H. A.; Bohn, K.; Miller, D. S.; Sharom, F. J.; Chmielewski, J.; Hrycyna, C. A. Reversible dimers of the atypical antipsychotic quetiapine inhibit P-glycoprotein-mediated efflux in vitro with increased binding affinity and in situ at the blood-brain barrier. *ACS Chem. Neurosci.* **2014**, *5* (4), 305–317.

35. Bohn, K.; Lange, A.; Chmielewski, J.; Hrycyna, C. A. Dual modulation of human P-glycoprotein and ABCG2 with prodrug dimers of the atypical antipsychotic agent paliperidone in a model of the blood-brain barrier. *Mol. Pharm.*, **2017**, *14* (4) 1107–1119.

36. Namanja-Magliano, H. A.; Bohn, K.; Agrawal, N.; Willoughby, M. E.; Hrycyna, C. A.; Chmielewski, J. Dual inhibitors of the human blood brain barrier efflux transporters P-glycoprotein and ABCG2 based on the antiviral azidothymidine. *Bioorg. Med. Chem.* **2017**, *25* (19), 5128-5132.

37. Schuster, I. I. A Carbon-13 NMR Study of electronic effects in the hydrogen bonding of trifluoroacetic acid with substituted benzenes, 1- and 2-substituted naphthalenes, and 9-substituted anthracenes in chloroform. *J. Org. Chem.* **1985**, *50* (10), 1656–1662.

38. Hrycyna, C. A.; Ramachandra, M.; Pastan, I.; Gottesman, M. M. Functional expression of human P-glycoprotein from plasmids using vaccinia virus-bacteriophage T7 RNA polymerase system. *Methods Enzymol.* **1998**, *292*, 456–473.

39. Namanja, H. A. Development of dimeric prodrug inhibitors of P-glycoprotein and ABCG2 to enhance brain penetration of antiretroviral agents. Ph.D. Dissertation, Purdue University, **2012.**

40. Lee, C. G.; Pastan, I.; Gottesman, M. M. Retroviral transfer of human MDR1 gene into human T lymphocytes. *Methods Enzymol.* **1998**, *292*, 557–572.

41. Weksler, B. B.; Subileau, E. A.; Perrière, N.; Charneau, P.; Holloway, K.; Leveque, M.; Tricoire-Leignel, H.; Nicotra, A.; Bourdoulous, S.; Turowski, P.; Male, D. K.; Roux, F.; Greenwood, J.; Romero, I. A.; Couraud, P. O. Blood-brain barrier-specific properties of a human adult brain endothelial cell line. *FASEB J.* **2005**, *19* (13), 1872–1874.

42. Carl, S. M.; Lindley, D. J.; Das, D.; Couraud, P. O.; Weksler, B. B.; Romero, I.; Mowery, S. A.; Knipp, G. T. ABC and SLC transporter expression and proton oligopeptide transporter (POT) mediated permeation across the human blood-brain barrier cell line, HCMEC/D3. *Mol. Pharm.* **2010**, *7* (4), 1057–1068.

43. Poller, B.; Gutmann, H.; Krähenbühl, S.; Weksler, B.; Romero, I.; Couraud, P.-O.; Tuffin, G.; Drewe, J.; Huwyler, J. The human brain endothelial cell line HCMEC/D3 as a human blood-brain barrier model for drug transport studies. *J. Neurochem.* **2008**, *107* (5), 1358–1368.

44. Mosmann, T. Rapid colorimetric assay for cellular growth and survival: application to proliferation and cytotoxicity assays. *J. Immunol. Methods* **1983**, *65* (1–2), 55–63.

45. Richman, D. D.; Kornbluth, R. S.; Carson, D. A. Failure of dideoxynucleosides to inhibit human immunodeficiency virus replication in cultured human macrophages. *J. Exp. Med.* **1987**, *166* (4), 1144–1149.

46. Davis, D. A.; Brown, C. A.; Singer, K. E.; Wang, V.; Kaufman, J.; Stahl, S. J.; Wingfield, P.; Maeda, K.; Harada, S.; Yoshimura, K.; Kosalaraksa, P.; Mitsuya, H.; Yarchoan, R. Inhibition of HIV-1 replication by a peptide dimerization inhibitor of HIV-1 protease. *Antiviral Res.* **2006**, *72* (2), 89–99.

47. Tang, M. W.; Shafer, R. W. HIV-1 antiretroviral resistance: scientific principles and clinical applications. *Drugs* **2012**, *72* (9), e1-e25.

CHAPTER 3. THE SYNTHESIS OF KANAMYCIN-ARG$_8$ USING A UV ACTIVE STRATEGY

3.1 Introduction

There are many classes of pathogenic bacteria which are able to hide within mammalian cells and promote bacterial genesis, such as *M. tuberculosis*, *A. baumannii,* MRSA, *Listeria monocytogenes,* and *Salmonella enterica*. Intracellular bacteria are notoriously difficult to treat, namely because these pathogens have developed mechanisms to evade the host's immune system.[1,2] To exacerbate the problem further, many commonly prescribed antibiotics, such as aminoglycosides and β lactams, are unable to penetrate the mammalian cell membrane and, therefore, cannot accumulate inside the cell in therapeutic concentrations.[3] The intracellular environment becomes a sanctuary for these pathogenic bacteria, where their growth is left unchecked. Thus, infected carriers of these bacteria chronically suffer or die from the bacterial infection.[4] Therefore, there is an imperative need for therapies which can accumulate inside the mammalian cell and clear these pathogenic bacteria.

A potential strategy to circumvent this problem uses cell penetrating peptides (CPP) to carry antibiotic cargo past the plasma membrane of a mammalian cell. CPP have successfully delivered a wide variety of cargo intracellulary, such as DNA and proteins.[5-15] CPP are a promising tool to enhance intracellular delivery of antibiotics. Various CPP are discussed herein, such as octarginine (Arg$_8$),[14] HIV-1 transactivator of transcription peptide (Tat),[12] and α1H/α2H.[15]

A number of groups have conjugated antibiotics with CPPs for the clearance of intracellular bacteria and these data are summarized herein. In 2018, N2, an antimicrobial peptide, has been shown to display potent antimicrobial activity against Gram negative bacteria, such as *E. coli* and *S. enteritidis.*[16] However, previous studies showed that N2 does not effectively clear intracellular *S. typhimurium* due to its limited membrane permeability. Therefore, Li *et al.* in 2018 conjugated N2 with the CPP Tat, which showed approximately two times more potent clearance of intracellular *S. typhimurium* as compared to N2 alone.[16] Further, N6 is also an antimicrobial peptide, with potent antibacterial activity against Gram negative infections, such as *Salmonella* and *E. coli.*[12] In 2018 Li *et al*. described enhanced intracellular antibacterial activity of N6 by conjugating N6 to Tat with a cathepsin cleavable linker.[12] Moreover, the enhanced intracellular activity was further seen *in vivo* where the N6-Tat conjugate protected 83-100% of the mice from

the lethal *S. typhimurium* infection, as compared to 33% survival with N6 alone. Sparr *et al.* observed enhanced antibacterial activity of the antibiotic fosmidomycin against *Mycobacterium* strains after conjugating fosmidomycin to Arg_8.[14] In 2019, Ruczynski and coworkers improved the bioavailablity of vancomycin by conjugating it to the cell penetrating peptide, transportan 10.[17] The vancomycin-transportan 10 conjugate displayed a 14-fold reduction of intracellular MRSA as compared to vancomycin alone. Using bacteria derived cell penetrating peptides, α1H/α2H, Gomarasca *et al*. in 2017, overcame gentamicin's poor cell permeability by conjugating it to α1H/α2H. These gentamicin- α1H/α2H conjugates were able to significantly reduce various intracellular bacteria, such as *E. coli*, *Salmonella*, and *Shigella*.[15]

The Kelley lab has introduced methotrexate cell penetrating peptide conjugates to target intracellular pathogens, namely Gram-positive pathogens such as *Enterococcus faecalis* and *Bacillus subtilis.*[18] This work was later expanded towards the clearance of intracellular *L. monogenes* and *M. tuberculosis*.[19, 20] The cell penetrating peptide used in this work was a mitochondria penetrating peptide, designed by the Kelley lab.[21, 22] This CPP-methotrexate conjugate allows for greater than 3000-fold and 10,000-fold improvements against *Enterococcus faecalis* and *Bacillus subtilis*, respectively, as compared to methotrexate alone.[18] Further modifications of the peptide conjugate allowed for enhanced clearance of intracellular *L. monogenes* and *M. smegmatis*.[19, 20] Thus, this tunable CPP-drug conjugate is able to effectively clear various intracellular pathogens.

Chmielewski and coworkers were the first to report a dual antibiotic-CPP strategy, whereby the CPP akone also has antibiotic activity. In their work, the cell penetrating peptide with inherent antibacterial activity P14LRR, was conjugated to the aminoglycoside kanamycin via a reversible linker to yield P14KanS. P14KanS significantly reduced intracellular bacteria across a wide variety of pathogens, including *M. tuberculosis*, *S. enteritidis*, *B. abortus*, and *S. flexeri*, wherein, P14KanS cleared 70-95% of the bacteria.[9] Further, within a *C. elegans in vivo* model, P14KanS was able to clear 90% of the bacteria across all concentrations. Together, these studies confirm the advantage of a delivery vehicle, enhancing each of the known antibiotics' activity against intracellular pathogens.

Linking known antibiotics to CPPs is a very promising strategy to clear intracellular bacteria, and a number of synthetic strategies have been used to make these conjugates. Here, we will specifically focus on the conjugation of aminoglycoside antibiotics. Aminoglycosides are non-

UV active antibiotics which contain sugar-like ring moieties with amines (blue) and hydroxyl (red) functionalities (Figure 3.1). Aminoglycoside conjugation is challenging for a couple of reasons; (1) visualization of the antibiotic conjugates during synthesis and purification is difficult without a UV active moiety and (2) multiple isomers will result upon conjugation due to multiple amine and hydroxyl functionalities.

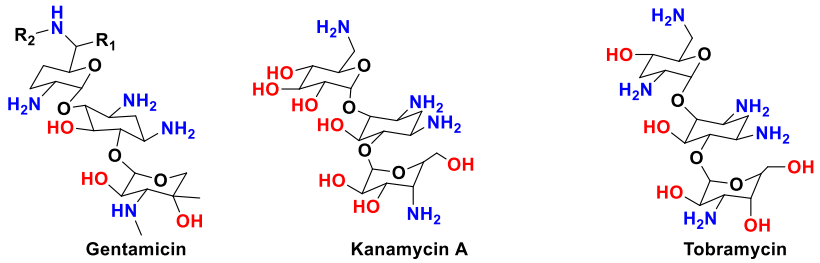

Figure 3.1 A selection of aminoglycoside structures.

Conjugation of aminoglycosides with carboxylic acid linkers may result in either amide or ester functionalization. When functionalized as an amide, these aminoglycosides, in general, do not revert back to their corresponding monomer, such as the cases of paromomycin[10] and gentamicin.[15] Conversely, when conjugated at the hydroxyl functional groups, the resulting ester may be labile if a reversible tether design is used. P14KanS is a prime example of this design.[9] Within the tether of P14KanS is a disulfide moiety which, in the reducing environment of the cell, may reduce to free thiols, tethered to kanamycin and P14LRR. For kanamycin-SH, the free thiol may intramolecularly attack the carbonyl on the tether and release the active kanamycin, intracellularly (Figure 3.2).

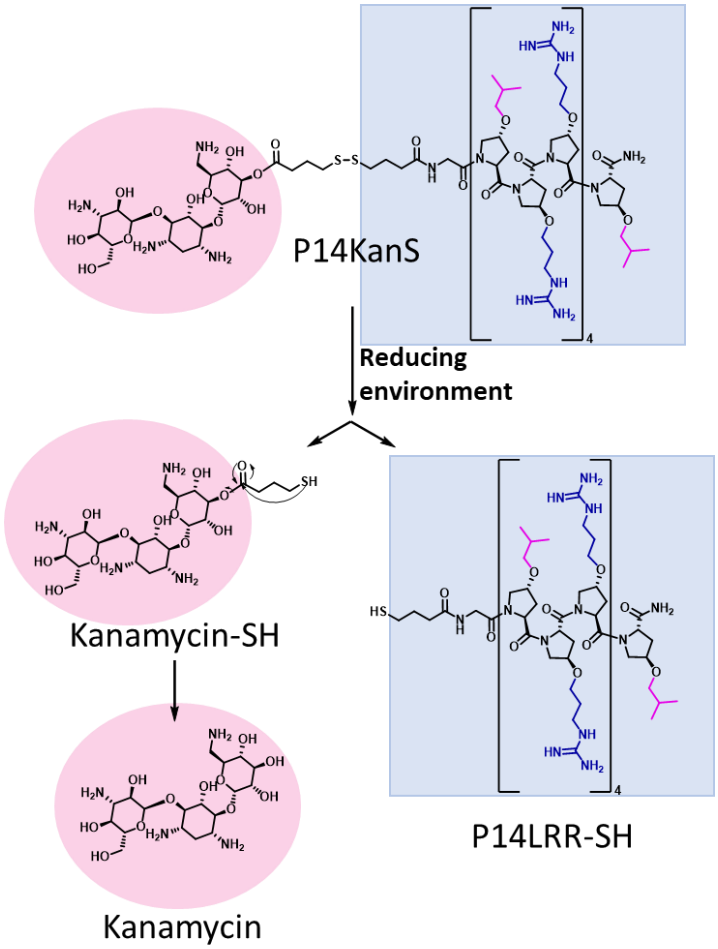

Figure 3.2 P14KanS reversible tether design, which in the reducing environment of the cell may revert to monomeric kanamycin and P14LRR-SH.

As previously mentioned, aminoglycoside antibiotics contain multiple alcohol functionalities within a molecule, usually one primary alcohol and multiple secondary alcohols (Figure 3.1). Selectively conjugating one of these alcohol groups is a difficult challenge. The literature contains methods to selectively conjugate at the primary hydroxyl. This method works by first protecting the amines with *tert*-butyloxycarbonyl. At this point, functionality was directed onto the primary hydroxyl of an aminoglycoside with 2,4,6-triisopropyl-benzenesulfonyl chloride.[23] This bulky reagent is sterically demanding and, therefore, should only react with the primary hydroxyl, and this group may act as a leaving group in further chemistry. Previous groups have utilized this directing group strategy in order to guarantee the isolation of one distinct isomer. However, this creates extra steps in the synthesis, and will not necessarily produce a reversible tether design.

In the recent synthesis of P14KanS (Figure 3.3) this directing group chemistry was not used and a mixture of esterified product isomers was observed.[9] Using their methodology only one of the isomers in mixture was isolated in pure form. The isolated isomer was not the ester of the primary alcohol, as is often targeted, but an ester from one of the secondary alcohols (3', Figure 3.3). This mixture of isomers was difficult to separate because there was no UV active moiety to allow for easy detection of the isomers during purification. Therefore, isolation of multiple distinct isomers of the aminoglycoside conjugates was not accomplished.

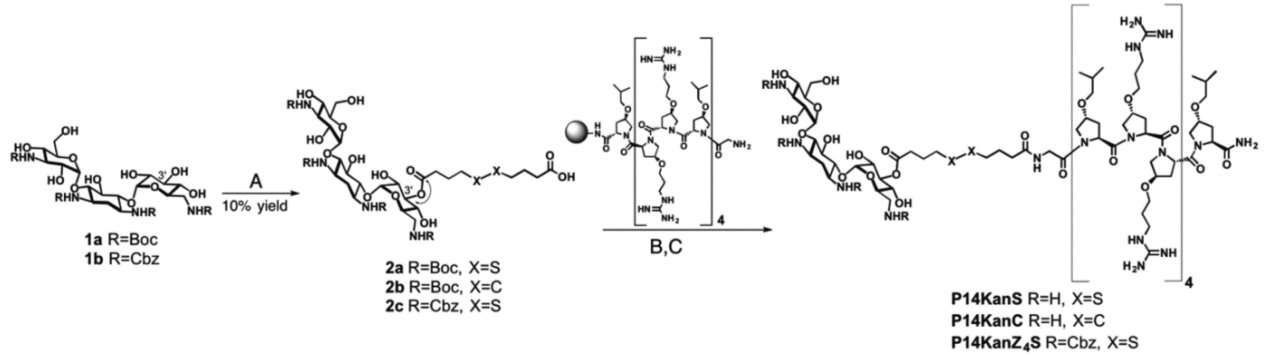

Figure 3.3 Synthesis of P14KanS[9]

3.2 Results and Discussion

3.2.1 Design

Here, we utilize a UV active tether strategy in order to visualize analogs of the aminoglycoside kanamycin (Figure 3.4). This strategy uses 2-mercaptopyridinyl-4-mercaptobutyric acid disulfide as part of the tether functionality that will be linked to a thiol containing CPP (Arg_8-SH). This modification allows for the detection of distinct isomers of kanamycin esters by UV.[24-26] Kanamycin esters with 2-mercaptopyridinyl-4-mercaptobutyric acid disulfide are useful as they will allow facile linkage of the aminoglycoside conjugate with a free thiol-containing CPP. Such CPP-kanamycin conjugates would then contain a tether which, in the reducing environment of the cell, will allow for the release of the kanamycin, or any aminoglycoside, inside the cell.

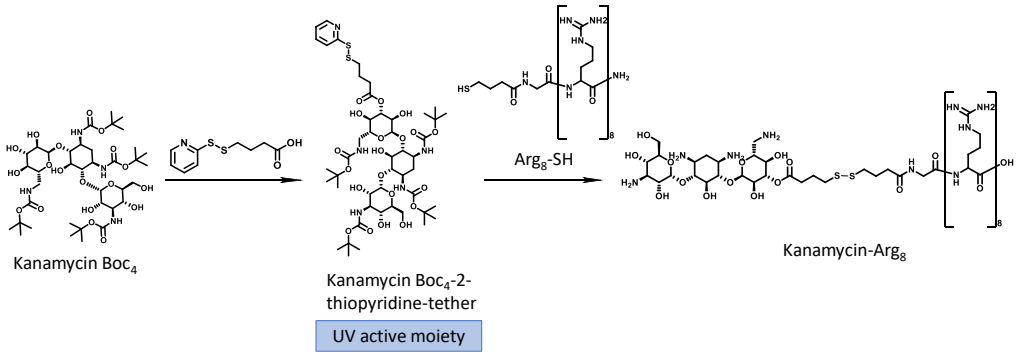

Figure 3.4 New synthetic strategy, utilizing a UV active intermediate of kanamycin

The kanamycin-Arg_8 proof of concept synthesis was designed for two functions: (1) allow for the visualization of kanamycin during the synthesis using a UV active intermediate and (2) to isolate more than one isomer of kanamycin-Arg_8 to determine if there are differences in the release of kanamycin from differing isomers of the conjugates. These aims were accomplished via a new synthetic design, utilizing a 2-mercaptopyridine activated thiol disulfide exchange chemistry, that allowed for the isolation of more than one isomer of the desired conjugate. These isomers were further tested to evaluate if a difference in reductive release of the aminoglycoside existed between the isomers.

3.2.2 Synthesis

For the synthesis of Kanamycin-Arg_8 (Scheme 3.1), first the amine groups of kanamycin were protected with the acid labile *tert*-butyloxycarbonyl group (boc) to afford kanamycin boc_4. Kanamycin boc_4 was then reacted with 2-mercaptopyridinyl-4-mercaptobutyric acid disulfide (a) using HATU, HOAt, DIEA in DMF to yield the UV active moiety Kanamycin Boc_4-2-thiopyridinyl tether. In this step, two distinct isomers were isolated by RP-HPLC, named isomer 1 and 2 at this point. Kanamycin-Boc_4-2-thiopyridyl tether isomer 1 and 2 were Boc-deprotected using 1:1 TFA:DCM yielding Kanamycin-2-thiopyridinyl tether, isomers 1 and 2.

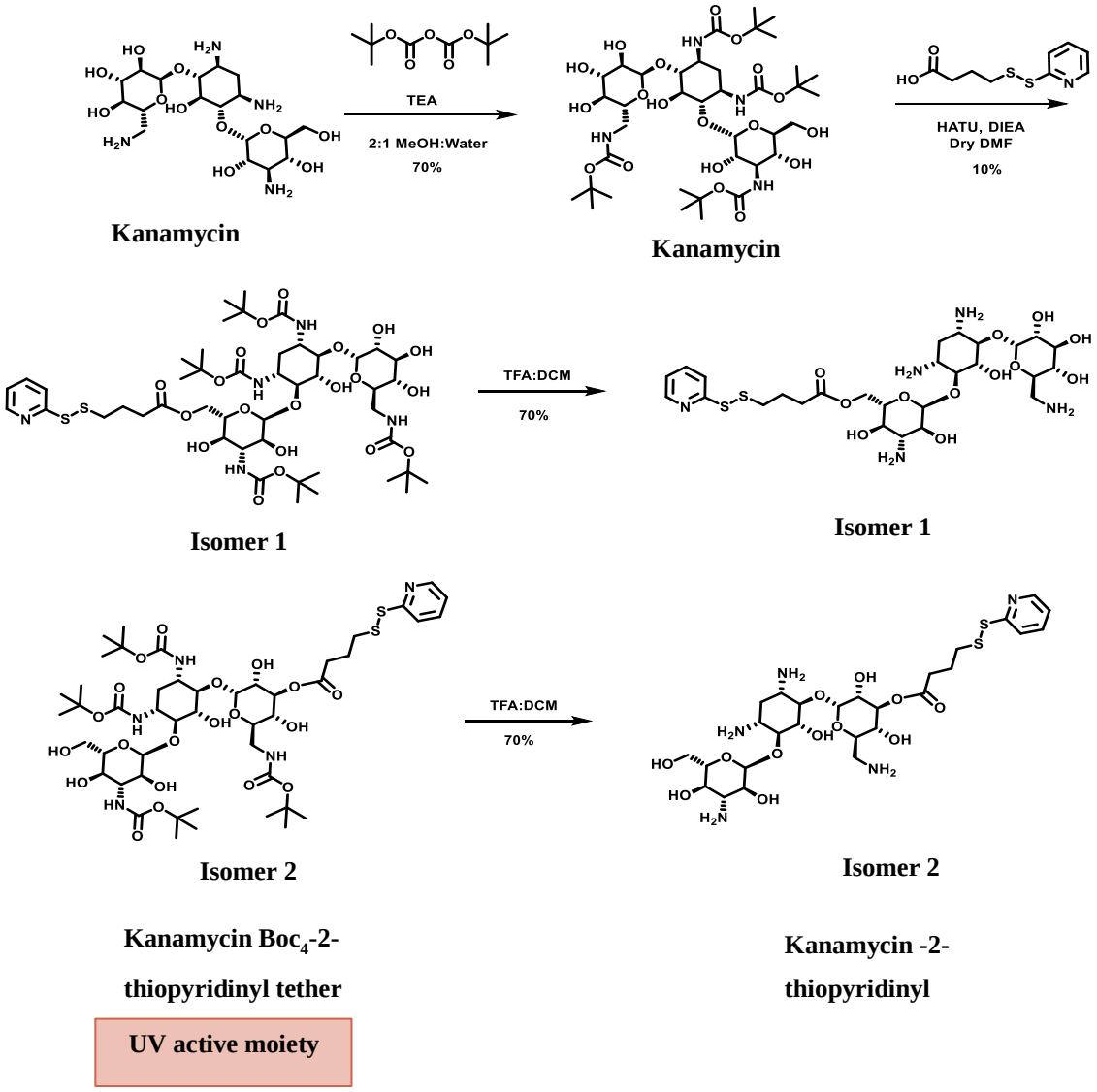

Scheme 3.1 Synthesis of Kanamycin-Arg$_8$ utilizing a UV active intermediate.

Each isomer was fully characterized by ^{1}H, ^{13}C, COSY, HSQC, and HMBC NMR spectroscopy in collaboration with Dr. John Harwood in the Purdue NMR facilities. Kanamycin Boc$_4$-2-thiopyridinyl tether isomers 1 and 2 were first isolated in step 2 of the synthesis (Scheme 3.1). At this point both Kanamycin Boc$_4$-2-thiopyridinyl tethers were dissolved in d$_6$-DMSO for NMR analysis. Each isomer was subjected to the 800 MHz NMR. It was clear from the ^{1}H NMR that isomer 1 had an impurity in the sample. Upon further analysis, the impurity was actually a third isomer of the Kanamycin Boc$_4$-2-thiopyridinyl tether. We determined that the best way to separate isomer 1 from the third isomer was by removing the Boc protecting groups and then separation by HPLC (Scheme 3.1). Therefore, in order to precisely identify the conjugation

location on isomer 1, it was necessary to use the Boc-deprotected version of the isomer (Kanamycin-2-thiopyridnyl tether isomer 1). Isomer 1 was dissolved in d_4-methanol for further NMR analyses. The ^{1}H NMR for Kanamycin Boc_4-2-thiopyrindinyl tether isomer 2, on the other hand, looked clean from the beginning. Therefore, this UV active intermediate was used to determine the conjugation location for isomer 2 in d_6-DMSO using the aforementioned NMR techniques.

3.2.2.1 Kanamycin-2-thiopyrinyl tether isomer 1 characterization

Kanamycin-2-thiopyridinyl tether isomer 1 was fully characterized ^{1}H, ^{13}C, COSY, TOCSY, DEPT-135, HSQC, and HMBC NMR techniques in order to determine the location of the ester in Kanamycin-2-thiopyridinyl tether isomer 1 (Figure 3.5). The comparison of the 2D techniques, namely the COSY, TOCSY, DEPT-135, HSQC and HMBC NMRs, allowed for the peak assignment of each ^{1}H (Figure 3.6) and ^{13}C (Figure A20) peak. Each 2D technique will be briefly described to explain the precise identification of each 1D NMR peak. First, it is important to note that DEPT-135 is a 2D carbon technique which identifies carbons as methylenes or methines based on their orientation in the spectrum. Within the DEPT-135 spectrum, positive peaks indicated a methine and a negative peak indicated a methylene. DEPT-135 was useful in identifying the different carbons within the molecule, as there were far fewer methylenes in the overall structure. After the identification of each of the methylenes and methines, their orientation in the overall molecule was then identified by other 2D techniques. COSY and TOCSY are proton versus proton 2D NMR techniques which help to identify which protons are directly adjacent to one another (COSY) and which protons are in close proximity, for example, which protons are on the same ring (TOCSY). Identification of each proton can be further facilitated by the heteroatom 2D NMR techniques, specifically HSQC and HMBC. These techniques compare protons with carbons. Starting with the short range 2D heteronuclear NMR technique HSQC. A correlation peak in an HSQC spectra indicated protons which are directly attached to the carbon. To facilitate the identification of each proton and carbon peak further, one additional technique, HMBC, was used. HMBC is a long-range proton and carbon correlation, which allowed for the identification of protons in close proximity to carbons. Using each of these techniques, each carbon and proton peak were precisely identified.

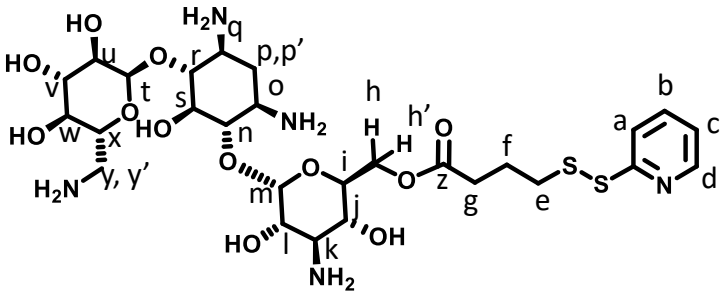

Figure 3.5 Kanamycin-2-thiopyridinyl tether isomer 1 labeled for NMR analysis purposes.

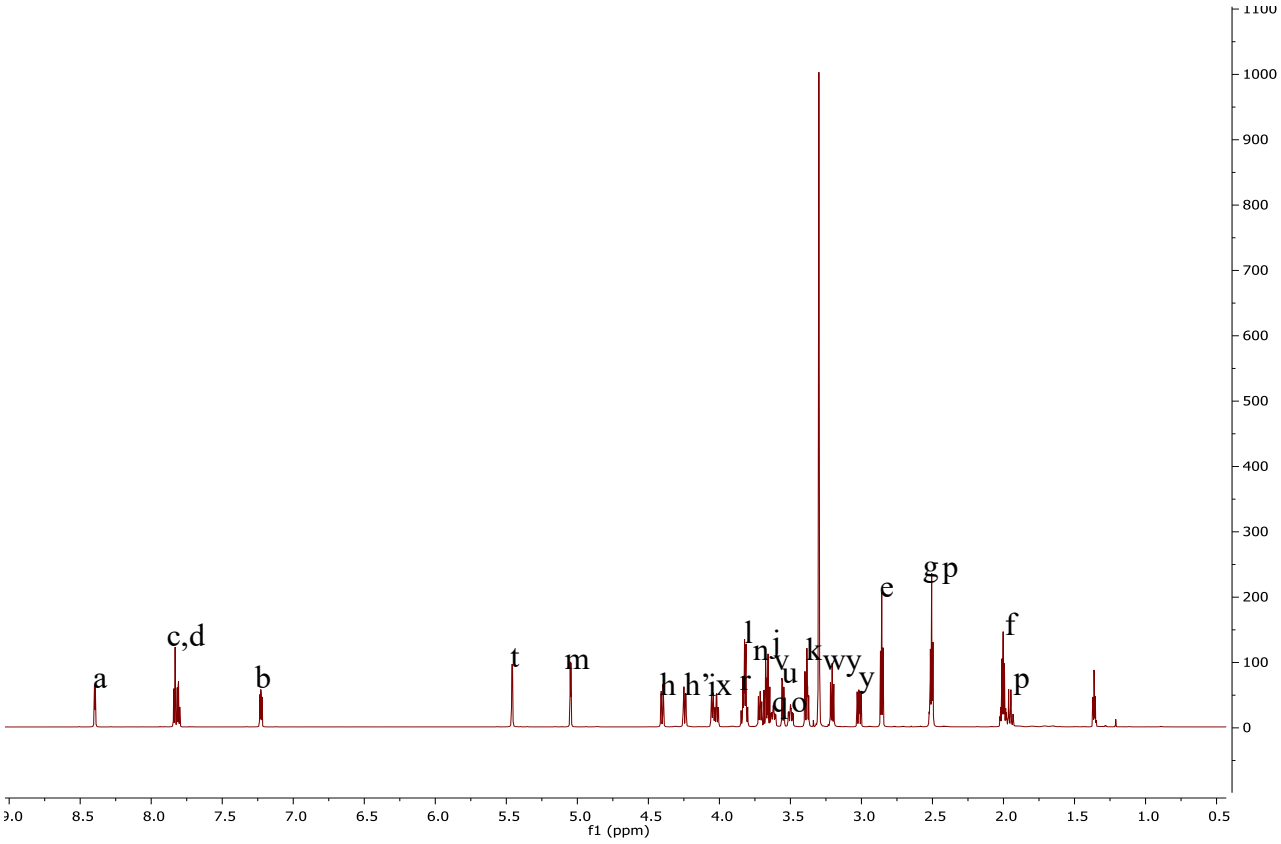

Figure 3.6 The ^{1}H NMR of Kanamycin-2-thiopyridinyl tether isomer 1 in CD_3OD. The peak assignments were made using ^{1}H, ^{13}C, COSY, TOCSY, DEPT-135, HSQC and HMBC NMR techniques.

In order to further corraborate the location of the ester on Kanamycin-2-thiopyridinyl tether isomer 1, the heteroatom 2D techniques, HSQC and the HMBC, were also used (Figure 3.7). Starting with the HSQC, which again is a 2D NMR technique which crosses carbon NMR with the proton NMR, correlation with this short-range technique indicated which protons were directly attached to the carbons. Therefore, in order to pinpoint the connectivity, the carbon technique DEPT-135 was crossed with the traditional ^{1}H NMR spectrum (Figure 3.7a). The DEPT-135 spectrum is seen vertically on the left-hand side of the chromatogram versus the proton NMR at the top. First, the carbon, labelled (h), is seen as a negative peak, which indicates that this is a methylene carbon. The cross of this methylene carbon (h) highlights the two expected protons (h) and (h'), identified in the top ^{1}H chromatogram. This, once again, indicates that these protons (h and h') are directly attached to methylene carbon (h). Next, in the HMBC (Figure 3.7b), which is a long-range heteroatom correlation, the ^{13}C spectrum (left) is crossed with the ^{1}H spectrum (top). In this case, proton (h), as identified before as a proton directly attached to methylene carbon (h), crosses with a carbon peak at 175 ppm. A carbon at this shift is a carbonyl carbon, identified as (z) (Figure 3.5). Therefore, there is a correlation between carbonyl carbon (z) and proton (h) on the HMBC chromatogram, indicating that Kanamycin-2-thiopyridinyl tether isomer 1 is esterified on the primary hydroxyl (h) of kanamycin.

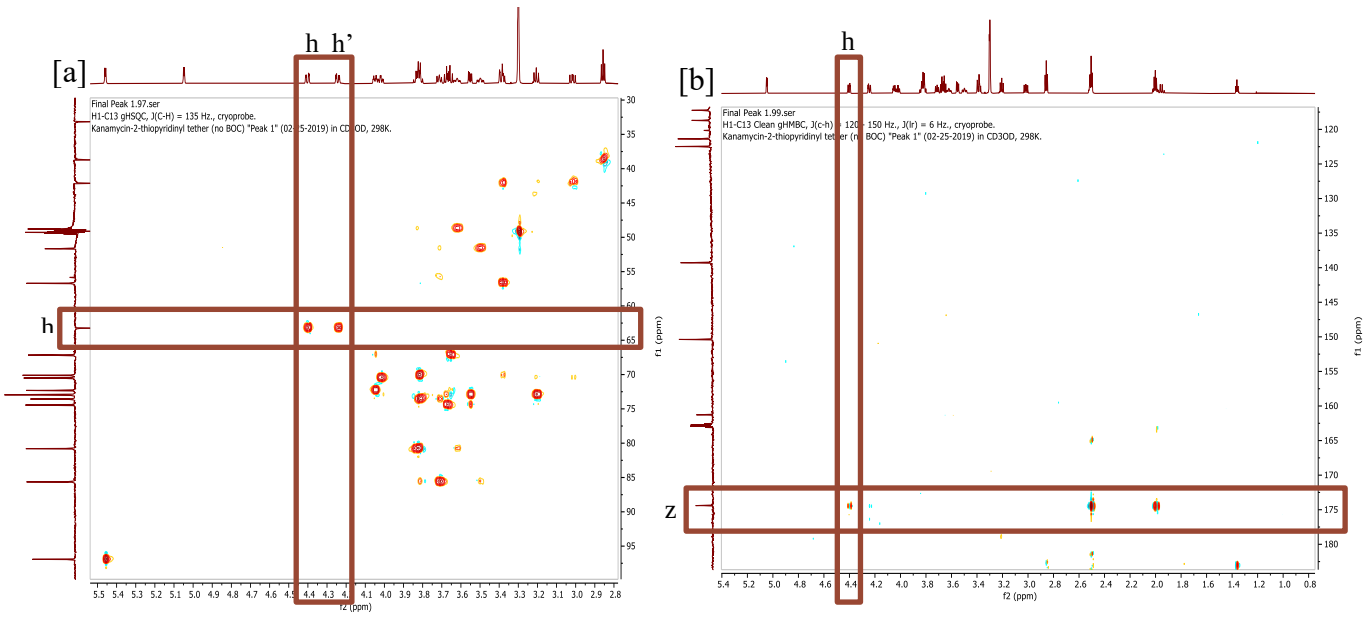

Figure 3.7 [a] The HSQC NMR of Kanamycin -2-thiopyrinyl tether isomer 1 and [b] the HMBC NMR of Kanamycin Boc$_4$-2-thiopyrinyl tether isomer 1 both in CD_3OD.

3.2.2.2 Kanamycin Boc$_4$-2-thiopyrinyl tether isomer 2 Characterization

Kanamycin Boc$_4$-2-thiopyridinyl tether isomer 2 was fully characterized ^{1}H, ^{13}C, COSY, TOCSY, DEPT-135, HSQC, and HMBC NMR techniques in order to determine the location of the ester in Kanamycin Boc$_4$-2-thiopyridinyl tether isomer 2 (Figure 3.8). The comparison of the 2D techniques, namely the COSY, TOCSY, DEPT-135, HSQC and HMBC NMRs, allowed for the peak assignment of each ^{1}H (Figure 3.9) and ^{13}C (Figure A27) peak. Each of the peaks were identified using the same techniques as previously described for Kanamycin-2-thiopyridinyl tether isomer 1.

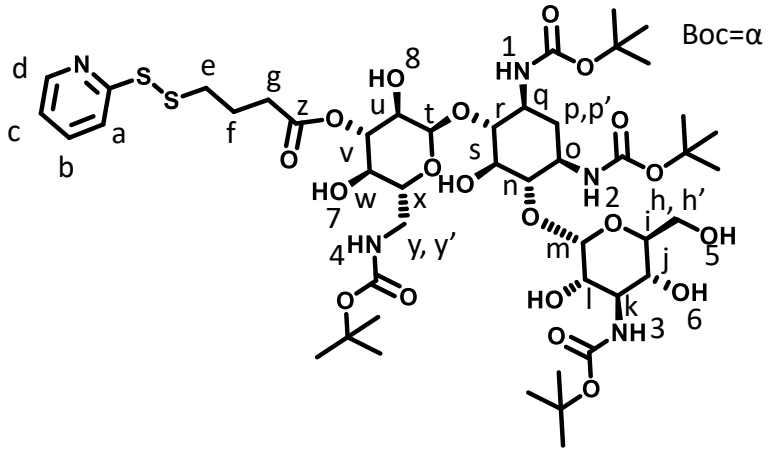

Figure 3.8 Kanamycin Boc$_4$-2-thiopyridinyl tether isomer 2 structure, labeled for NMR analysis.

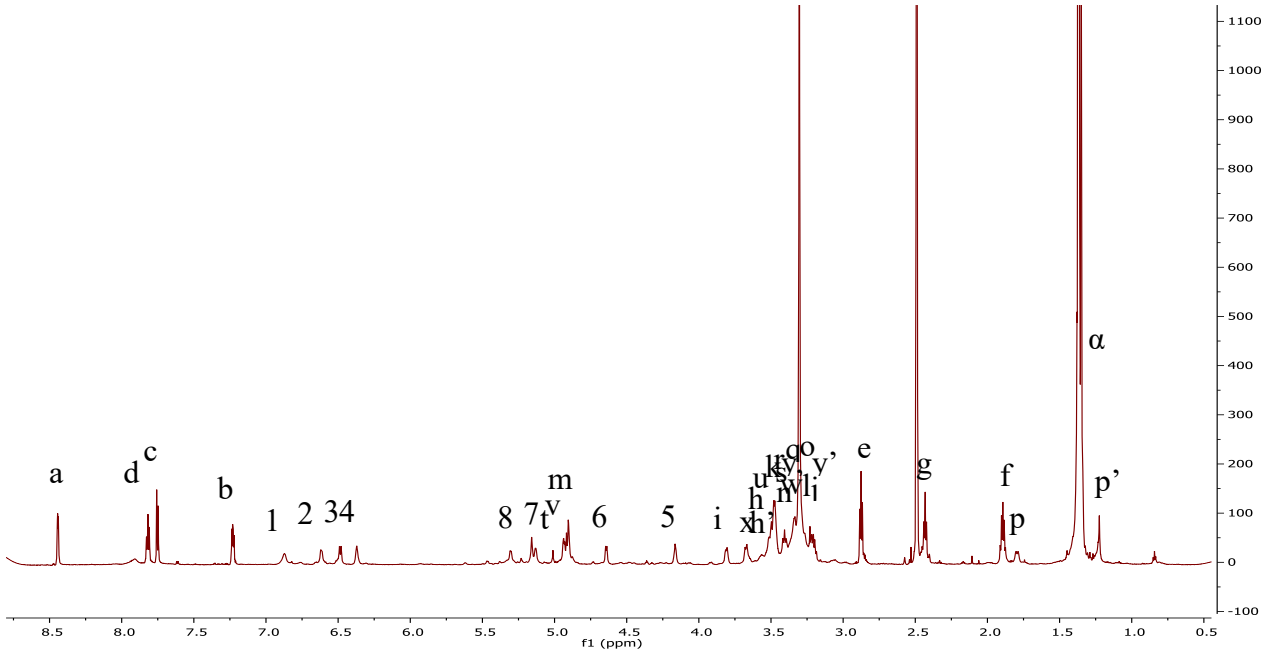

Figure 3.9 The ^{1}H NMR of Kanamycin-Boc$_4$-2-thiopyridinyl tether isomer 2 in d$_6$-DMSO. The peak assignments were made using ^{1}H, ^{13}C, COSY, TOCSY, DEPT-135, HSQC and HMBC NMR techniques.

In order to identify the location of the ester in Kanamycin Boc$_4$-2-thiopyridinyl tether isomer 2, the DEPT-135 spectrum (left) was crossed with the ^{1}H NMR spectrum (top) in the HSQC (Figure 3.10a). First, the carbon, labelled (v), is seen as a positive peak, which indicates that this is a methine carbon. The cross of this methine carbon (v) highlights the one expected proton (v), identified in the top ^{1}H spectrum. Once again, this indicates that this proton (v) is directly attached to methine carbon (v). Next, in the HMBC experiment (Figure 3.10b), which is a long-range heteroatom correlation, the ^{13}C spectrum (left) is crossed with the ^{1}H spectrum (top). In this case, proton (v), as identified before as a proton directly attached to methine carbon (v), crosses with a carbon peak at 175 ppm. A carbon at this shift is a carbonyl carbon, identified as (z) (Figure 3.8). Therefore, there is a correlation between carbonyl carbon (z) and proton (v) in the HMBC spectrum, indicating that Kanamycin Boc$_4$-2-thiopyridinyl tether isomer 2 is esterified on the secondary hydroxyl (v) of kanamycin. Interestingly, this is the same conjugation location as originally seen in P14KanS.[9]

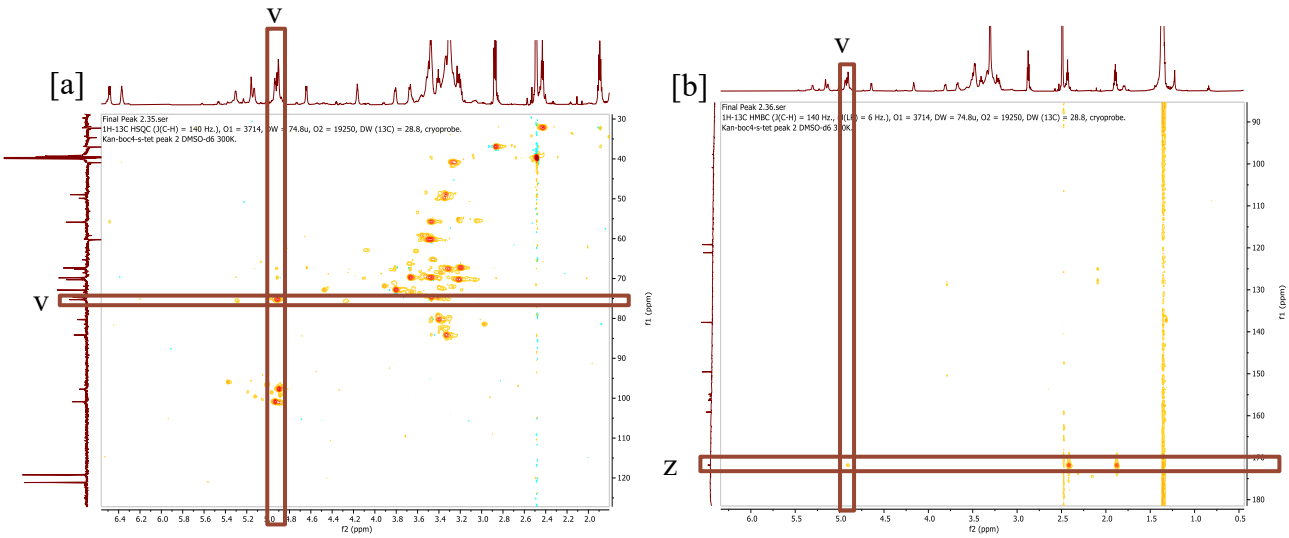

Figure 3.10 [a] The HSQC Kanamycin Boc_4-2-thiopyridinyl tether isomer 2 [b] The HMBC Kanamycin Boc_4-2-thiopyridinyl tether isomer 2 in d_6-DMSO.

The known cell penetrating peptide (CPP) Arg_8[14] was synthesized via solid phase peptide synthesis using high loading (0.45 mmol/g) Chem Matrix H-Rink Amide Resin (Scheme 3.2). Upon synthesis of the Arg_8 peptide, the resin was treated with trityl-4-mercaptobutyric acid (b), HATU and DIEA in DMF. After the reaction, the peptide was globally deprotected and cleaved from resin with a TFA cocktail containing ethanedithiol (EDT, 5%), TIPS (2.5%) and H_2O (2.5%). The resulting Arg_8-SH was purified on RP-HPLC to homogeneity and the mass was confirmed with MALDI-TOF mass spectrometry (Scheme 3.2).

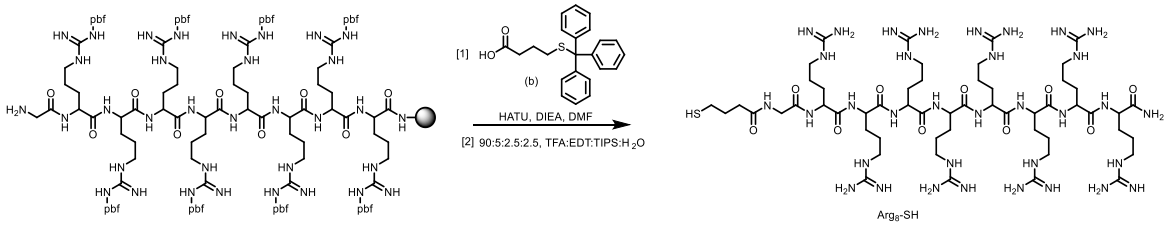

Scheme 3.2 Synthesis of Arg_8-SH.

Kanamycin-2-thiopyridinyl tether (isomer 1 or 2) and Arg_8-SH were combined in PBS buffer (pH 8) and allowed to stir at room temperature for 12 hours (Scheme 3.3). The final products

Kanamycin-Arg_8 isomer 1 and Kanamycin-Arg_8 isomer 2 were purified to homogeneity by RP-HPLC and their masses were confirmed by MALDI-TOF mass spectrometry.

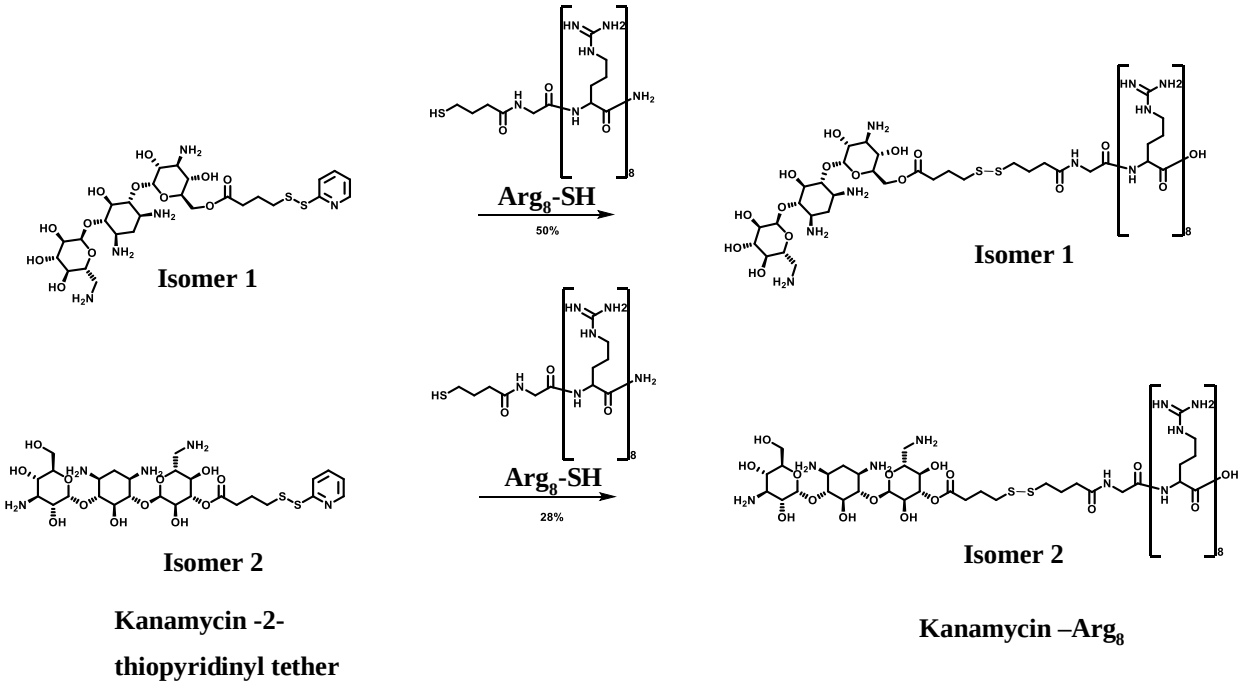

Scheme 3.3 Synthesis of Kanamycin-Arg_8 (isomers 1 and 2).

3.2.3 Reduction Kinetics of Kanamycin-Arg_8 Isomers 1 and 2

A hallmark of the compound design is the inclusion of a disulfide moiety within the tether. Within the intracellular reducing environment, this disulfide may reduce into two free thiols attached to kanamycin and the peptide. The thiol attached to kanamycin may then rearrange and release kanamycin. Each of the two isomers obtained during the synthesis will be tested in a reducing environment in order to determine the half-life ($t_{1/2}$) of release of kanamycin.

The reducing environment of the cell was mimicked using 10 mM DTT as it is within the normal range of free thiols present inside of a traditional cell.[27] In each experiment, ammonium acetate buffer (pH 7.4) was used, as it is compatible with electrospray ionization mass spectrometry (ESI-MS). The reactions were incubated at 37˚C and at the desired time points aliquots were removed for analysis by UPLC/MS. The mass of kanamycin (485 Da) was extracted from the overall mass spectrum of the reaction, and the integration was normalized with quinine

as an internal standard. From these data, the $t_{1/2}$ of kanamycin release was calculated for the two isomers, Figure 3.11.

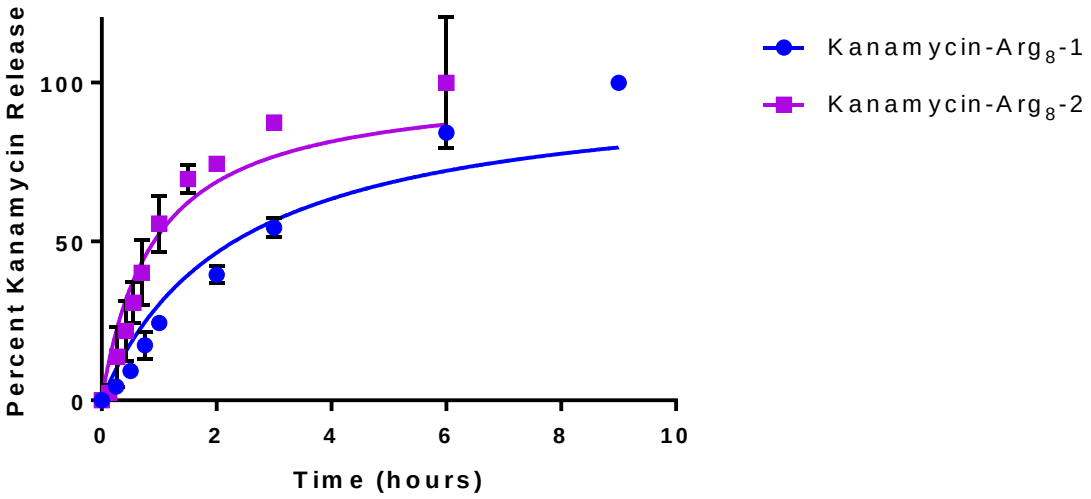

Figure 3.11 The release of kanamycin from Kanamycin-Arg_8 isomers 1 and 2 (50 μM) with DTT (10 μM) in ammonium acetate buffer (pH 7.4).

From the data, Kanamycin-Arg_8 isomer 1 has a $t_{1/2}$ of release of 2.3 ± 0.3 hours and Kanamycin-Arg_8 isomer 2 has a $t_{1/2}$ of release of 0.9 ± 0.1 hours. Therefore, isomer 2 releases kanamycin 2.5 times faster as compared to isomer 1. In an effort to understand this difference, we turned to some molecular modeling to gain insight on the difference in release between these isomers based on the environment of the ester groups.

3.2.3.1 Kanamycin-Arg_8 isomer 1

Kanamycin-SH isomer 1 was modelled in its fully protonated form, since the reaction was run at pH 7.4 (Figure 3.5). After an MM2 energy minimization, the carbonyl of the ester is seen to be in close proximity (<2 Å) to a protonated amine (k) of kanamycin (Figure 3.12). A proton in close proximity to the carbonyl could act as a Bronsted acid with the carbonyl, thus increasing the electrophilicity of the carbonyl carbon to the thiol, allowing for rapid release of the kanamycin.

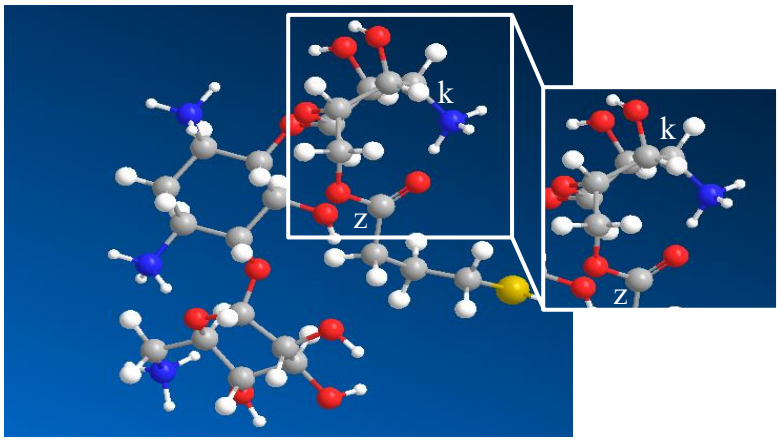

Figure 3.12 MM2 energy minimization of fully protonated kanamycin-SH (isomer 1), showing the protonated amine (K) in close proximity to carbonyl (Z) in the inset.

3.2.3.2 Kanamycin-Arg$_8$ isomer 2

Kanamycin-SH isomer 2 was modelled and energy minimized, as described for isomer 1 above (Figure 3.8). Interestingly, in the case of isomer 2, the carbonyl of the ester is in close proximity (<2 Å) to two protonated amines in kanamycin (O and Y) (Figure 3.13). Protons in close proximity to the carbonyl in 3-dimensional space could act as a Bronsted acid with the carbonyl, thus increasing the electrophilicity of the carbonyl carbon to the thiol even more, allowing for even more rapid release of the kanamycin, as compared to isomer 1.

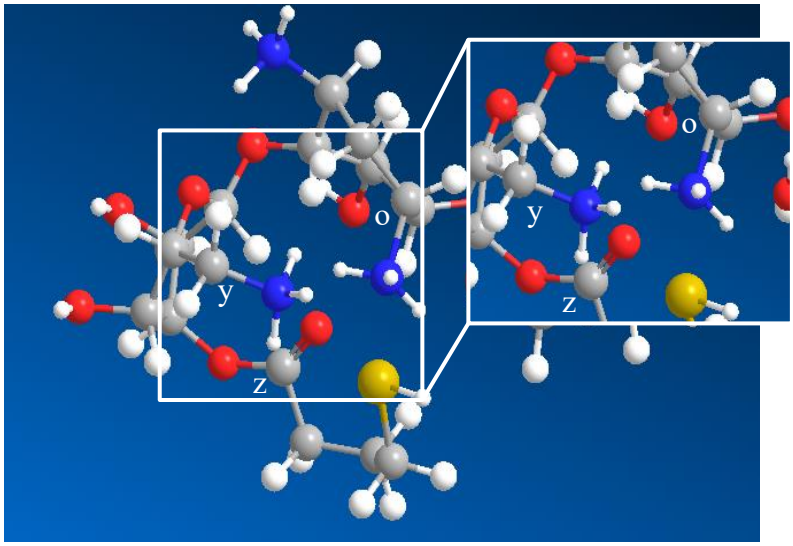

Figure 3.13 MM2 energy minimization of fully protonated kanamycin-SH (isomer 2), showing the protonated amines (Y and O) in close proximity to the carbonyl (Z) in the inset

3.3 Conclusions

Herein, a new synthetic methodology and its application are discussed. A new synthetic strategy was developed that includes a UV active kanamycin derivative that allows for the facile derivatization and purification of aminoglycosides. Two distinct isomers were isolated using this new methodology. These isomers were fully characterized using a range of 2D NMR techniques. Interestingly, there is a 2.5-fold difference in kanamycin release between these isomers. These differences were rationalized using an energy minimized models of each isomer. These models showed that the ester carbonyl is in close proximity to protonated amines (1 for isomer 1 and 2 for isomer 2), which may account for the observed difference in release of kanamycin. Overall, there is a perceivable difference in kanamycin release from Kanamycin-Arg_8 isomers 1 and 2. Therefore, this methodology can be used to expand the breadth of cell penetrating antibiotics in order to expedite the eradication of cellular bacterial reservoirs.

3.4 Materials and Methods

3.4.1 Materials

Kanamycin A was purchased from Santa Cruz Biotechnology (Dallas, TX). ChemMatrix Rink Amide Resin was purchased from PCAS BioMatrix Inc (Saint-Jean-sur-Richelieu, Quebec, Canada). Fmoc-Gly, Fmoc-Arg(pbf), 1-[Bis(dimethylamino)methylebe]-1H-1,2,3-triazolo[4,5-b]pyridium 3-oxid hexafluorophosphate (HATU), and 1-Hydroxy-7-azabenzotriazole (HOAt) were purchased from Ana Spec Inc (Fremont, CA). Dithiothreitol (DTT) was purchased from Roche (Indianapolis, IN). Ethanedithiol (EDT) was purchased from Alfa Aesar (Tewksbury, MA). 2,2' bisthiopyridine, Trifluoroacetic acid, N,N diisopropylethylamine (DIEA), N,N dimethylformamide (DMF), dichloromethane (DCM), methanol, triisopropylsilane (TIPS) and γ-thiobutriolactone were purchased from Sigma Aldrich (St. Louis, MO).

3.4.2 Methods

3.4.2.1 Synthesis of Kanamycin Boc_4

The synthesis of Kanamycin Boc_4 was carried out using a previously reported literature procedure, with some modifications.[28] Kanamycin (1g, 2.06 mmol), di-*tert*-butyldicarbonate (4.5 g, 20.6 mmol), with triethylamine (5.7 mL, 41.2 mmol) were added to a round bottom flask equipped with a stir bar. To this flask, a solution of methanol (20 mL) and water (10 mL) was added. The reaction was allowed to reflux at 50˚C overnight, during which time a white precipitate was formed. The reaction was then brought to room temperature and diluted with deionized water (100 mL). The white precipitate was then vacuum filtered and washed with water (100 mL, 3X). The white solid was collected, frozen and lyophilized. The desired product was obtained with a yield of 70%, and the ^{1}H NMR spectrum matched the previously reported NMR spectrum. ^{1}H NMR (400 MHz, DMSO) δ 6.88 (s, 1H), 6.57 (s, 1H), 6.49 (d, J = 9.2 Hz, 1H), 6.34 (s, 1H), 5.37 (d, J = 19.4 Hz, 1H), 5.24 (s, 1H), 4.89 (dd, J = 9.2, 4.3 Hz, 4H), 4.67 (d, J = 6.4 Hz, 1H), 4.19 (t, J = 5.2 Hz, 2H), 3.80 (d, J = 9.9 Hz, 1H), 3.61 – 3.17 (m, 28H), 3.06 (s, 2H), 1.79 (d, J = 12.7 Hz, 1H), 1.50 – 1.27 (m, 44H).

3.4.2.2 Synthesis of 2-mercaptopyridinyl-4-mercaptobutyric acid disulfide (a)

The synthesis of 2-mercaptopyridinyl-4-mercaptobutyric acid disulfide was carried out using previous literature procedure, with some modifications.[29] γ-thiobutriolactone (221 µL, 2.44 mmol) was added to a round bottom flask equipped with stir bar. Sodium hydroxide (aq, 262.5 mg/mL) was then added to the reaction flask. Upon addition, the reaction was refluxed at 110˚C for 15 min. The mixture was allowed to cool to room temperature and was combined with concentrated HCl (2 mL, 0˚C). The product was extracted with diethyl ether (4x, 5 mL), the combined organic layers were dried over sodium sulfate and concentrated *in vacuo*. The product was immediately suspended in degassed methanol (1.8 mL). In a separate flask, 2,2'-dithiodipyridine (1.35 g, 4.99 mmol) was suspended in N_2 degassed methanol, equipped with a stir bar. 4-thiobutyric acid solution was added dropwise to the stirring 2, 2'-dithiodipyridine solution. The reaction was allowed to stir for 12 hours at room temperature. The reaction mixture was concentrated under reduced pressure and subjected to flash silica gel chromatography (70:29:1, hexanes: ethyl acetate: acetic acid). The product fractions were pooled and concentrated under reduced pressure. The final product was isolated in a 65% yield. The NMR spectrum of the product matched the previously reported NMR spectrum. ^{1}H NMR (400 MHz, $CDCl_3$) δ 8.48 (d, *J* = 5.0 Hz, 1H), 7.68 (m, 2H), 7.10 (ddd, *J* = 7.2, 4.9, 1.3 Hz, 1H), 2.86 (t, *J* = 7.1 Hz, 2H), 2.51 (t, *J* = 7.2 Hz, 2H), 2.04 (p, *J* = 7.1 Hz, 2H).

3.4.2.3 Synthesis of Kanamycin Boc_4-2-thiopyridinyl tether (isomer 1 and 2)

Kanamycin Boc_4 (1.15g, 1.3 mmol), 2-mercaptopyridinyl-4-mercaptobutyric acid disulfide (a) (250 mg, 1.09 mmol), HATU (304 mg, 1.3 mmol), HOAt (177 mg, 1.3 mmol) and diisopropylethylamine (2.3 mL, 13 mmol) were added to a round bottomed flask equipped with stir bar and activated 4Å molecular sieves under a nitrogen atmosphere. To this flask, dry DMF (10 mL) was added at room temperature. The reaction was allowed to react for 72 hours at room temperature. The resulting crude reaction mixture was diluted with DMF (50 mL) and purified using RP-HPLC. The RP-HPLC solvents used were acetonitrile with 0.1% TFA (solvent A) and water with 0.1% TFA (solvent B). The crude mixture was purified using a C18 column (Phenomenex, USA) with a gradient of 50-65% solvent A (curve 9) at a flow rate of 12 mL/min over 60 minutes and visualized by UV at 254 nm. The product peaks (isomer 1 and 2) eluted at 27

and 29 minutes, respectively, with a yield of 5% and 5%, respectively. Isomer products (isomer 1 and 2) were characterized by ESI-MS (Expected: 1096, Observed: 1097.0, 1096.9 respectively). Isomer 2 was at this point fully characterized by NMR. ^{1}H NMR (800 MHz, DMSO) δ 8.45 (ddd, *J* = 4.6, 3.1, 1.7 Hz, 1H), 7.82 (tt, *J* = 7.7, 2.3 Hz, 1H), 7.76 (d, *J* = 8.0 Hz, 1H), 7.29 – 7.20 (m, 1H), 6.88 (s, 1H), 6.64 (d, *J* = 27.6 Hz, 1H), 6.49 (d, *J* = 9.3 Hz, 1H), 6.38 (s, 1H), 5.31 (s, 1H), 5.15 (dd, *J* = 22.0, 4.3 Hz, 1H), 5.02 – 4.85 (m, 2H), 4.65 (d, *J* = 6.8 Hz, 1H), 4.17 (d, *J* = 6.1 Hz, 1H), 3.86 – 3.79 (m, 1H), 3.68 (d, *J* = 9.5 Hz, 1H), 3.53 – 3.44 (m, 4H), 3.41 (t, *J* = 9.7 Hz, 1H), 3.34 (s, 8H), 3.29 – 3.17 (m, 2H), 2.88 (t, *J* = 7.2 Hz, 2H), 2.44 (t, *J* = 7.1 Hz, 2H), 1.90 (p, *J* = 7.2 Hz, 2H), 1.57 – 1.29 (m, 37H). ^{13}C NMR (800 MHz, DMSO) δ 13.92, 22.06, 23.66, 23.92, 27.99, 28.11, 28.20, 28.31, 28.98, 29.74, 31.25, 32.26, 34.67, 37.00, 37.03, 39.19, 39.29, 39.40, 39.50, 39.60, 39.71, 39.81, 39.86, 39.97, 40.94, 48.96, 49.87, 55.87, 60.24, 67.34, 67.63, 69.81, 70.29, 72.89, 74.73, 75.29, 77.17, 77.74, 77.79, 80.30, 84.16, 97.73, 100.88, 119.22, 121.09, 121.15, 137.77, 149.55, 154.87, 155.33, 156.04, 156.31, 159.14, 171.77. (Isomer 2 (1 and 2 D NMR spectra): Figures A26-A32)

3.4.2.4 Synthesis of Kanamycin-2-thiopyridinyl tether (isomer 1 and 2)

TFA (350 µL (isomer 1) or 305 µL (isomer 2)) and DCM (350 µL (isomer 1) or 305 µL (isomer 2)) were added to kanamycin boc_4-2-thiopyridinyl tether (isomer 1 or 2; 15.9 mg, 0.015mmol or 13.9 mg, 0.1268 mmol, respectively) in a 1 dram vial. The reaction was allowed to proceed at room temperature for 1 hour. The TFA was removed from the reaction vessel via rotary evaporation. The reaction mixture was treated with methanol (1 mL, 3X) and DCM (1 mL, 3X), and concentrated after each addition to facilitate the full removal of the TFA. The mixture of isomer 1 was placed on the high vacuum overnight. Isomer 2 was 96% pure before deprotection, therefore it was not further purified, just resuspended in deionized water, frozen and lyophilized. The mixture of isomer 2 was resuspended in deionized water and purified using RP-HPLC. The RP-HPLC solvents used were acetonitrile with 0.1% TFA (solvent A) and water with 0.1% TFA (solvent B). The mixture was purified using C18 column (Phenomenex, USA) with a gradient of 5-30% solvent A with a flow rate of 12 mL/min over 60 minutes and visualized by UV at 254 nm and eluted at 36 mins. Yields of 66% and quantitative were obtained, respectively for Kanamycin-2-thiopyridinyl tether (isomers 1 and 2) and were characterized via ESI-MS (Expected mass: 696.8 Da, Observed mass: 696.3 Da, 696.3 Da). At this point, isomer 1 was fully characterized by NMR.

^{1}H NMR (800 MHz, CD_3OD) δ 8.41 (ddd, *J* = 4.9, 1.8, 0.9 Hz, 1H), 7.85 (dt, *J* = 8.1, 1.2 Hz, 1H), 7.82 (td, *J* = 8.1, 7.7, 1.8 Hz, 1H), 7.24 (ddd, *J* = 7.3, 4.9, 1.2 Hz, 1H), 5.47 (d, *J* = 3.9 Hz, 1H), 5.06 (d, *J* = 3.6 Hz, 1H), 4.41 (dd, *J* = 12.2, 2.5 Hz, 1H), 4.25 (dd, *J* = 12.2, 3.4 Hz, 1H), 4.08 – 4.01 (m, 2H), 3.87 – 3.80 (m, 3H), 3.74 – 3.71 (m, 1H), 3.68 (dt, *J* = 14.7, 9.6 Hz, 2H), 3.63 (ddd, *J* = 12.4, 10.0, 4.2 Hz, 1H), 3.56 (dd, *J* = 9.6, 3.9 Hz, 1H), 3.51 (ddd, *J* = 12.6, 10.3, 4.2 Hz, 1H), 3.42 – 3.37 (m, 2H), 3.22 (dt, *J* = 10.0, 6.8 Hz, 1H), 3.03 (dd, *J* = 13.0, 9.1 Hz, 1H), 2.87 (t, *J* = 7.1 Hz, 2H), 2.54 – 2.50 (m, 3H), 2.01 (p, *J* = 7.2 Hz, 2H), 1.97 (q, *J* = 12.4 Hz, 1H). ^{13}C NMR (800 MHz, CD_3OD) δ 17.27, 18.70, 25.04, 28.97, 33.15, 38.73, 42.15, 48.68, 48.79, 48.90, 49.00, 49.11, 49.22, 49.32, 51.66, 55.85, 56.71, 63.24, 67.17, 70.11, 70.51, 72.31, 72.94, 72.96, 73.57, 74.44, 80.80, 85.64, 96.93, 102.44, 115.80, 117.25, 118.70, 120.16, 121.37, 122.48, 139.28, 150.38, 161.28, 162.57, 162.75, 162.92, 163.10, 174.40. (Isomer 1 (1 and 2D NMR spectra): Figures A19-25)

3.4.2.5 Synthesis of trityl-4-mercaptobutyric acid (b)

The synthesis of trityl-4-mercaptobutyric acid was carried out following a previous literature procedure with some modifications.[30] γ-thiobutriolactone (221 µL, 2.44 mmol) was added to a round bottom flask equipped with a stir bar. Sodium hydroxide (aq, 262.5 mg/mL) was then added to the reaction mixture. Upon addition, the reaction was refluxed at 110˚C for 15 min. The mixture was allowed to cool to room temperature and was combined with concentrated HCl (2 mL, 0˚C). The product was extracted with diethyl ether (4x, 5 mL), dried over sodium sulfate and concentrated. 4-thiobutyric acid was immediately added to trityl chloride (750 mg, 2.65 mmol) in 2.8 mL dry N,N' dimethylformamide. The reaction was allowed to stir for 48 hours. To an Erlenmeyer flask, 10% sodium acetate (Aq, 30 mL) was added. The reaction mixture was added to the Erlenmeyer flask. The mixture solidified upon addition. The precipitate was filtered and washed with water (50 mL, 3X). The precipitate was then collected and added to a round bottom flask equipped with a stir bar. The mixture was stirred in acetone at 50˚C for 30 min, allowed to cool to room temperature and was rotovapped to dryness. The precipitate was resuspended in methanol and left at 4˚C overnight. The supernatant was removed and the product was subjected to flash silica gel chromatography (60:40, ethyl acetate: hexanes). The product fractions were combined and concentrated. The final product was a white solid with a total 41.3% yield. The NMR spectrum of the product matched the previously reported NMR spectrum. ^{1}H NMR (400

MHz, $CDCl_3$) δ 7.29 (m, 17H), 2.31 (t, *J* = 7.4 Hz, 2H), 2.22 (t, *J* = 7.2 Hz, 2H), 1.67 (p, *J* = 7.3 Hz, 2H).

3.4.2.6 Synthesis of Arg_8-SH

Arg_8-SH peptide was synthesized via solid phase peptide synthesis using high loading (200 mg, 0.45 mmol/g) Chem Matrix H-Rink Amide Resin. Fmoc-arginine(pbf) (175.2 mg, 3 mmol) or Fmoc-glycine (80.3 mg, 3 mmol) was combined with HATU (102.7 mg, 3 mmol) and diisopropylethylamine (94 µL, 6 mmol) in DMF (8 mL). Each coupling reacted for 3 hours at room temperature. The amino acid mixture was drained and resin was washed with DMF, DCM, MeOH, DCM, and DMF (4 mL, 2X each). Next, piperidine (25% in DMF, 8mL) was added to the reaction flask. The contents of the reaction flask were allowed to react for 30 minutes. The piperidine solution was then drained and the resin was washed with DMF, DCM, MeOH, DCM, and DMF (4 mL, 2X). This process was repeated until all the amino acids were coupled to the resin. Couplings were monitored by Kaiser and Chloranil tests.

Upon synthesis of the Arg_8 peptide, the trityl-4-mercaptobutyric acid (97.9 mg, 3 mmol) was added to the resin with HATU (102.7 mg, 3 mmol) and diisopropylethylamine (94 µL, 6 mmol) in DMF (8 mL). This mixture was allowed to stir at room temperature for 3 hours. Amino acid solution was drained and the resin was washed with DMF, DCM, MeOH, DCM, and DMF (4 mL, 2X). Arg_8-SH was cleaved from resin and globally deprotected by treatment with a cleavage cocktail of 90:5:2.5:2.5, TFA:EDT:TIPS:H_2O and was reacted for 3 hours. The crude mixture was collected into a preweighed plastic falcon tube. The resin was washed with DCM (4 mL, 3X) and drained into the preweighed plastic falcon tube. The crude mixture was concentrated in vacuo. Cold diethyl ether (15 mL) was then added to the crude mixture, which will cause the crude peptide to precipitate. The supernatant was removed and the crude Arg_8-SH was dried under vacuum overnight. The crude Arg_8-SH was then resuspended in deionized water and was purified to homogeneity by RP-HPLC. The RP-HPLC solvents used were acetonitrile with 0.1% TFA (solvent A) and water with 0.1% TFA (solvent B). The crude was purified using a C18 column (Phenomenex, USA) with a gradient of 5-50% solvent A with a flow rate of 12 mL/min over 60 minutes and visualized by UV at 214 nm. The compound eluted at 20 minutes over this gradient. Final compound was obtained in 99% purity as measured on analytical RP-HPLC using a C18

column. The mass was confirmed using MALDI-TOF mass spectrometry (Expected Mass: 1424.87 Da, Observed Mass: 1426.1 Da).

3.4.2.7 Synthesis of Kanamycin-Arg_8 (isomer 1 and 2)

First, PBS buffer (pH 8) was degassed under nitrogen for 1 hour. Then, Kanamycin-2-thiopyridinyl tether (isomer 1: 9.7 mg, 0.014 mmol or isomer 2: 8.7 mg, 0.013 mmol) was dissolved in the PBS buffer (139 µL or 125 µL) and added to a 1.5 mL Eppendorf tube equipped with stir bar. Then, Arg_8-SH (8 mg, 0.006 mmol) was dissolved in the PBS (56 µL) and was added dropwise to the reaction vessel. The reaction was allowed to stir at room temperature for 12 hours. The crude mixture (isomer 1 or 2) was diluted with deionized water and purified using RP-HPLC. The RP-HPLC solvents used were acetonitrile with 0.1% TFA (solvent A) and water with 0.1% TFA (solvent B). The mixtures were purified using a C18 column (Phenomenex, USA) with a gradient of 5-30% solvent A with a flow rate of 12 mL/min over 60 minutes and visualized by UV at 214 nm. Isomer 1 eluted from the column at 35 mins and isomer 2 eluted at 37 minutes. Kanamycin-Arg_8 (isomer 1 and 2) were isolated in 99% purity with a yield of 50% and 28%, respectively. The conjugates were characterized by MALDI-TOF mass spectrometry (Expected mass: 2009 Da, Observed mass: 2009 Da, 2010 Da, respectively). (Analytical purity trace: Figure A2 and A3, MALDI: Figure A7 and A8).

3.4.2.8 Reduction of Kanamycin-Arg_8 isomers in the presence of DTT

The stability studies with DTT were adapted from a previously published protocol with some changes.[9] Kanamycin-Arg_8 (isomer 1 or 2, 50 µM) were incubated at 37 °C with 10 mM DTT in degassed ammonium acetate buffer (pH ~7.4) containing 5 µM quinine as the internal standard in 1.5 mL total volume. When monitoring kanamycin release, an aliquot of the reaction mixture was taken at different time points and directly analyzed by UPLC-MS. The time points were analyzed using UPLC/MS with a T3-C18 column consisting of solvent A (water and 0.1% formic acid) and solvent B (acetonitrile and 0.1% formic acid), a gradient of 0 - 3 (3 mins) – 50 (2 mins) % of solvent B, a flow rate of 0.5 ml/min, and a column temperature 40˚C. The peaks corresponding to the m/z for quinine (325.4), Kanamycin-Arg_8 (+5:403, +4:503), Kanamycin-SH (585), Kanamycin (485), and Arg_8-SH (+5:286, +4:357, +3:476, +2:713) were detected and extracted

using the MassLynx software. The experiments were run in triplicate, and the average percentage of release vs time was fitted using Graph Pad Prism 7 to generate $t_{1/2}$'s.

3.5 References

1. Thakur, A.; Mikkelsen, H.; Jungersen, G., Intracellular pathogens: host immunity and microbial persistence strategies. *J. Immunol. Res.* **2019**, 1356540.

2. Casadevall, A., Evolution of intracellular pathogens. *Annu. Rev. Microbiol.* **2008,** *62*, 19-33.

3. Carryn, S.; Chanteux, H.; Seral, C.; Mingeot-Leclercq, M.-P.; Van Bambeke, F.; Tulkens Paul, M., Intracellular pharmacodynamics of antibiotics. *Infect Dis Clin North Am* **2003,** *17* (3), 615-34.

4. Monack, D. M.; Mueller, A.; Falkow, S., Persistent bacterial infections: the interface of the pathogen and the host immune system. *Nat. Rev. Microbiol.* **2004,** *2* (9), 747-765.

5. Habault, J.; Poyet, J.-L., Recent advances in cell penetrating peptide-based anticancer therapies. *Molecules* **2019,** *24* (5), 927/1-927/17.

6. Bolhassani, A.; Jafarzade, B. S.; Mardani, G., In vitro and in vivo delivery of therapeutic proteins using cell penetrating peptides. *Peptides* **2017,** *87*, 50-63.

7. Gagat, M.; Zielinska, W.; Grzanka, A., Cell-penetrating peptides and their utility in genome function modifications (review). *Int. J. Mol. Med.* **2017,** *40* (6), 1615-1623.

8. Abdul Ghaffar, K.; Hussein, W. M.; Khalil, Z. G.; Capon, R. J.; Skwarczynski, M.; Toth, I., Levofloxacin and indolicidin for combination antimicrobial therapy. *Curr. Drug Delivery* **2015,** *12* (1), 108-114.

9. Brezden, A.; Mohamed, M. F.; Nepal, M.; Harwood, J. S.; Kuriakose, J.; Seleem, M. N.; Chmielewski, J., Dual targeting of intracellular pathogenic bacteria with a cleavable conjugate of kanamycin and an antibacterial cell-penetrating peptide. *J. Am. Chem. Soc.* **2016,** *138* (34), 10945-10949.

10. Defaus, S.; Gallo, M.; Andreu, D.; Abengozar Maria, A.; Rivas, L., A Synthetic strategy for conjugation of paromomycin to cell-penetrating Tat(48-60) for delivery and visualization into Leishmania parasites. *Int J Pept* **2017,** *2017*, 4213037.

11. Garcia, C. B.; Shi, D.; Webster, T. J., Tat-functionalized liposomes for the treatment of meningitis: an in vitro study. *Int. J. Nanomed.* **2017,** *12*, 3009-3021.

12. Li, Z.; Teng, D.; Mao, R.; Wang, X.; Hao, Y.; Wang, X.; Wang, J., Improved antibacterial activity of the marine peptide N6 against intracellular Salmonella typhimurium by conjugating with the cell-penetrating peptide Tat11 via a cleavable linker. *J. Med. Chem.* **2018,** *61* (17), 7991-8000.

13. Wang, Y.; Li, S.; Liu, L.; Feng, L., Photothermal-responsive conjugated polymer nanoparticles for the rapid and effective killing of bacteria. *ACS Appl. Bio Mater.* **2018,** *1* (1), 27-32.

14. Sparr, C.; Purkayastha, N.; Kolesinska, B.; Gengenbacher, M.; Amulic, B.; Matuschewski, K.; Seebach, D.; Kamena, F., Improved efficacy of fosmidomycin against Plasmodium and Mycobacterium species by combination with the cell-penetrating peptide octaarginine. *Antimicrob. Agents Chemother.* **2013,** *57* (10), 4689-4698.

15. Gomarasca, M.; Martins, T. F. C.; Greune, L.; Hardwidge, P. R.; Schmidt, M. A.; Rueter, C., Bacterium-derived cell-penetrating peptides deliver gentamicin to kill intracellular pathogens. *Antimicrob. Agents Chemother.* **2017,** *61* (4), e02545-16/1-e02545-16/20.

16. Li, Z.; Wang, X.; Teng, D.; Mao, R.; Hao, Y.; Yang, N.; Chen, H.; Wang, X.; Wang, J., Improved antibacterial activity of a marine peptide-N2 against intracellular Salmonella typhimurium by conjugating with cell-penetrating peptides-bLFcin6/Tat11. *Eur. J. Med. Chem.* **2018,** *145*, 263-272.

17. Ruczynski, J.; Kozlowska, A.; Alenowicz, M.; Rekowski, P.; Rusiecka, I.; Iwona, G. A.; Kocic, I.; Turecka, K.; Waleron, K.; Kawiak, A., Transportan 10 improves the pharmacokinetics and pharmacodynamics of vancomycin. *Sci Rep* **2019,** *9* (1), 3247.

18. Pereira, M. P.; Kelley, S. O., Maximizing the therapeutic window of an antimicrobial drug by imparting mitochondrial sequestration in human cells. *J. Am. Chem. Soc.* **2011,** *133* (10), 3260-3263.

19. Lei, E. K.; Pereira, M. P.; Kelley, S. O., Tuning the intracellular bacterial targeting of peptidic vectors. *Angew. Chem., Int. Ed.* **2013,** *52* (37), 9660-9663.

20. Pereira, M. P.; Shi, J.; Kelley, S. O., Peptide targeting of an antibiotic prodrug toward phagosome-entrapped mycobacteria. *ACS Infect. Dis.* **2015,** *1* (12), 586-592.

21. Horton, K. L.; Stewart, K. M.; Fonseca, S. B.; Guo, Q.; Kelley, S. O., Mitochondria-penetrating peptides. *Chem. Biol. (Cambridge, MA, U. S.)* **2008,** *15* (4), 375-382.

22. Yousif, L. F.; Stewart, K. M.; Horton, K. L.; Kelley, S. O., Mitochondria-penetrating peptides: sequence effects and model cargo transport. *ChemBioChem* **2009,** *10* (12), 2081-2088.

23. Fair, R. J.; Hensler, M. E.; Thienphrapa, W.; Dam, Q. N.; Nizet, V.; Tor, Y., Selectively guanidinylated aminoglycosides as antibiotics. *ChemMedChem* **2012,** *7* (7), 1237-1244, S1237/1-S1237/26.

24. Onyango, J. O.; Chung, M. S.; Eng, C.-H.; Klees, L. M.; Langenbacher, R.; Yao, L.; An, M., Noncanonical amino acids to improve the pH response of pHLIP insertion at tumor acidity. *Angew. Chem., Int. Ed.* **2015,** *54* (12), 3658-3663.

25. Cheetham, A. G.; Ou, Y.-C.; Zhang, P.; Cui, H., Linker-determined drug release mechanism of free camptothecin from self-assembling drug amphiphiles. *Chem. Commun. (Cambridge, U. K.)* **2014,** *50* (45), 6039-6042.

26. Lin, R.; Cheetham, A. G.; Zhang, P.; Lin, Y.-a.; Cui, H., Supramolecular filaments containing a fixed 41% paclitaxel loading. *Chem. Commun.* **2013,** *49* (43), 4968-4970.

27. Meister, A., Glutathione metabolism and its selective modification. *J. Biol. Chem.* **1988,** *263* (33), 17205-8.

28. Disney, M. D.; Barrett, O. J., An aminoglycoside microarray platform for directly monitoring and studying antibiotic resistance. *Biochemistry* **2007,** *46* (40), 11223-11230.

29. Tokutake, N.; Miyake, Y.; Regen, S. L., Bridging group effects on nearest-neighbor recognition within fluid phospholipid membranes. *Langmuir* **2000,** *16* (1), 81-86.

30. Yang, Q.; Bai, L.; Zhang, Y.; Zhu, F.; Xu, Y.; Shao, Z.; Shen, Y.-M.; Gong, B., Dynamic covalent diblock copolymers: instructed coupling, micellation and redox responsiveness. *Macromolecules* **2014,** *47* (21), 7431-7441.

CHAPTER 4. A CELL PENETRATING DUAL ANTIBIOTIC CONJUGATE, TOBRAMYCIN-P14LRR

4.1 Introduction

Peptides are ubiquitous in nature and are very useful as antibiotics. For instance, antimicrobial peptides (AMPs) have commonly been referred to as host defense peptides.[1] AMPs are effective antibacterial agents with unique modes of action, and therefore may be an attractive avenue for new antibiotics.[2] Another subclass of peptides that are particularly useful for antibiotic purposes are cell penetrating peptides. Cell penetrating peptides (CPPs) are effective intracellular delivery vehicles, able to deliver a wide variety of cargo including protein, nucleic acids and antibiotics.[3-8] Therefore, CPPs are useful tools in order to deliver therapeutics intracellularly, as described in Chapter 3. [8-10]

Recently, a new scaffold that exhibits both, cell penetration and antibacterial effectiveness has been developed. This class of peptides has become known as cationic amphipathic polyproline helices or CAPHs. Structurally, CAPHs are comprised of unnatural proline amino acids functionalized with hydrophobic and cationic groups, that adopt a polyproline II helix with three residues per turn. Therefore, every third residue is displayed on the same face with a 10 Å pitch (Figure 4.1a and b).[11] In this way, the hydrophobic residues are clustered on one face of the helix and the cationic groups occupy the other face (Figure 4.1c). The design and utility of CAPHs has evolved overtime. The important characteristics inherent in CAPHs design, and ultimately effectiveness, are the rigidity, amphiphilicity and length.[7, 11-20]

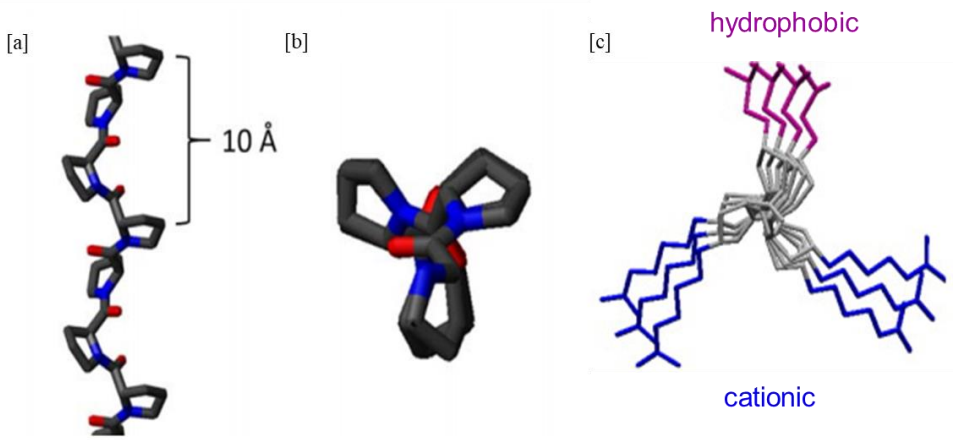

Figure 4.1 Polyproline type II helix [a] side view, [b] top down view, [c] CAPHs scaffold (top down) showing the amphipathic faces, with hydrophobic in purple and the cationic groups in blue.

The importance of amphiphilicity, for instance was probed with a scrambled CAPH where the hydrophobic and cationic residues were mixed on the face of the helix.[11] A 7-fold decrease in cell uptake was found when scrambling the residues as compared to the amphipathic CAPH. Therefore, the importance of amphiphilicity on cell uptake of the CAPH scaffold was solidified (Figure 4.1c).

It was of further interest to determine the ideal hydrophilic and hydrophobic residues in order to design the most potent CAPHs, for intracellular accumulation and antibacterial efficacy. First, the hydrophilic moiety was probed with a proline residues containing either an amino or guanidinium group.[11] There was 23-fold higher intracellular accumulation of the CAPH containing guanidinum groups as compared to the amine variant (Figure 4.2).

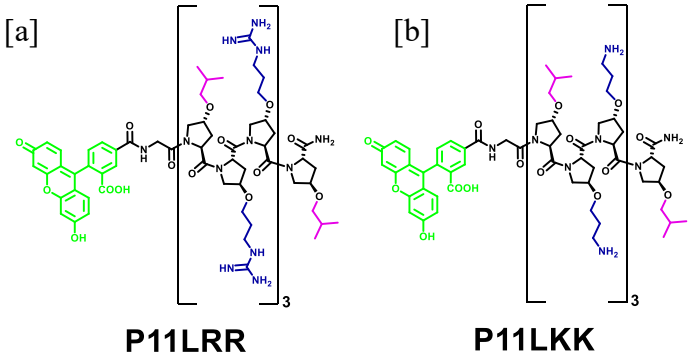

Figure 4.2 [a] P11LRR structure and [b] P11LKK structures compared for intracellular accumulation.

With the ideal hydrophilic residue for intracellular accumulation determined, the effect of the variation of the hydrophobic moiety has been probed. In an initial study, the isobutyl functionality of P11LRR was substituted for a phenyl, in two of the four repeating hydrophobic residues of P11, making P11LRR and P11F/LRR (Figure 4.3a and b), respectively.[19] P11LRR, P11F/LRR and Tat were tested against a variety of cancer cell lines (MCF7 (breast cancer), HOS (bone cancer), HT1080 (connective tissue cancer), HeLa (cervical cancer), KB 3-1(HeLa derivative) and KB-FD(KB with overexpression of folate receptor) and a non-cancer cell line (WI 38) in order to probe cellular accumulation within certain cell types. P11LRR and P11F/LRR preferentially localized into specific cells over others (MCF7 cells and KB 3-1, respectively) as compared to Tat which accumulated in all the tested cell types without discrimination. Subcellular localization of P11LRR and P11F/LRR were then probed in MCF7 cells. P11LRR colocalization matched previously reported results, wherein it was visualized across the cell and in a few punctate vesicles.[11, 14] Conversely, P11F/LLR was visualized exclusively in punctate vesicles. Overall, changing the hydrophobic moiety seems to direct cellular specificity and subcellular localization.

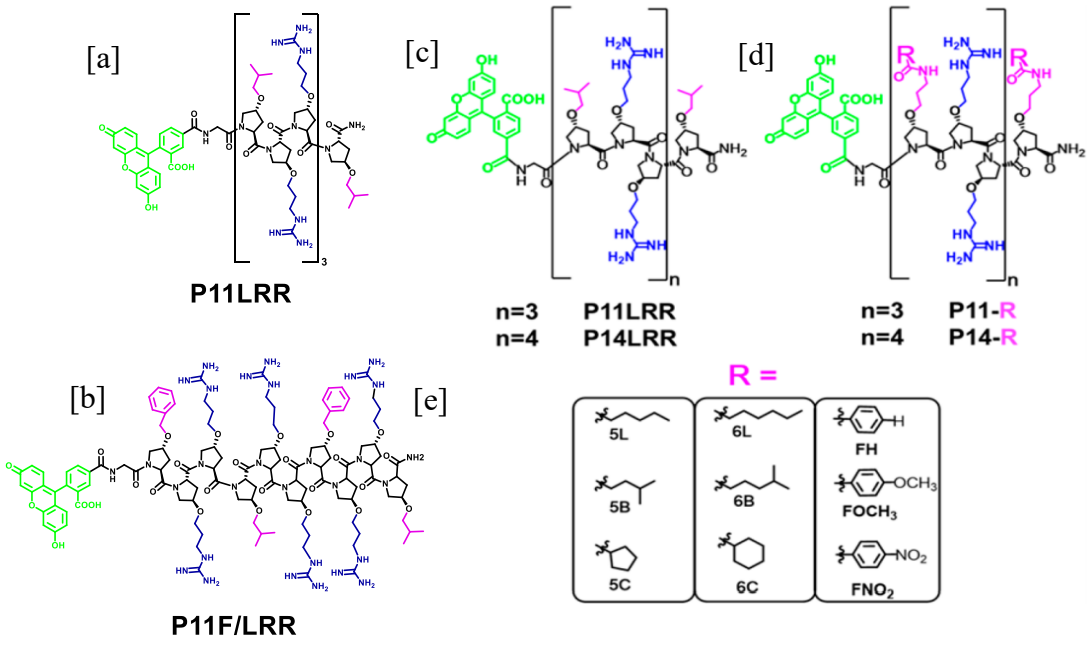

Figure 4.3 CAPHs library to probe the effects of changing the hydrophobic moieties; [a] the parent P11LRR, and [b] a benzyl substituted P11F/LRR derivative. [c] The parent peptides P11LRR and P14LRR, with 3 and 4 triad repeats, respectively, and [d] the peptide library with hydrophobic modifications, with [e] the different hydrophobic moieties that make up this library.

Further studies changed the hydrophobic residues to probe the difference in cellular accumulation, antibiotic efficacy and subcellular localization, using a library-based approach.[16] Instead of synthesizing unique amino acids for each member of the library, as was previously done, an on resin derivatization method was used, in order to efficiently synthesize a diverse library. The library contained three and four repeating triads, P11 and P14, respectively (Figure 4.3 c) with hydrophobic residues containing either 5 carbon moieties (linear (L), branched (B), or cyclic (C)), 6 carbon groups (linear (L), branched (B), or cyclic (C)), or phenyl substituents (phenyl, p-methoxyphenyl, or p-nitrophenyl) (Figure 4.3d and e). The library was first assessed based on intracellular accumulation of the peptides. The peptides which were able to accumulate inside of the cell as well or better than P14LRR were targeted. Based on intracellular accumulation and cell viability, three members of the library emerged as superior, the P14-5L, P14-5B and P14-5C. The P14 5-carbon compounds were further characterized to determine antibacterial activity and subcellular localization.

Starting with confocal experiments, it was determined that there was a difference in the subcellular localization of the 3 CAPHs, with the linear and branched compounds localizing in the cytoplasm within a 15 minute incubation, with some endosomal, mitochondrial and nuclear localization. Conversely, the P14-5C showed mostly endosomal localization after 15 min and 1 hour incubation times. All 3 CAPHs demonstrated good activity against *Salmonella*, *Shigella*, and *Listeria in vitro*. These CAPHs, however, demonstrated different levels of intracellular clearance based on their colocalization with bacteria within mammalian cells. For instance, with intracellular *Salmonella*, which commonly localizes in endosomes,[21, 22] the P14-5C peptide (80% clearance) more effectively cleared the *Salmonella* infection as compared to the P14-5L peptide (60% clearance). Thus, the peptide's subcellular localization confers specificity towards effective clearance of pathogens in different subcellular compartments. Therefore, overall, modification of the hydrophobic residues allows for increased intracellular accumulation and antibacterial potency. Further, modifying the hydrophobic residue also directs subcellular localization of the peptide, which may allow for targeted antibacterial agents.

Changing the residues of CAPHs can drastically change intracellular accumulation and antibiotic activity, and this effect has also been seen in changing the peptide length of CAPHs (Figure 4.4). The first generation of CAPHs, P11LRR, was able to accumulate inside cells approximately 9-fold better than the known cell penetrating peptide Tat.[11] When the 3 repeat

residues of P11LRR were expanded to 4, in P14LRR, the cellular accumulation increased 7 and 12-fold at concentrations of 10 and 15 µM, respectively.[15] Similarly, the modest antibiotic activity of P11LRR against *E. coli* and *S. aureus* (60 µM and 60 µM, respectively) was enhanced significantly, by elongating the peptide to P14LRR (4 µM and 12 µM, respectively). The peptide was further elongated to 5 repeating units, P17LRR, and again there was an observed increase in intracellular accumulation by 2.5 to 3.5-fold across concentrations of 5 to 25 µM, as compared to P14LRR. Further, antibacterial efficacy of P17LRR was enhanced by 2 and 3-fold, respectively, with MIC of 2 µM for *E. coli* and 4 µM for *S. aureus*. The increase, though significant, was certainly not as dramatic as the increase from P11LRR to P14LRR.[13] Hence, there seems to be a threshold in the elongation of CAPHs to obtain effective cell penetration and antibacterial activity.

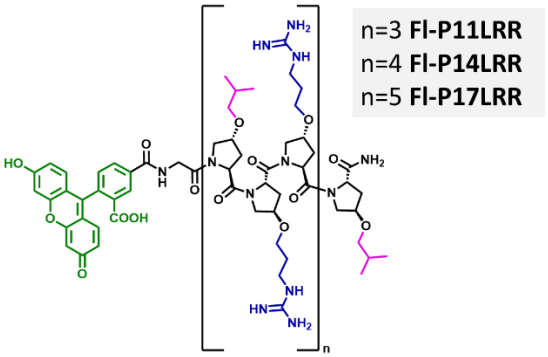

Figure 4.4 CAPHs structures investigating the affect of length on overall intracellular accumulation and antibacterial activity.

As described in Chapter 3, this class of peptides was further modified to enhance antibacterial efficacy. A known aminoglycoside antibiotic, kanamycin, was conjugated to the CAPH peptide P14LRR to generate P14KanS (Figure 4.5).[7]

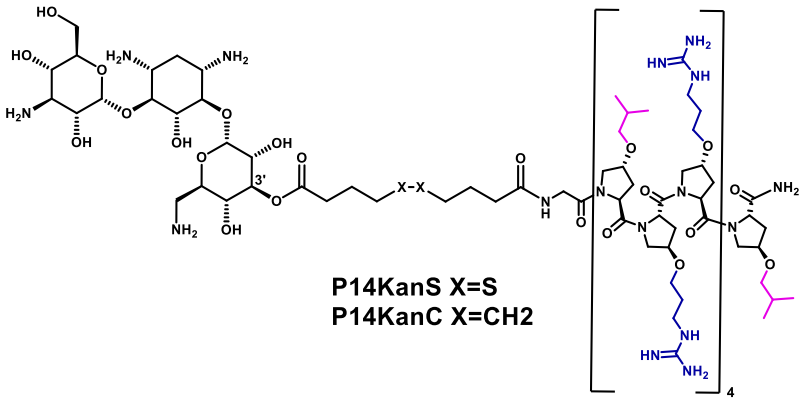

Figure 4.5 Structures of P14KanC and P14KanS, which were probed for increased intracellular antibiotic efficacy, as compared to the parent peptide P14LRR.

The conjugation of kanamycin to P14LRR (reversibly with disulfide and irreversibly without disulfide) enhanced the antibacterial activity as compared to both component monomers. For instance, the reversibly linked conjugate, P14KanS, showed synergistic clearance of *S. enteritidis*, *B. abortus*, and *M. tuberculosis* with 95, 85 and 93% bacterial clearance, respectively. The irreversibly linked kanamycin-P14LRR conjugate, P14KanC, cleared 60%, 50%, and 30% bacterial clearance, against the same bacteria. Therefore, it has been shown there is a therapeutic advantage to a reversible linker, and this reversible design will be utilized herein.

Even though the P14KanS conjugate is a potent antibiotic, kanamycin on its own is traditionally considered a second-line antibiotic due to its many side effects, such as damage to hearing, sense of balance, and the kidneys.[23] Therefore, replacing kanamycin with a first-line treatment would result in enhanced antibacterial efficacy. Tobramycin, an aminoglycoside antibiotic, is a first-line treatment against Gram negative infections, such as *P. aeruginosa*, particularly in patients with cystic fibrosis.[24] *P. aeruginosa* is an opportunistic infection which has the propensity to infect mammalian cells and to form biofilms, making it particularly difficult to treat. Therefore, a cell-penetrating conjugate of tobramycin could be particularly advantageous.

Tobramycin has previously been conjugated to antibiotics and cell-penetrating peptides. For instance, the Schweizer group conjugated tobramycin to other antibiotics, such as polymyxin B_3, in order to make antibiotic adjuvants against various bacteria, such as *P. aeruginosa* (Figure 4.7a).[25-31] These conjugates demonstrated potent activity against multidrug resistant and extensively drug resistant clinical isolates of *P. aeruginosa*. Further, the Kasko/Wong groups engineered a cell-penetrating peptide that disrupts bacterial cell membranes.[32, 33] The peptide

conjugate, Pentobra, successfully killed *E. coli* and *S. aureus* persister strains 4-6 logs better than tobramycin alone. These studies confirm that tobramycin is an ideal candidate for conjugation with P14LRR to further enhance its antibacterial activity.

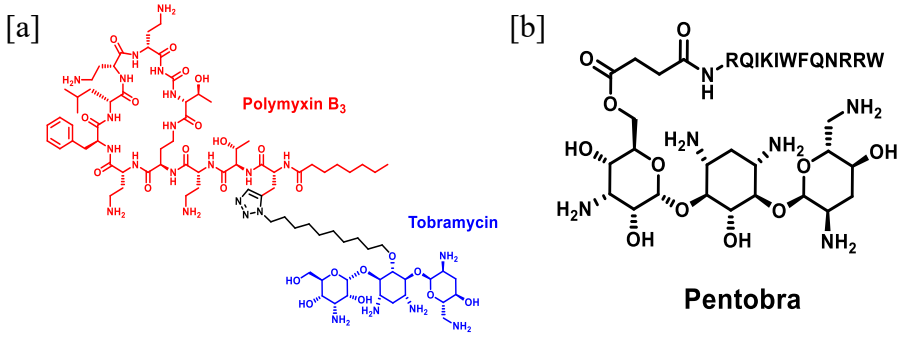

Figure 4.6 [a] The Tobramycin-Polymycin B_3 conjugate for enhanced antibiotic efficacy and [b] Pentobra, the cell penetrating peptide with tobramycin conjugate for increased antibiotic efficacy against persister cells.

Herein, we disclose the synthesis and application of reversible tobramycin-P14LRR conjugates for the treatment of intracellular pathogens. Tobramycin, a non-UV active aminoglycoside moiety, was conjugated to P14LRR using the new UV active intermediate strategy developed in Chapter 3. The synthesis, isolation, characterization, antibacterial activity, reversibility in a reducing environment, cytotoxicity and intracellular antibacterial activity for the tobramycin-P14LRR conjugates are reported herein.

4.2 Results and Discussion

4.2.1 Design

We created a reversibly-linked, cell-penetrating conjugate with the aminoglycoside, tobramycin, and the broad-spectrum antibiotic/cell-penetrating peptide, P14LRR, conjugated with a reversible disulfide linker (Figure 4.8). Within the reducing environment of the cell, the disulfide moiety should reduce into free thiols (Figure 4.9). The free thiol, tobramycin-SH, should intramolecularly rearrange to release active tobramycin inside the cell. The P14LRR-SH will retain the thiol tether, but it contains the same antibacterial activity of P14LRR alone.[7] We hypothesize

that this design will lead to a cell-penetrating dual antibiotic conjugate, that will synergistically clear intracellular bacteria.

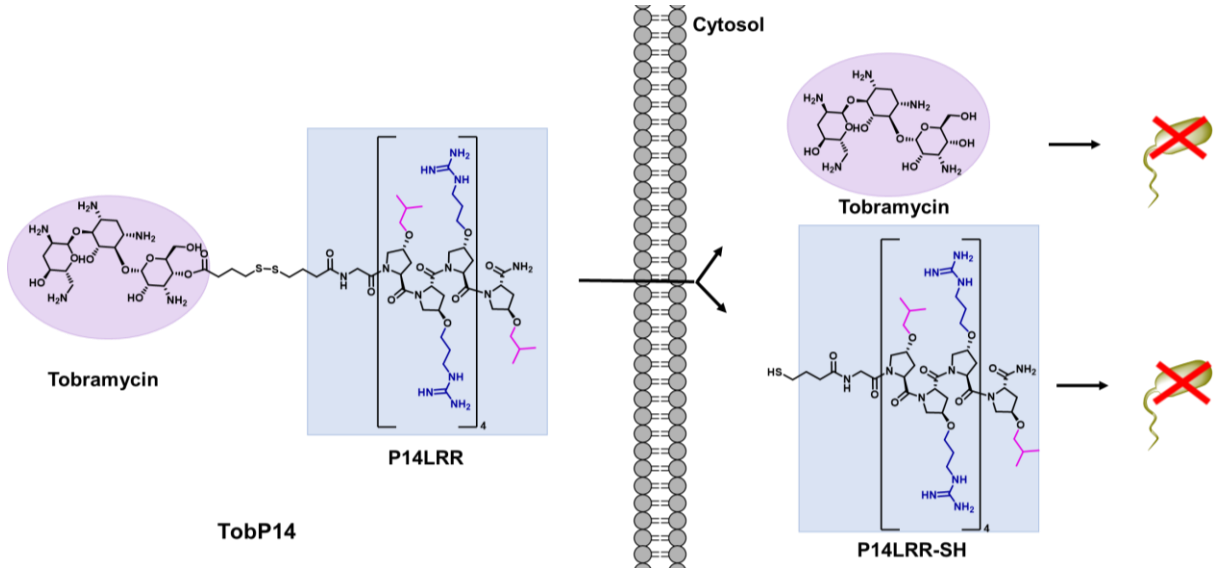

Figure 4.7 Dual TobP14 conjugate for cellular delivery of two antibiotic agents: tobramycin and P14LRR-SH.

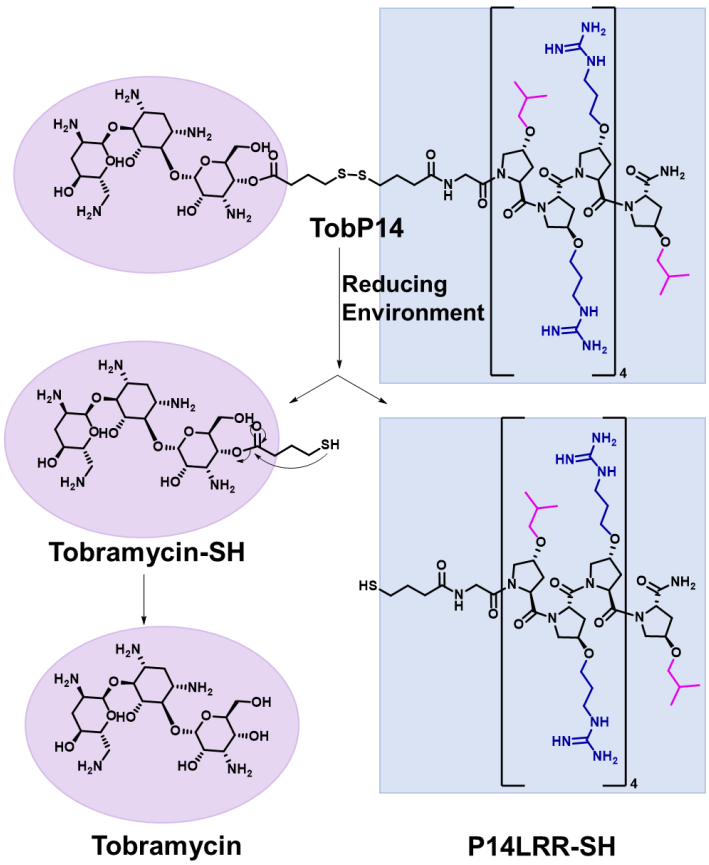

Figure 4.8 Reversible TobP14 conjugate design that allows for the release of tobramycin and P14LRR-SH in the reducing environment of the cell.

4.2.2 Synthesis

4.2.2.1 Synthesis of the P14LRR-SH Peptide

The unnatural amino acids Fmoc-P_L and Fmoc-P_R were synthesized as previously described (Scheme 4.1).[11]

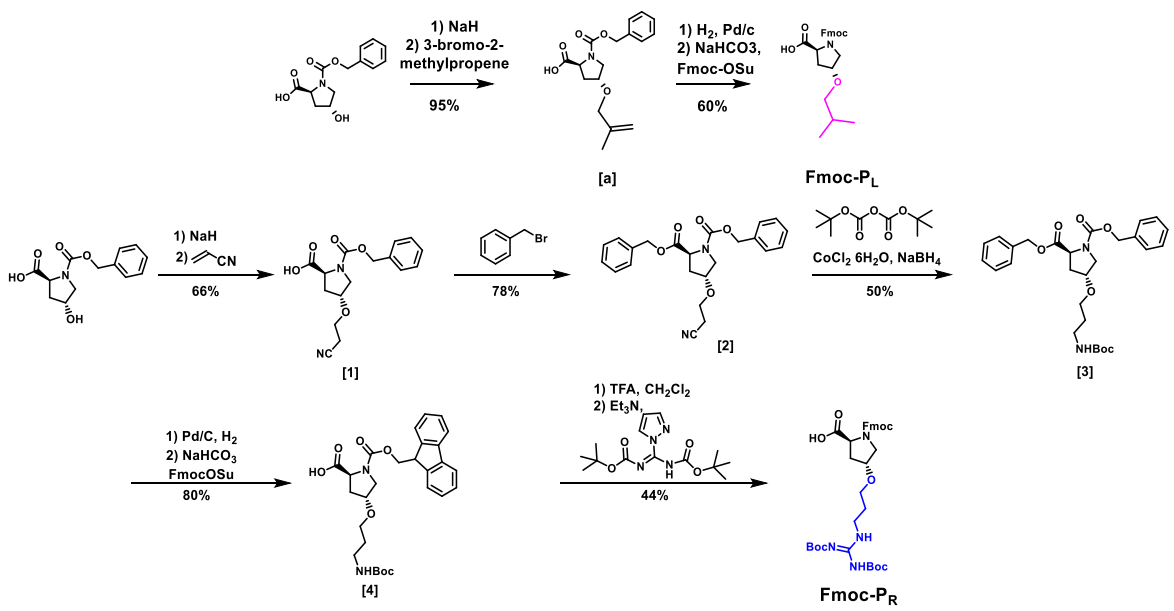

Scheme 4.1 Synthesis of non-natural amino acids, Fmoc-P_L and Fmoc-P_R.

P14LRR-SH was synthesized via solid phase peptide synthesis using high loading (0.45 mmol/g) ChemMatrix H-Rink Amide Resin (Scheme 4.2). Upon synthesis of the P14LRR peptide, the trityl-4-mercaptobutyric acid [b] was coupled via HATU and DIEA in DMF. At this point, P14LRR-SH was globally deprotected and cleaved from the resin. P14LRR-SH was purified on RP-HPLC to homogeneity, and the mass was confirmed via MALDI-TOF mass spectroscopy.

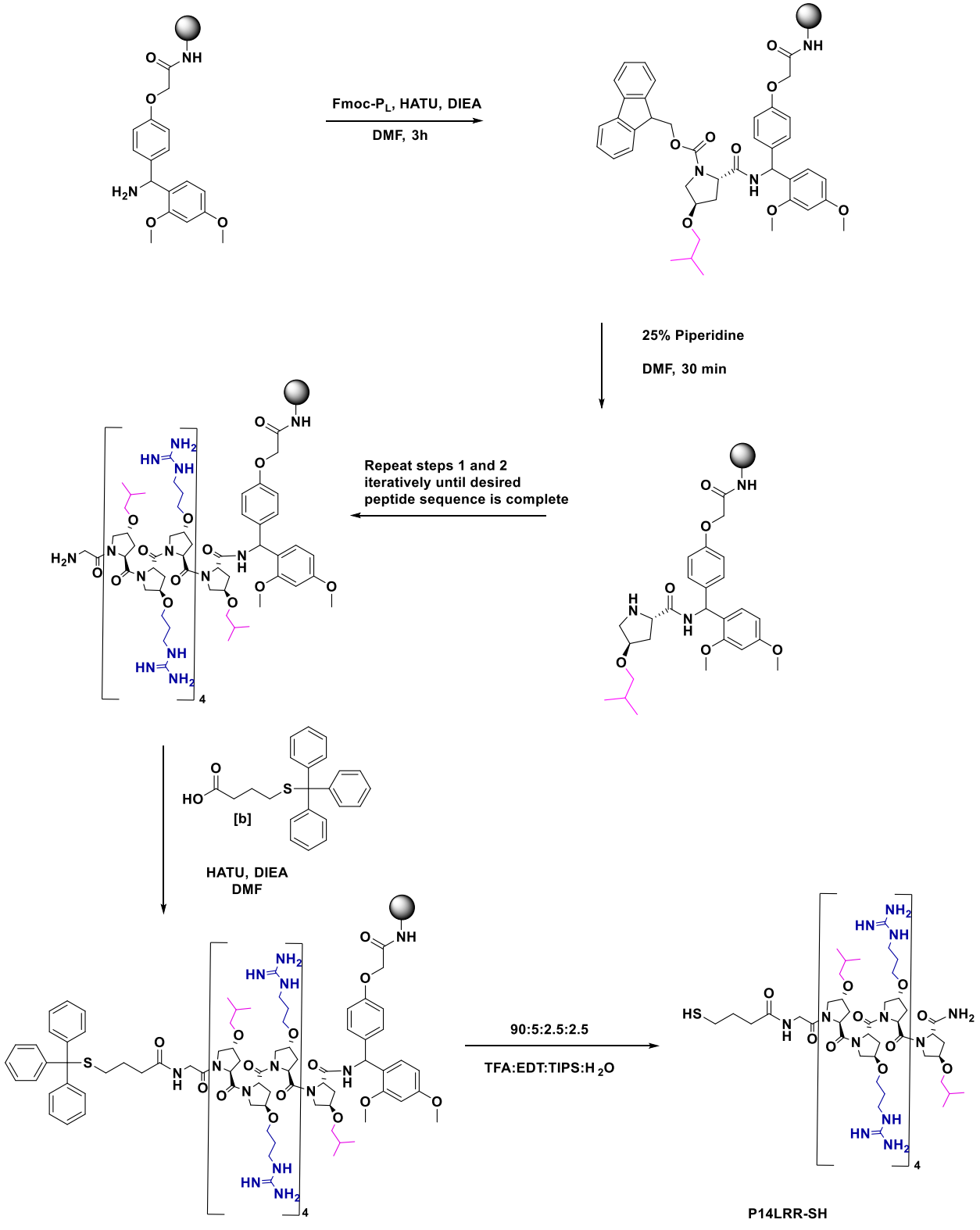

Scheme 4.2 Synthesis of P14LRR-SH.

4.2.2.2 Synthesis of Tobramycin-activated thiol conjugates

For the synthesis of Tobramycin-P14LRR, first the amine groups of tobramycin were protected with the acid labile *tert*-butyloxycarbonyl group (boc) to afford Tobramycin Boc_5 (Scheme 4.3). Tobramycin Boc_5 was then reacted with 2-mercaptopyridinyl-4-mercaptobutyric acid disulfide [c] using HATU, HOAt, and DIEA in DMF to yield the UV active Tobramycin Boc_5-2-thiopyridinyl tether. In this step, two distinct isomers were isolated by RP-HPLC, isomer A and isomer B (Scheme 4.3). Tobramycin Boc_5-2-thiopyridyl tether isomer A and B were then Boc-deprotected using 1:1 TFA:DCM to yield Tobramycin-2-thiopyridinyl tether, isomers A and B. At this point, each isomer was fully characterized by ^{1}H, ^{13}C, COSY, HSQC, and HMBC NMR spectroscopy in collaboration with Dr. John Harwood in the Purdue NMR facilities, as described below.

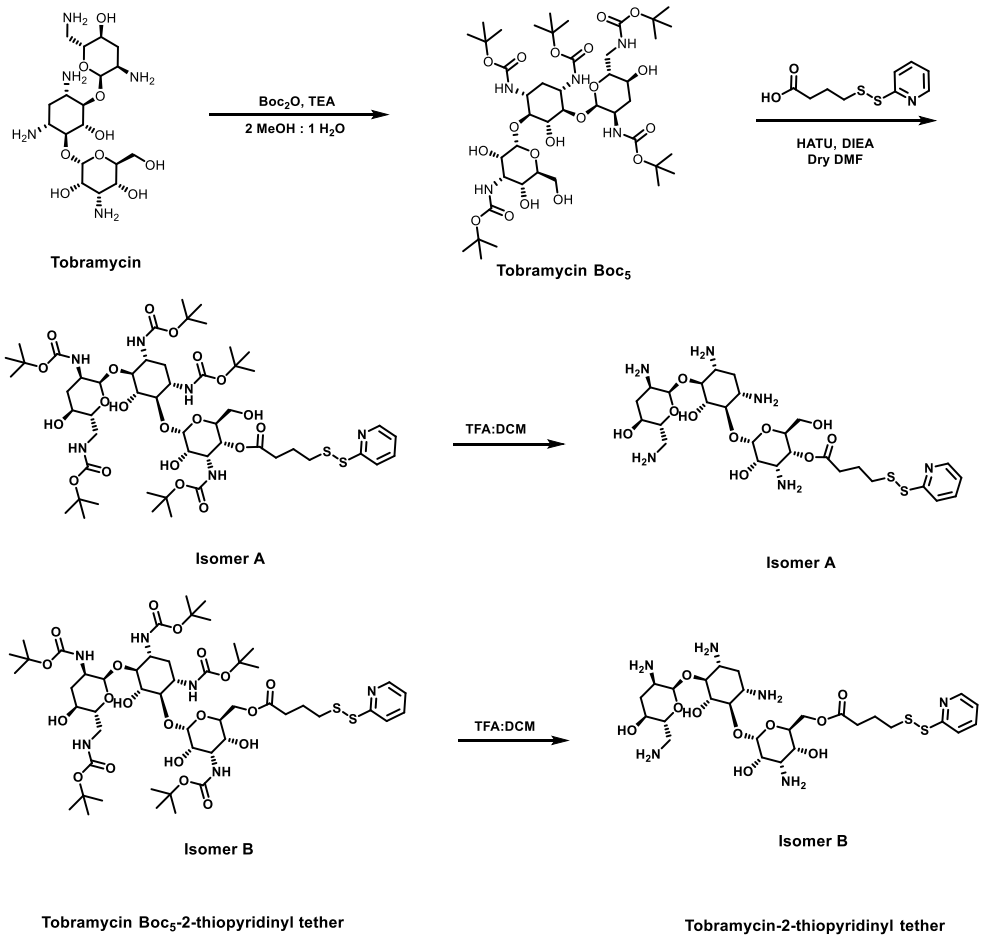

Scheme 4.3 Synthesis of Tobramycin-2-thiopyridinyl tether isomers A and B.

4.2.2.3 NMR characterization of Tobramycin-2-thiopyridinyl tether-A

Tobramycin-2-thiopyridinyl tether isomer A was fully characterized ^{1}H, ^{13}C, COSY, TOCSY, DEPT-135, HSQC, and HMBC NMR techniques in order to determine the location of the ester in Tobramycin-2-thiopyridinyl tether isomer A (Figure 4.10). The comparison of the 2D techniques, namely the COSY, TOCSY, DEPT-135, HSQC and HMBC NMRs, allowed for the peak assignment of each ^{1}H (Figure 4.11) and ^{13}C (Figure A34) peak. Each 2D technique will be briefly described to explain the precise identification of the 1D NMR peaks. First, it is important to note that DEPT-135 is a 2D carbon technique which identifies carbons as methylenes or methines based on their orientation in the spectrum. Within the DEPT-135 spectrum, positive peaks indicated a methine or a methyl and a negative peak indicated a methylene. DEPT-135 was useful in identifying the different carbons within the molecule, as there were far fewer methylenes in the overall structure. After the identification of each of the methylenes and methines, their orientation in the overall molecule was then identified by other 2D techniques. COSY and TOCSY are proton versus proton 2D NMR techniques which helped to identify which protons were directly adjacent to one another (COSY) and which protons were in close proximity, for instance, which protons are on the same ring (TOCSY). Identification of each proton was further facilitated by heteroatom 2D NMR techniques, specifically HSQC and HMBC. These techniques compare protons with carbons. Starting with the short range 2D heteronuclear NMR technique HSQC. A correlation peak in an HSQC spectra indicated protons which are directly attached to the carbon. To facilitate the identification of each proton and carbon peak further, one additional technique, HMBC, was used. HMBC correlates protons and carbons that are separated by multiple bonds (2-4), which allowed for the identification of protons in close proximity to carbons. Using each of these techniques, each carbon and proton peak were precisely identified.

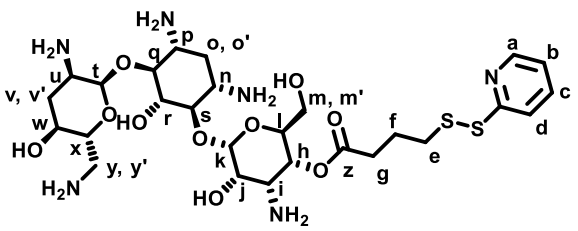

Figure 4.9 Tobramycin-2-thiopyridinyl tether isomer A.

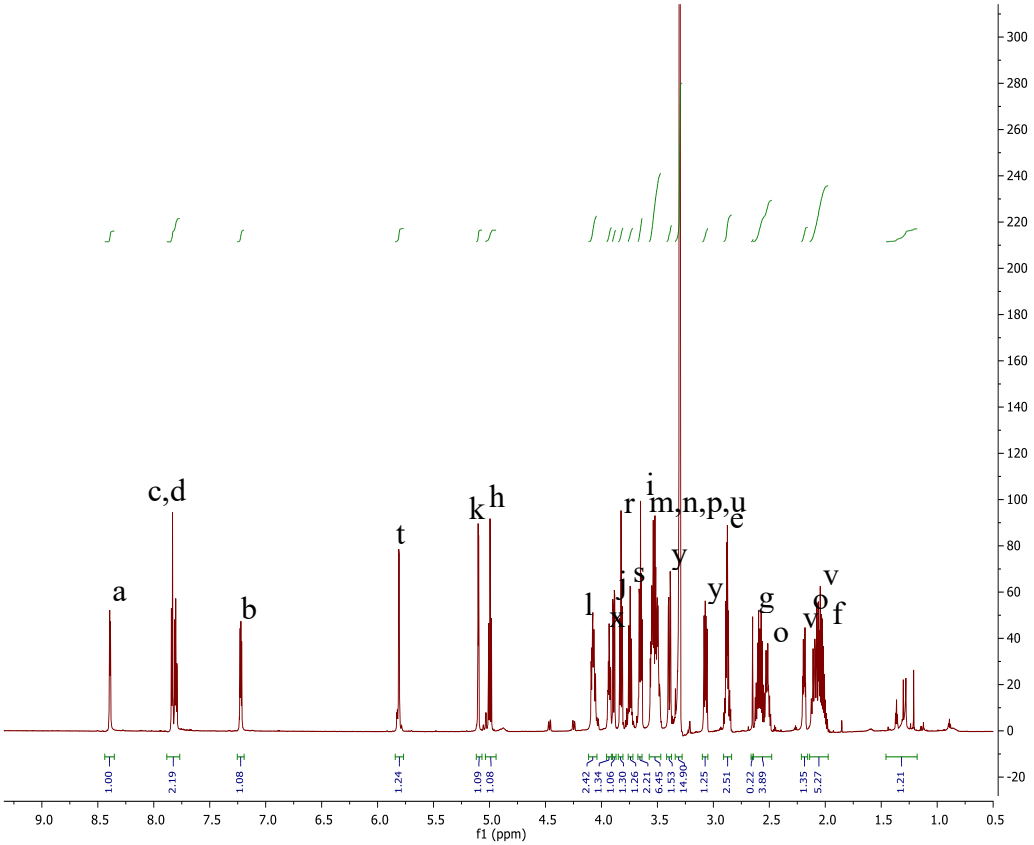

Figure 10 Tobramycin-2-thiopyridinyl tether isomer A ^{1}H NMR in CD_3OD. Each of the peaks were identified by comparison of the ^{1}H, ^{13}C, COSY, TOCSY, DEPT-135, HSQC and HMBC.

In order to further corroborate the identification of the location of the ester on Tobramycin-2-thiopyridinyl tether isomer A, the heteroatom 2D techniques, HSQC and the HMBC, were also used (Figure 3.12). Starting with the HSQC, which is a 2D NMR technique which crosses carbon NMR with the proton NMR, correlation with this short-range technique indicated which protons were directly attached to the carbons. Therefore, in order to pinpoint the connectivity, the carbon technique DEPT-135 was crossed with the ^{1}H NMR spectrum (Figure 4.12a). The DEPT-135 spectrum is seen vertically on the left-hand side of the chromatogram. First, the carbon, labelled (h), is seen as a positive peak, which indicates that this is a methine carbon. The cross of this methine carbon (h) highlights the one expected proton (h), identified in the top ^{1}H chromatogram. This, once again, indicates that this proton (h) is directly attached to methine carbon (h). Further, in the HMBC (Figure 4.12b), which is a long-range heteroatom correlation, the ^{13}C spectrum (left) is crossed with the ^{1}H spectrum (top). In this case, proton (h), as identified before as a proton

directly attached to methine carbon (h), crosses with a carbon peak at 175 ppm. A carbon at this shift is a carbonyl carbon, as identified as (z) (Figure 3.10). Therefore, there is a correlation between carbonyl carbon (z) and proton (h) on the HMBC spectrum, indicating that Tobramycin-2-thiopyridinyl tether isomer A is esterified on the secondary hydroxyl (h) of tobramycin.

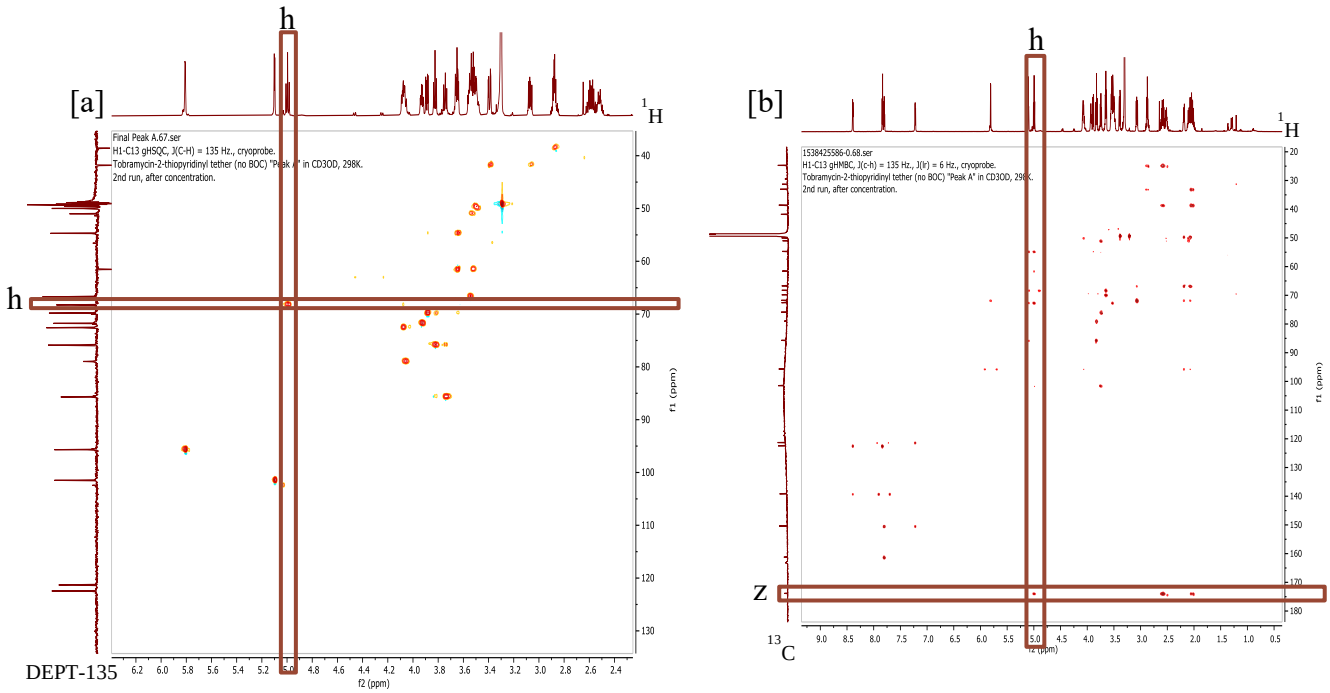

Figure 4.11 [a] The DEPT-135 -^{1}H HSQC of Tobramycin-2-thiopyridinyl tether A showing the correlation between methine carbon (h) and proton (h). [b] The ^{13}C -^{1}H HMBC of Tobramycin-2-thiopyrdinyl tether A showing the correlation between methine proton (h) and carbonyl carbon (z).

4.2.2.4 NMR characterization of Tobramycin-2-thiopyridinyl tether-B

Tobramycin-2-thiopyridinyl tether isomer B was fully characterized ^{1}H, ^{13}C, COSY, TOCSY, DEPT-135, HSQC, and HMBC NMR techniques in order to determine the location of the ester in Tobramycin-2-thiopyridinyl tether isomer B (Figure 4.11). The comparison of the 2D techniques, namely the COSY, TOCSY, DEPT-135, HSQC and HMBC NMRs, allowed for the peak assignment of each ^{1}H (Figure 4.14) and ^{13}C (Figure A41) peak. Each of the peaks were identified using the same techniques as previously described for Tobramycin-2-thiopyridinyl tether isomer A.

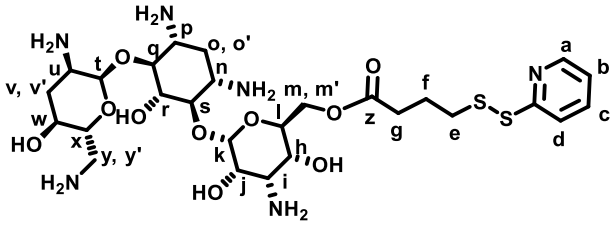

Figure 4.12 Tobramycin-2-thiopyridinyl tether isomer B.

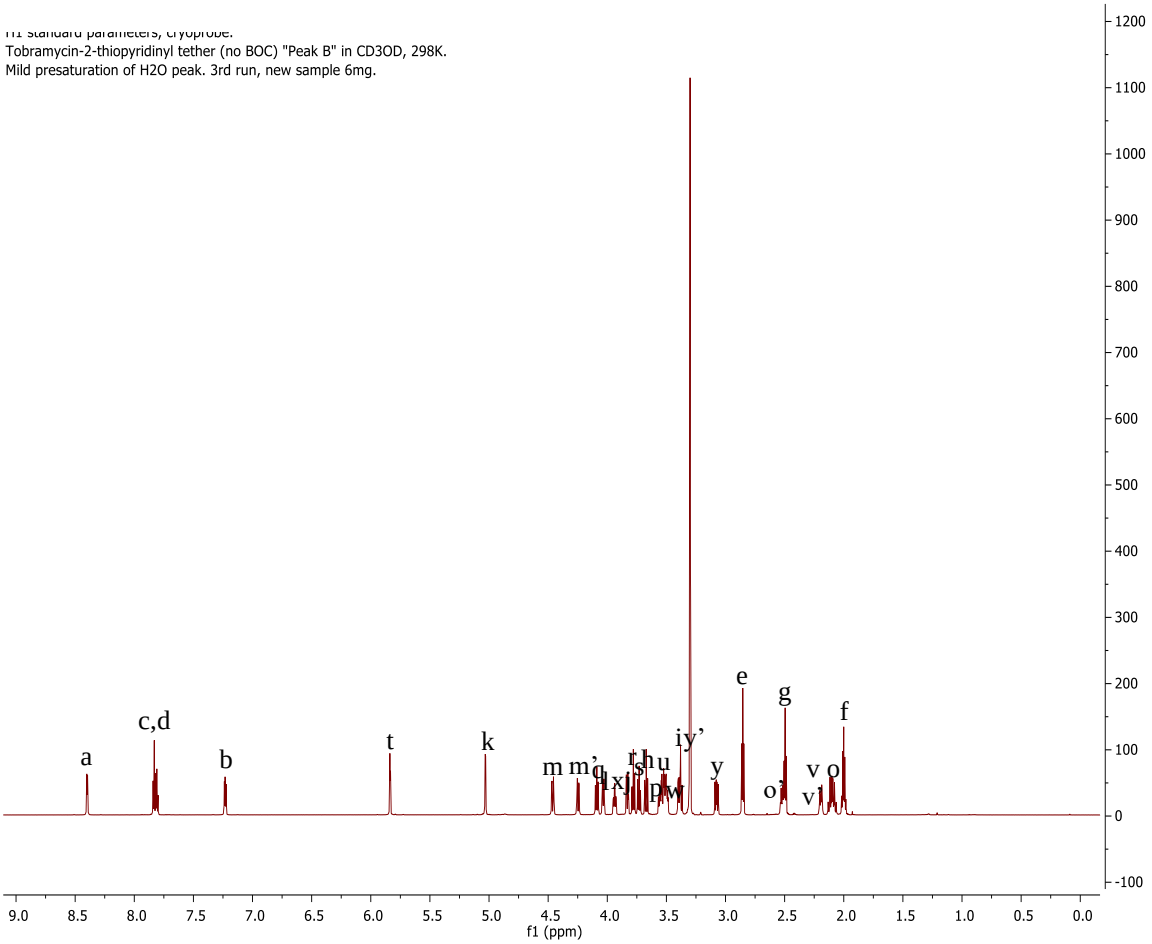

Figure 4.13 Tobramycin-2-thiopyridinyl tether B ^{1}H NMR in CD_3OD. Each of the peaks were identified by comparison of the ^{1}H, ^{13}C, COSY, TOCSY, DEPT-135, HSQC and HMBC.

To identify the location of the Tobramycin-2-thiopyridinyl tether isomer B, DEPT-135 spectrum (left) was crossed with the ^{1}H NMR spectrum in the HSQC (Figure 4.15a). First, the carbon, labelled (m), is seen as a negative peak, which indicates that this is a methylene carbon.

The cross of this methylene carbon (m) highlights the two expected protons (m) and (m'), identified in the top ^{1}H spectrum. This, once again, indicates that these protons (m and m') are directly attached to methylene carbon (m). Next, in the HMBC (Figure 4.15b), which is a long-range proton-carbon correlation, the ^{13}C spectrum (left) is crossed with the ^{1}H spectrum (top). In this case, proton (m), as identified before as a proton directly attached to methylene carbon (m), crosses with a carbon peak at 175 ppm. A carbon at this shift is a carbonyl carbon, as identified as (z) (Figure 3.13). Therefore, there is a correlation between carbonyl carbon (z) and proton (m) on the HMBC spectrum, indicating that Tobramycin-2-thiopyridinyl tether isomer B is esterified on the primary hydroxyl (m) of tobramycin.

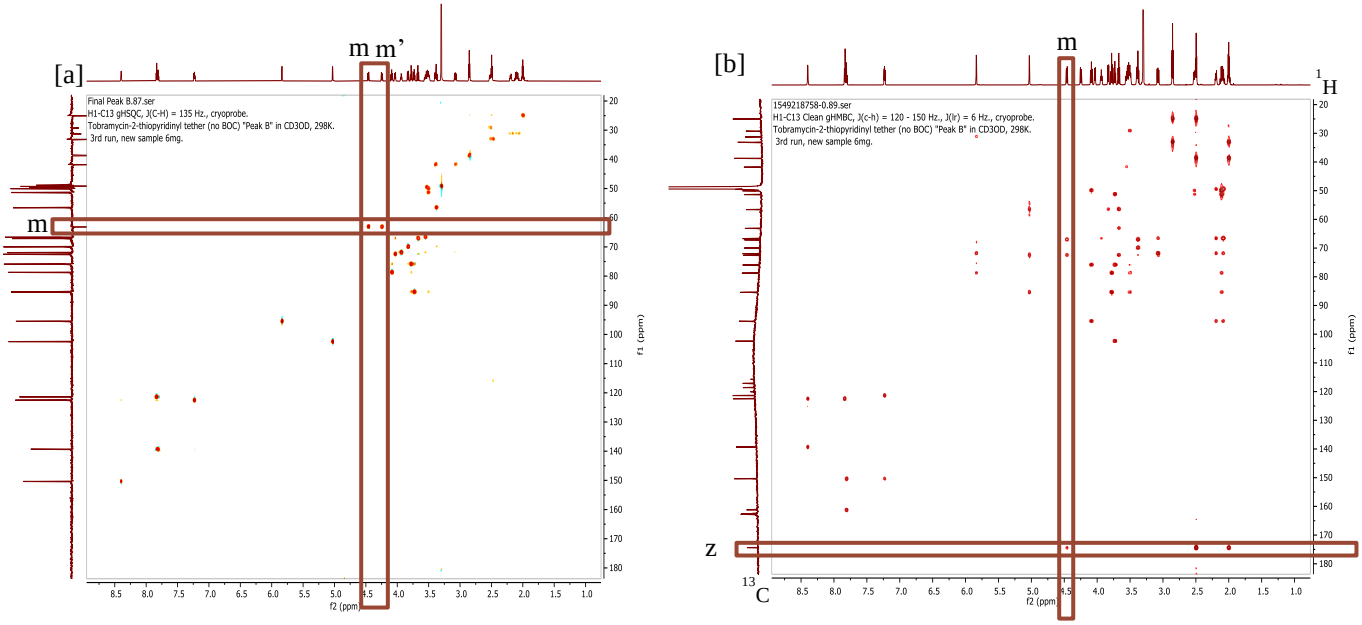

Figure 4.14 [a] The DEPT-135-^{1}H HSQC of Tobramycin-2-thiopyridinyl tether isomer B showing the correlation between methylene carbon (m) and proton (m). [b] The ^{13}C -^{1}H HMBC of Tobramycin-2-thiopyridinyl tether isomer B showing the correlation between methylene proton (m) and carbonyl carbon (z).

4.2.2.5 Synthesis of Tobramycin-P14LRR isomers A and B

Each of the tobramycin-2-thiopyridinyl tether compounds (isomer A or B) and P14LRR-SH were combined in PBS pH 8 buffer and allowed to stir for 12 hours. Upon RP-HPLC purification, the final products Tobramycin-P14LRR isomer A (TobP14-A) and Tobramycin-P14LRR isomer B (TobP14-B) were isolated (Scheme 4.4). After synthesis and isolation of the

two distinct isomers of the desired conjugate, TobP14, their mass was confirmed by MALDI-TOF mass spectroscopy.

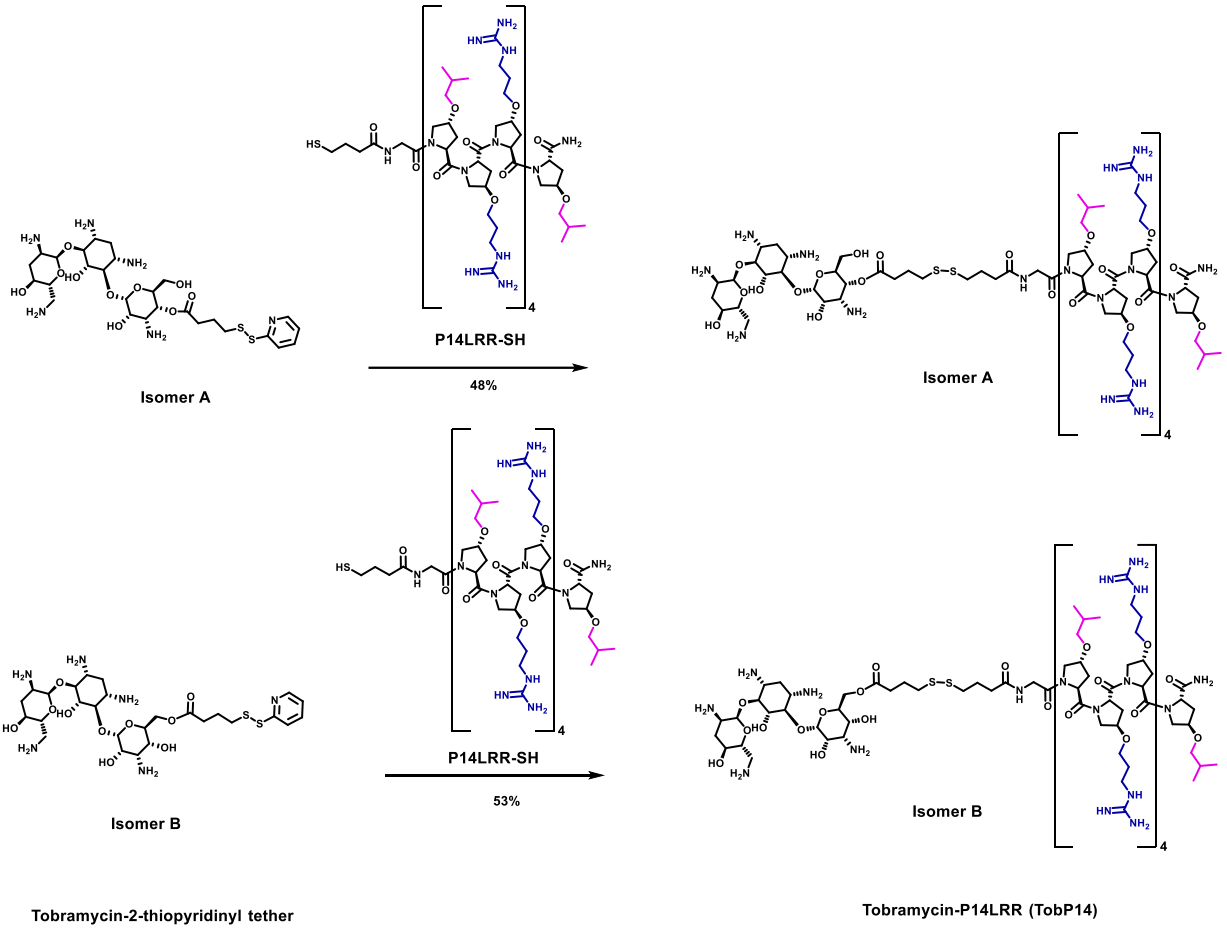

Scheme 4.4 The synthesis of tobramycin-P14LRR, TobP14 (isomers A and B).

4.2.3 Antibiotic Activity of TobP14 A and B

The antibiotic activity of TobP14 isomers (A and B) were probed against various Gram positive and negative strains of the bacteria *A. baumannii*, *P. aeruginosa*, *S. aureus*, and *S. epidermidis*. For each bacteria strain, a minimum inhibitory concentration (MIC) for TobP14 (isomers A and B) and various controls (P14LRR, tobramycin, a 1:1 mixture of tobramycin:P14LRR, gentamicin, and vancomycin), were determined using a microbroth dilution assay (Table 4.1).

For *A. baumannii*, two drug resistant strains (1605 and 19606) were tested with TobP14 isomers A and B and the various controls. Across both strains of *A. baumannii* (1605 and 19606), TobP14 isomers (A and B) displayed potent MIC values of A: 4 and 2 μM and B: 2 and 2 μM, respectively (Table 4.1). Further, TobP14 isomers A and B were more effective in clearing bacteria than tobramycin, gentamicin and vancomycin (Table 4.1). TobP14 (A and B) were also at least as potent as P14LRR alone for each strain, and both TobP14 isomers were approximately as potent as the 1:1 mixture of tobramycin:P14LRR.

Next, two drug resistant strains of *P. aeruginosa* (48982 and 31040) were then tested with TobP14 A and B, with the various controls. For *P. aeruginosa* 48982, TobP14 A and B displayed MICs of 16 and 8 μM, respectively and for *P. aeruginosa* 31040 had MICs of 4 and 4 μM, respectively (Table 4.1). Though potent MIC values were obtained against both strains, there was a difference between the strains as compared to the controls. First, for *P. aeruginosa* 48982, both TobP14 isomers (A and B) were more potent than all of the controls (tobramycin, P14LRR, a 1:1 mixture of tobramycin:P14LRR, gentamicin and vancomycin). However, in the case of *P. aeruginosa* 31040, TobP14 A and B were more effective in clearing bacteria than gentamicin, vancomycin and P14LRR alone. Though both isomers displayed impressive MICs (4μM) both TobP14 A and B were less potent than tobramycin and a 1:1 mixture of tobramycin:P14LRR with MICs of 1 μM (Table 4.1). Though less potent, all MIC values are within the same order of magnitude. Perhaps the covalent linkage within the isomers has slightly perturbed the potency against this strain (31040). If this is the case, in an intracellular environment, the release of the individual antibiotics (tobramycin and P14LRR) should mitigate this effect. Regardless, across both *P. aeruginosa* strains (48982 and 31040), TobP14 A and B were more potent than gentamicin, vancomycin, and P14LRR alone. For *P. aeruginosa* 31040, tobramycin and 1:1 tobramycin:P14LRR were more potent than TobP14 A and B, however for *P. aeruginosa* 48982, TobP14 A and B contained superior antibacterial activity as compared to tobramycin and a 1:1 mixture of tobramycin:P14LRR (Table 4.1).

Next, three *S. aureus* strains were tested (6538, MRSA 300 and MRSA 400) with TobP14 A and B and the various controls, as described above. Across all strains, TobP14 isomers (A and B) displayed MICs of ≤4 μM (Table 4.1). In all cases, TobP14 A and B were able to more effectively clear bacteria than P14LRR alone. Conversely, tobramycin, a 1:1 mixture of tobramycin:P14LRR, gentamicin and vancomycin were all more potent than TobP14 A and B

against all strains of *S. aureus* tested. Although not as efficacious as many of the controls, TobP14 isomers (A and B) still displayed MIC values of ≤4 μM across all strains, which is potent activity against *S. aureus*, overall.

Finally, a strain of *S. epidermidis* (NRS 101) was tested with TobP14 A and B, with the various controls, as above. TobP14 A and B displayed MICs of 1 and 0.5 μM, respectively. TobP14 A and B were able to more effectively clear bacteria than tobramycin, P14LRR, a 1:1 mixture of tobramycin:P14LRR and gentamicin. TobP14 A and B were also at least as potent as vancomycin against this strain of *S. epidermidis*. Therefore, TobP14 A and B are extremely potent against *S. epidermidis* NRS 101.

Table 4.1 MIC (μM) of TobP14 A and B compared to P14LRR, Tobramycin, a 1:1 mixture of Tobramycin:P14LRR, Gentamicin and Vancomycin against various strains of opportunistic pathogens

	A baumannii 1605	*A baumannii 19606*	*P. aeruginosa 48982*	*P. aeruginosa 31040*	*S aureus 6538*	*MRSA 300*	*MRSA 400*	*S. epidermidis NRS 101*
P14LRR	4	8	>32	>32	16	>32	>32	4
Tobramycin + P14LRR	2	2	32	1	0.25	2	1	2
Free Tobramycin	16	16	>32	1	0.25	1	0.5	8
Isomer A	4	2	16	4	2	4	2	1
Isomer B	2	2	8	4	1	2	2	0.5
Gentamicin	64	64	128	128	0.25	0.5	0.25	32
Vancomycin	128	128	>128	>128	0.5	0.5	1	1

4.2.4 Cell Viability in the presence of TobP14 A and B

Inherent in the design of the TobP14 conjugates is selective toxicity against invasive bacteria without harming the mammalian cell. Such a feature would allow the conjugates to be used as antibiotics against intracellular pathogens. In order to probe the conjugates' cytotoxicity, an MTT assay was performed using J774A.1 macrophage cells. J774A.1 macrophage cells were

chosen as the model cell line because macrophage cells are commonly infected with intracellular bacteria. J774A.1 macrophage cells were incubated with the TobP14 A and B and compared to the parent peptide P14LRR for 9 hours when administered at concentrations ranging from 1-32 µM (Figure 4.16).

TobP14 B and the control (P14LRR) remained ≥ 80% viable up to 16 µM. TobP14A is approximately 100% viable, until 16 µM, where it dips to approximately 70% viable. By 32 µM, all compounds dip below 40% viability. TobP14 A remains approximately 100% viable from 1-8 µM. By 16 µM, TobP14 A becomes approximately 80% viable. At 32 µM, TobP14 A dips to less than 40% viable (Figure 4.16). Taken together, TobP14 A and B are ≥70% viable up to 16 µM. Therefore, both conjugates can be used with J774A.1 macrophage cells up to 16 µM in the various intracellular antibacterial studies with minimal cytotoxicity.

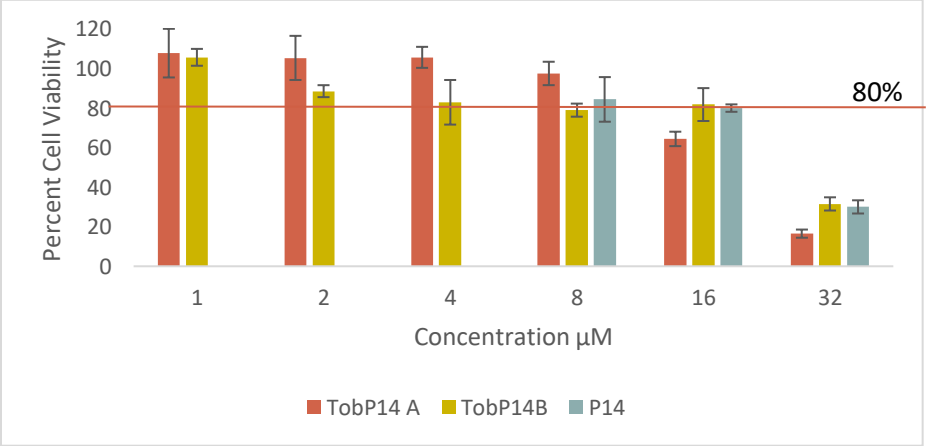

Figure 4.15 The cytotoxicity of TobP14 A and B with J774A.1 macrophage cells using an MTT assay after a 9 hour incubation of compounds.

4.2.5 Kinetics of Release of tobramycin from TobP14 A and B

TobP14 (isomers A and B) conjugates were designed to enter a mammalian cell and, within the intracellular reducing environment, ultimately release tobramycin and P14LRR-SH (Figure 4.9). In order to probe this design, the TobP14 isomers (A or B, 50 µM) were treated with 10 mM dithiothreitol (DTT) in ammonium acetate buffer (pH 7.4). Tobramycin release was monitored using UPLC/MS and the half-life of release ($t_{1/2}$) was calculated for the two isomers, Figure 4.17.

Interestingly, the different TobP14 isomers (A and B) had different $t_{1/2}$ of tobramycin release. For TobP14 A the $t_{1/2}$ for tobramycin release was 0.01 ± 0.008 hr. In contrast, TobP14 B

has a $t_{1/2}$ for tobramycin release of 1.3 ± 0.2 hrs. While both TobP14 isomers demonstrate rapid tobramycin release, this 130-fold difference in their half-lives is significant.

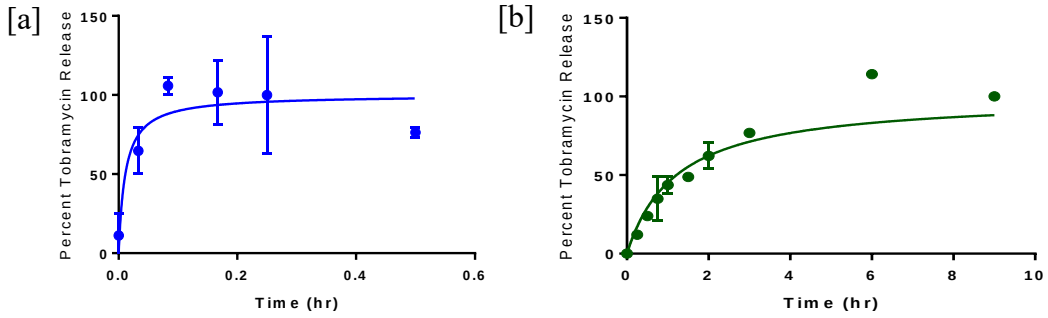

Figure 4.16 [a] Tobramycin release from TobP14 A (50 µM) when incubated with DTT (10 mM) in ammonium acetate buffer (pH 7.4). [b] Tobramycin release from TobP14 B 50 µM) when incubated with DTT (10 mM) in ammonium acetate buffer (pH 7.4).

4.2.5.1 Energy minimization of TobP14 A

In an effort to understand this difference between the reductive release of tobramycin between the isomers, we turned to molecular modelling. Initially, Tobramycin-SH isomer A was modelled in its fully protonated form, since the reduction reaction was performed at a pH of 7.4 (Figure 4.10). After MM2 energy minimization, the alkoxy group of the ester (h) seems to be in close proximity with a protonated amine moiety (i) (Figure 4.18). To further probe the distance between the alkoxy and the protonated amine, the model was visualized in PyMol, and this intramolecular distance was measured. According to the PyMol measurement, the proton on the amine is approximately 2.4 Å from the alkoxy group. This close proximity is hypothesized to stabilize the leaving group of tobramycin by effectively protonating the alkoxy moiety upon leaving group release.

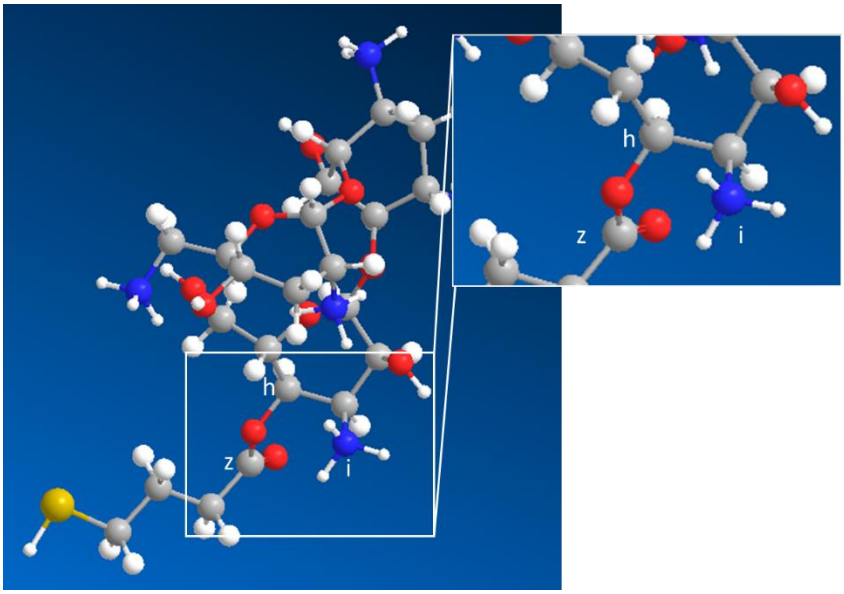

Figure 4.17 MM2 energy minimization of fully protonated tobramycin-SH (isomer A), showing protonated amine (i) in close proximity to the alkoxy of the ester (h) in the inset.

4.2.5.2 Energy minimization of TobP14 B

As with isomer A, Tobramycin-SH isomer B was modelled fully protonated (Figure 4.13). After MM2 energy minimization, the carbonyl oxygen seems to be in close proximity with two protonated amines (n and u, Figure 4.19). This distance was further probed using PyMol. In PyMol, the intramolecular distance from the proton on the protonated amine to the carbonyl oxygen on the energy minimized Tobramycin-SH isomer B model was found to be 0.3 and 1.8 Å, respectively. Due to this close proximity, it is hypothesized that these protons act as Bronstead acids with the carbonyl oxygen, enhancing the electrophilicity of the carbonyl to the thiol nucleophile, allowing for rapid tobramycin release.

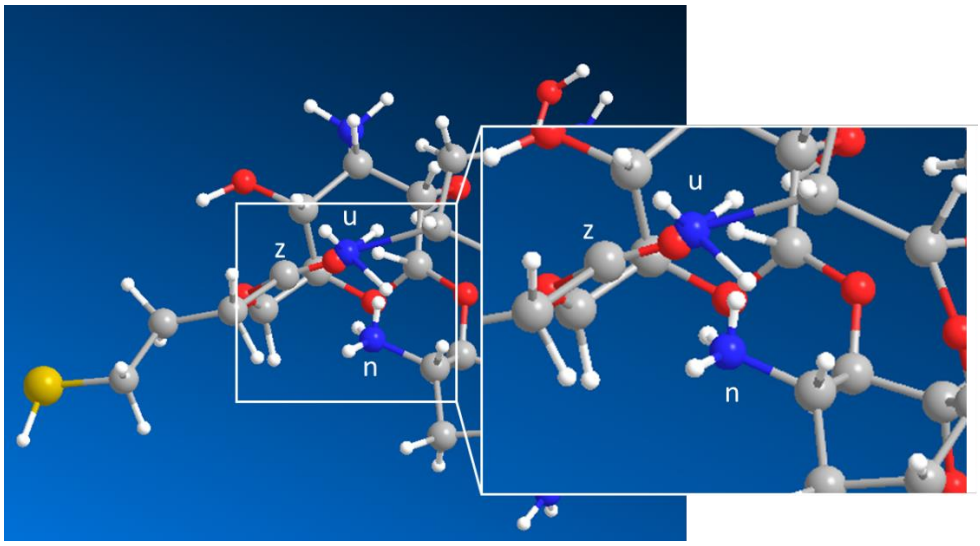

Figure 4.18 [a] MM2 energy minimization of full protonated tobramycin-SH (isomer B), showing the protonated amines (u and n) in close proximity to the carbonyl (z) in the inset.

There was a 130-fold difference in tobramycin release within a reducing environment between TobP14 isomers A and B, as previously discussed. Interestingly, these energy minimization studies revealed a difference in the electrostatic interactions observed in the two isomers. Namely, the enhanced leaving group ability of TobP14 A allows for the most rapid regeneration of tobramycin. This is compared to the enhanced electrophilicity of the carbonyl seen in TobP14 B. These structural observations may account for the marked difference in the release kinetics of the two isomers in the reducing environment.

4.2.6 Intracellular antibiotic activity of TobP14 A and B

As we have demonstrated, the TobP14 A and B conjugates have significant antibacterial activity against various strains of bacterial pathogens, such as *A. baumannii*, *P. aeruginosa*, *S. aureus*, and *S. epidermidis*. TobP14 A and B conjugates also have the advantages of being nontoxic to mammalian cells up to 16 μM and, within a reducing environment, they rapidly release the active monomers of TobP14 A and B (tobramycin and P14LRR-SH). Next, the TobP14 A and B isomers were tested against the intracellular pathogen *A. baumannii* (strains 19299 and 19606). J774A.1 macrophage cells were infected with *A. baumannii* (Strain 19299) and treated with

TobP14 A and B, tobramycin, P14LRR, and a 1:1 mixture of tobramycin:P14LRR for 12 hours over a range of concentrations (2.5-10 µM), Figure 4.20.

TobP14 A and B displayed concentration dependent intracellular clearance of *A. baumannii*. At a concentration of 2.5 µM, P14LRR and TobP14 B reduced the intracellular *A. baumannii* levels by 20% (Figure 4.20a). However, when the concentration was increased to 5 µM, P14LRR and TobP14 A reduced intracellular *A. baumannii* by 40%. Similarly, at 5 µM concentration, TobP14 A and the 1:1 mixture of tobramycin:P14LRR reduced the intracellular *A. baumannii* by 50%. These reductions in bacterial populations were significantly greater than those in the cases of the untreated control and tobramycin (Figure 4.20b). Finally, when the concentration was increased to 10 µM, TobP14 A and B and P14LRR were able to clear 90% of the intracellular *A. baumannii* and the 1:1 mixture of tobramycin:P14LRR cleared 95% (Figure 4.20c). Once again, the conjugates were able to clear significantly more bacteria as compared to the untreated control and the tobramycin treatment.

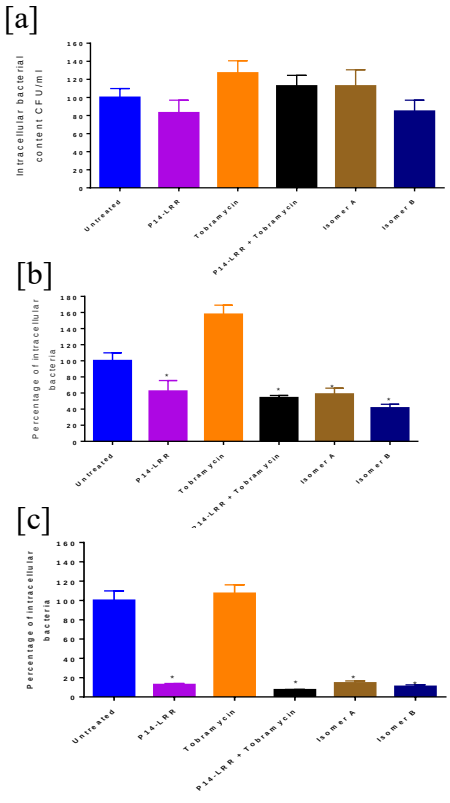

Figure 4.19 Intracellular *A. baumannii* (strain 19299) clearance using tobramycin, P14LRR. 1:1 tobramycin:P14LRR and TobP14 A and B at concentrations [a] 2.5 µM, [b] 5 µM, and [c]10 µM after 12 hour incubation of treatments with the bacterial infected J774A.1 cells.

The N-terminus of P14LRR is modified to either include fluorescein (for fluorescent monitoring) or else is acetyl capped. In the above experiments, the P14LRR control was attached to fluorescein at the N-terminus. Previous studies suggest that when P14LRR is attached to fluorescein, the antibacterial activity of the peptide (P14LRR) increases somewhat (unpublished results). Therefore, we were curious if this trend is the reason behind the observed antibacterial efficacy of P14LRR and the 1:1 mixture of tobramycin:P14LRR.

To test this hypothesis, J774A.1 macrophage cells were once again infected with *A. baumannii* strain 19299 and treated with TobP14 A and B, tobramycin, Ac-P14LRR, a 1:1 mixture of tobramycin:P14LRR, and cetazidime at the most potent concentration, 10 µM. In this case, both TobP14 A and B once again significantly cleared the intracellular *A. baumannii*, 56 and 53% respectively, Figure 4.21. Interestingly, the acylated P14LRR and the 1:1 mixture of tobramycin:P14LRR demonstrated dramatically reduced efficacy against *A. baumannii* 19299, as compared to the previous fluorescein-P14LRR results. Therefore, highlighting the significant clearance of intracellular *A. baumannii* 19299 with the TobP14 isomers (A and B). Together, the TobP14 A and B conjugates are able to significantly clear the intracellular *A. baumannii* 19299 as compared to the controls, tobramycin, Ac-P14LRR, and a 1:1 mixture of tobramycin:Ac-P14LRR.

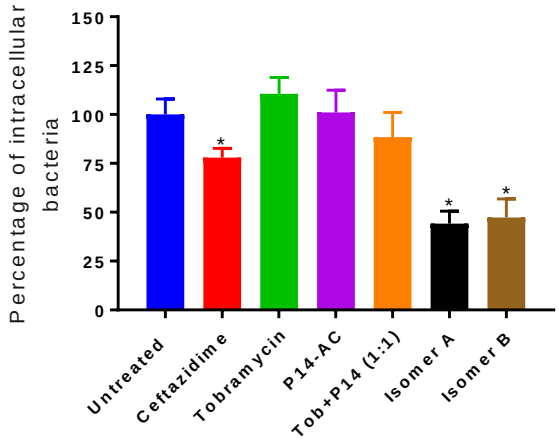

Figure 4.20 Intracellular *A. baumannii* (19299) treated with ceftazidime, tobramycin, Ac-P14LRR, 1:1 tobramycin:AcP14LRR, TobP14 A and B at 10 µM after 12 hour incubation of treatments with the bacterial infected J774A.1 cells.

Further, it was important to discern whether there is a difference in TobP14 A and B activity between strains of *A. baumannii*. Therefore, J774A.1 macrophage cells were infected with *A. baumannii* (19606) and treated with TobP14 A and B, tobramycin, Ac-P14LRR, a 1:1 mixture of tobramycin:P14LRR, and cetazidime at the most potent concentration, 10 µM, Figure 4.22. Ac-P14LRR and the 1:1 mixture of tobramycin:Ac-P14LRR cleared the intracellular *A. baumannii* 19606 by 92 and 91%, respectively. TobP14 A and B cleared the intracellular *A. baumannii* 19606 by 96 and 95%, respectively. Therefore, Ac-P14LRR, the 1:1 mixture of tobramycin:Ac-P14LRR, TobP14 A and B significantly cleared intracellular *A. baumannii* (19606) as compared to the untreated control and free tobramycin.

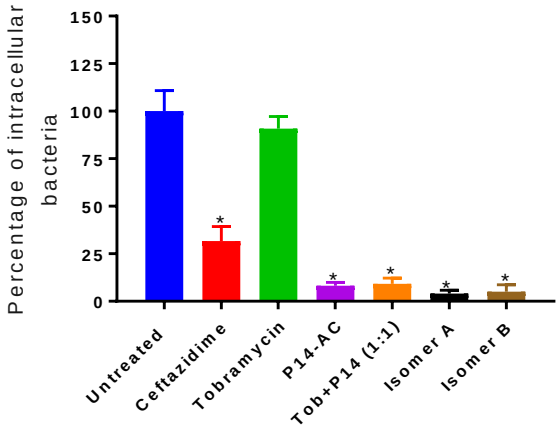

Figure 4.21 Intracellular *A. baumannii* (19606) treated with ceftazidime, tobramycin, Ac-P14LRR, 1:1 tobramycin:AcP14LRR, TobP14 A and B at 10 µM after 12 hour incubation of treatments with the bacterial infected J774A.1 cells.

Overall, TobP14 A and B conjugates were able to significantly clear intracellular *A. baumannii* (strains 19299 and 19606). Replacing the N-terminal fluorescein on the control P14LRR with an acyl substitution helped to highlight the significant clearance of intracellular *A. baumannii* 19299 with the TobP14 isomers (A and B) as compared to the controls (P14LRR, tobramycin, 1:1 tobramycin:P14LRR). TobP14 isomers (A and B) were able to clear 56% and 53% intracellular *A. baumannii* (19299), and 96% and 95% of intracellular *A. baumannii* (19606), respectively.

4.3 Conclusions

Here, a novel dual cell penetrating antibiotic, TobP14, was introduced. Two distinct isomers of the TobP14 conjugate (A and B) were synthesized, isolated, and fully characterized. It was shown that TobP14 A and B displays potent antibacterial activity against a variety of Gram positive and negative pathogens, such as *S. aureus*, *S. epidermidis*, *A. baumannii*, and *P. aeruginosa*. Both TobP14 isomers (A and B) were found to be minimally cytotoxic to mammalian cells when administered at concentrations up to 16 μM. In a reducing environment, TobP14 isomers (A and B) were able to revert back to monomeric tobramycin at a rapid rate ($t_{1/2}$ = 0.01± 0.008 hrs and 1.3 ± 0.2 hrs, respectively). Interestingly, there was a significant difference between TobP14 A and TobP14 B in terms of tobramycin release in a reducing environment. A modelling experiment of each tobramycin-SH intermediate (A and B) may explain this marked difference in release kinetics via the differences in the positioning of protonated amines near the ester carbonyls. TobP14 isomers (A and B) were able to clear 56% and 53% intracellular *A. baumannii* (19299), and 96% and 95% of intracellular *A. baumannii* (19606), respectively. Thus, we have demonstrated that TobP14 A and B are potent antibiotics that are nontoxic to mammalian cells, able to quickly regenerate into their component monomers in a reducing environment and effectively clear intracellular *A. baumannii* (19299 and 19606). With the evidence we have in hand, we believe that TobP14 A and B have the potential to be effective treatments in the continuing war against antibiotic resistant pathogens.

4.4 Future Directions

While we have made promising initial strides with our TobP14 A and B isomers, there is still more work to be done. First, the isomers should be tested against even more bacteria strains, both extra- and intracellularly. The mechanism of action of TobP14 A and B isomers must also be elucidated. Furthermore, the Tobramycin-2-thiopyridinyl tether isomers (A and B) should be conjugated to other CAPHs peptides (such as P17LRR, P14-5C, P14-5L, and P14-5B) in order to enhance their antibiotic potency. Tobramycin could also be replaced with other more potent antibiotics such as vancomycin or linezoid, which should also enhance the antibiotic potency of the conjugate.

4.5 Materials and Methods

4.5.1 Materials

Cbz-hydroxyproline was purchased from Chem-Impex Inc (Wood Dale, IL, USA). All other materials required for unnatural amino acid monomers were purchased from AK Scientific (Union City, CA) or Sigma Aldrich (St. Louis, MO). Tobramycin was purchased from Cayman Chemical (Ann Arbor, Michigan). ChemMatrix Rink Amide Resin was purchased from PCAS BioMatrix Inc (Saint-Jean-sur-Richelieu, Quebec, Canada). Fmoc-Gly, 1-[Bis(dimethylamino)methylebe]-1H-1,2,3-triazolo[4,5-b]pyridium 3-oxid hexafluorophosphate (HATU), and 1-Hydroxy-7-azabenzotriazole (HOAt) were purchased from Ana Spec Inc (Fremont, CA). Dithiothreitol (DTT) was purchased from Roche (Indianapolis, IN). Ethanedithiol (EDT) was purchased from Alfa Aesar (Tewksbury, MA). 2,2' bisthiopyridine, Trifluoroacetic acid, N,N diisopropylethylamine (DIEA), N,N dimethylformamide (DMF), dichloromethane (DCM), methanol, triisopropylsilane (TIPS) and γ-thiobutriolactone were purchased from Sigma Aldrich (St. Louis, MO).

Cell culture media Dulbecco's modified Eagles medium (DMEM), phosphate buffered saline (PBS), penicillin streptomycin, L-glutamine, and trypsin were purchased from VWR (Batavia, IL). Fetal Bovine Serum (FBS) was purchased from Atlanta Biologicals (Flowery Branch, GA). Tryptic Soy Broth (TSB), Muller Hilton Broth (MHB), 3-(4,5-dimethylthiazol-2-yl)-2,5-diphenyltetrazolium bromide (MTT) and dimethyl sulfoxide (DMSO) were purchased from Sigma Aldrich (St. Louis, MO). All the bacteria and cell lines were purchased from ATCC.

4.5.2 Methods

4.5.2.1 P14LRR-SH Synthesis

The P14LRR-SH peptide was synthesized via solid phase peptide synthesis using high loading (200 mg, 0.45 mmol/g) Chem Matrix H-Rink Amide Resin. Fmoc-P_L (110.6 mg, 3 mmol), P_R (176mg, 3 mmol) or Fmoc-glycine (80.3 mg, 3 mmol) was combined with HATU (102.7 mg, 3 mmol) and diisopropylethylamine (94 µL, 6 mmol) in DMF (8 mL) in a peptide synthesis flask. Each coupling was allowed to spin on a rotory spinner for 3 hours at room temperature. The amino

acid mixture was drained and the resin was washed with DMF, DCM, MeOH, DCM, and DMF (4 mL, 2X each). Next, piperidine (25% in DMF, 8mL) was added to the reaction flask. The reaction flask was allowed to spin for 30 minutes. The piperidine solution was then drained and the resin was washed with DMF, DCM, MeOH, DCM, and DMF (4 mL, 2X). This process was repeated until all the amino acids were coupled to the resin. Couplings were monitored by Kaiser and/or Chloranil tests.

Upon synthesis of the P14LRR peptide, the trityl-4-mercaptobutyric acid (97.9 mg, 3 mmol) was coupled via HATU (102.7 mg, 3 mmol) and diisopropylethylamine(94 µL, 6 mmol) in DMF (8 mL), which was allowed to stir at room temperature for 3 hours. The reaction solution was drained and the resin was washed with DMF, DCM, MeOH, DCM, and DMF (4 mL, 2X). P14LRR-SH was then globally deprotected and cleaved from the resin using a cleavage cocktail of 90:5:2.5:2.5, TFA:EDT:TIPS:H_2O. The cleavage cocktail with the peptide on resin was allowed to spin for 3 hours. The crude mixture was collected into a preweighed plastic falcon tube. The resin was washed with DCM (4 mL, 3X) and drained into the preweighed plastic falcon tube. The crude mixture was concentrated in vacuo. Cold diethyl ether (15 mL) was then added to the crude mixture, which caused the crude peptide to precipitate. The supernatant was removed and the crude P14LRR-SH was dried under vacuum overnight. Crude P14LRR-SH was resuspended in deionized water and was purified on RP-HPLC to homogeneity. RP-HPLC solvent used were acetonitrile with 0.1% TFA (solvent A) and water with 0.1% TFA (solvent B). The crude was purified using C18 column (Phenomenex, USA) with a gradient of 25-65% solvent A with a flow rate of 12 mL/min over 60 minutes and was visualized by UV at 214 nm. The mass was confirmed using MALDI-TOF (Expected Mass: 2718 Da, Observed Mass: 2717.75 Da). (Analytical purity trace: Figure A4, MALDI: Figure A9).

4.5.2.2 Tobramycin Boc_5

The synthesis of tobramycin boc_5 was carried out using previous literature procedure with some modifications.[27] Tobramycin (1 g, 2.13 mmol), di-*tert*-butyl dicarbonate (4.65 g, 21.3 mmol), triethylamine (6 mL, 42.8 mmol) were added to a round bottom flask that was equipped with stir bar at room temperature. Methanol (20 mL) and water (5 mL) were added to the reaction flask. The resultant mixture was refluxed at 55˚C for 12 hours. The mixture was concentrated under reduced pressure to afford a white solid, which was carried on to the next step without further

purification, in 81% yield. The ^{1}H NMR spectrum matched previously reported NMR spectrum. ^{1}H NMR (400 MHz, DMSO) δ 6.86 (s, 1H), 6.48 (ddd, *J* = 33.2, 15.1, 6.0 Hz, 5H), 4.86 (dd, *J* = 21.5, 4.4 Hz, 5H), 4.68 (d, *J* = 6.2 Hz, 1H), 4.21 (t, *J* = 5.7 Hz, 1H), 3.73 (d, *J* = 9.9 Hz, 2H), 3.57 – 3.42 (m, 8H), 3.40 – 3.16 (m, 14H), 1.83 (t, *J* = 10.1 Hz, 3H), 1.55 – 1.44 (m, 2H), 1.42 – 1.28 (m, 64H).

4.5.2.3 Tobramycin Boc_5 2-thiopyridinyl Tether

Tobramycin Boc_5 (1.3 g, 1.3 mmol), 2-mercaptopyridinyl-4-mercaptobutyric acid disulfide (250 mg, 1.09 mmol), diisopropylethylamine (2.3 mL, 13 mmol), HATU (304 mg, 1.3 mmol) were added to a flame dried flask that was equipped with stir bar and 4 Å molecular sieves. Dry N, N' dimethylformamide (10 mL) was added to the reaction mixture and the mixture was purged under N_2. The reaction was allowed to react undisturbed for 72 hours at room temperature. The reaction was diluted in DMF (30 mL) and purified using RP-HPLC. The solution was purified using a C18 Phenomenex HPLC column. The solvents used were acetonitrile with 0.1% TFA (solvent A) and water with 0.1% TFA (solvent B). The mixture was purified with a gradient of 60-75% A and were visualized at 254 nm to afford 2 major isomers that eluted at 23 min and 24.5 min, respectively. Isomer fractions were combined and concentrated under reduced pressure. Resulting aqueous solutions were lyophilized to yield white solid isomers, "A" and "B", with yields 6% and 14%, respectively. MS (ESI) m/z: calculated [M+H]: 1179.5, Observed: 1179.6, 1180.2, respectively

4.5.2.4 Tobramycin-2-thiopyridinyl Tether A

Dichloromethane (268 µL, DCM) and trifluoroacetic acid (268 µL, TFA) were added to a vial containing Tobramycin Boc_5-2-thiopyridinyl tether A (12.2 mg, 0.005 mmol) that was equipped with a stir bar. The reaction was allowed to stir for 1.5 hour at room temperature. The solvent was removed under reduced pressure. The reaction mixture was redissolved in methanol (1 mL, 2x) and dichloromethane (1 mL, 2x) and concentrated under reduced pressure until the residual TFA had been removed. The reaction was resuspended in water and purified using RP-HPLC. The solution was purified using a C18 Phenomenex HPLC column. The solvents used were acetonitrile with 0.1% TFA (solvent A) and water with 0.1% TFA (solvent B). The mixture was purified with a gradient of 10-40% solvent A using curve 8 and were visualized at a wavelength

of 254 nm and it eluted at 42 mins. The product fractions were collected, combined and concentrated under reduced pressure. The resultant aqueous solution was lyophilized to provide a white solid in 79% yield and is 99% pure. MS (ESI) m/z: calculated [M+H]: 679.3, Observed: 679.3. ^{1}H NMR (800 MHz, MeOD) δ 8.39 (dq, *J* = 4.7, 0.6 Hz, 1H), 7.84 (dt, *J* = 8.1, 1.1 Hz, 1H), 7.80 (td, *J* = 8.2, 7.0, 2.0 Hz, 1H), 7.22 (ddd, *J* = 7.3, 4.9, 1.2 Hz, 1H), 5.81 (d, *J* = 3.6 Hz, 1H), 5.10 (d, *J* = 3.7 Hz, 1H), 5.00 (t, *J* = 10.2 Hz, 1H), 4.10 – 4.04 (m, 2H), 3.93 (td, *J* = 8.7, 3.3 Hz, 1H), 3.89 (dd, *J* = 10.7, 3.6 Hz, 1H), 3.83 (t, *J* = 9.1 Hz, 1H), 3.69 – 3.62 (m, 2H), 3.58 – 3.45 (m, 5H), 3.39 (dd, *J* = 13.3, 3.3 Hz, 1H), 3.10 – 3.04 (m, 1H), 2.91 – 2.85 (m, 2H), 2.65 (s, 0H), 2.63 – 2.54 (m, 2H), 2.55 – 2.48 (m, 2H), 2.19 (dt, *J* = 12.0, 4.5 Hz, 1H), 2.14 – 1.97 (m, 5H). ^{13}C NMR (800 MHz, MeOD) δ 24.75, 29.46, 31.31, 33.07, 38.60, 41.81, 48.68, 48.79, 48.89, 49.00, 49.11, 49.21, 49.32, 50.00, 51.00, 54.71, 61.56, 66.71, 68.27, 69.83, 71.76, 72.58, 75.89, 78.98, 85.70, 95.68, 101.48, 121.31, 122.44, 139.19, 150.42, 161.26, 163.34, 173.89. (1 and 2D NMR spectra: Figures A33-A39)

4.5.2.5 Tobramycin-2-thiopyridnyl Tether B

Dichloromethane (268 µL, DCM) and trifluoroacetic Acid (268 µL, TFA) were added to a vial containing the lyophilized white powder of Tobramycin Boc_5-2-thiopyridinyl tether B (12.2 mg, 0.005 mmol) that was equipped with a stir bar. The reaction was allowed to stir for 1.5 hour at room temperature. The reaction was monitored by TLC (30% methanol:70% dichloromethane). The reaction vial was concentrated under reduced pressure. The reaction mixture was redissolved in methanol (1 mL, 2x) and dichloromethane (1 mL, 2x) and concentrated under reduced pressure until the residual TFA had been removed. The reaction was resuspended in water and purified using RP-HPLC. The solvents used were acetonitrile with 0.1% TFA (solvent A) and water with 0.1% TFA (solvent B). The solution was purified using a C18 (Phenomenex, USA) HPLC column. The mixture was purified with a gradient of 10-40% solvent A using curve 8 and were visualized at a wavelength of 254 nm and it eluted at 41 mins. The product fractions were collected, combined and concentrated under reduced pressure. The resultant aqueous solution was lyophilized to provide a white solid in 82.9% and is 99% pure. MS (ESI) m/z: calculated [M+H]: 679.3, Observed: 679.3 ^{1}H NMR (800 MHz, MeOD) δ 8.40 (ddd, *J* = 4.9, 1.8, 1.0 Hz, 1H), 7.86 – 7.80 (m, 2H), 7.23 (ddt, *J* = 7.4, 4.7, 1.3 Hz, 1H), 5.84 (d, *J* = 3.6 Hz, 1H), 5.03 (d, *J* = 3.7 Hz, 1H), 4.46 (dd, *J* = 12.3, 2.6 Hz, 1H), 4.25 (dd, *J* = 12.3, 3.0 Hz, 1H), 4.09 (dd, *J* = 10.3, 9.1 Hz, 1H), 4.03 (dt, *J* =

9.8, 2.8 Hz, 1H), 3.94 (td, *J* = 8.7, 3.3 Hz, 1H), 3.83 (dd, *J* = 10.8, 3.6 Hz, 1H), 3.78 (t, *J* = 9.2 Hz, 1H), 3.73 (t, *J* = 9.7 Hz, 1H), 3.67 (t, *J* = 10.0 Hz, 1H), 3.58 – 3.47 (m, 4H), 3.41 – 3.36 (m, 2H), 3.08 (dd, *J* = 13.3, 8.4 Hz, 1H), 2.85 (t, *J* = 7.1 Hz, 2H), 2.52 (dt, *J* = 12.4, 4.2 Hz, 1H), 2.50 (t, *J* = 6.7 Hz, 2H), 2.19 (dt, *J* = 12.1, 4.5 Hz, 1H), 2.14 – 2.05 (m, 2H), 2.00 (p, *J* = 7.1 Hz, 2H). ^{13}C NMR (800 MHz, MeOD) δ 25.02, 29.26, 31.27, 33.14, 38.74, 41.81, 48.68, 48.79, 48.89, 49.00, 49.11, 49.21, 49.32, 50.04, 51.36, 56.58, 63.16, 66.70, 67.14, 69.98, 71.94, 72.53, 75.92, 78.72, 85.43, 95.50, 102.45, 115.72, 117.17, 118.62, 120.07, 121.39, 122.51, 139.31, 150.38, 161.22, 162.47, 162.64, 162.82, 163.00, 174.38. (1 and 2D NMR spectra: Figures A40-A46)

4.5.2.6 P14LRR-Tobramycin A and B

P14LRR-SH peptide (8.6 mg, 0.00316 mmol) in degassed PBS (31.6 µL, pH 8) was added dropwise to an eppendorf containing Tobramycin-2-thiopyridnyl tether (A or B) (7.8 mg, 3 µmol), which was equipped with a stir bar. The reaction was allowed to react at room temperature for 12 hours. The crude mixture (isomer A or B) was diluted in deionized water (2 mL) and purified using RP-HPLC. The RP-HPLC solvents used were acetonitrile with 0.1% TFA (solvent A) and water with 0.1% TFA (solvent B). The crude mixture was purified using a C18 column (Phenomenex, USA) with a gradient of 20-80% solvent A with a flow rate of 12 mL/min over 60 minutes and visualized by UV at 214 nm. TobP14A eluted at 30.5 mins and TobP14B eluted at 29.5 mins. The product fractions were combined, the acetonitrile was removed under reduced pressure and the resulting aqueous solution was lyophilized to afford the white solid in 48% and 53% yield, respectively. Both products were 99% pure. MS (MALDI) m/z: calculated: 3285.9, observed: 3284.95 and 3285.94, respectively. (Analytical purity trace: Figure A5 and A6, MALDI: Figure A10 and A11).

4.5.2.7 Reduction of TobP14 (A and B) isomers in the presence of DTT

Stability studies with DTT were adapted from a previously published protocol with some changes.[7] TobP14 (isomer A or B, 50 µM) was incubated at 37 °C with 10 mM DTT in degassed ammonium acetate buffer (pH ~7.4) containing 5 µM quinine as the internal standard in 1.5 mL total volume. When monitoring tobramycin release, an aliquot of the reaction mixture was taken at different time points and directly analyzed by UPLC-MS. The time points were analyzed using

RP-UPLC with a T3-C18 column consisting of solvent A (water and 0.1% formic acid) and solvent B (acetonitrile and 0.1% formic acid), a gradient of 0-3 (3mins)-65 (4min)% of solvent B, a flow rate of 0.5 ml/min, and a column temperature of 40˚C. The peaks corresponding to the m/z for quinine (325.4), TobP14 (+5: 658, +4: 822), Tobramycin-SH (571), Tobramycin (468), and P14LRR-SH (+5: 545, +4: 681) were detected and extracted using MassLynx software. The experiments were run in triplicate, and the average percentage of release vs time was fitted using Graph Pad Prism 7 to generate $t_{1/2}$'s.

4.5.2.8 Cell Culture

J774A.1 macrophage cells were cultured in DMEM supplemented with 10% Fetal Bovine Serum, 1% L-glutamine, 1% penicillin and streptomycin. The cells were grown at 37˚C in 5% carbon dioxide atmosphere and were subcultured biweekly.

4.5.2.9 *In vitro* cytotoxicity assessment

Cytotoxicity was assessed using the MTT cell viability assay. Briefly, 20,000 cells (J774A.1) were cultured using DMEM supplemented with 10% FBS, 1% L-glutamine and 1% penicillin and streptomycin were plated in 96 well plates and incubated for 18 hours at 37˚C in a 5% carbon dioxide atmosphere. The spent media was then aspirated and then the drug treatments (50 µL) in complete DMEM media, ranging in concentration from 1-32 µM. The drug treatments were then added to the cells and incubated for 9 hours. After incubation, the treatments were aspirated and washed with PBS (100 µL). The PBS was then aspirated. Complete DMEM media was added to each well (100 µL), followed by 10 µL MTT solution (5 mg/mL in PBS). The plate was incubated for an additional 2 hours. After incubation, the MTT solution was aspirated from each well, and then DMSO (100 µL) was added to each well. The plate was covered with foil and allowed to shake on a shaker for 5 minutes. The absorbance was measured at 590 nm on a plate reader. All samples were run in duplicate and each experiment was duplicated.

4.5.2.10 TobP14 A and B antibacterial activity assay

TobP14 Isomers (A and B) and controls were tested against various bacterial strains (*A. baumannii* (19299 and 19606), *P. aeruginosa* (48982 and 31040), *S. aureus* (6538, MRSA 300,

MRSA 400), and *S. epidermidis* (NRS 101)) using a microbroth dilution assay. Briefly, the bacteria were diluted to an inoculum of 5 x 10^5 colony forming units (CFU/mL) in Muller-Hinton Broth (MHB). They were then transferred to 96 well plates. The treatments were then added to their respective well, sterile water or treatments of compounds (at desired concentrations). The plates were incubated at 37˚C for 24 hr. MIC was defined as the lowest concentration of drug which inhibited visible growth of the bacteria.

4.5.2.11 Intracellular *A. baumannii* activity assay

To determine the activity of tobramycin conjugates against intracellular *A. baumannii* (19299 and 19606). J774A.1 murine macrophage-like cells were seeded at a density of 1×10^5 cells per well in 96-well plates (Corning Incorporated) for 24 hours before being infected with bacteria. The cells were routinely grown in Dulbecco's Modified Eagle Medium (DMEM) supplemented with 10% heat-inactivated fetal bovine serum. Following incubation, the cells were washed once with DMEM. Then cells were infected *A. baumannii* 19606 (multiplicity of infection 1:10), for 45 min. At the end of the infection, cells were washed three times with DMEM medium containing 100 µg/ mL gentamicin (Sigma) and was further incubated for 3 hours with gentamicin (100 µg/ mL) to kill and non-phagocytized bacteria. Then DMEM medium supplemented with 10% fetal bovine serum containing the tested compounds at 10 µM (subtoxic concentration based on the toxicity study) were added to the cells. Control cells received sterile phosphate buffered saline (PBS). The plate was then returned to the incubator and the intracellular clearance activity of tobramycin conjugates and the tested controls were assessed after 12 hours. At the end of the incubation time, the infected cells were washed three times with PBS and lysed with 100 µL of 0.01% triton-x to collect the intracellular bacteria. The colony forming units (CFUs) of the bacteria in the lysates were determined by plating a series of 10-fold serial dilutions onto tryptic soy agar (TSA) and incubating the plates at 37 °C for 24 hours. Statistical significance was assessed with one-way ANOVA, with post hoc Dunnet's multiple comparisons test ($P < 0.05$), utilizing GraphPad Prism 6.0 (GraphPad Software, La Jolla, CA).

4.6 References

1. Bahar, A. A.; Ren, D., Antimicrobial peptides. *Pharmaceuticals* **2013,** *6* (12), 1543-1575, 33 pp.

2. Mahlapuu, M.; Haakansson, J.; Ringstad, L.; Bjoern, C., Antimicrobial peptides: an emerging category of therapeutic agents. *Front. Cell. Infect. Microbiol.* **2016,** *6*, 194/1-194/12.

3. Habault, J.; Poyet, J.-L., Recent advances in cell penetrating peptide-based anticancer therapies. *Molecules* **2019,** *24* (5), 927/1-927/17.

4. Bolhassani, A.; Jafarzade, B. S.; Mardani, G., *In vitro* and *in vivo* delivery of therapeutic proteins using cell penetrating peptides. *Peptides* **2017,** *87*, 50-63.

5. Gagat, M.; Zielinska, W.; Grzanka, A., Cell-penetrating peptides and their utility in genome function modifications (review). *Int. J. Mol. Med.* **2017,** *40* (6), 1615-1623.

6. Abdul Ghaffar, K.; Hussein, W. M.; Khalil, Z. G.; Capon, R. J.; Skwarczynski, M.; Toth, I., Levofloxacin and Indolicidin for combination antimicrobial therapy. *Curr. Drug Delivery* **2015,** *12* (1), 108-114.

7. Brezden, A.; Mohamed, M. F.; Nepal, M.; Harwood, J. S.; Kuriakose, J.; Seleem, M. N.; Chmielewski, J., Dual Targeting of intracellular pathogenic bacteria with a cleavable conjugate of kanamycin and an antibacterial cell-penetrating peptide. *J. Am. Chem. Soc.* **2016,** *138* (34), 10945-10949.

8. Lee, H.; Lim, S. I.; Shin, S.-H.; Lim, Y.; Koh, J. W.; Yang, S., Conjugation of cell-penetrating peptides to antimicrobial peptides enhances antibacterial activity. *ACS Omega* **2019,** *4* (13), 15694-15701.

9. Li, Z.; Teng, D.; Mao, R.; Wang, X.; Hao, Y.; Wang, X.; Wang, J., Improved antibacterial activity of the marine peptide N6 against intracellular *Salmonella typhimurium* by conjugating with the cell-penetrating peptide Tat11 via a cleavable linker. *J. Med. Chem.* **2018,** *61* (17), 7991-8000.

10. Li, Z.; Wang, X.; Teng, D.; Mao, R.; Hao, Y.; Yang, N.; Chen, H.; Wang, X.; Wang, J., Improved antibacterial activity of a marine peptide-N2 against intracellular *Salmonella typhimurium* by conjugating with cell-penetrating peptides-bLFcin6/Tat11. *Eur. J. Med. Chem.* **2018,** *145*, 263-272.

11. Fillon, Y. A.; Anderson, J. P.; Chmielewski, J., Cell penetrating agents based on a polyproline helix scaffold. *J. Am. Chem. Soc.* **2005,** *127* (33), 11798-11803.

12. Kuriakose, J.; Hernandez-Gordillo, V.; Nepal, M.; Brezden, A.; Pozzi, V.; Seleem, M. N.; Chmielewski, J., Targeting intracellular pathogenic bacteria with unnatural proline-rich peptides: coupling antibacterial activity with macrophage penetration. *Angew. Chem., Int. Ed.* **2013,** *52* (37), 9664-9667.

13. Nepal, M.; Thangamani, S.; Seleem, M. N.; Chmielewski, J., Targeting intracellular bacteria with an extended cationic amphiphilic polyproline helix. *Org. Biomol. Chem.* **2015,** *13* (21), 5930-5936.

14. Geisler, I.; Chmielewski, J., Probing length effects and mechanism of cell penetrating agents mounted on a polyproline helix scaffold. *Bioorg. Med. Chem. Lett.* **2007,** *17* (10), 2765-2768.

15. Kalafut, D.; Anderson, T. N.; Chmielewski, J., Mitochondrial targeting of a cationic amphiphilic polyproline helix. *Bioorg. Med. Chem. Lett.* **2012,** *22* (1), 561-563.

16. Nepal, M.; Mohamed, M. F.; Blade, R.; Eldesouky, H. E.; N. Anderson, T.; Seleem, M. N.; Chmielewski, J., A library approach to cationic amphiphilic polyproline helices that target intracellular pathogenic bacteria. *ACS Infect. Dis.* **2018,** *4* (9), 1300-1305.

17. Geisler, I. M.; Chmielewski, J., Dimeric cationic amphiphilic polyproline helices for mitochondrial targeting. *Pharm. Res.* **2011,** *28* (11), 2797-2807.

18. Li, L.; Geisler, I.; Chmielewski, J.; Cheng, J.-X., Cationic amphiphilic polyproline helix P11LRR targets intracellular mitochondria. *J. Controlled Release* **2010,** *142* (2), 259-266.

19. Geisler, I.; Chmielewski, J., Cationic amphiphilic polyproline helices: side-chain variations and cell-specific internalization. *Chem. Biol. Drug Des.* **2009,** *73* (1), 39-45.

20. Thangamani, S.; Nepal, M.; Chmielewski, J.; Seleem, M. N., Antibacterial activity and therapeutic efficacy of FI-PRPRPL-5, a cationic amphiphilic polyproline helix, in a mouse model of staphylococcal skin infection. *Drug Des., Dev. Ther.* **2015,** *9*, 5749-5754.

21. Figueira, R.; Holden, D. W., Functions of the *Salmonella* pathogenicity island 2 (SPI-2) type III secretion system effectors. *Microbiology* **2012,** *158* (5), 1147-1161.

22. Ibarra, J. A.; Steele-Mortimer, O., *Salmonella*, the ultimate insider: *Salmonella* virulence factors that modulate intracellular survival. *Cell. Microbiol.* **2009,** *11* (11), 1579-1586.

23. Erlanson, P.; Lundgren, A., Ototoxic side effects following treatment with streptomycin, dihydrostreptomycin, and kanamycin. Connection with dosage and renal function; preventive measures. *Acta Med Scand* **1964,** *176*, 147-63.

24. Li, X.; Vogt Frederick, G.; Hayes, D., Jr.; Mansour Heidi, M., Design, characterization, and aerosol dispersion performance modeling of advanced co-spray dried antibiotics with mannitol as respirable microparticles/nanoparticles for targeted pulmonary delivery as dry powder inhalers. *J Pharm Sci* **2014,** *103* (9), 2937-2949.

25. Domalaon, R.; Yang, X.; Lyu, Y.; Zhanel, G. G.; Schweizer, F., Polymyxin B3-Tobramycin hybrids with *Pseudomonas aeruginosa*-selective antibacterial activity and strong potentiation of rifampicin, minocycline, and vancomycin. *ACS Infect. Dis.* **2017,** *3* (12), 941-954.

26. Yang, X.; Domalaon, R.; Lyu, Y.; Zhanel, G. G.; Schweizer, F., Tobramycin-linked efflux pump inhibitor conjugates synergize fluoroquinolones, rifampicin and fosfomycin against multidrug-resistant *Pseudomonas aeruginosa*. *J. Clin. Med.* **2018,** *7* (7), 158/1-158/12.

27. Yang, X.; Goswami, S.; Gorityala, B. K.; Domalaon, R.; Lyu, Y.; Kumar, A.; Zhanel, G. G.; Schweizer, F., A tobramycin vector enhances synergy and efficacy of efflux pump inhibitors against multidrug-resistant Gram-negative bacteria. *J. Med. Chem.* **2017,** *60* (9), 3913-3932.

28. Idowu, T.; Ammeter, D.; Rossong, H.; Zhanel, G. G.; Schweizer, F., Homodimeric tobramycin adjuvant repurposes novobiocin as an effective antibacterial agent against Gram-negative bacteria. *J. Med. Chem.* **2019**, 62 (20), 9103-9115.

29. Ammeter, D.; Idowu, T.; Zhanel, G. G.; Schweizer, F., Development of a nebramine-cyclam conjugate as an antibacterial adjuvant to potentiate β-lactam antibiotics against multidrug-resistant P. aeruginosa. *J. Antibiot.* **2019,** *72* (11), 816-826.

30. Guchhait, G.; Altieri, A.; Gorityala, B.; Yang, X.; Findlay, B.; Zhanel, G. G.; Mookherjee, N.; Schweizer, F., Amphiphilic tobramycins with immunomodulatory properties. *Angew. Chem., Int. Ed.* **2015,** *54* (21), 6278-6282.

31. Lyu, Y.; Yang, X.; Goswami, S.; Gorityala, B. K.; Idowu, T.; Domalaon, R.; Zhanel, G. G.; Shan, A.; Schweizer, F., Amphiphilic tobramycin-lysine conjugates sensitize multidrug resistant Gram-negative bacteria to rifampicin and minocycline. *J. Med. Chem.* **2017,** *60* (9), 3684-3702.

32. Schmidt, N. W.; Deshayes, S.; Hawker, S.; Blacker, A.; Kasko, A. M.; Wong, G. C. L., Engineering persister-specific antibiotics with synergistic antimicrobial functions. *ACS Nano* **2014,** *8* (9), 8786-8793.

33. Deshayes, S.; Xian, W.; Schmidt, N. W.; Kordbacheh, S.; Lieng, J.; Wang, J.; Zarmer, S.; Germain, S. S.; Voyen, L.; Thulin, J.; Wong, G. C. L.; Kasko, A. M., Designing hybrid antibiotic peptide conjugates to cross bacterial membranes. *Bioconjugate Chem.* **2017,** *28* (3), 793-804.

34. Yang, Q.; Bai, L.; Zhang, Y.; Zhu, F.; Xu, Y.; Shao, Z.; Shen, Y.-M.; Gong, B., Dynamic covalent diblock copolymers: instructed coupling, micellation and redox responsiveness. *Macromolecules* **2014,** *47* (21), 7431-7441.

35. Tokutake, N.; Miyake, Y.; Regen, S. L., Bridging group effects on nearest-neighbor recognition within fluid phospholipid membranes. *Langmuir* **2000,** *16* (1), 81-86.

APPENDIX

Purity Analyticals

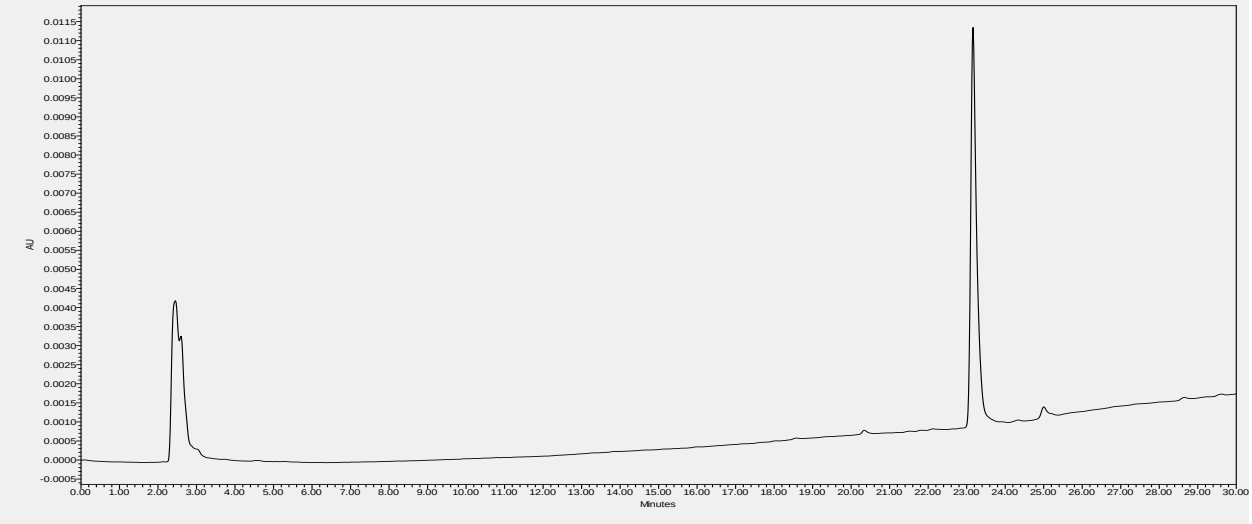

Figure A 1: Analytical purity HPLC of Aba-S_2-DRV8: C18 column, 20-95% acetonitrile with a flow rate of 1.2 mL/min, and visualized at 254 nm. The product is 99% pure.

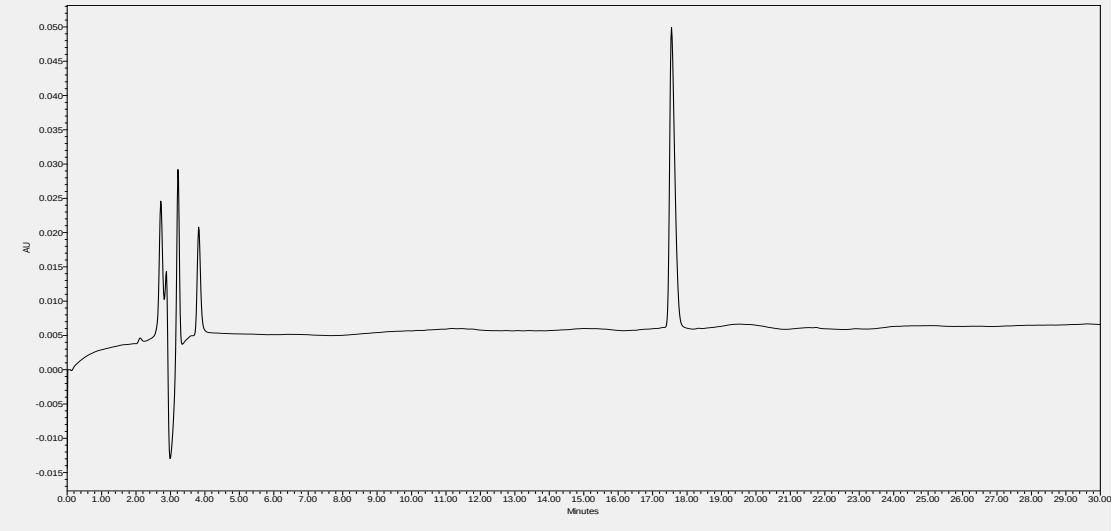

Figure A 2: Analytical purity HPLC of Kanamycin-Arg_8 Isomer 1: C18 column, 5-30% acetonitrile with a flow rate of 1.2 mL/min, and visualized at 254 nm. The product is 99% pure.

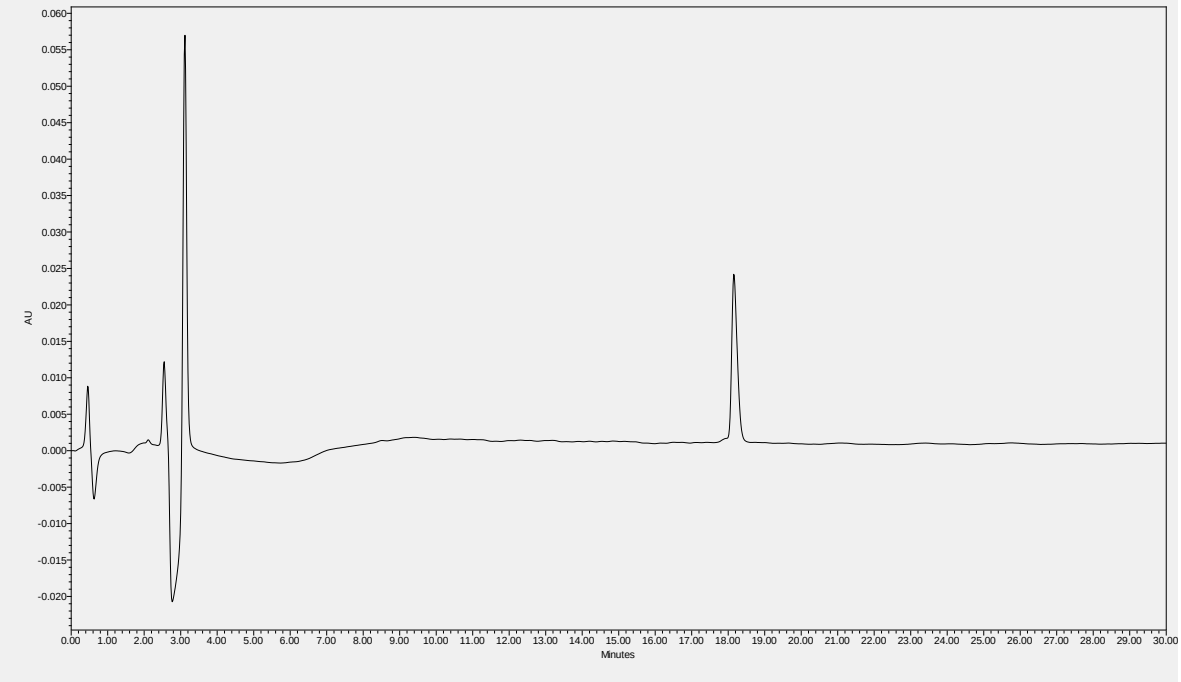

Figure A 3: Analytical purity HPLC of Kanamycin-Arg_8 Isomer 2: C18 column, 5-30% acetonitrile with a flow rate of 1.2 mL/min, and visualized at 254 nm. The product is 99% pure.

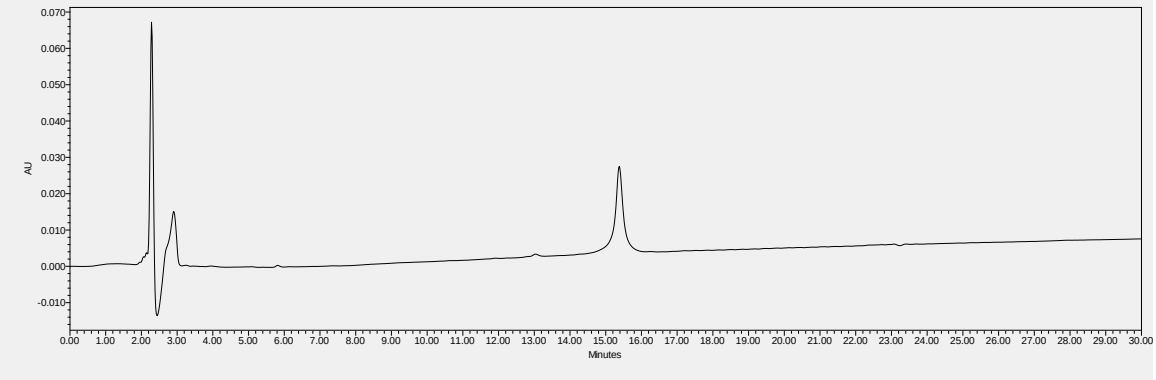

Figure A 4: Analytical purity HPLC of P14LRR-SH: C18 column, 25-65% acetonitrile with a flow rate of 1.2 mL/min, and visualized at 214 nm. The product is 99% pure.

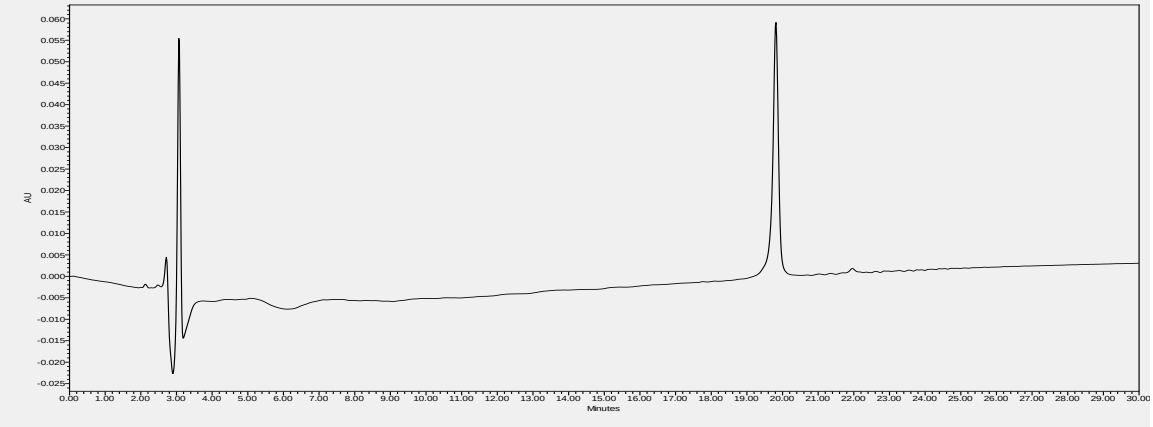

Figure A 5: Analytical purity chromatogram of TobP14 Isomer A: C18, 10-70% Acetonitrile, 214 nm. Product is 99% pure.

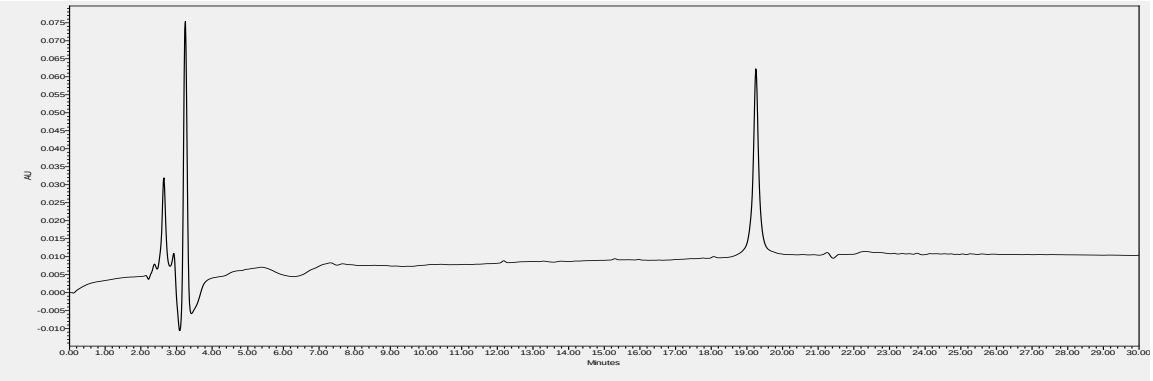

Figure A 6: Analytical purity chromatogram of TobP14 Isomer B: C18, 10-70% Acetonitrile, 214 nm. Product is 99% pure.

Mass Spectra

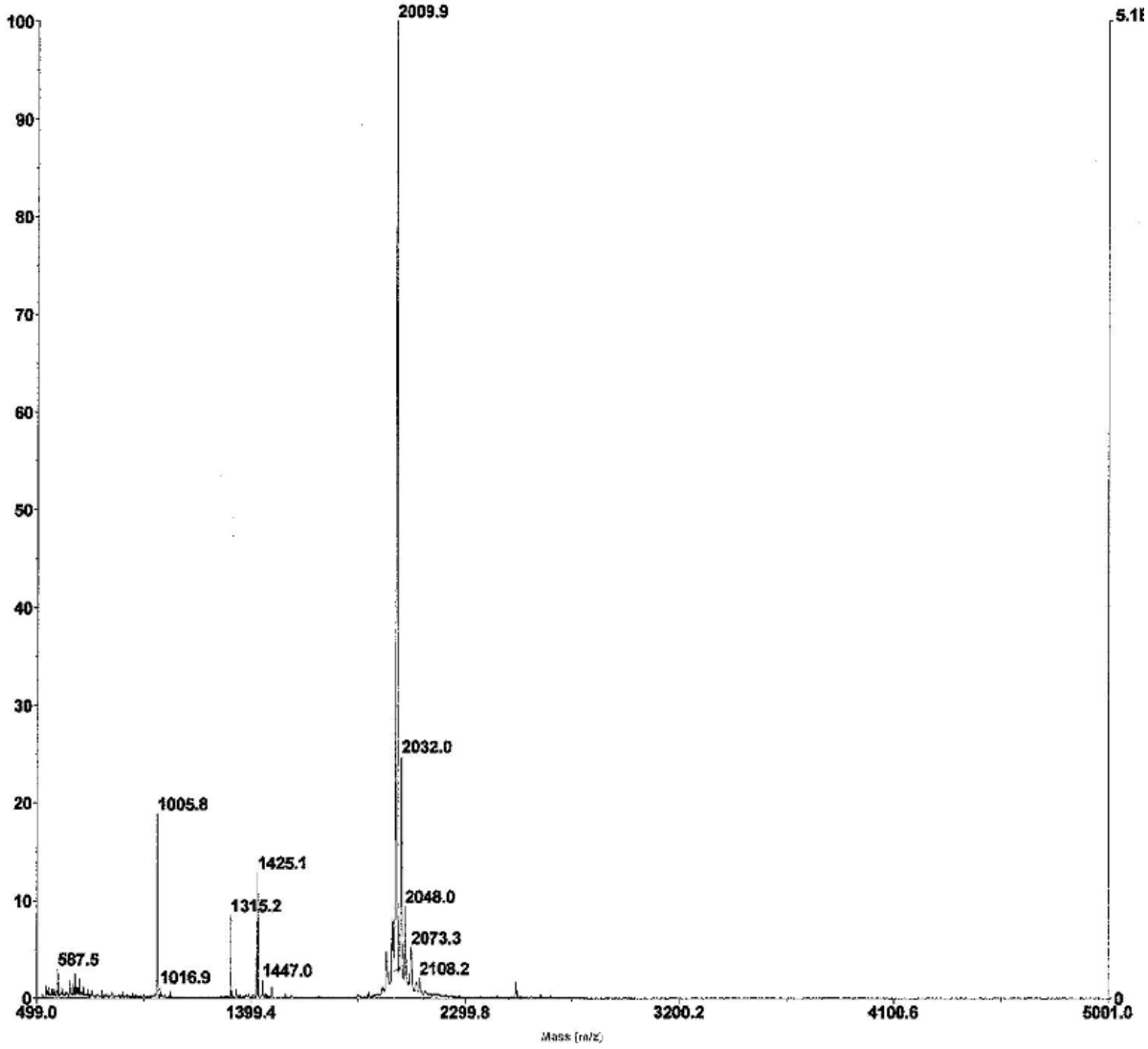

Figure A 7: MALDI mass spectra of Kanamycin-Arg_8 Isomer 1 (Expected Mass: 2010.09, Observed Mass: 2009.94).

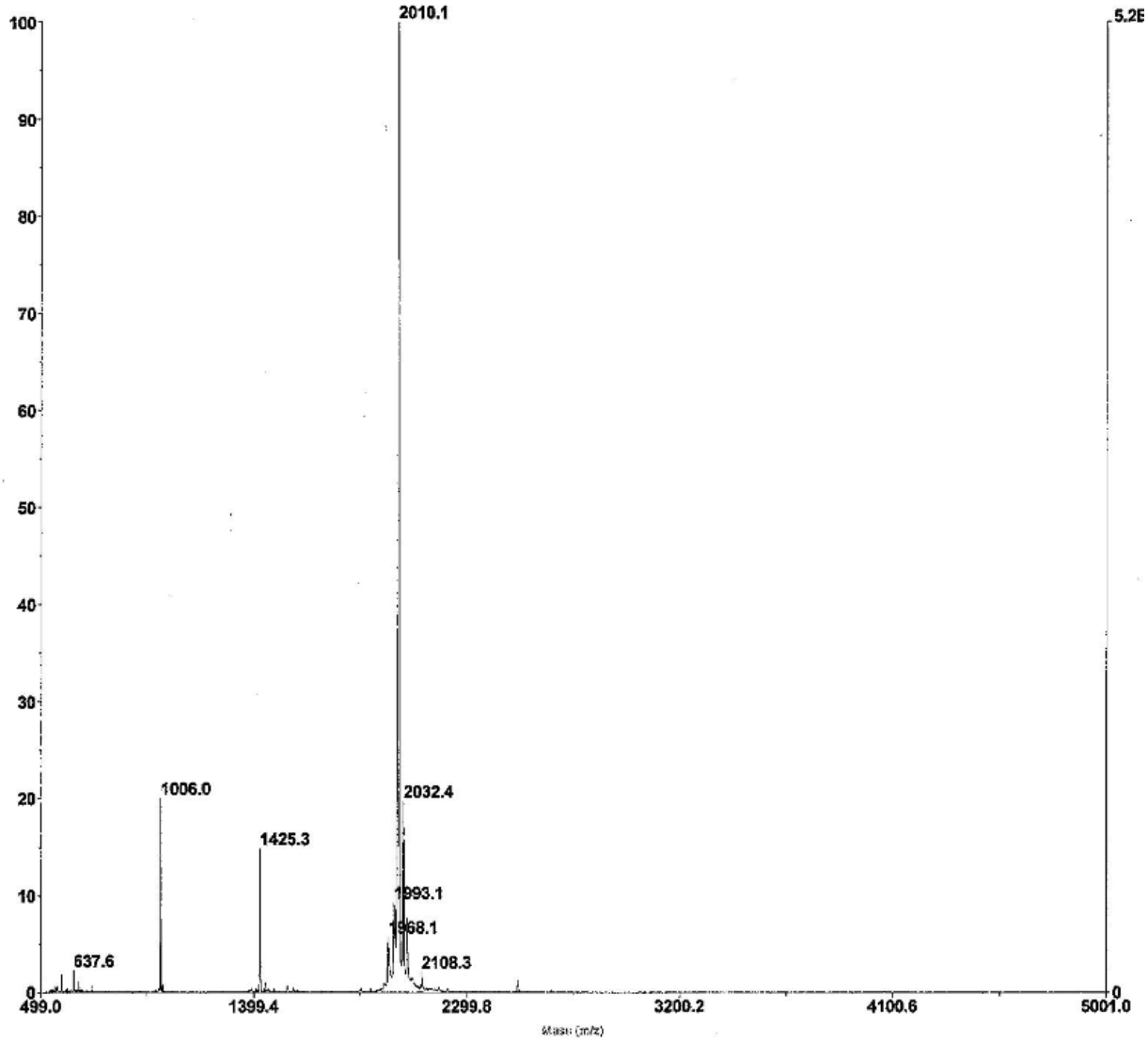

Figure A 8: MALDI mass spectra of Kanamycin-Arg_8 Isomer 2 (Expected Mass: 2010.09, Observed Mass: 2010.13).

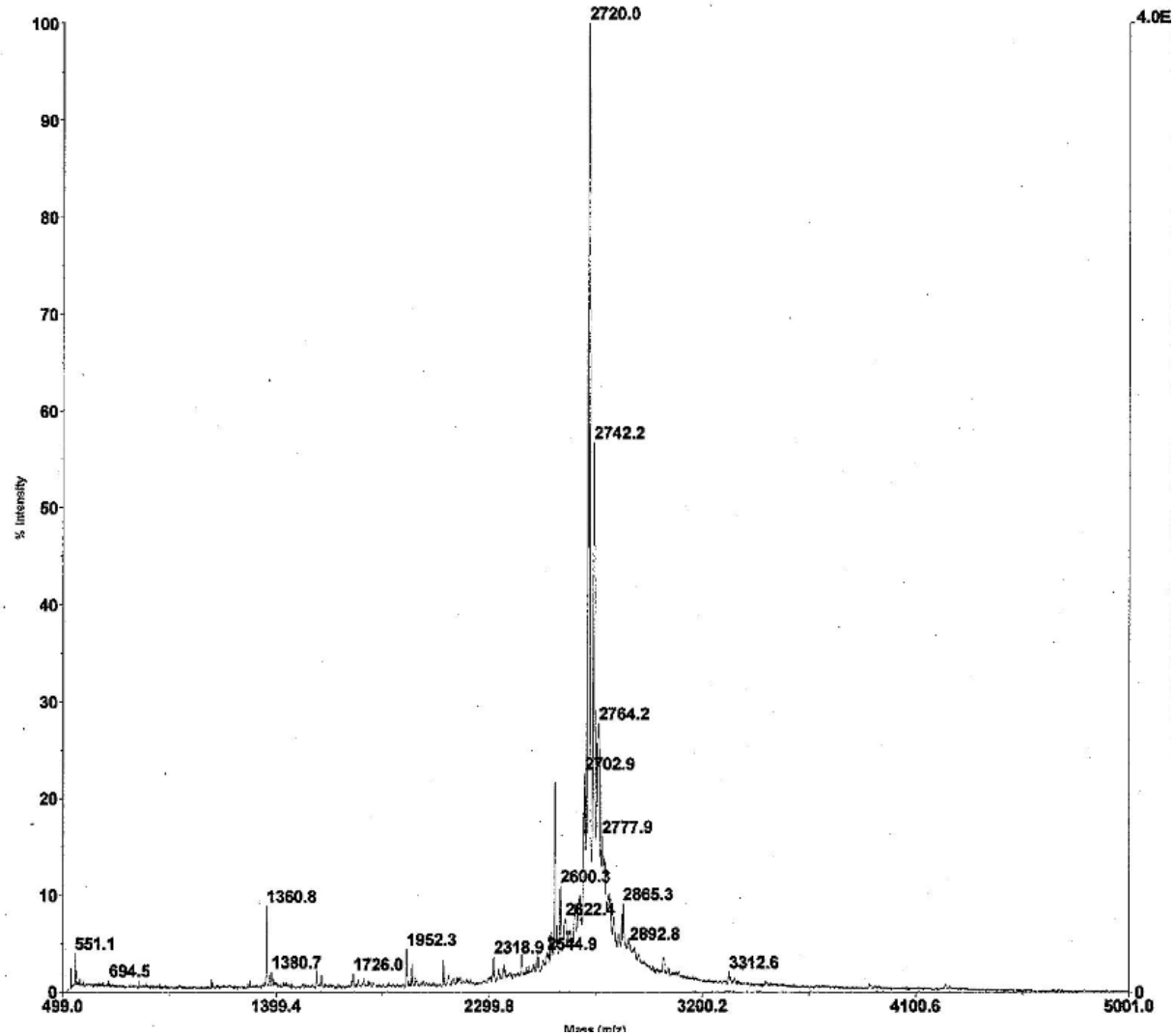

Figure A 9: MALDI mass spectra of P14LRR-SH (Expected Mass: 2718, Observed Mass: 2720.0).

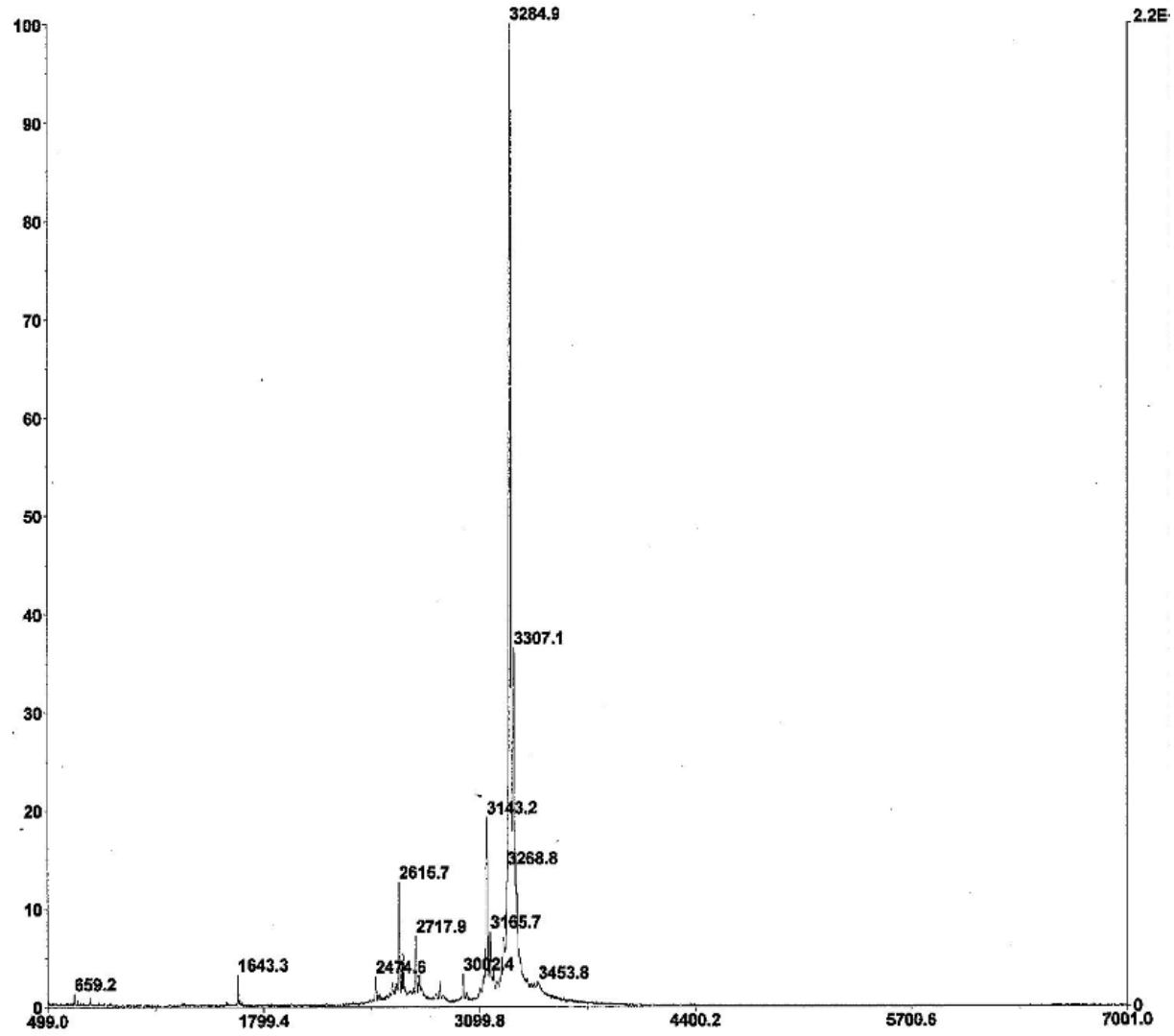

Figure A 10: MALDI mass spectra of TobP14 Isomer A (Expected Mass: 3285.89, Observed Mass: 3284.9).

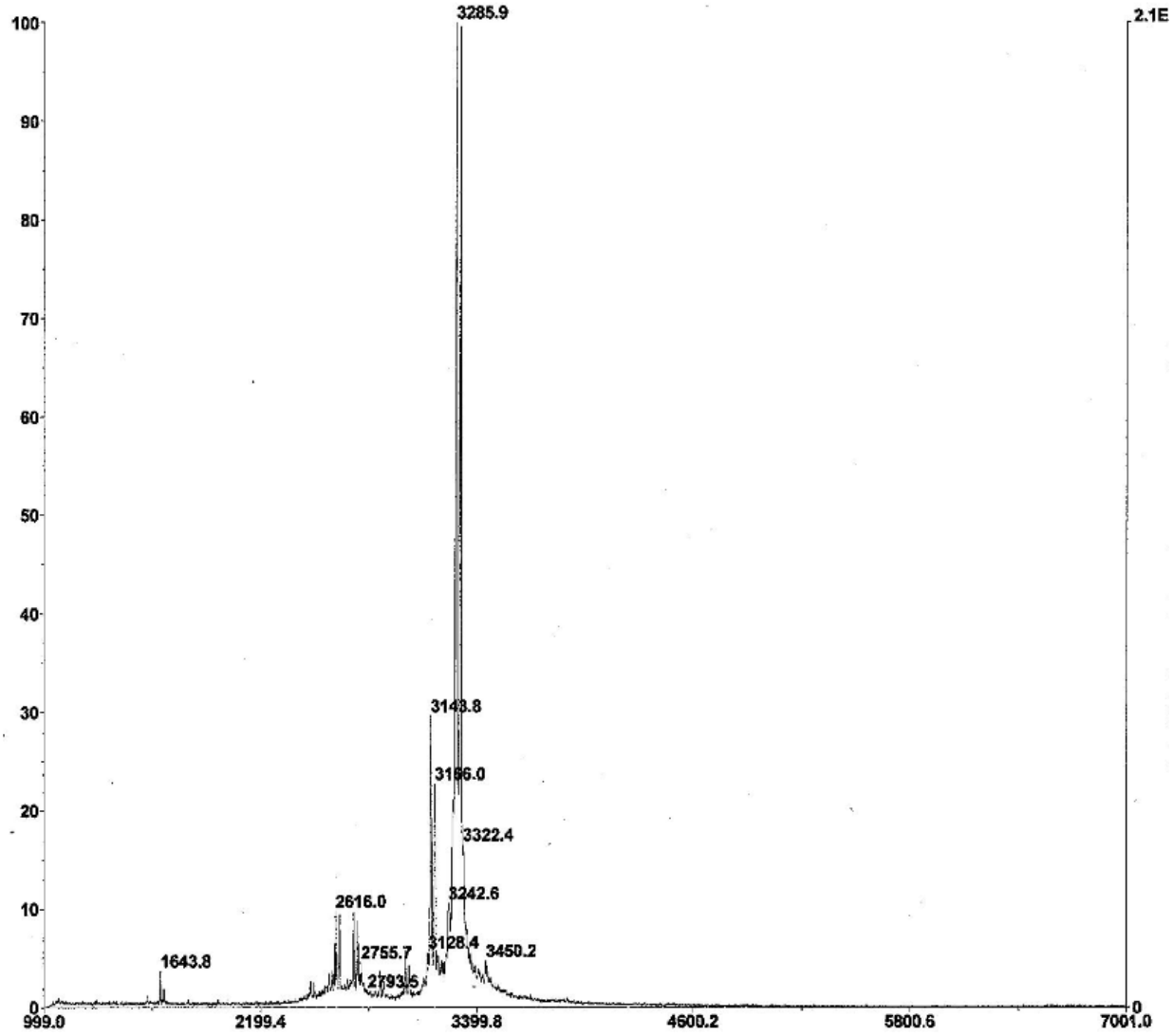

Figure A 11: MALDI mass spectra of TobP14 Isomer B (Expected Mass: 3285.89, Observed Mass: 3285.9).

NMR Spectra

Spectra A12-A18 are taken from Agrawal, N.; Rowe, J.; Lan, J.; Yu, Q.; Hrycyna, C. A.; Chmielewski, J., Potential tools for eradicating HIV reservoirs in the brain: development of trojan horse prodrugs for the inhibition of P-glycoprotein with anti-HIV-1 activity. *J. Med. Chem.* **2019**, DOI: 10.1021/acs.jmedchem.9b00779. Spectra A11 and A12 were acquired by Neha Agrawal.

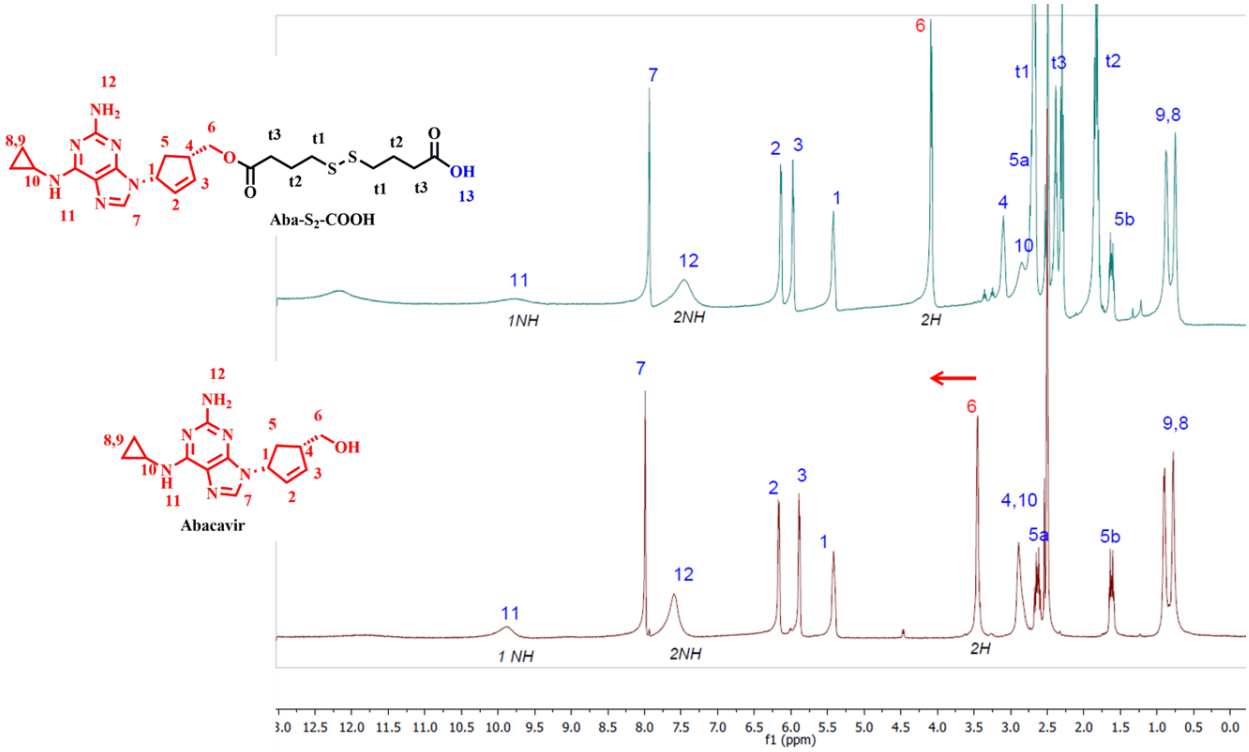

Figure A 12: Comparison of ^{1}H Aba-S_2-COOH as compared to ^{1}H of parent abacavir. Proton 6 corresponds with the proton off the methylene carbon in abacavir adjacent to the primary hydroxyl. Note the downfield shift in the case of Aba-S_2-COOH.

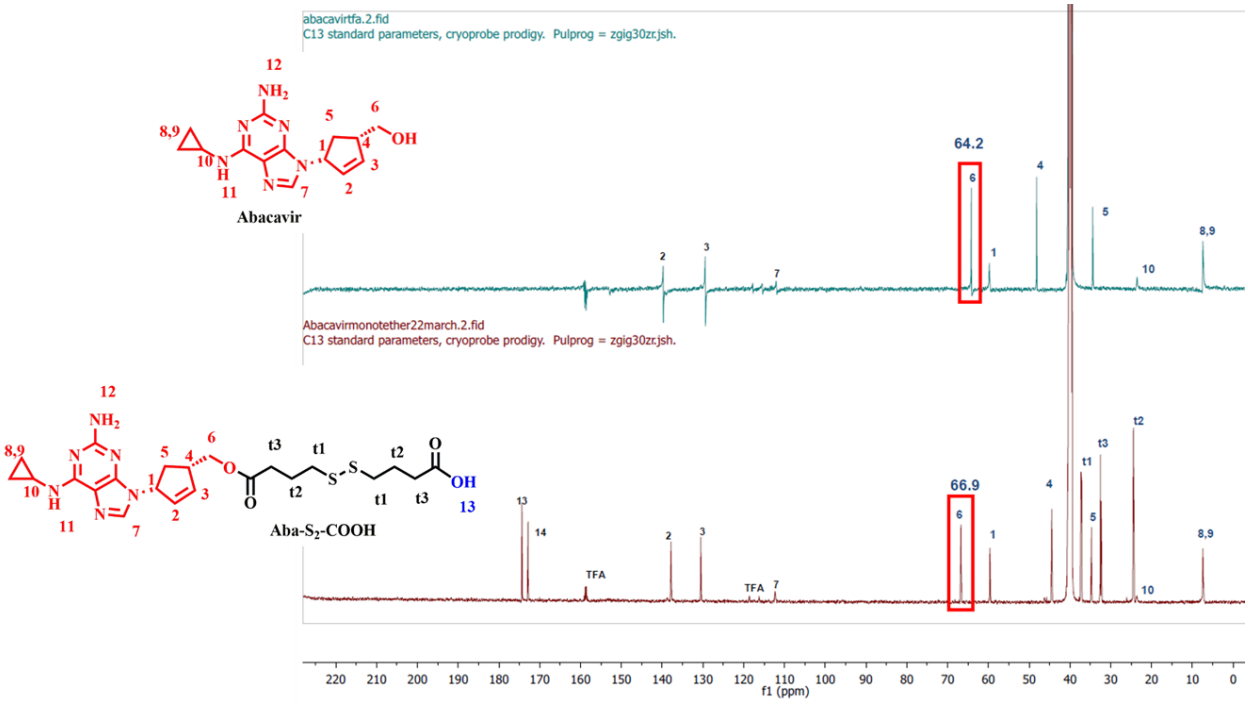

Figure A 13: Comparison of ^{13}C from Aba-S_2-COOH as compared to ^{13}C from parent abacavir. Carbon 6 corresponds to the methylene carbon in abacavir adjacent to the primary hydroxyl. Note the downfield shift in the case of Aba-S_2-COOH.

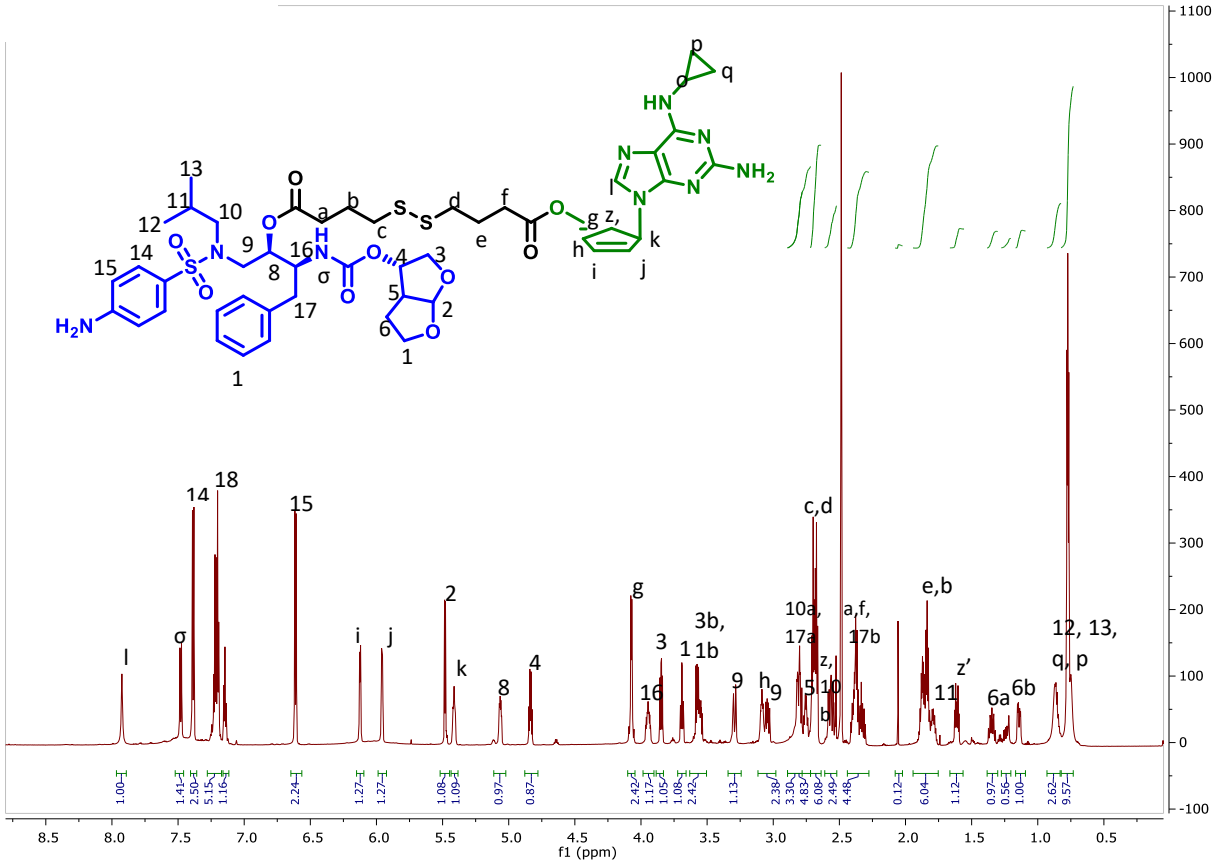

Figure A 14: ^{1}H for Aba-S_2-DRV8 in DMSO-*d6*. Assignments made by ^{1}H, ^{13}C, COSY, TOCSY, HMQC.

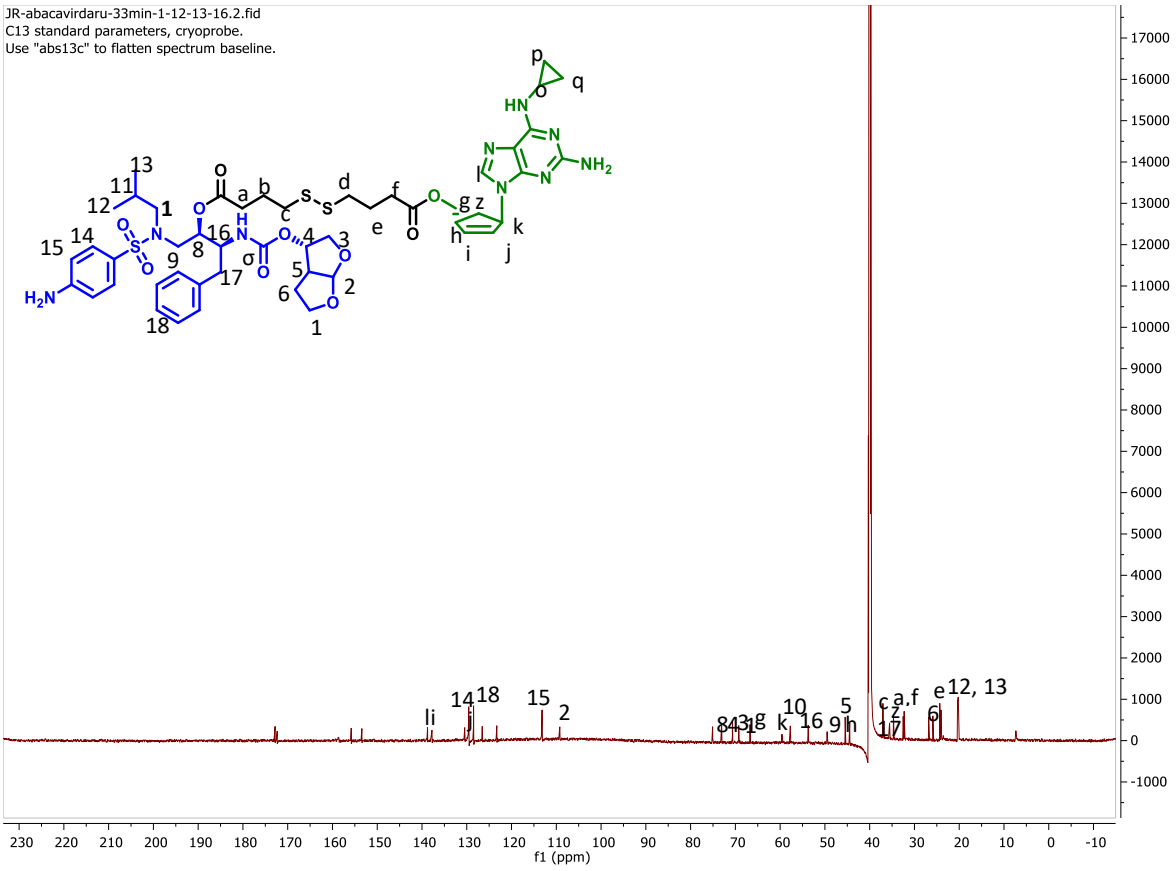

Figure A 15: ^{13}C for Aba-S_2-DRV8 in in DMSO-*d6*: Assignments made by ^{1}H, ^{13}C, COSY, TOCSY, HMQC.

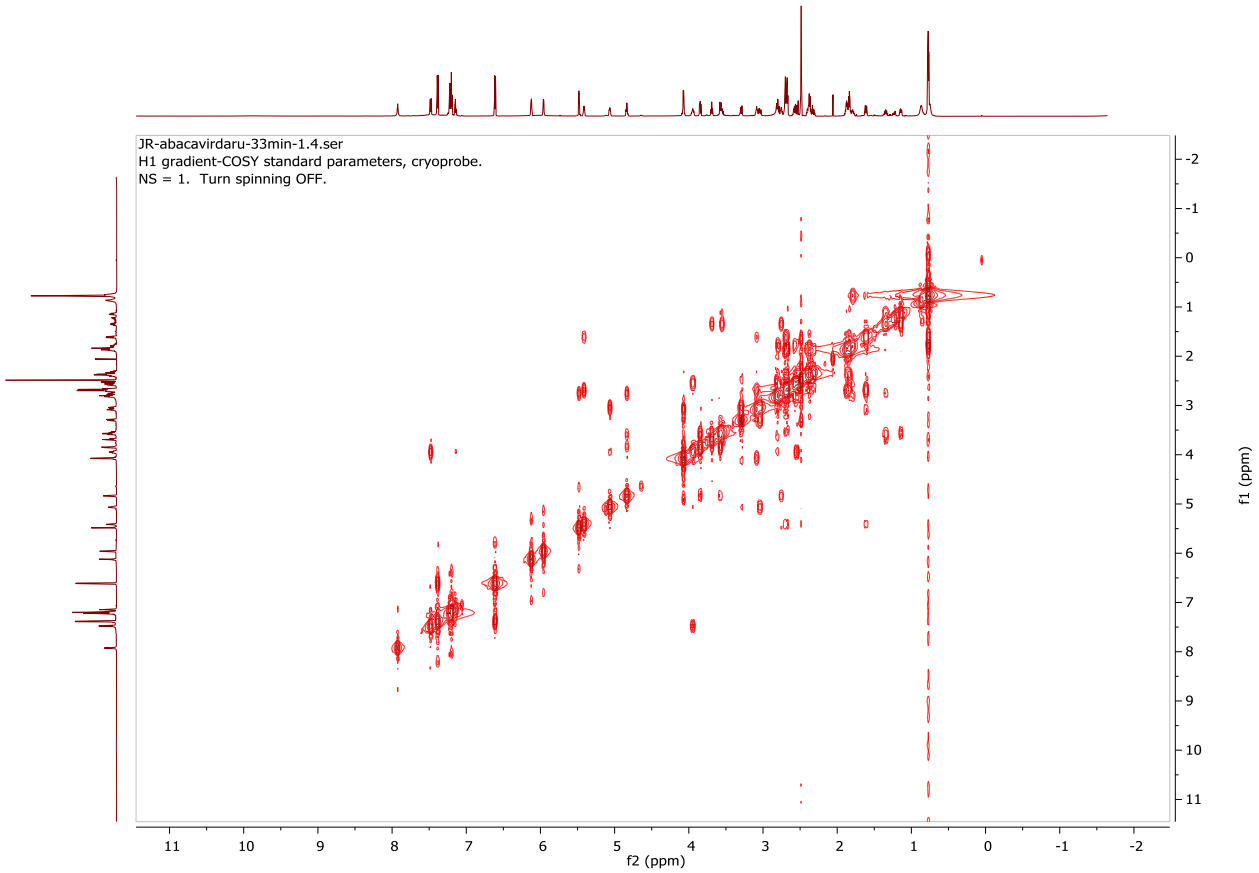

Figure A 16: ^{1}H-^{1}H COSY for Aba-S_2-DRV8.

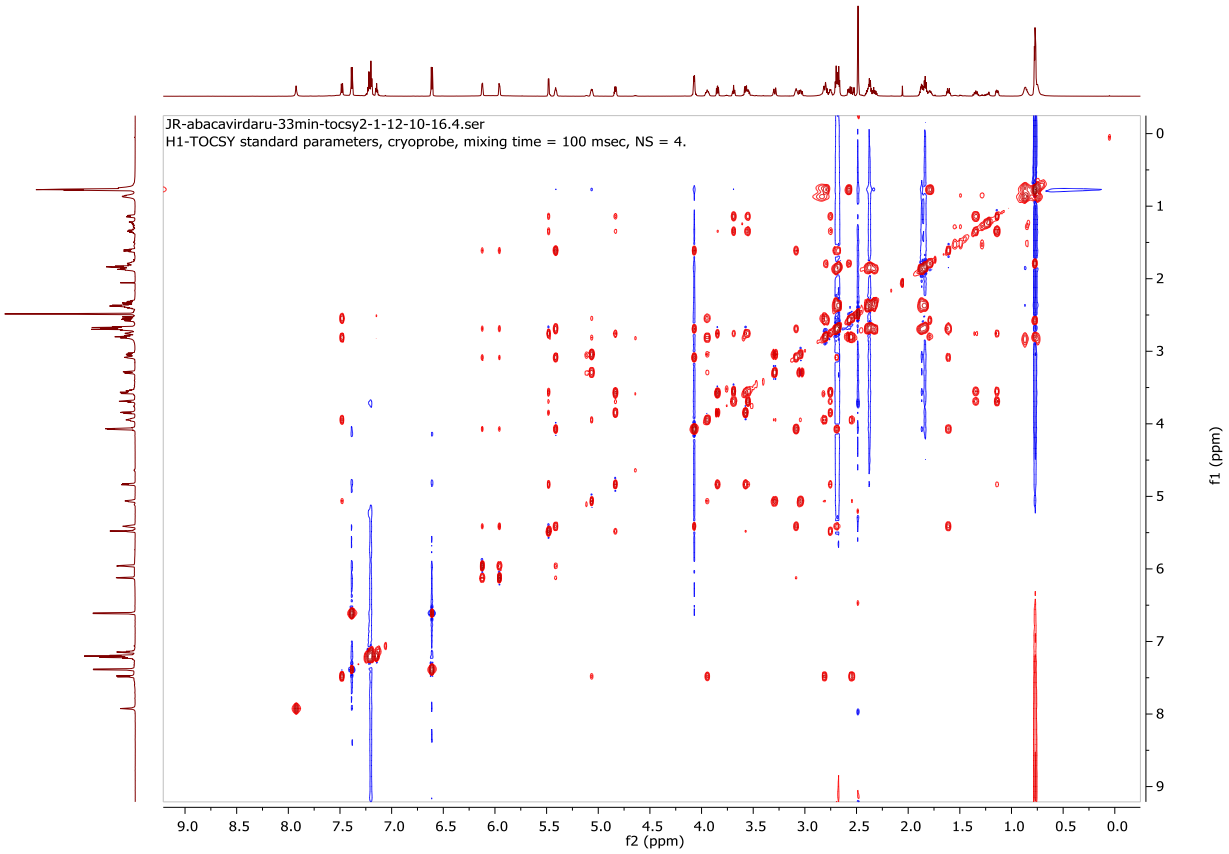

Figure A 17: ^{1}H-^{1}H TOCSY for Aba-S_2-DRV8.

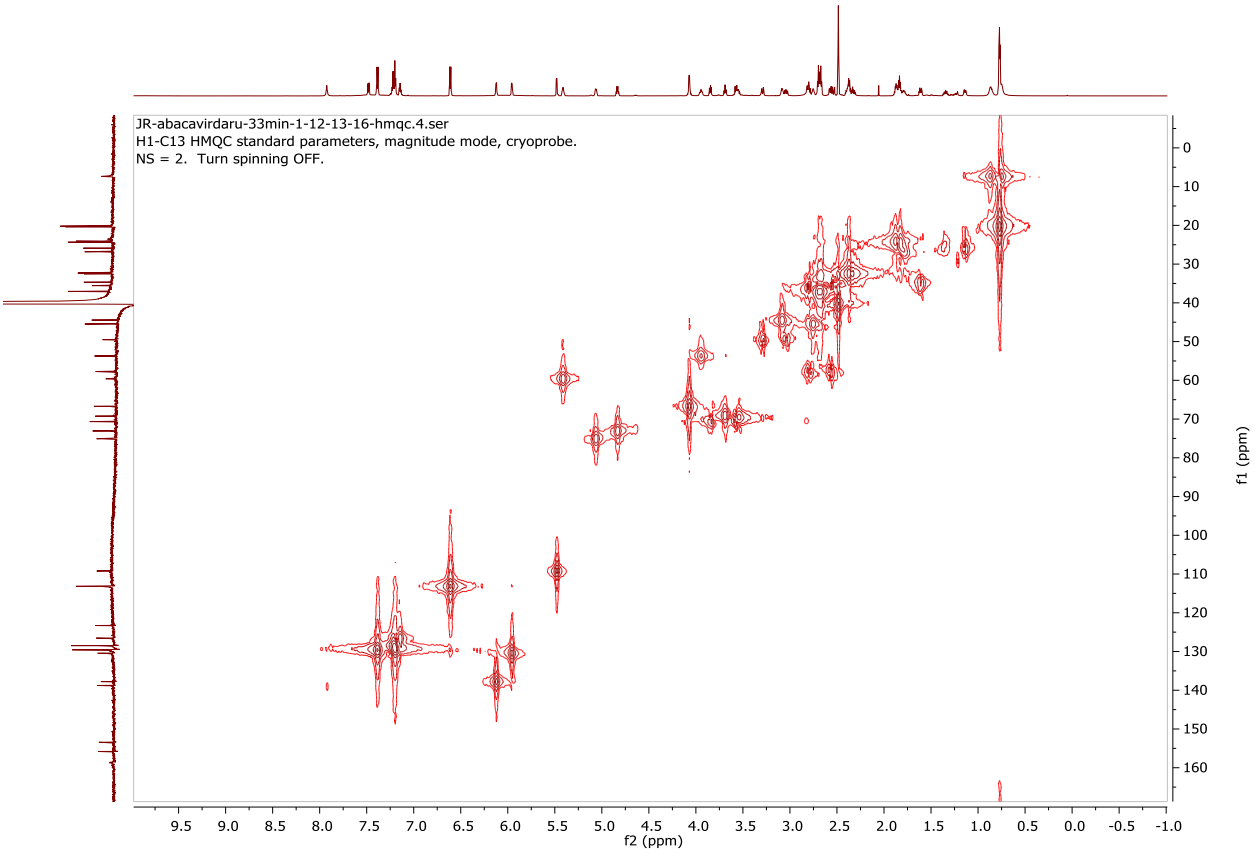

Figure A 18: ^{1}H-^{13}C HMQC for Aba-S_2-DRV8.

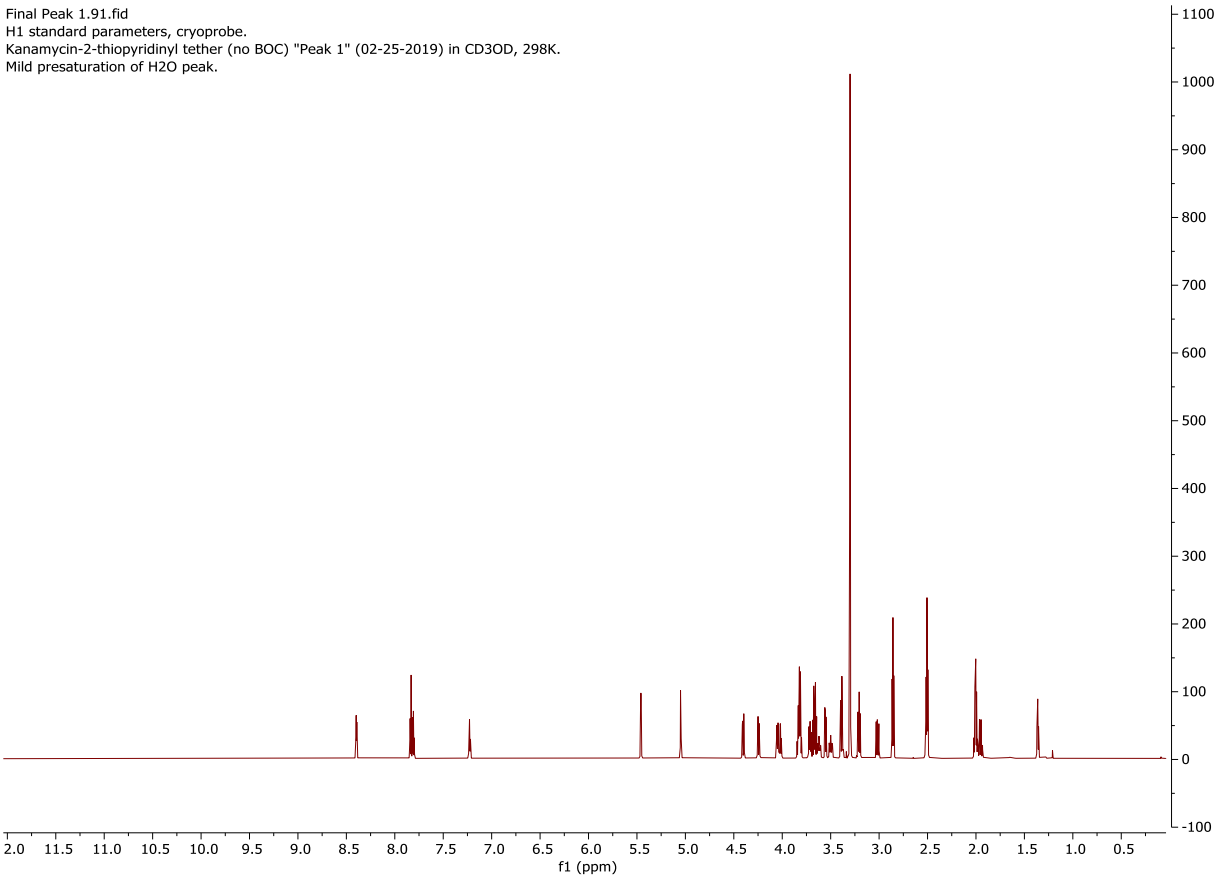

Figure A 19: ^{1}H NMR for Kanamycin-2-thiopyridinyl tether (Isomer 1) in CD_3-OD: Assignments made by ^{1}H, ^{13}C, DEPT-135, COSY, TOCSY, HSQC, and HMBC.

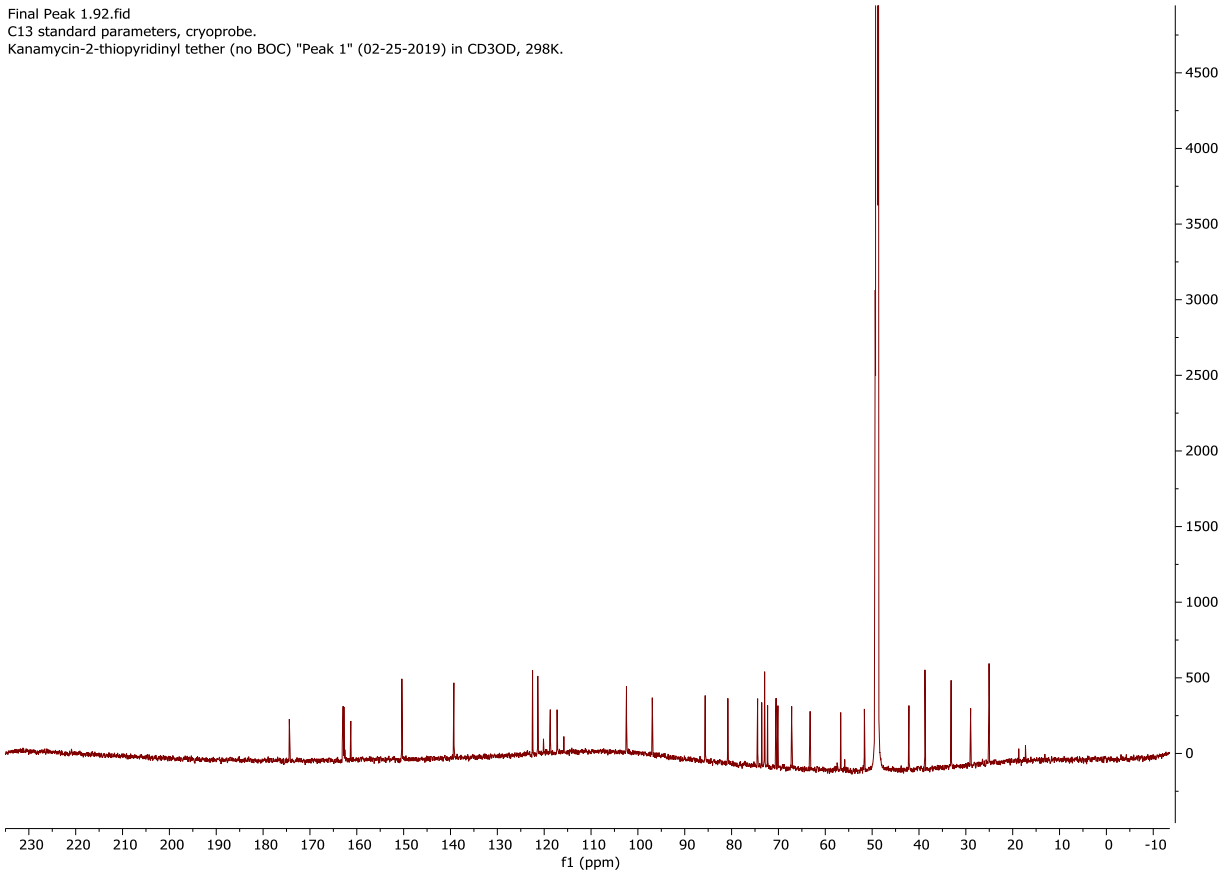

Figure A 20: ^{13}C NMR for Kanamycin-2-thiopyridinyl tether (Isomer 1) in CD_3-OD: Assignments made by ^{1}H, ^{13}C, DEPT-135, COSY, TOCSY, HSQC, and HMBC.

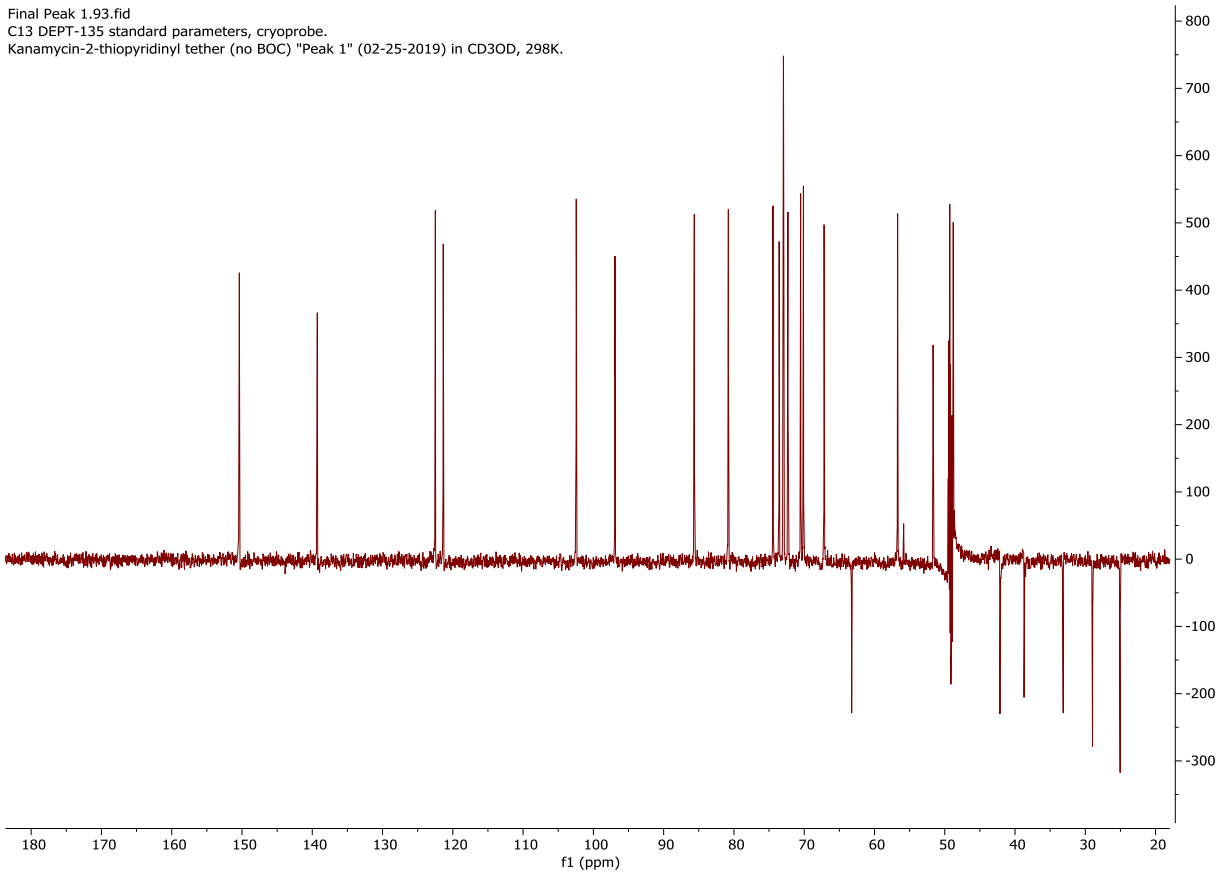

Figure A 21: DEPT-135 for Kanamycin-2-thiopyridinyl tether (Isomer 1).

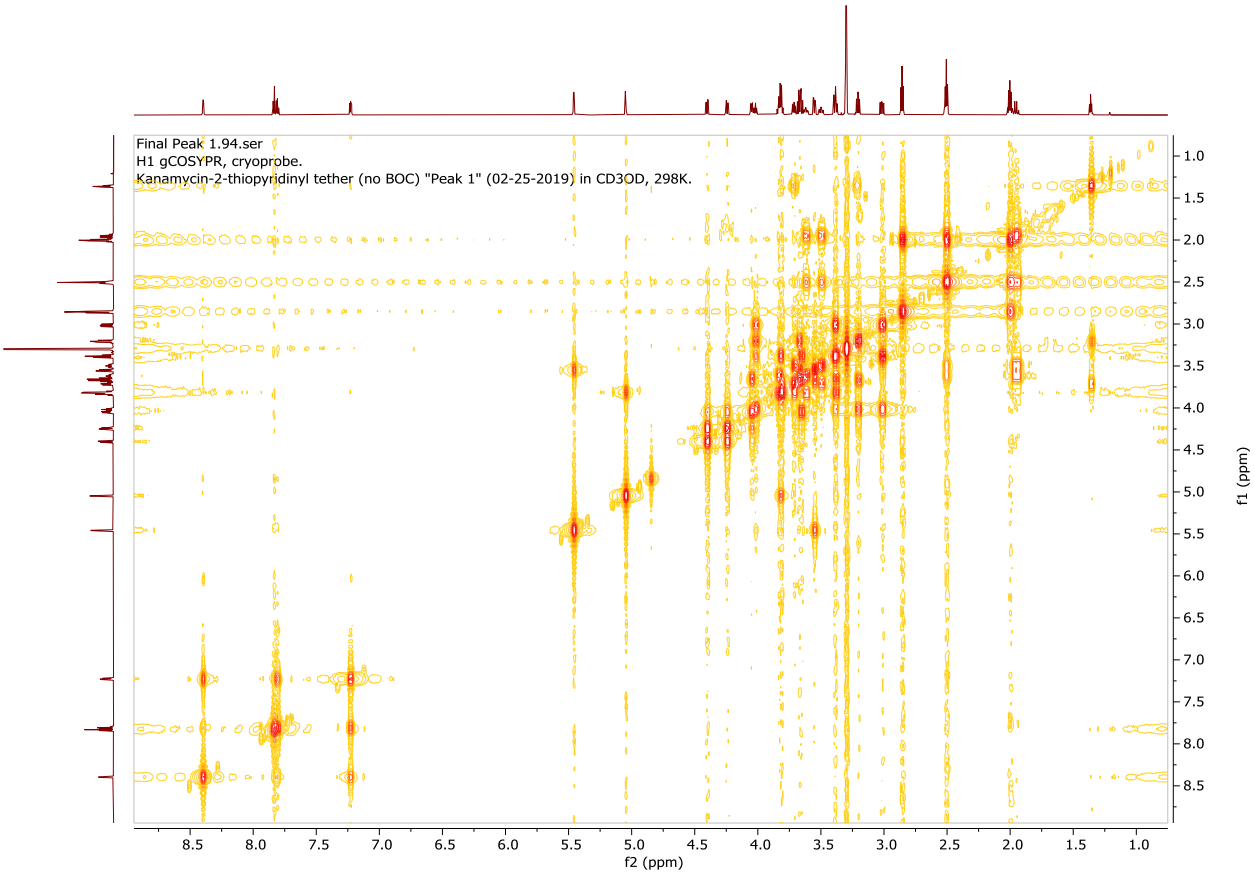

Figure A 22: COSY for Kanamycin-2-thiopyridinyl tether (Isomer 1).

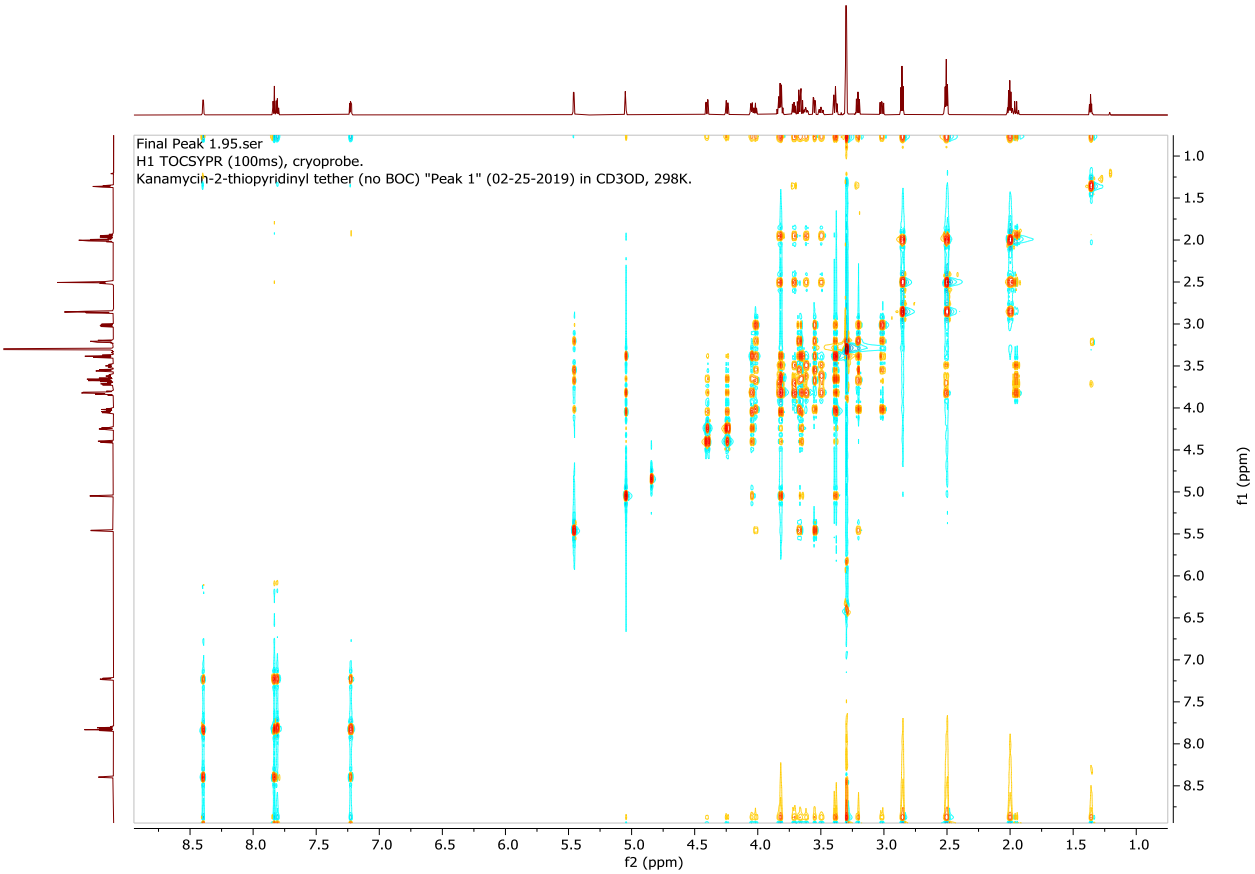

Figure A 23: TOCSY for Kanamycin-2-thiopyridinyl tether (Isomer 1).

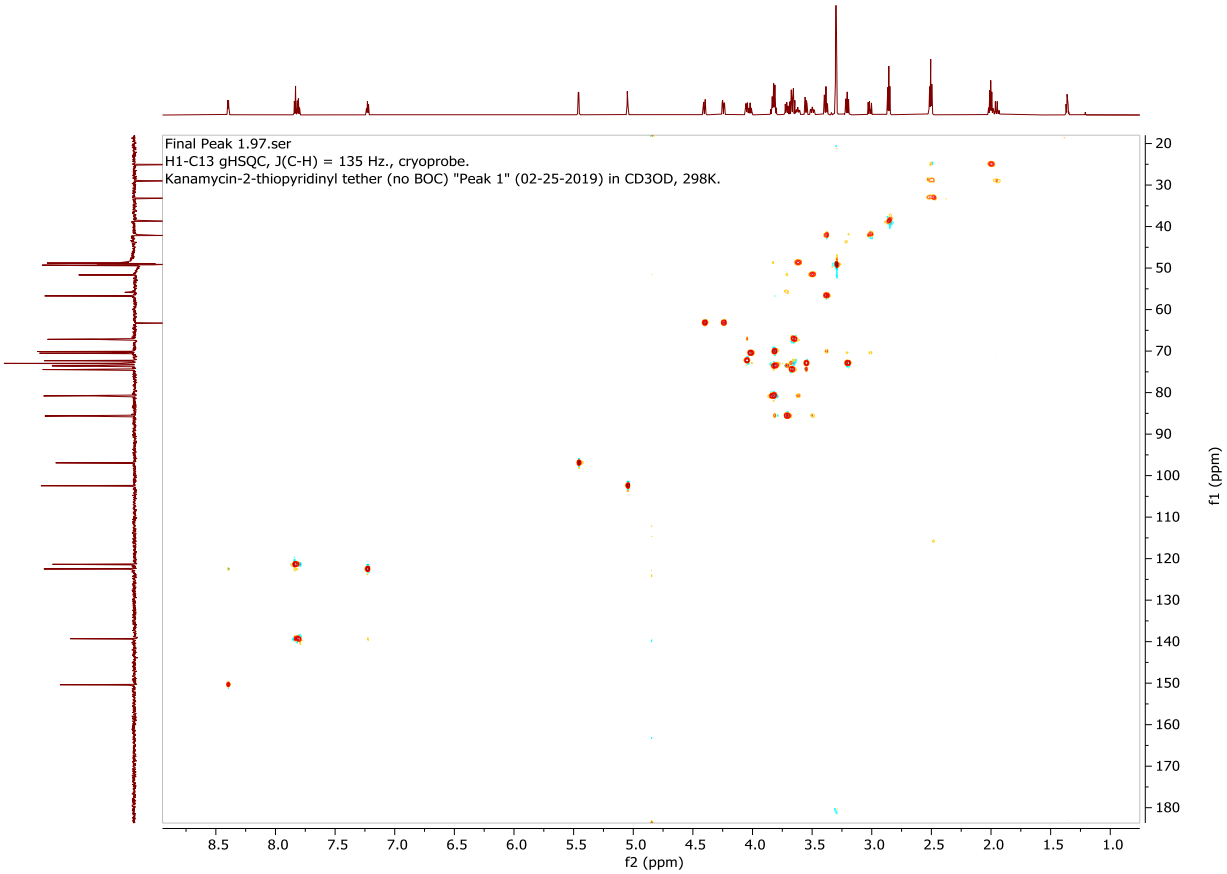

Figure A 24: HSQC for Kanamycin-2-thiopyridinyl tether (Isomer 1). Cross with DEPT-135 and ^{1}H Spectra.

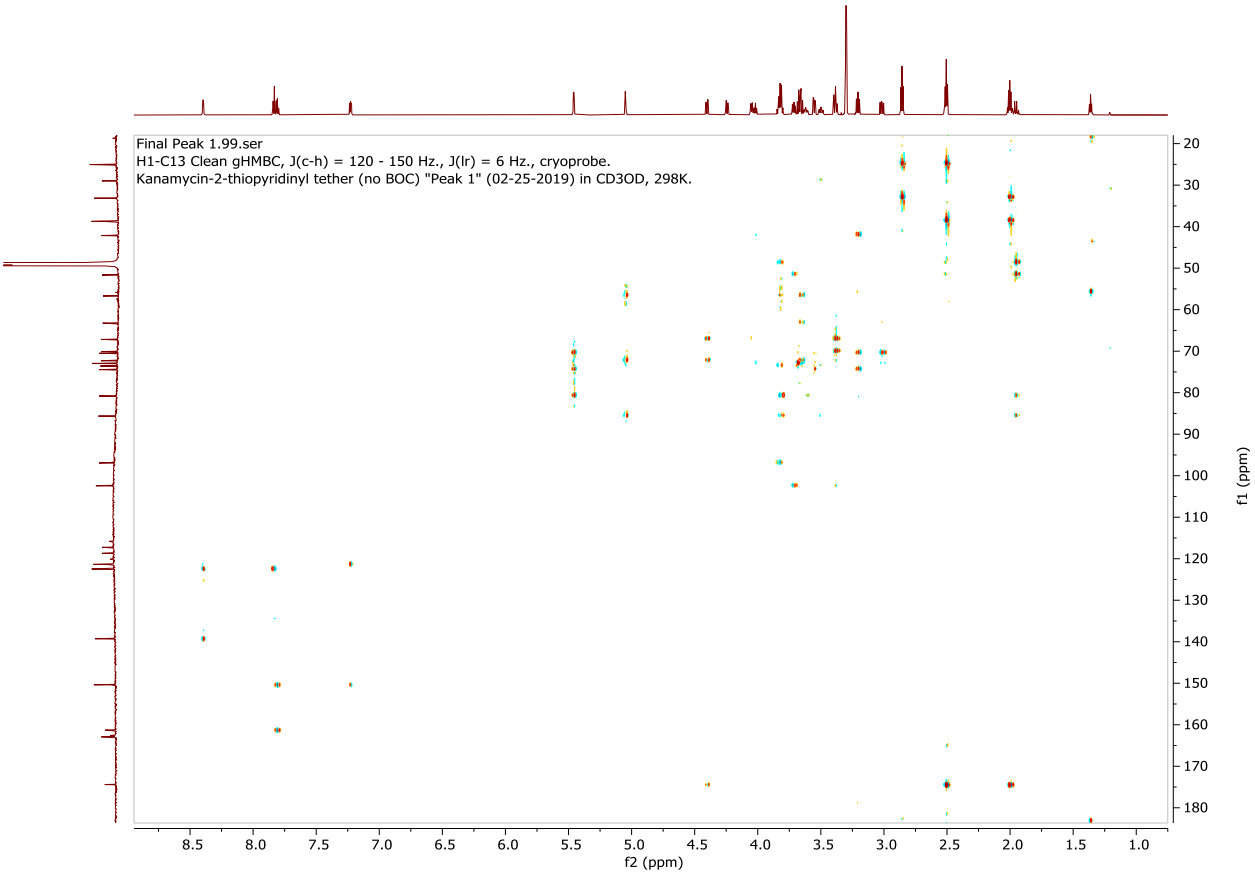

Figure A 25: HMBC for Kanamycin-2-thiopyridinyl tether (Isomer 1). Cross with ^{13}C and ^{1}H Spectra.

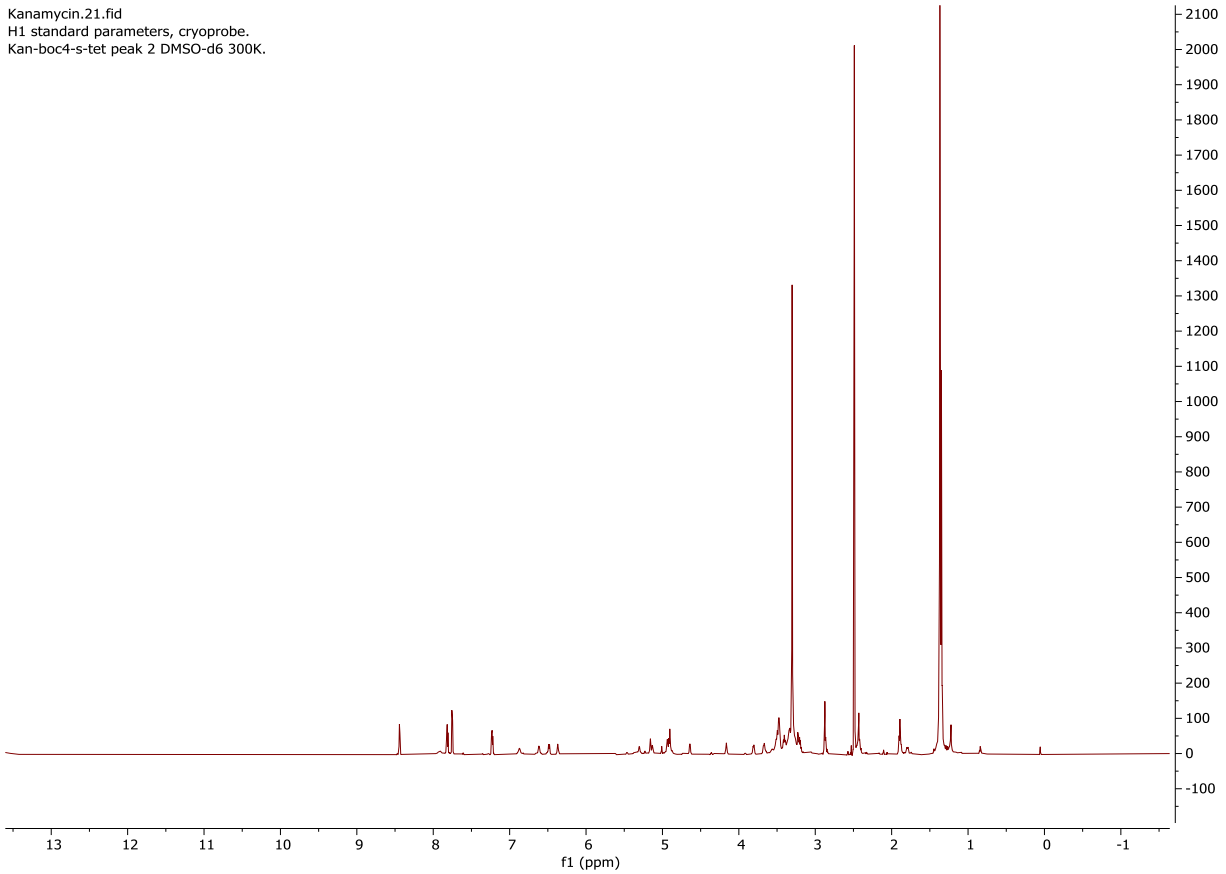

Figure A 26: ^{1}H for Kanamycin Boc_4- 2-thiopyridinyl tether (Isomer 2). in DMSO-d_6: Assignments made by ^{1}H, ^{13}C, DEPT-135, COSY, TOCSY, HSQC, and HMBC.

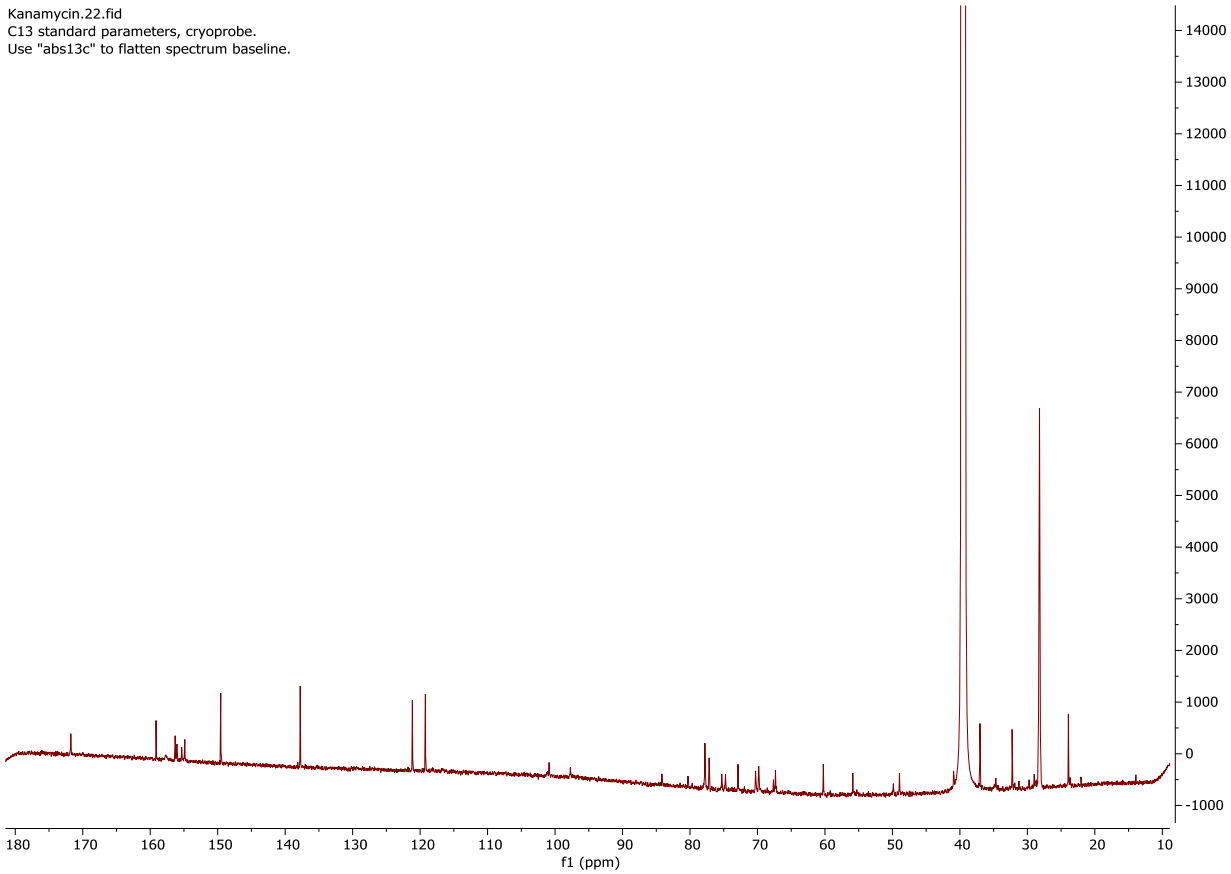

Figure A 27: ^{13}C for Kanamycin Boc_4-2-thiopyridinyl tether (Isomer 2). in DMSO-d_6: Assignments made by ^{1}H, ^{13}C, DEPT-135, COSY, TOCSY, HSQC, and HMBC.

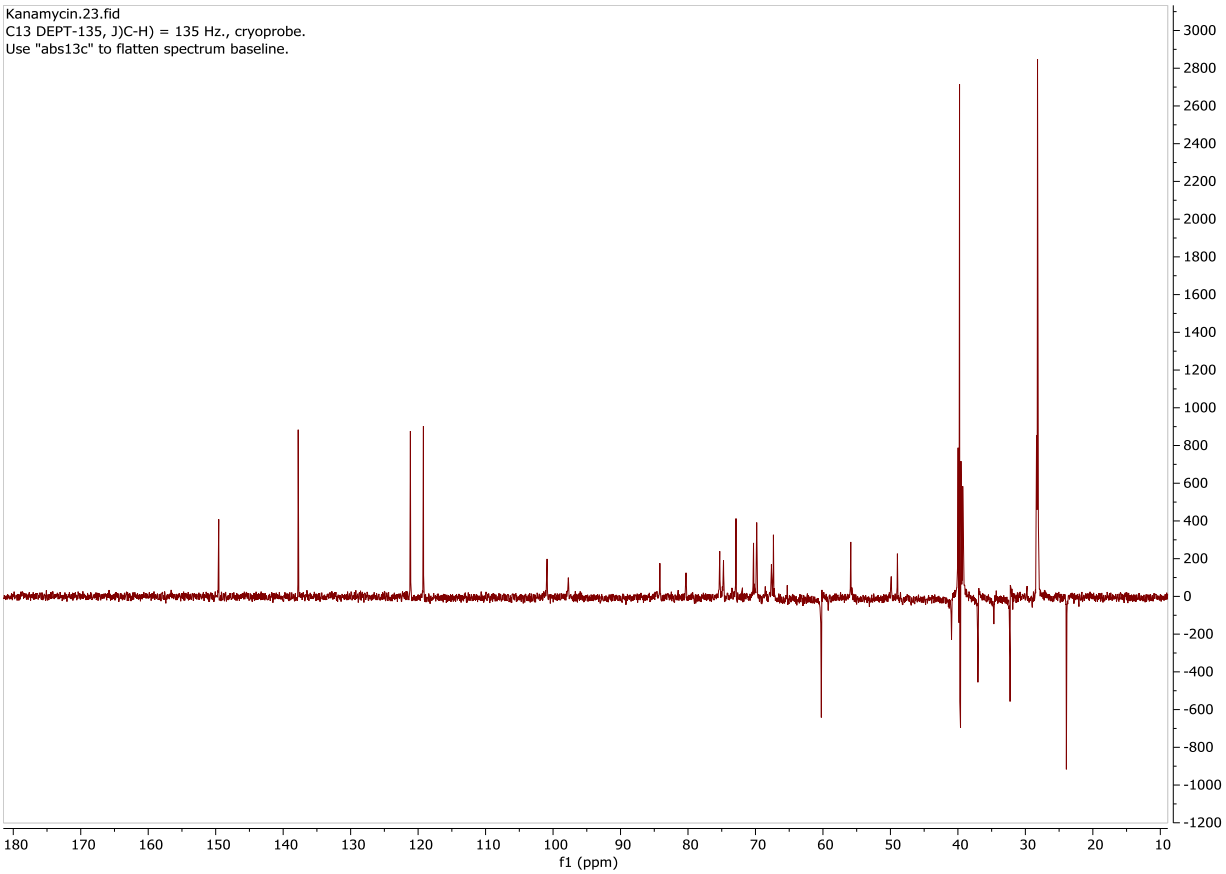

Figure A 28: DEPT-135 for Kanamycin Boc_4-2-thiopyridinyl tether (Isomer 2).

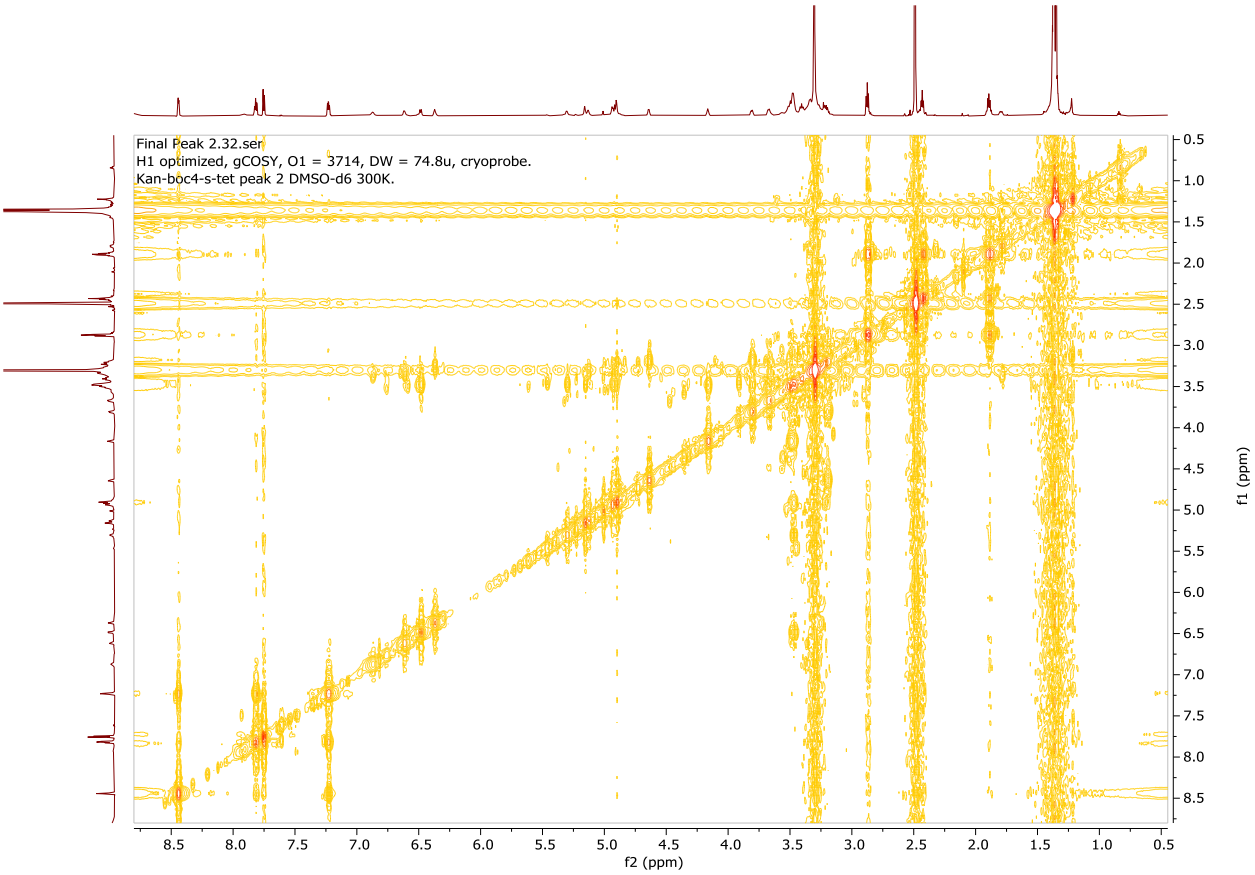

Figure A 29: COSY for Kanamycin Boc_4-2-thiopyridinyl tether (Isomer 2).

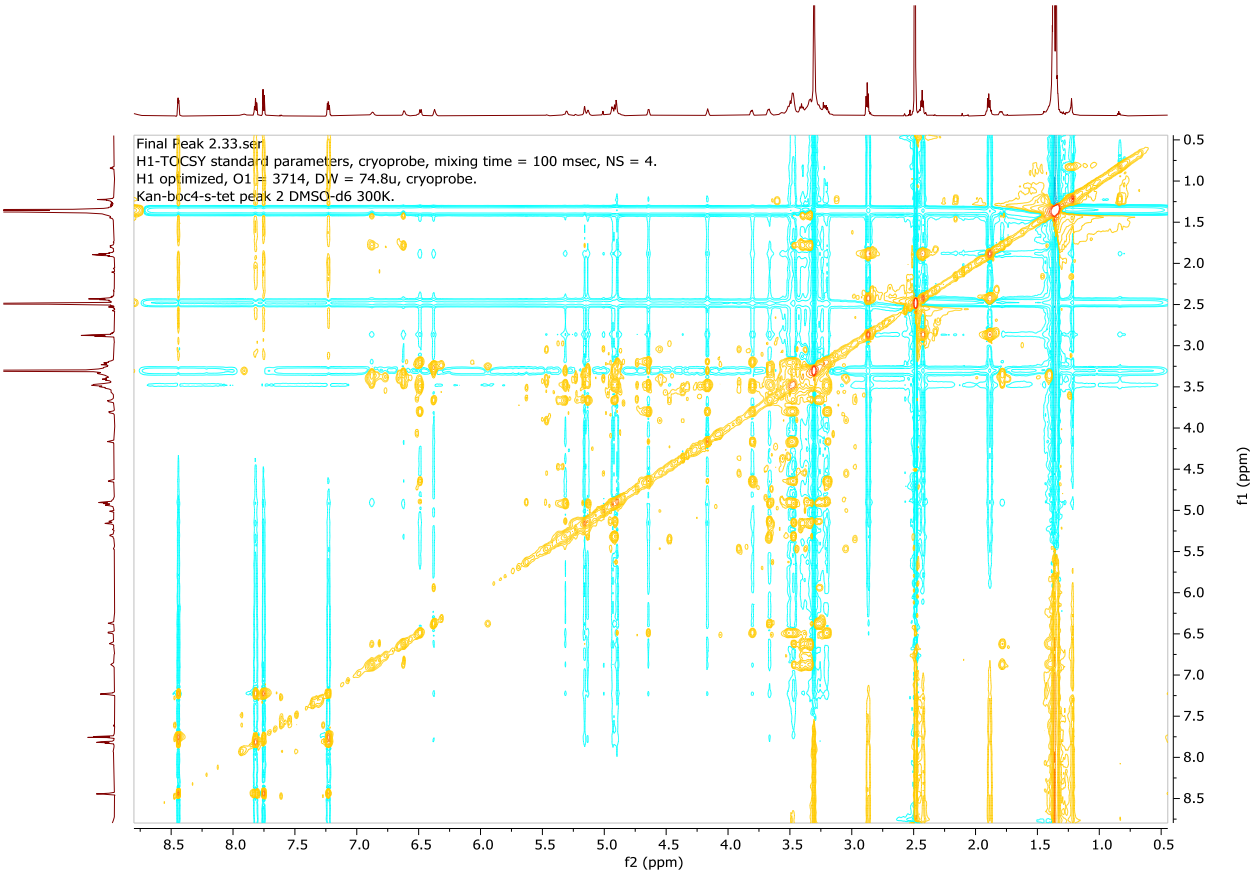

Figure A 30: TOCSY for Kanamycin Boc_4-2-thiopyridinyl tether (Isomer 2).

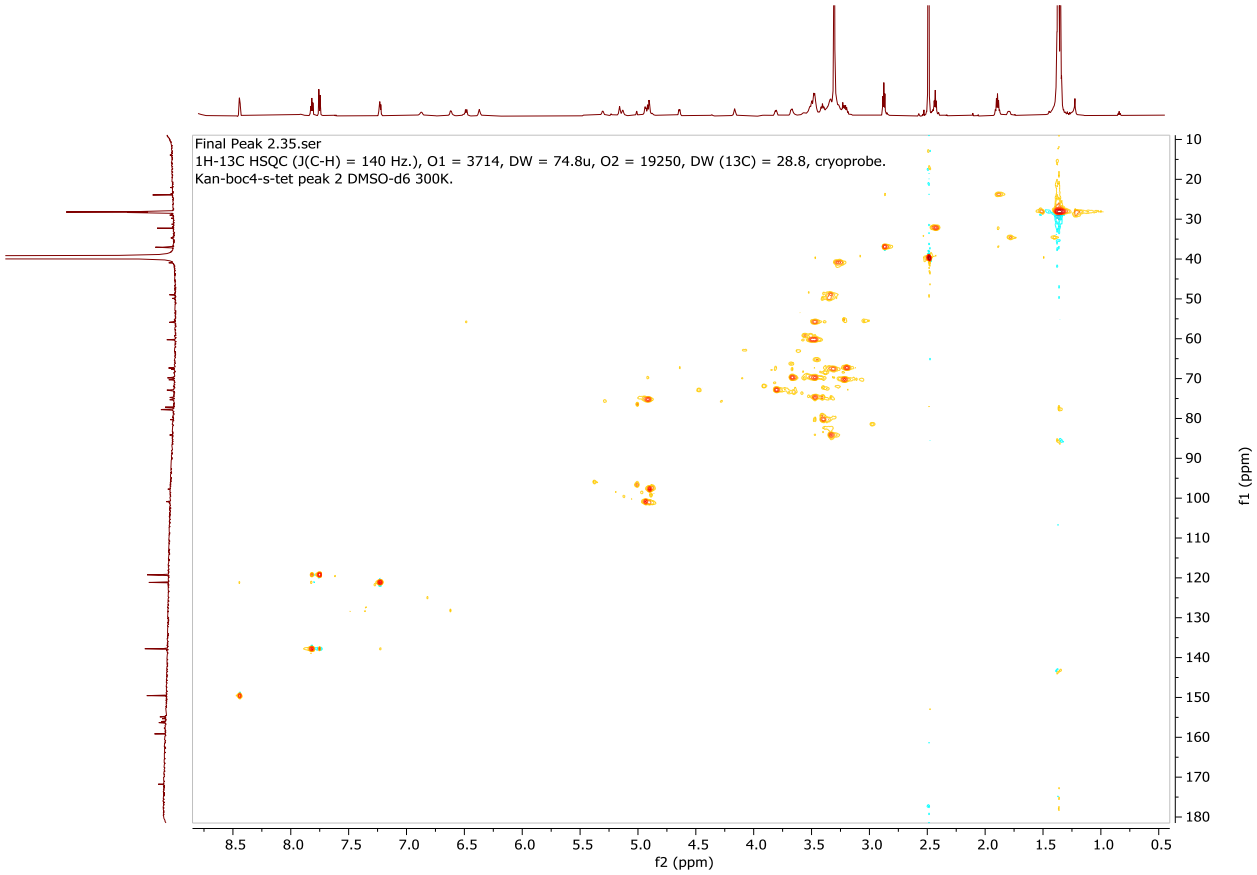

Figure A 31: HSQC for Kanamycin Boc_4-2-thiopyridinyl tether (Isomer 2). Cross of ^{13}C and ^{1}H spectra.

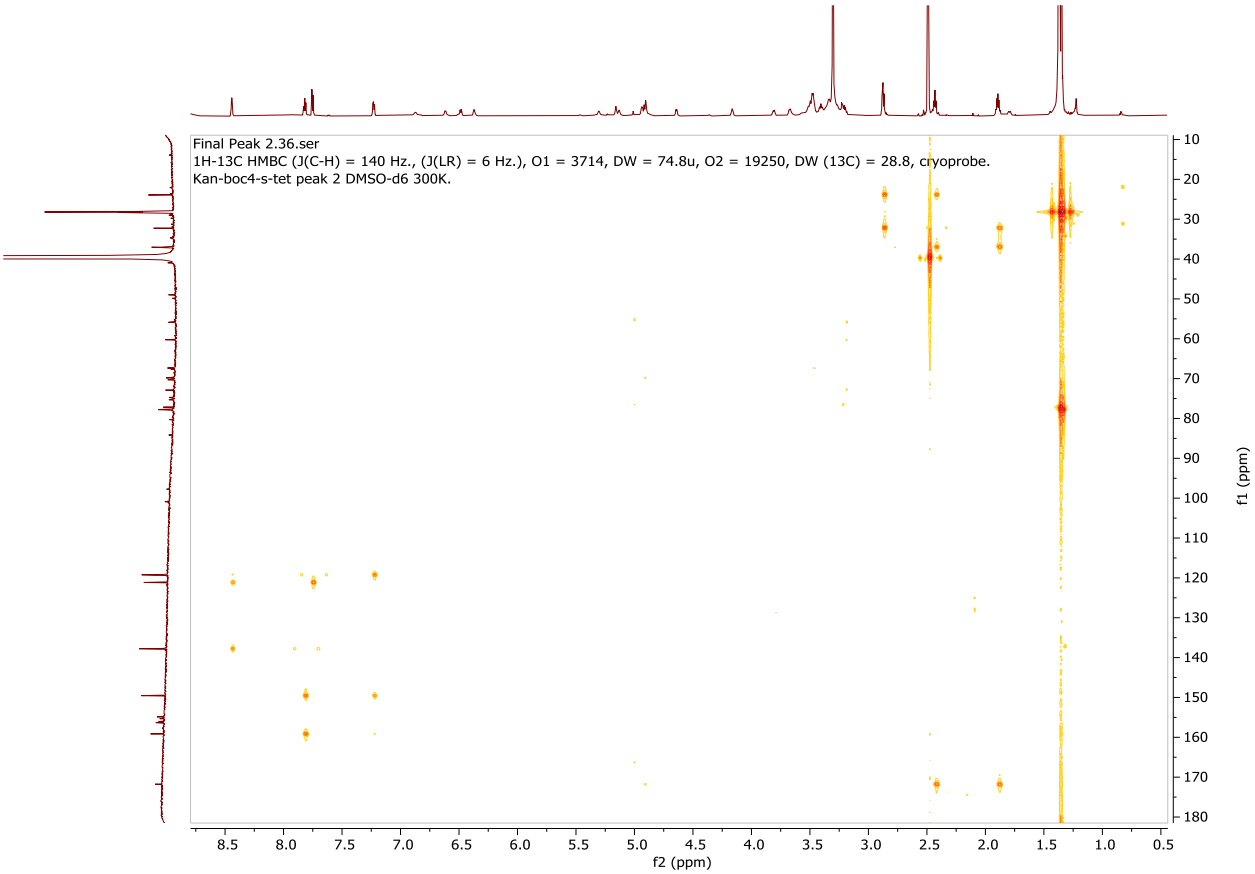

Figure A 32: HMBC for Kanamycin Boc_4-2-thiopyridinyl tether (Isomer 2). Cross of ^{13}C and ^{1}H spectra.

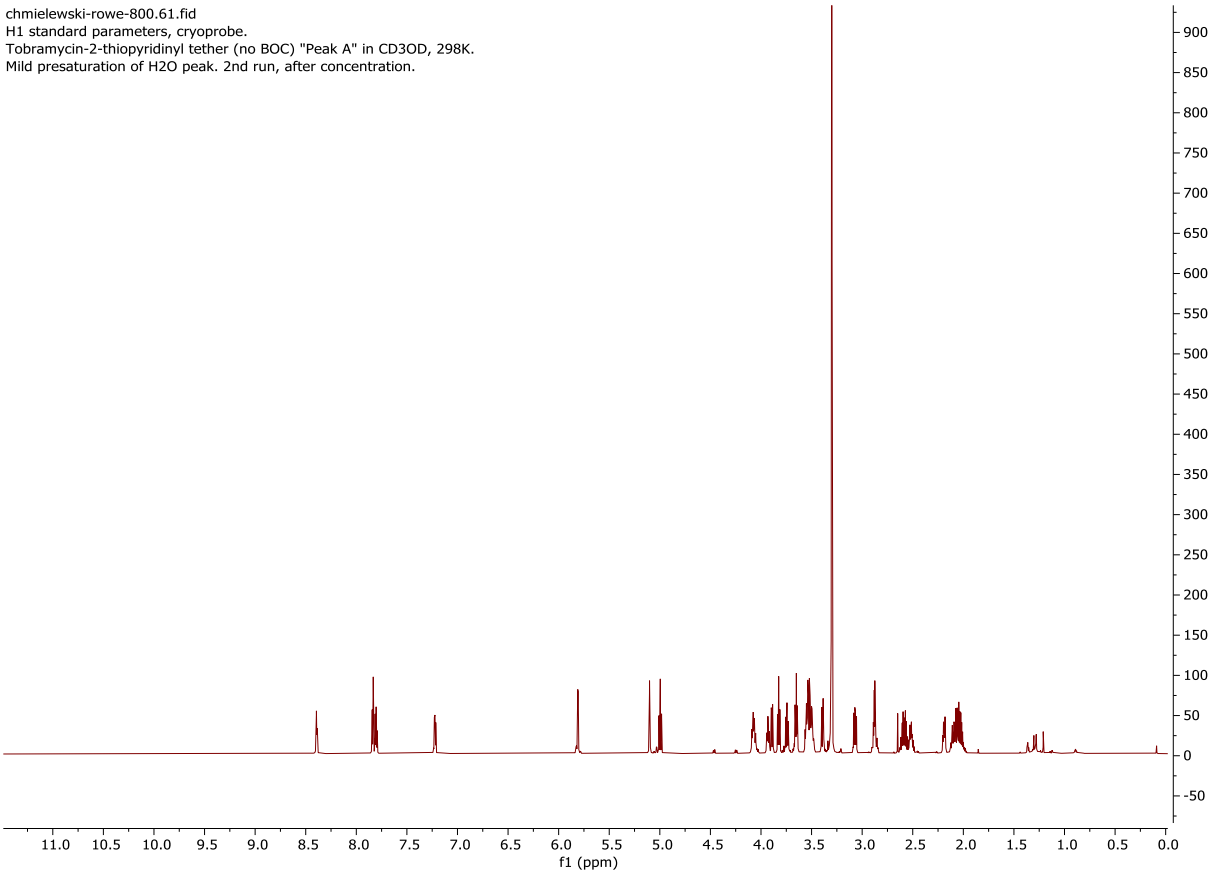

Figure A 33: ^{1}H for Tobramycin-2-thiopyridinyl tether (Isomer A) in CD_3-OD: Assignments made by ^{1}H, ^{13}C, DEPT-135, COSY, TOCSY, HSQC and HMBC.

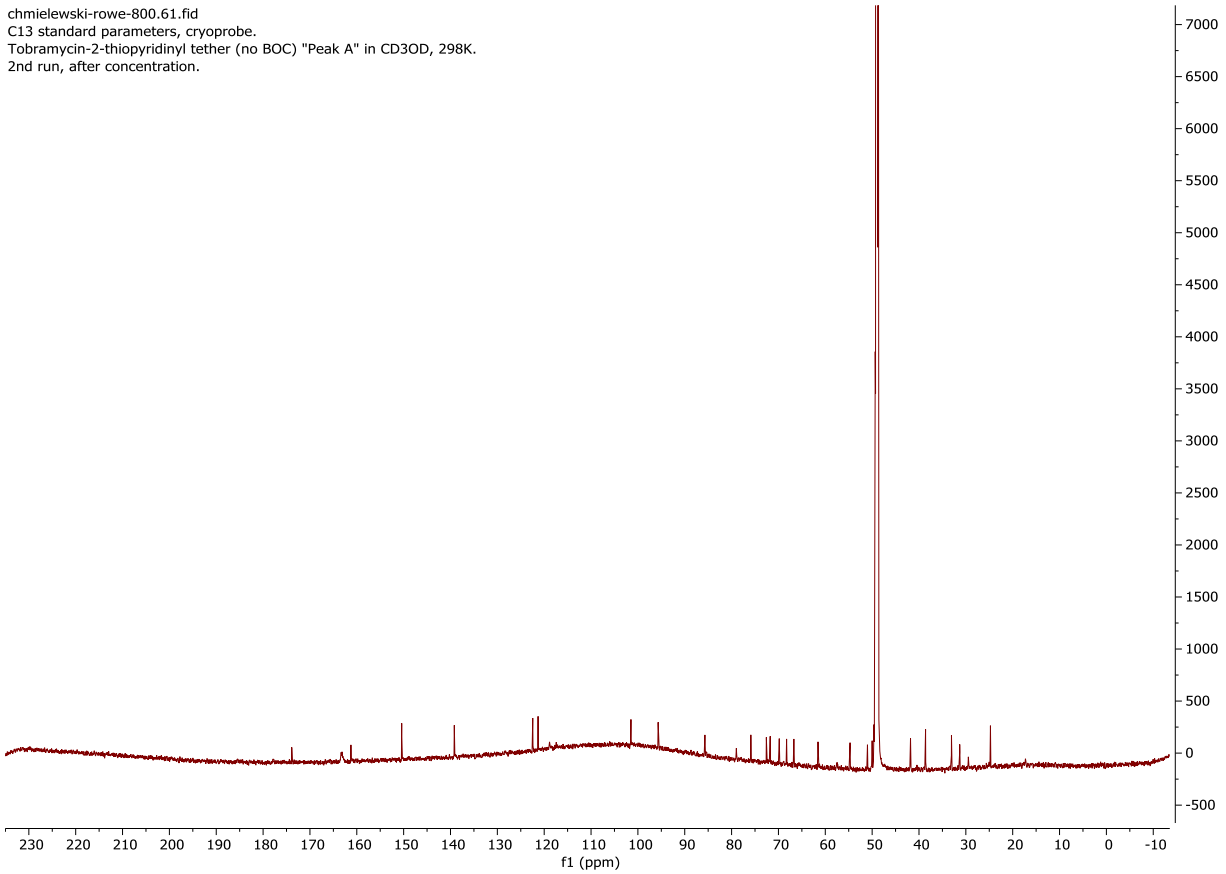

Figure A 34: ^{13}C for Tobramycin-2-thiopyridinyl tether (Isomer A) in CD_3-OD: Assignments made by ^{1}H, ^{13}C, DEPT-135, COSY, TOCSY, HSQC and HMBC.

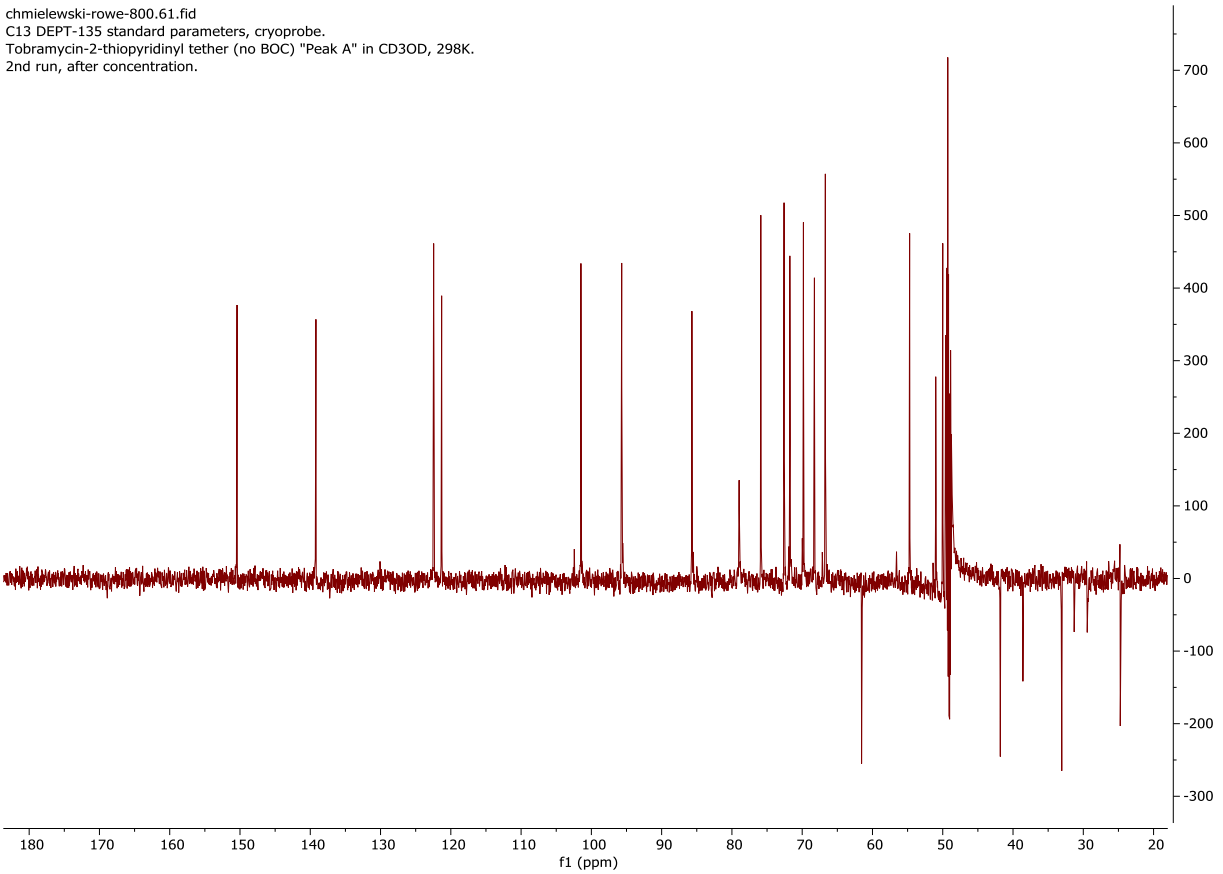

Figure A 35: DEPT 135 for Tobramycin-2-thiopyridinyl tether (Isomer A).

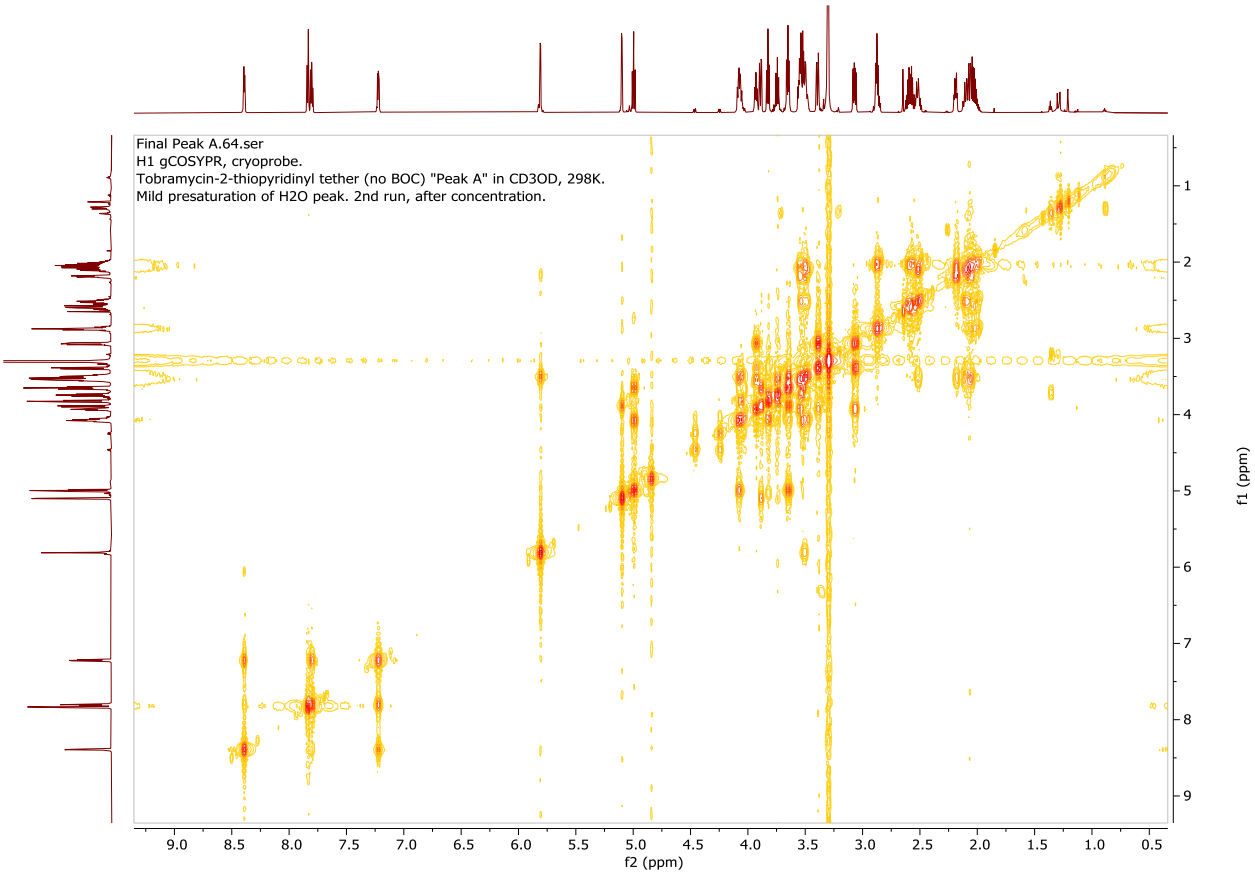

Figure A 36: ^{1}H-^{1}H COSY for Tobramycin-2-thiopyridinyl tether (Isomer A).

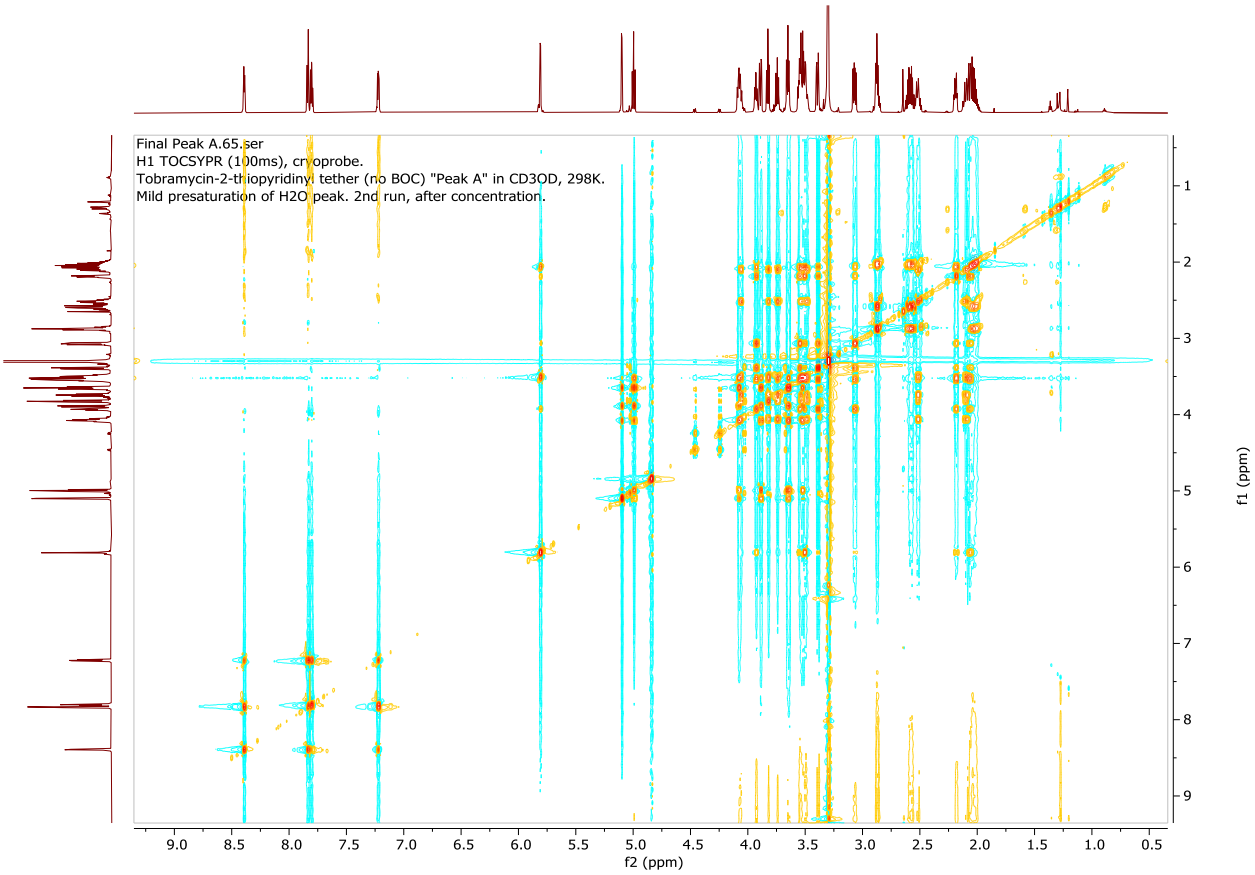

Figure A 37: ^{1}H-^{1}H TOCSY for Tobramycin-2-thiopyridinyl tether (Isomer A).

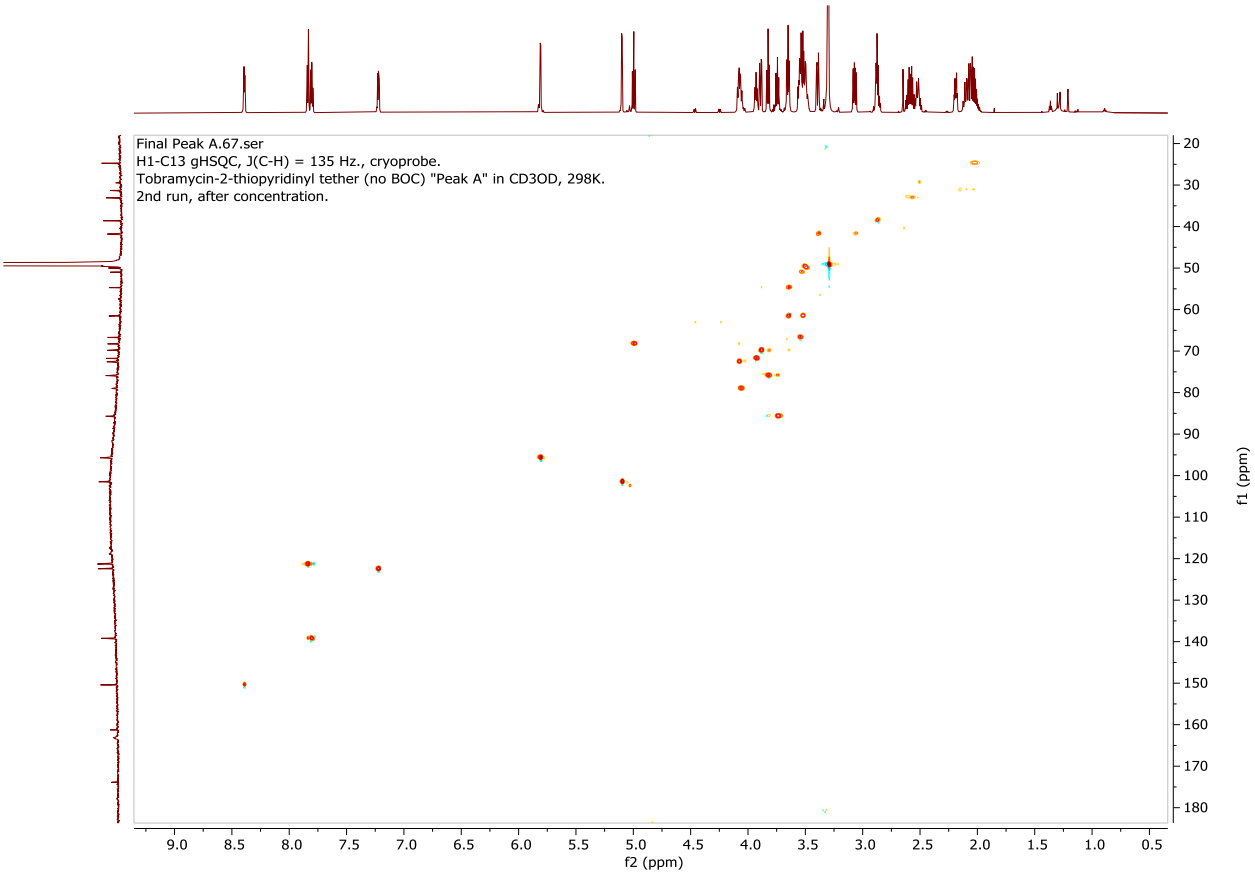

Figure A 38: ^{1}H-^{13}C HSQC for Tobramycin-2-thiopyridinyl tether (Isomer A).

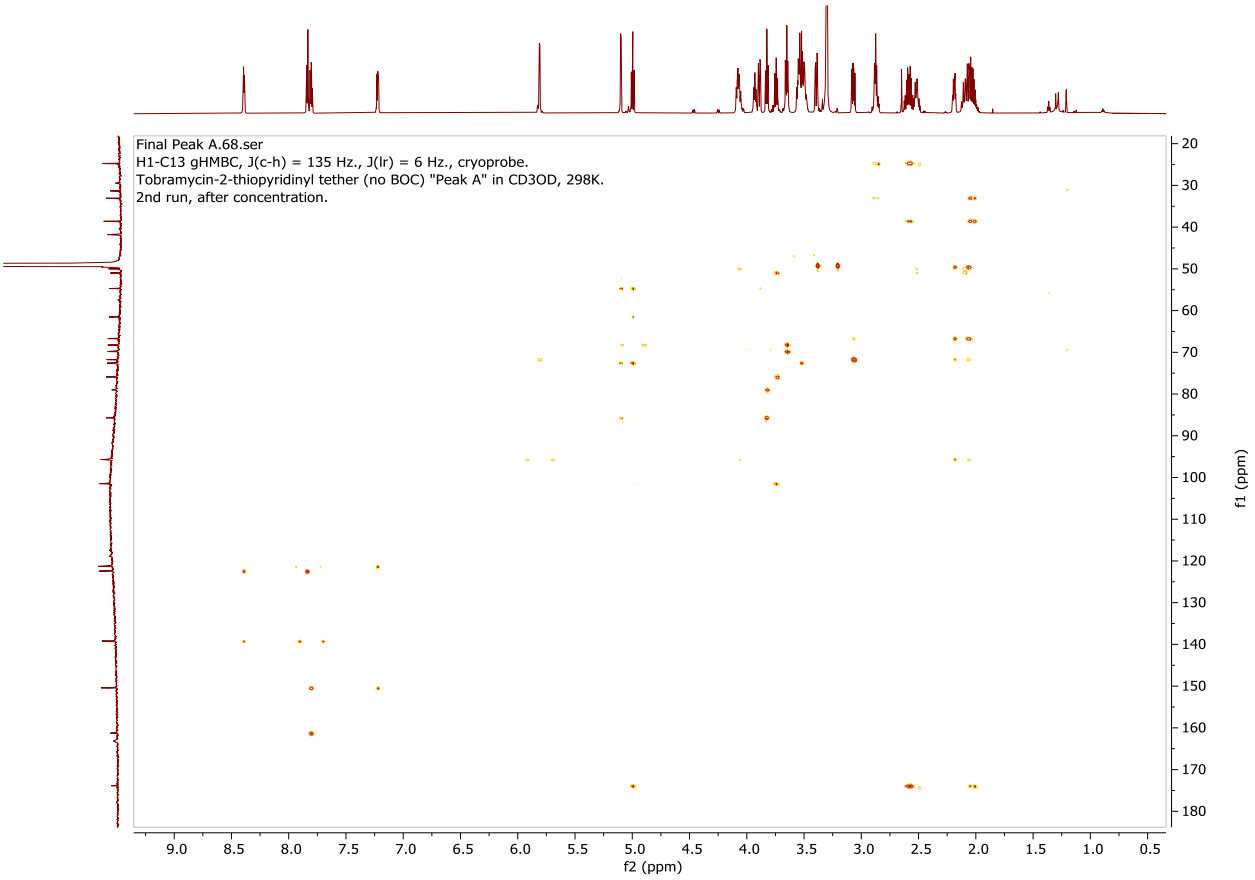

Figure A 39: ^{1}H-^{13}C HBMC for Tobramycin-2-thiopyridinyl tether (Isomer A).

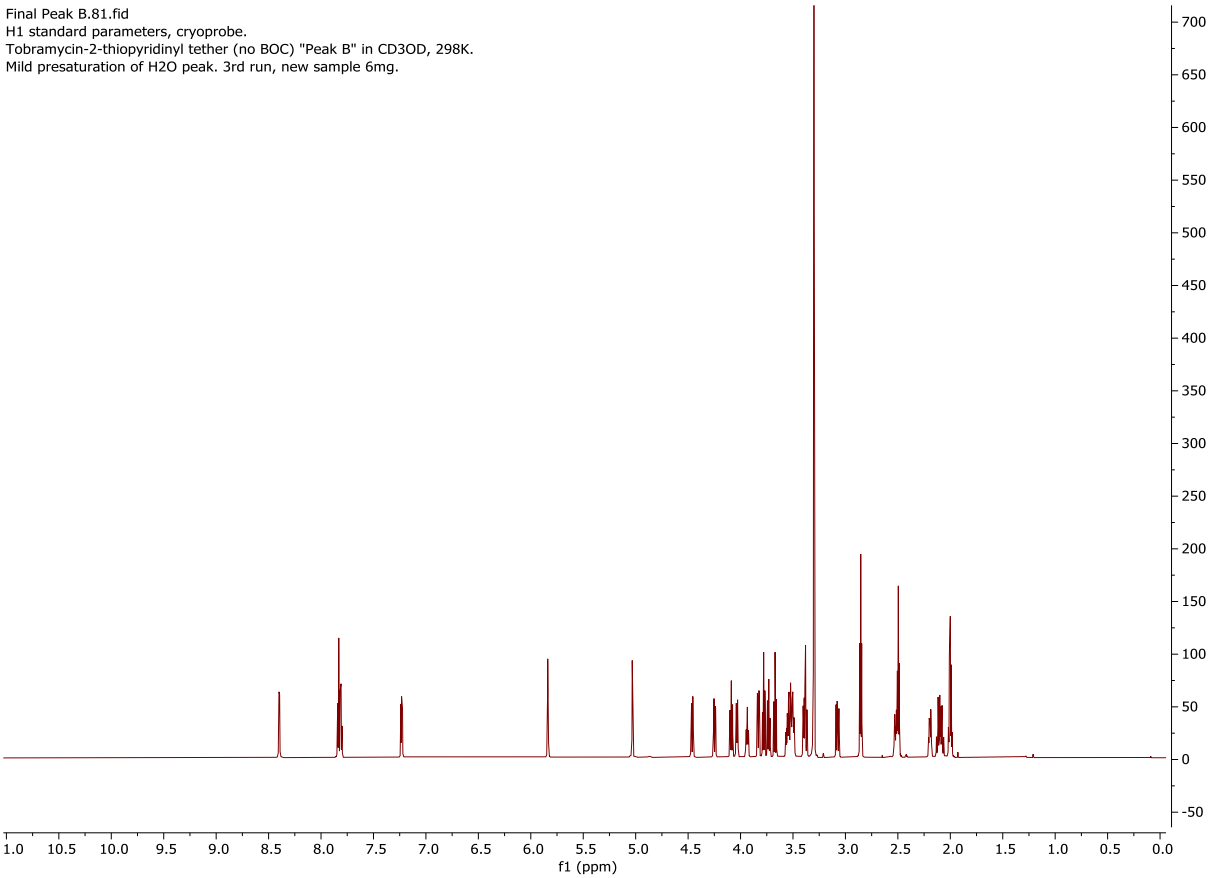

Figure A 40: ^{1}H for Tobramycin-2-thiopyridinyl tether (Isomer B) in CD_3-OD: Assignments made by ^{1}H, ^{13}C, DEPT-135, COSY, TOCSY, HSQC and HMBC.

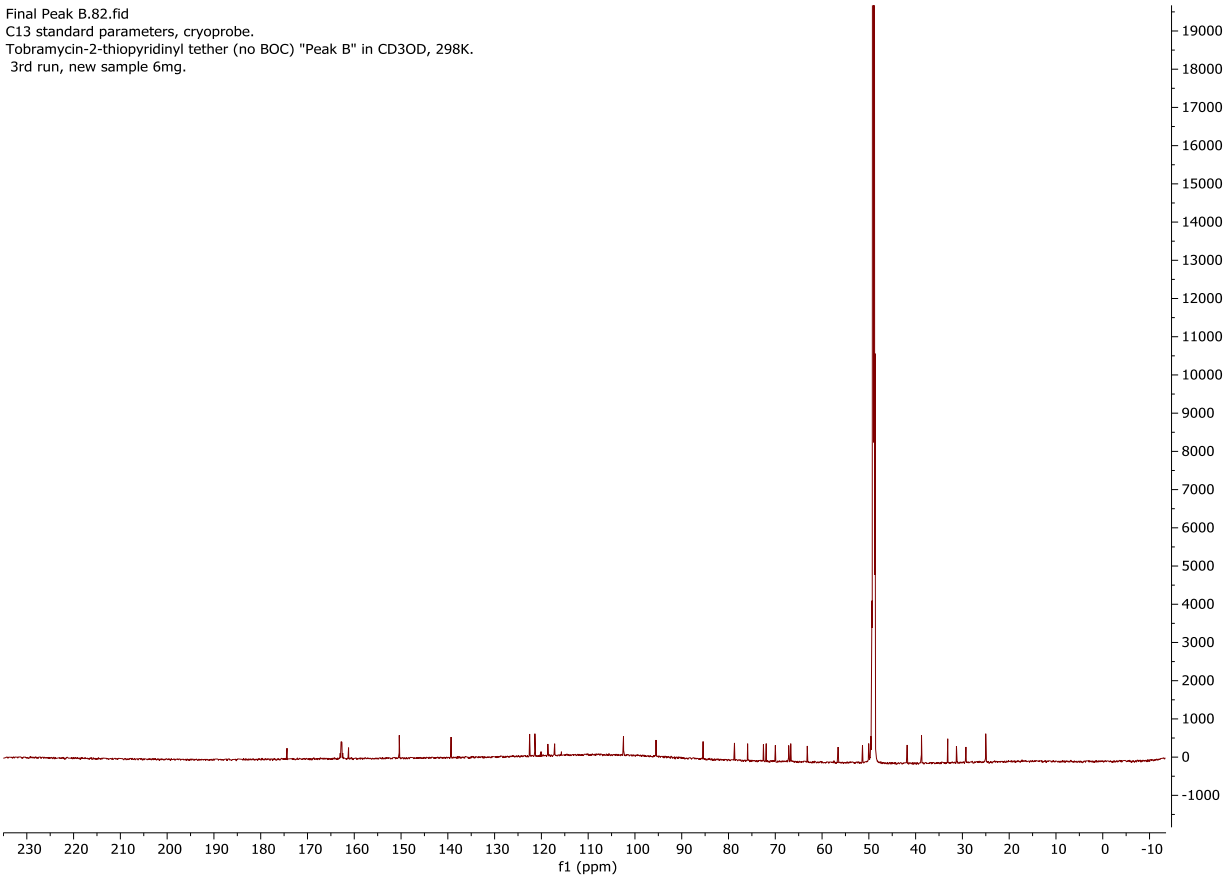

Figure A 41: ^{13}C for Tobramycin-2-thiopyridinyl tether (Isomer B) in CD_3-OD: Assignments made by ^{1}H, ^{13}C, DEPT-135, COSY, TOCSY, HSQC and HMBC.

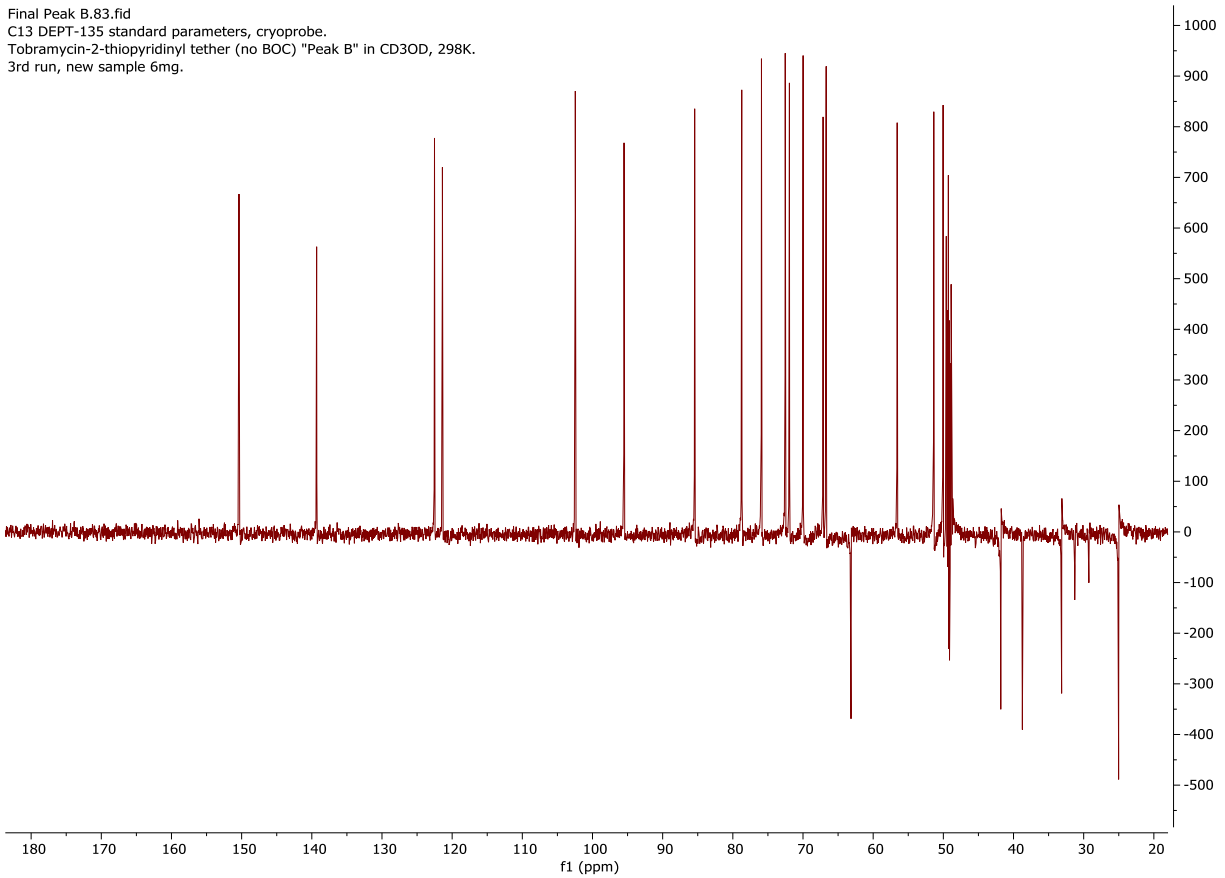

Figure A 42: DEPT 135 for Tobramycin-2-thiopyridinyl tether (Isomer B).

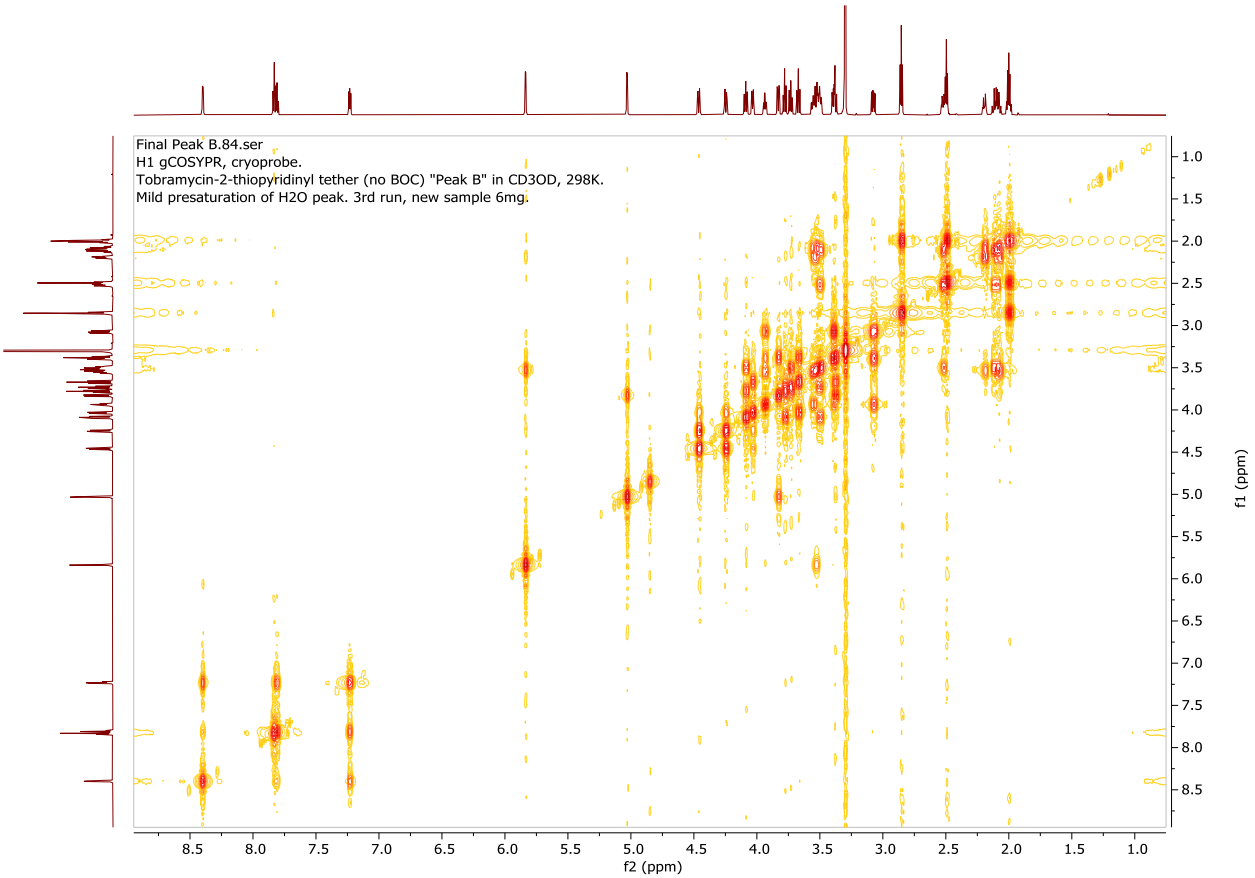

Figure A 43: ^{1}H-^{1}H COSY for Tobramycin-2-thiopyridinyl tether (Isomer B).

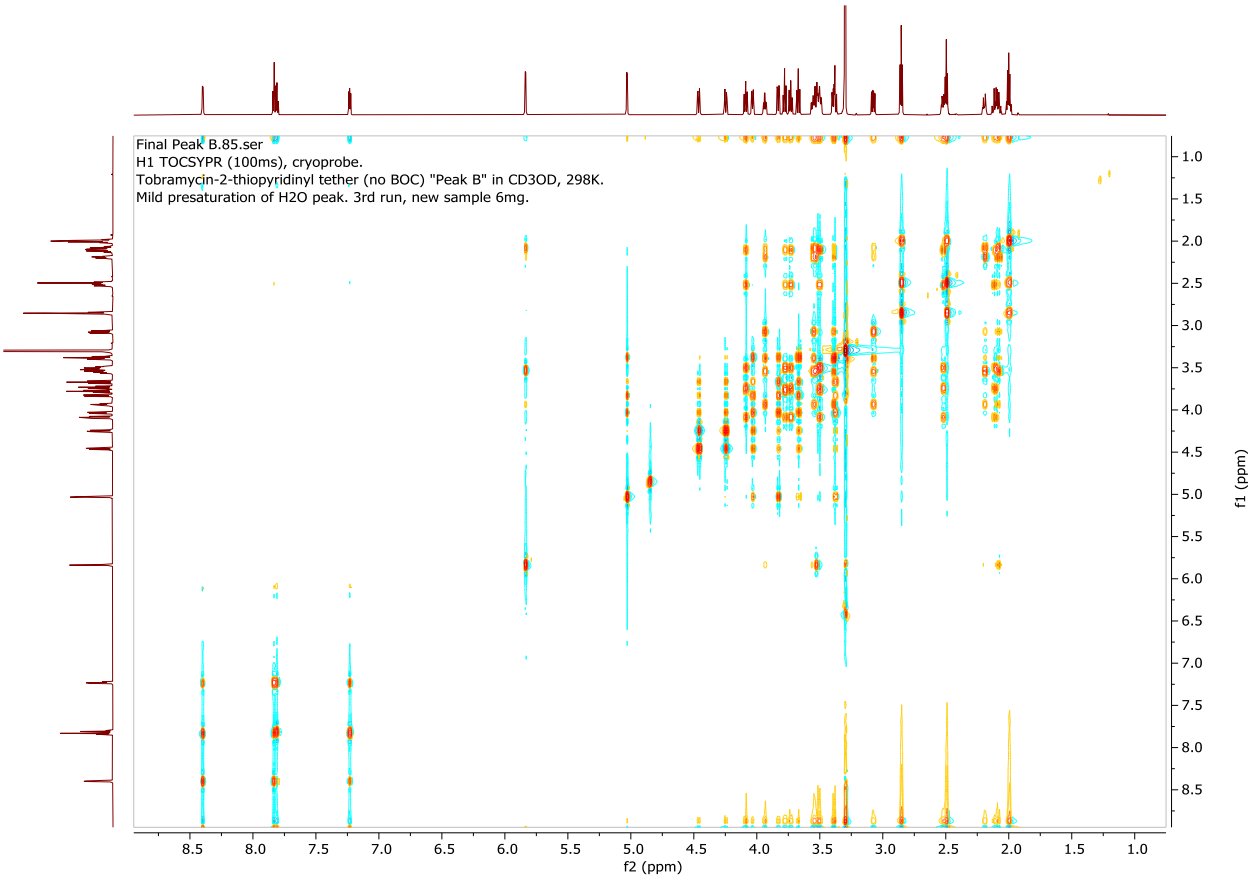

Figure A 44: ^{1}H-^{1}H TOCSY for Tobramycin-2-thiopyridinyl tether (Isomer B).

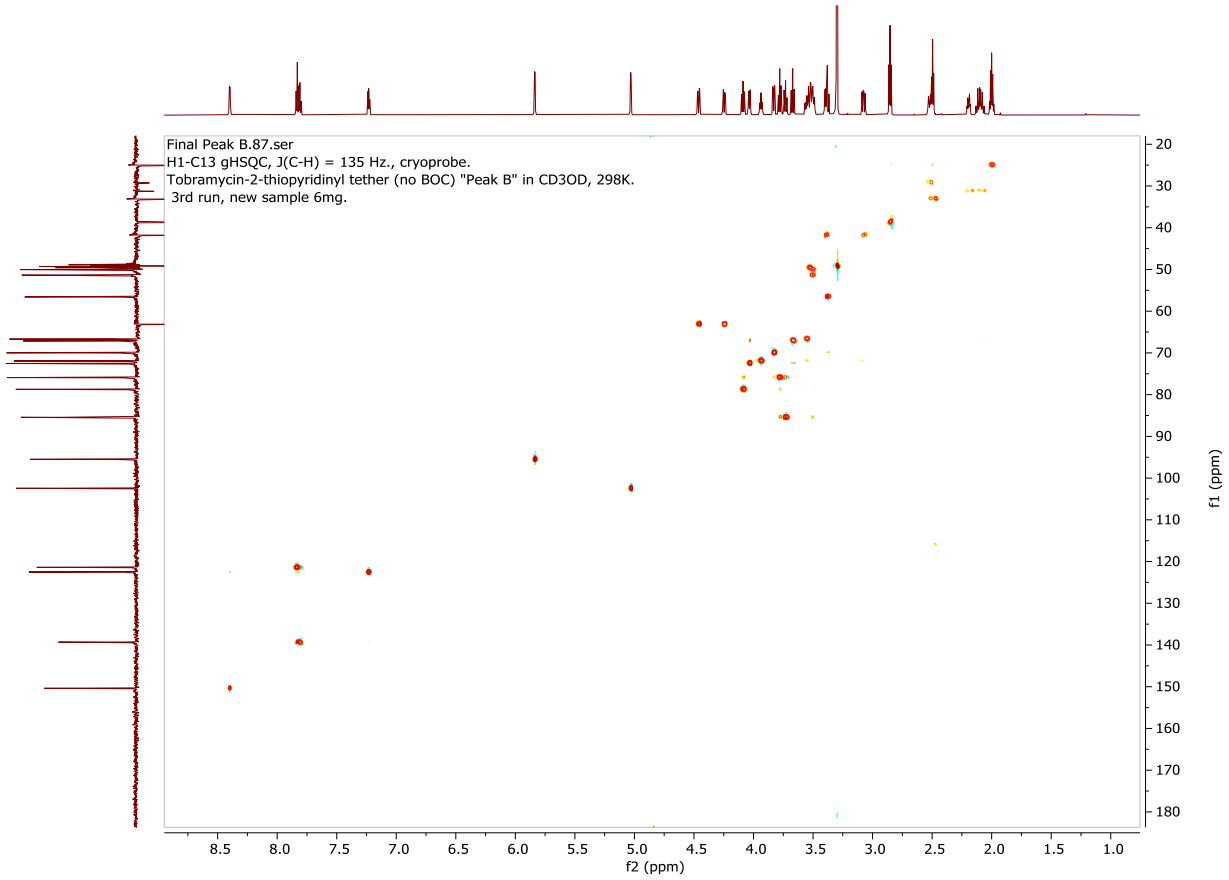

Figure A 45: ^{1}H-^{13}C HSQC for Tobramycin-2-thiopyridinyl tether (Isomer B).

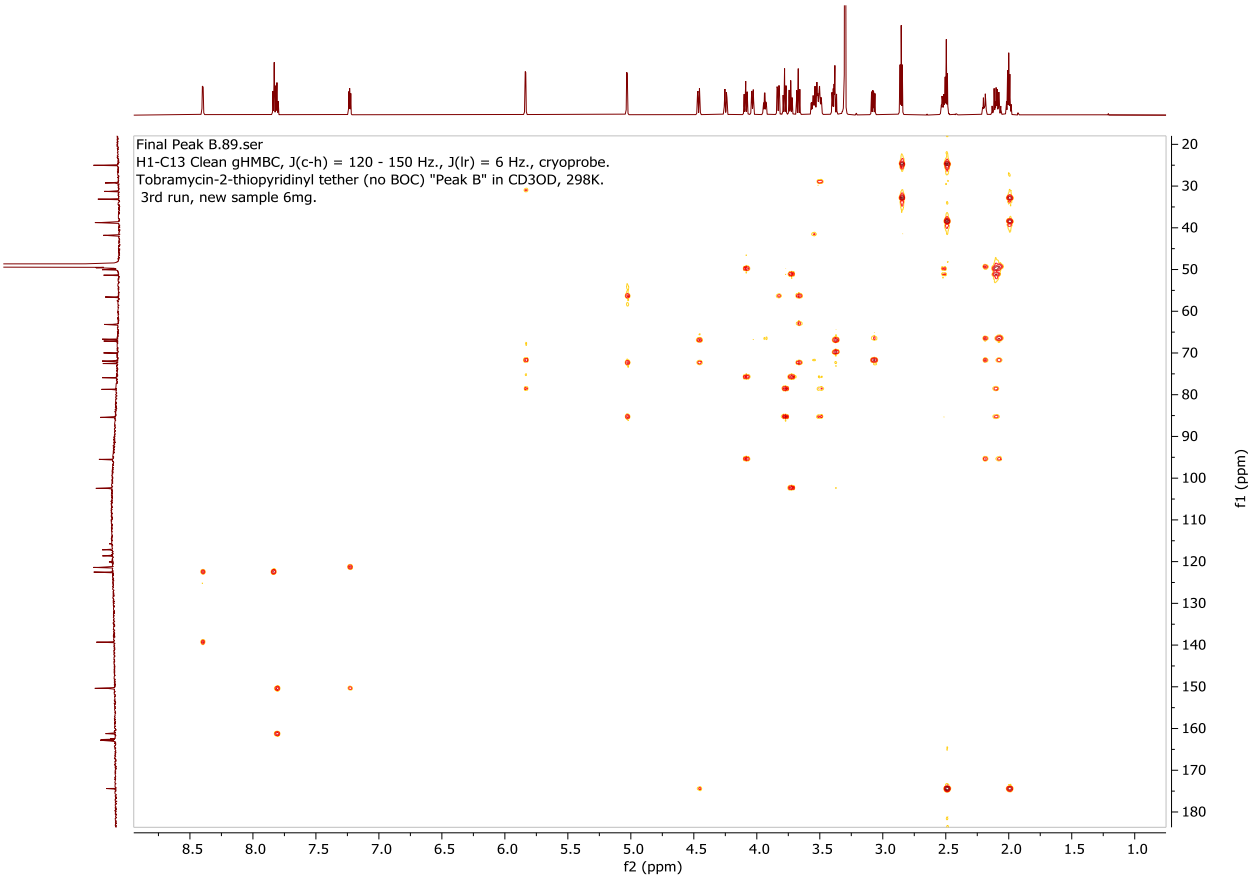

Figure A 46: ^{1}H-^{13}C HMBC for Tobramycin-2-thiopyridinyl tether (Isomer B).

VITA

Jennifer L. Rowe was born in Princeton, New Jersey on December 18, 1991. She attended high school at Mater Dei High School in Santa Ana, California. Upon graduation, she moved to Saint Paul, MN where she attended St. Catherine University for her undergraduate studies. During her undergraduate studies, she performed research in the laboratory of Professor James Wollack from 2012-2014. In the summer of 2013, she completed a summer undergraduate research fellowship at the Massachusetts Institute of Technology, under the direction of Professor John Essigmann. She then graduated from St. Catherine University Summa Cum Laude with a Bachelor of Arts in Chemistry in May 2014. After graduating, she started her graduate work at Purdue University Chemistry Department in August 2014, where she joined Professor Jean Chmielewski's laboratory studying bio-organic chemistry. She completed her Ph.D. in Organic Chemistry in December 2019. After graduation, she will continue her career at the University of Notre Dame as a Postdoctoral Fellow in the laboratory of Professor Juan Del Valle. She will work on disrupting protein-protein interactions with small molecules and peptides.

Journal of Medicinal Chemistry

Article

Cite This: J. Med. Chem. XXXX, XXX, XXX−XXX

pubs.acs.org/jmc

Potential Tools for Eradicating HIV Reservoirs in the Brain: Development of Trojan Horse Prodrugs for the Inhibition of P-Glycoprotein with Anti-HIV-1 Activity

Neha Agrawal,[†,§] Jennifer Rowe,[†,§] Jie Lan,[‡] Qigui Yu,[‡] Christine A. Hrycyna,[†] and Jean Chmielewski*[,†]

[†]Department of Chemistry, Purdue University, 560 Oval Drive, West Lafayette, Indiana 47907-2084, United States

[‡]Department of Microbiology and Immunology, Indiana University School of Medicine, Indianapolis, Indiana 46202, United States

Supporting Information

ABSTRACT: Combination antiretroviral therapy is the mainstay of HIV treatment, lowering plasma viral levels below detection. However, eradication of HIV is a major challenge due to cellular and anatomical viral reservoirs that are often protected from treatment by efflux transporters, such as P-glycoprotein (P-gp) at the blood−brain barrier (BBB). Herein we described a Trojan horse approach to therapeutic evasion of P-gp based on a reversibly linked combination of HIV reverse transcriptase and protease inhibitors. Potent inhibition of P-gp efflux in cells, including human brain endothelial cells, was observed with the linked heterodimeric compounds. In vitro regeneration of active monomeric drugs was observed in a reducing environment with these dimeric prodrugs, with the superior leaving group promoting more facile release from the tether. These release trends were mirrored in the efficacy of the in cyto anti-HIV-1 activity of the Trojan horse heterodimers.

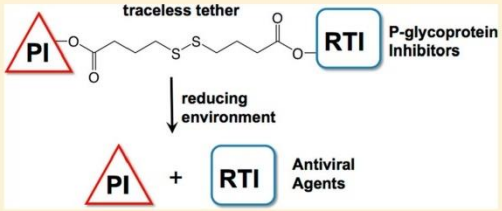

1. INTRODUCTION

HIV treatment has progressed substantially since the first documented case with combination antiretroviral therapies (cART) successfully reducing of plasma viral levels below the detectable limit.[1] Although cART has been a significant advancement in HIV treatment, HIV has not been eradicated due, in part, to viral reservoirs.[2,3] These viral reservoirs exist in a number of cellular and anatomical locations, including the central nervous system (CNS), macrophages, and lymphocytes. Viral accumulation in the brain, for instance, has been proposed to mainly proceed through paracellular or transcellular diapedesis.[4] While HIV is able to enter the brain through these mechanisms, numerous cART treatments do not accumulate well in the brain due to the physiochemical properties of the drugs, the presence of tight junctions, and the high concentration of efflux transporters at the blood−brain barrier (BBB).[5−7] One of the well studied efflux transporter, P-glycoprotein (P-gp), resides in the apical membrane of brain capillary endothelial cells where it is known to efflux many therapies.[8,9]

P-gp has many substrates, including various cART drugs targeting HIV-1 protease (PR), reverse transcriptase (RT), and integrase (IN). In vitro and in vivo experiments confirm that RT inhibitor drugs, such as abacavir, PR inhibitors, such as nelfinavir and darunavir, and IN inhibitor drugs, such as raltegravir, for instance, are P-gp substrates.[6,10−16] Notably, in P-gp null mice studies, abacavir and nelfinavir accumulated in the brain at increased levels as compared to wild-type mice (20-fold and 36-fold, respectively).[10,17] Further, chemical inhibition of P-gp efflux with a known inhibitor, LY-335979, was shown to increase the brain accumulation of four different PR inhibitors (PI) in vitro and in vivo.[18] Such studies strongly support the hypothesis that P-gp efflux limits the accumulation of cART drugs in the brain, leaving viral replication unchecked.

An X-ray structure of P-gp has shown a large binding site region that can accommodate the binding of two cyclic peptides.[19,20] To block P-gp efflux, we wished to take advantage of this multiplicity of binding sites within the transmembrane domain of P-gp.[19−26] In this way we envisioned that taking two antiviral agents that are substrates of P-gp and combining them into the same molecule with a linker would allow the heterodimeric compounds to occupy the multiple binding sites within P-gp, thereby turning two substrates into one inhibitor. Dimerizing a P-gp substrate has been demonstrated to be an effective means to inhibit P-gp efflux in cells and in situ at the BBB.[27−36] By use of this concept for antiviral substrates, reversibly linked homodimeric prodrugs of abacavir demonstrated potent P-gp inhibition with cellular anti-HIV-1 activity.[32] This proof of concept study

Special Issue: Women in Medicinal Chemistry

Received: May 13, 2019
Published: September 11, 2019

DOI: 10.1021/acs.jmedchem.9b00779
J. Med. Chem. XXXX, XXX, XXX−XXX

paved the way for the current Trojan horse (TH) design (Figure 1), a reversible combination therapy in one molecule

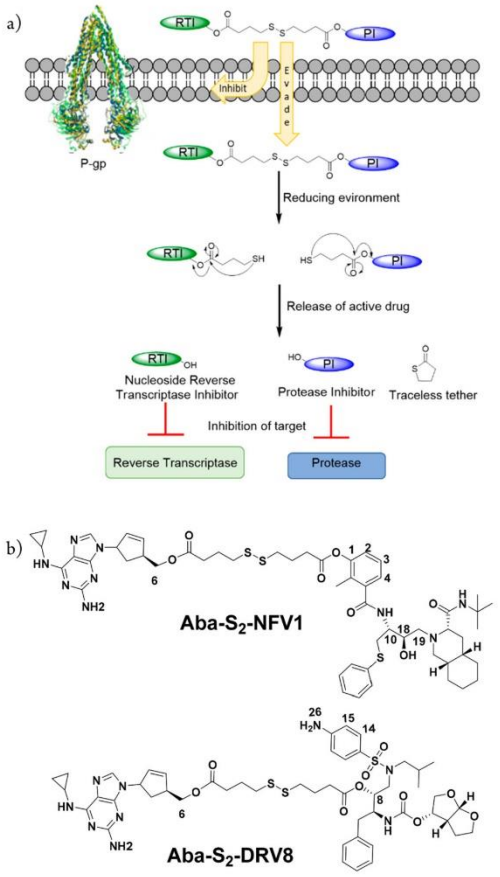

Figure 1. (a) Design of Trojan horse (TH) prodrugs containing a reverse transcriptase inhibitor (RTI), abacavir (Aba), a protease inhibitor (PI) (nelfinavir (NFV) or darunavir (DRV)), and a disulfide-containing tether. (b) Structures of abacavir-S_2-nelfinavir-1 (Aba-S_2-NFV1) and abacavir-S_2-darunavir-8 (Aba-S_2-DRV8).

that also may act as a P-gp inhibitor to improve cell accumulation. Specifically, agents were designed as an cART prodrug containing the RT inhibitor (RTI) abacavir (Aba) and one of two PR inhibitors (PI), nelfinavir (NFV) or darunavir (DRV), linked via a disulfide-containing tether. Such compounds were designed to inhibit P-gp efflux and, in the reducing environment of an HIV infected cell, release two monomeric therapies within the cell. Herein, we discuss the successful synthesis and application of two cART heterodimers, abacavir-S_2-nelfinavir (Aba-S_2-NFV1) and abacavir-S_2-darunavir (Aba-S_2-DRV8), as P-gp inhibitors and antiviral prodrugs that highlight the importance of the chemical connectivity on their antiviral activity.

2. RESULTS AND DISCUSSION

2.1. Design. TH combination cART prodrugs were designed to provide two functions: (1) inhibit P-gp efflux in brain endothelial cells and T-cells and (2) in the reducing environment of cells, release the monomeric therapies for interaction with target enzymes (Figure 1). This was accomplished by conjugating two classes of known FDA approved HIV-1 drugs, a RTI (Aba) and PIs (NFV and DRV) connected by ester linkages via a disulfide-containing tether. This tether contains a central disulfide moiety that is reduced in the reducing environment of the cell. The thiols that are generated can then rearrange to release the monomeric drugs of interest within the cell. Thus, the design creates TH heterodimers that may be useful tools in the treatment of cellular and anatomical reservoirs of HIV-1.

2.2. Synthesis and Characterization of TH Dimers Aba-S_2-NFV and Aba-S_2-DRV. The TH heterodimers were synthesized over two-steps. The presence of an alcohol functional group within Aba and NFV (C1 and C18) or DRV (C8) allowed us to introduce ester linkages to generate Aba-S_2-NFV and Aba-S_2-DRV analogs (Scheme 1).

Scheme 1. Synthesis of Aba-S_2-NFV and Aba-S_2-DRV Analogs[a]

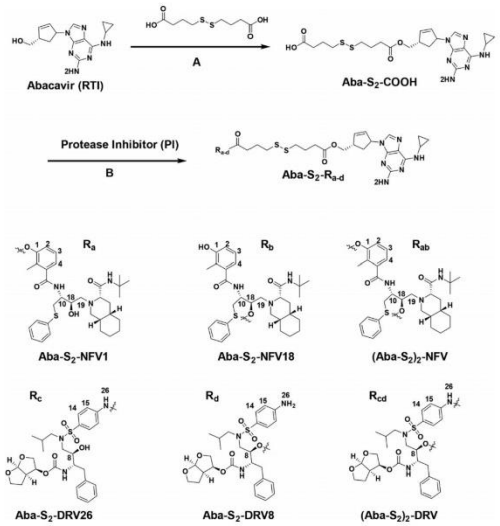

[a]Reagents and conditions: (A) PyBOP, DMAP, DIEA, DMF, rt 24 h, 70% yield; (B) EDC, DMAP, DIEA, CH_2Cl_2, 4 Å molecular sieves, 0 °C for 2 h, rt for 48 h; Aba-S_2-NFV1, 62% yield; Aba-S_2-NFV18, 3% yield; (Aba-S_2)$_2$-NFV, 2% yield; Aba-S2-DRV8, 27% yield; (Aba-S_2)$_2$-DRV, 21% yield. Atom numbering used for NMR analysis of Aba-S_2-COOH, darunavir, and nelfinavir derivatives.

In the first step of the synthesis of the heterodimers, Aba was treated with PyBOP-activated 4,4′-dithiodibutyric acid in the presence of DMAP and DIEA to produce Aba-S_2-COOH (Scheme 1) in 70% yield after purification by reverse phase HPLC (RP-HPLC). The selective acylation of the primary alcohol in Aba was established based on the resonances corresponding to the H-6 proton and the C-6 carbon of Aba-S_2-COOH, which were shifted downfield from the correspond-

DOI: 10.1021/acs.jmedchem.9b00779
J. Med. Chem. XXXX, XXX, XXX−XXX

Table 1. Inhibition of P-gp Mediated Efflux of Calcein-AM and NBD-Aba in 12D7-MDR and hCMEC/D3 Cells[a]

	IC_{50} (μM)			
	12D7-MDR cells		hCMEC/D3 cells	
compd	calcein-AM	NBD-Aba	calcein-AM	NBD-Aba
NFV	9.1 ± 3.0	5.8 ± 1.4	2.0 ± 0.2	1.7 ± 0.3
Aba-S_2-NFV1	0.77 ± 0.05	0.65 ± 0.09	0.59 ± 0.07	0.41 ± 0.06
DRV	33.2 ± 6.5	60 ± 9.4	6.6 ± 1.9	15.4 ± 3.2
Aba-S_2-DRV8	0.50 ± 0.04	0.51 ± 0.08	0.08 ± 0.02	0.09 ± 0.02

[a]Cells were treated with calcein-AM (0.25 μM) or NBD-Aba (5 μM) with different concentrations of compound. The accumulated fluorescence was analyzed using flow cytometery.

ing proton H-6 and carbon C-6 signals in Aba by 0.7 ppm (4.1 ppm from 3.4 ppm) and 2.7 ppm (66.9 ppm from 64.2 ppm), respectively (Figures S3–S6).

Acylation of NFV with Aba-S_2-COOH was accomplished using the PI and Aba-S_2-COOH in the presence of EDC/DMAP (Scheme 1). NFV has two possible sites of acylation (C1 (phenolic) and C18 (secondary hydroxyl)) that could potentially lead to three products: monoesters at C1 (Aba-S_2-NFV1) and C18 (Aba-S_2-NFV18) and a diester at both sites (Aba-S_2)$_2$-NFV (Scheme 1). Upon RP-HPLC separation, Aba-S_2-NFV1 was isolated in 62% yield with <5% of the other possible ester derivatives obtained. The structure of Aba-S_2-NFV1 was elucidated by ^{1}H and ^{13}C NMR spectroscopy, with peak assignments confirmed using COSY, TOCSY, HMQC, and HMBC NMR (Figures S7–S16). The acylation of the phenolic alcohol of NFV in Aba-S_2-NFV1 was confirmed by the observed deshielding of the protons H-2, H-3, and H-4 by 0.41, 0.22, and 0.31 ppm, respectively, as compared to the parent NFV (Figure S14). The formation of the phenyl ester was further confirmed by ^{13}C NMR, with shielding of the C-1 carbon signal by 6.4 ppm in Aba-S_2-NFV1 as compared to NFV (Figure S15)[37] and the deshielding of C-2, C-3, and C-4 by 8–13 ppm (Figure S15). Furthermore, ^{1}H and ^{13}C resonances in the vicinity of the secondary alcohol (H-10/C-10, H-18/C-18, and H-19/C-19) showed no significant change in the spectra of Aba-S_2-NFV1 as compared to NFV (Figure S16). These NMR data taken together confirm the structure of Aba-S_2-NFV1 as the phenyl ester derivative.

The acylation of DRV was accomplished as described above (Scheme 1). DRV, like NFV, has two possible conjugation locations, the secondary alcohol on C8 (Aba-S_2-DRV8) or the aniline N26, with the possible acylation at both sites ((Aba-S_2)$_2$-DRV). Upon RP-HPLC separation of the reaction mixture, Aba-S_2-DRV8 was obtained in 27% yield with the diacylated product ((Aba-S_2)$_2$-DRV) in 21% yield. The structure of Aba-S_2-DRV8 was also elucidated by ^{1}H and ^{13}C NMR spectroscopy using COSY, TOCSY, and HMQC NMR (Figure S17–S24). The acylation of the secondary alcohol of darunavir in Aba-S_2-DRV8 was confirmed by the observed deshielding of the protons H-8 by 1.5 ppm, as compared to the parent darunavir (Figure S22). The formation of secondary ester was further confirmed by ^{13}C NMR with the deshielding of the C-8 signal by 2.3 ppm in Aba-S_2-DRV8 as compared to DRV (Figure S23). Furthermore, ^{1}H and ^{13}C NMR resonances in the vicinity of the aniline nitrogen (H-14/C-14 and H-15/C-15) showed no significant change in Aba-S_2-DRV8 as compared to DRV (Figure S24). These NMR data taken together confirmed that acylation proceeded on the secondary alcohol of darunavir. (Data for diacylated darunavir are not shown.) In all, this synthetic method allowed the preparation of two TH heterodimers, Aba-S_2-NFV1 and Aba-S_2-DRV8, for biological analysis.

2.3. Inhibition of P-gp Efflux with Aba-S_2-NFV1 and Aba-S_2-DRV8. One of the goals of the designed TH heterodimers is to inhibit P-gp-mediated efflux. A substrate accumulation assay was used to evaluate the potency of Aba-S_2-NFV1 and Aba-S_2-DRV8 as P-gp inhibitors using the P-gp substrates calcein-AM and NBD-Aba.[38,39] Two cell lines were used to monitor the accumulation of these fluorescent P-gp substrates: 12D7-MDR cells which are CD4+ T lymphocytes with overexpression of P-gp,[40] and hCMEC/D3 cells as an in vitro BBB model cell line.[41] hCMEC/D3 cells are an immortalized human brain capillary endothelial cell line that expresses endogenous levels of P-gp.[42,43] Inhibition of P-gp efflux was measured by monitoring the increase in cellular fluorescence with added heterodimer by flow cytometry. While the dimeric prodrugs have limited water solubility, they were fully soluble in 1% DMSO up to 100 μM, and, therefore, the cell-based P-gp experiments used 1% DMSO with no observed cytotoxicity.

With the 12D7-MDR and hCMEC/D3 cell lines, Aba-S_2-NFV1 and Aba-S_2-DRV8 demonstrated dose-dependent, potent inhibition of P-gp efflux of calcein-AM and NBD-Aba with submicromolar IC_{50} values (Table 1). Aba-S_2-DRV8 was the more potent of the two dimers with IC_{50} values of 80–90 nM in hCMEC/D3 cells. Interestingly, the IC_{50} values obtained with the hCMEC/D3 cells are lower than 12D7-MDR cells, especially with Aba-S_2-DRV8, likely due to the lower expression of P-gp in the brain capillary endothelial cells. Analogous experiments were performed with monomeric NFV and DRV using the fluorescent substrates. About a 3- to 12-fold increase in inhibition of P-gp was found with Aba-S_2-NFV1 as compared to NFV, and a striking 66- to 118-fold increase in inhibition of P-gp was found for Aba-S_2-DRV8 with respect to DRV alone (Table 1). Abacavir has been shown to minimally inhibit (<10%) P-gp in 12D7-MDR in cells up to 500 μM in these assays, whereas the known P-gp inhibitor verapamil had an IC_{50} value of 1.2 ± 0.4 μM in 12D7-MDR cells with the calcein-AM substrate.[32] These data substantiate that the TH heterodimers are inhibitors of P-gp efflux in both T-cells and in a BBB cell model. Together, these IC_{50} data confirm that the dimerization of two antivirals that are P-gp substrates (Aba and DRV/NFV) into one molecule successfully led to the generation of potent P-gp inhibitors.

An MTT assay was used to determine the cell toxicity of Aba-S_2-NFV1 and Aba-S_2-DRV8 in the 12D7-MDR cell lines after 24 h.[44] In this assay, Aba-S_2-NFV1 demonstrated high cell viability (>95%) at the maximum concentration used (20 μM). Aba-S-DRV8, though slightly more cytotoxic than Aba-S_2-NFV1, still maintained 70% cell viability at 20 μM, which is 40

DOI: 10.1021/acs.jmedchem.9b00779
J. Med. Chem. XXXX, XXX, XXX−XXX

times its IC_{50} for inhibition of P-gp. These data suggest that the TH heterodimers are minimally cytotoxic to 12D7-MDR cells at bioactive concentrations and can be used for further biological assays without detrimental effect on cell growth.

2.4. Probing the Reversion of TH Heterodimers into Monomers in a Reducing Environment. In a reducing environment the disulfide bonds within the TH heterodimers would yield two thiols (Figure 1a) that may rearrange to produce monomeric drugs (Aba, NFV, and DRV). The breakdown of the TH heterodimers with DTT and glutathione (GSH) and the release of monomers were monitored using UPLC−MS at various time points. The reduction of the heterodimers to free thiols occurs rapidly, with full reduction observed within 1 h. Upon appearance of free thiols, the subsequent rearrangement led to the generation of the component monomeric drugs. Aba regeneration from each TH heterodimer (Aba-S_2-NFV1 and Aba-S_2-DRV8) was consistent between heterodimers with a half-life ($t_{1/2}$) of 31.8 ± 6.8 and 34.5 ± 1.5 h, respectively, with DTT and 29.4 ± 3 and 21.6 ± 2 h, respectively, with with GSH. DRV and NFV were regenerated with a $t_{1/2}$ of 21.3 ± 0.8 and 1.2 ± 0.2 h with DTT, respectively, and 36.3 ± 4 and 10.3 ± 1 h with GSH. Interestingly, NFV was released significantly faster than the release of DRV and Aba. This significant difference in monomer release is likely due to the differences in the chemical connectivity of the monomers. NFV, as described above, is connected to the tether via a phenolic moiety, whereas DRV is linked by a secondary alcohol. The better leaving group ability of the phenol versus the secondary alcohol likely leads to the observed difference in monomer regeneration.

2.5. Anti-HIV-1 Potency of Each TH Heterodimer As Compared to Their Monomers, Alone and Combined. To investigate if Aba-S_2-NFV1 and Aba-S_2-DRV8 are effective against HIV-1 in cells, an in vitro HIV-1 titer assay was performed using the 12D7 cell line. 12D7 cells were infected with HIV-1_{LAI}, and anti-HIV-1 activity was measured by monitoring p24 protein levels as previously described.[45,46] First the stability of the prodrugs was monitored in PBS and cell culture media using UPLC−MS. Aba-S_2-NFV1 was greater than 95% intact after 1 week under both conditions, whereas Aba-S_2-DRV8 was also greater than 95% intact after 3 days under both conditions, but with decomposition observed after day 4. Therefore, for the cell-based anti-HIV-1 experiments, the medium, with drugs, was changed every 3 days. The anti-HIV-1 activity of different concentrations of monomeric drugs alone (Aba, NFV, or DRV), 1:1 combinations of an RTI with a PI (Aba and NFV or Aba and DRV), or the TH heterodimer was determined after 6 days. All drugs and drug combinations demonstrated a decrease in p24 levels as compared to the control, which corresponds to an increase in anti-HIV-1 activity. The PIs used are known to be superior antivirals as compared to the RTI Aba,[47] and this was also observed (Figure 2). Therefore, the antiretroviral activity of the 1:1 mix of Aba with NFV or DRV was dominated by the PI potency. For the TH heterodimers, the anti-HIV-1 activity of Aba-S_2-NFV was similar to the 1:1 mixture of Aba and NFV, whereas Aba-S_2-DRV was less potent than the 1:1 mixture of Aba and DRV. DRV alone is a highly potent antiviral and is more potent than NFV alone[48] (Figure 2). Therefore, one might expect that Aba-S_2-DRV8 would have superior anti-HIV-1 activity as compared to Aba-S_2-NFV1. However, the release of NFV from Aba-S_2-NFV1 is 18-fold faster than DRV release from Aba-S_2-DRV8 due to the better phenolic leaving group.

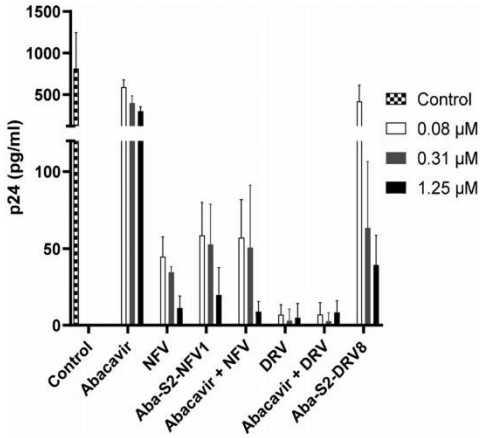

Figure 2. Anti-HIV-1 activity of individual RTI or PI antivirals, a 1:1 mixture of RTI and PI, and the TH heterodimers in HIV-1_{LAI} infected 12D7 cells. The plotted data are the average of HIV-1 p24 with the standard deviation derived from two independent experiments.

Thus, this difference in chemical connectivity leads to a difference in monomer release that may be responsible for the differences in anti-HIV-1 potency.

3. CONCLUSION

Herein, the successful synthesis and application of two TH heterodimers, Aba-S_2-NFV1 and Aba-S_2-DRV8, as P-gp inhibitors and antiviral prodrugs are discussed. Each heterodimer was synthesized, and the connectivity points within the monomers was fully characterized by NMR. Both TH heterodimers are potent P-gp inhibitors with activity in T-cells and endothelial cells from the BBB. These dimers were found to revert to their component monomers (Aba, NFV, and DRV) in a reducing environment, with NFV releasing significantly faster than DRV. Both TH heterodimers displayed anti-HIV-1 activity in T cells, with Aba-S_2-NFV1 displaying superior potency as compared to Aba-S_2-DRV8. The quicker regeneration of monomeric NFV in the reducing environment and, in turn, the superior anti-HIV potency of Aba-S_2-NFV1 as compared to Aba-S_2-DRV8 are likely due to the better phenolic leaving group in Aba-S_2-NFV. Thus, chemical connectivity to the tether within these TH heterodimers has a notable effect on the observed anti-HIV-1 activity. Future studies may probe alternative linking chemistry to promote more facile release of the combination therapies from the TH prodrugs.

4. EXPERIMENTAL SECTION

Materials. Abacavir, darunavir, and nelfinavir were provided by the NIH AIDS Reagent Program (Germantown, MD). ((1*H*-Benzo[*d*]-[1,2,3]triazol-1-yl)oxy)tri(pyrrolidin-1-yl)phosphonium hexafluorophosphate (PyBOP) was bought from GenScript Corporation (Piscataway, NJ). DTT was purchased from Roche (Indianapolis, IN). 1-(3-Dimethylaminoproyl)-3-ethylcarbodiimide hydrochloride (EDC) was purchased fom AK Scientific (Union City, CA). 4,4′-Dithiodibutyric acid, *N*,*N*-dimethylpyridin-4-amine (DMAP), and *N*-ethyl-*N*-isopropylpropan-2-amine (DIEA) were purchased from Sigma-Aldrich (St. Louis, MO). hCMEC/D3 cells were donated from Institut National de la Sante et de la Recherche Medicale

DOI: 10.1021/acs.jmedchem.9b00779
J. Med. Chem. XXXX, XXX, XXX−XXX

(INSERM, Paris, France). Rat tail collagen I was purchased from BD Biosciences (San Jose, CA). EBM-2 growth medium was purchased from Lonza (Basel, Switzerland). Calcein-AM was bought from Invitrogen (Carlsbad, CA), All other reagents were purchased from Sigma-Aldrich (St. Louis, MO) or Invitrogen (Carlsbad, CA) and used without further purification. ^{1}H, ^{13}C, and 2D NMR spectra were recorded with a Bruker AC 800 and Bruker AC 500 MHz. DMSO-d_6 was used to prepare NMR samples.

Methods. Synthesis of Aba-S_2-COOH. To a solution of 4,4′-dithiodibutyric acid (400 mg, 1.7 mmol) were added PyBOP (114 mg, 0.22 mmol), DIEA (0.20 mL, 0.75 mmol), and DMAP (2.6 mg, 0.022 mmol) under nitrogen atmosphere at room temperature in dry DMF (2 mL). After 20 min, abacavir sulfate (50 mg, 0.15 mmol) was added. The mixture was left to stir at room temperature for 24 h. The resulting reaction mixture was dissolved in DMSO and purified using RP-HPLC. The RP-HPLC solvent consisted of acetonitrile with 0.1% TFA (solvent A) and water with 0.1% TFA (solvent B). A gradient of 20−70% of solvent A with the flow rate of 12.0 mL/min and UV detection at 214 and 280 nm with a C8 column (Phenomenex, USA) was used for purification. Purity of the product (~99%) was estimated by C8 analytical RP-HPLC using a flow rate of 1.2 mL/min and UV detection at 214 and 280 nm and a gradient from 20% to 70% (solvent A) over 30 min. The retention time for Aba-S_2-COOH was found to be 16.2 min. The yield for this reaction was calculated to be 70%. Calculated mass for Aba-S_2-COOH 506.18, observed mass by ESI-MS 507.2 $[M + H]^+$. Aba-S_2-COOH: ^{1}H NMR (500 MHz, DMSO-d_6) δ 12.18 (s, 2H), 9.77 (s, 1H), 7.93 (s, 1H), 7.45 (s, 2H), 6.13 (dd, J = 5.3, 2.5 Hz, 1H), 5.98 (dt, J = 5.1, 2.2 Hz, 1H), 5.43 (ddd, J = 8.6, 6.1, 2.4 Hz, 1H), 4.09 (d, J = 6.1 Hz, 2H), 3.11 (ddt, J = 12.0, 8.5, 4.1 Hz, 1H), 2.85 (s, 1H), 2.68 (qd, J = 8.1, 7.2, 4.4 Hz, 5H), 2.38 (td, J = 7.3, 4.4 Hz, 2H), 2.29 (t, J = 7.2 Hz, 2H), 1.82 (dp, J = 11.4, 7.2 Hz, 4H), 1.62 (dt, J = 13.8, 5.9 Hz, 1H), 0.88 (s, 2H), 0.74 (s, 2H); ^{13}C NMR (126 MHz, DMSO-d_6) δ 174.34, 172.85, 159.09, 158.84, 158.59, 137.79, 130.49, 118.60, 116.23, 66.72, 59.61, 45.70, 44.48, 40.48, 40.32, 40.15, 39.98, 39.82, 39.65, 39.48, 37.28, 37.10, 34.71, 32.54, 32.34, 26.07, 24.43, 24.40, 7.39.

Synthesis of Aba-S_2-NFV1. To a flame-dried round-bottom flask under nitrogen were added NFV (20 mg, 34.8 μmol), Aba-S_2-COOH (21.5 mg, 34.8 μmol), EDC (10 mg, 52.2 μmol), DMAP (8.5 mg, 69.7 μmol), DIEA (60 μL, 348 μmol), and 4 Å powdered molecular sieves followed by dry DCM (1 mL) at 0 °C. The reaction mixture was stirred at room temperature for 24 h, and the progress of the reaction was monitored by RP-HPLC. An additional aliquot of EDC (10 mg, 52.2 μmol) was added after 24 h, and the reaction mixture was stirred for an additional 2 days. The mixture was diluted with DMSO, and components were separated by RP-HPLC on a C18 column (Phenomenex, USA) with a flow rate of 12 mL/min, a gradient of 20−60% solvent A over 60 min, and UV detection at 214 and 254 nm. Aba-S_2-NFV1 was obtained (62% yield, major product) with Aba-S_2-NFV18 and (Aba-S_2)$_2$-NFV (5% yield, minor products). Aba-S_2-NFV1 (major product) had a purity of 99% by RP-HPLC (Figure S2), and the compound was fully characterized by NMR (see below and Figures S7−S16). ESI-MS: calculated mass, 1056.5; observed mass, 1057.0. High resolution MS: calculated mass, 1056.4868; observed mass, 1056.4890. Aba-S_2-NFV1: ^{1}H NMR (800 MHz, DMSO-d_6) δ 9.85 (s, 1H), 9.20 (s, 1H), 8.37 (d, J = 8.9 Hz, 1H), 8.21 (s, 1H), 7.97 (s, 1H), 7.63 (s, 2H), 7.38−7.29 (m, 5H), 7.28 (t, J = 7.8 Hz, 1H), 7.23−7.19 (m, 1H), 7.16 (dt, J = 8.0, 1.9 Hz, 1H), 6.14 (dt, J = 5.7, 2.1 Hz, 1H), 5.98 (dt, J = 5.7, 2.2 Hz, 1H), 5.43 (ddd, J = 10.7, 4.8, 2.0 Hz, 1H), 4.14−4.05 (m, 3H), 3.94 (q, J = 10.5 Hz, 1H), 3.87 (s, 1H), 3.56 (d, J = 12.9 Hz, 1H), 3.41 (dd, J = 13.7, 2.9 Hz, 1H), 3.28 (s, 1H), 3.23 (d, J = 13.4 Hz, 1H), 3.10 (ddq, J = 8.3, 6.3, 2.1 Hz, 1H), 3.03−2.98 (m, 2H), 2.84−2.67 (m, 8H), 2.45−2.34 (m, 2H), 2.16 (d, J = 3.8 Hz, 3H), 2.08−1.98 (m, 2H), 1.96−1.90 (m, 3H), 1.86 (dp, J = 21.4, 7.2 Hz, 2H), 1.76 (m, 1H), 1.71 (d, J = 12.7 Hz, 2H), 1.63 (dt, J = 13.9, 5.9 Hz, 1H), 1.54 (t, J = 6.3 Hz, 2H), 1.40 (d, J = 12.4 Hz, 1H), 1.36−1.32 (m, 1H), 1.29−1.15 (m, 11H), 0.92−0.88 (m, 2H), 0.78 (s, 2H). ^{13}C NMR (126 MHz, DMSO-d_6) δ 172.85, 171.51, 169.09, 167.53, 158.91, 158.63, 152.99, 149.67, 139.23, 137.89, 136.34, 130.38, 129.55, 128.93, 128.21, 126.71, 126.44, 125.41, 123.90, 112.11, 68.91, 67.15, 66.72, 59.74, 58.96, 57.91, 52.60, 51.43, 44.48, 36.99, 34.68, 34.13, 33.99, 32.33, 32.25, 31.72, 30.21, 29.48, 28.84, 28.62, 25.99, 25.04, 24.37, 24.31, 23.61, 20.40, 13.32, 7.41.

Synthesis of Aba-S_2-DRV8. To a flame-dried round-bottom flask under nitrogen were added DRV (20 mg, 36 μmol), Aba-S_2-COOH (21.5 mg, 34.8 μmol), EDC (10 mg, 52.2 μmol), DMAP (8.5 mg, 69.7 μmol), DIEA (60 μL, 348 μmol), and 4 Å powdered molecular sieves followed by dry DCM (1 mL) at 0 °C. The reaction mixture was stirred at room temperature for 72 h, and the progress of the reaction was monitored by RP-HPLC. The reaction mixture was diluted with DMSO, and components were separated by RP-HPLC on a C18 column (Phenomenex, USA) with a flow rate of 12 mL/min, a gradient of 20−95% solvent A over 60 min, and UV detection at 214 and 254 nm. Aba-S_2-DRV was obtained (27% yield, major product) with (Aba-S_2)$_2$-DRV (21% yield, minor product). The retention time of Aba-S_2-DRV8 (major product) had a purity of 99% (Figure S1), and the compound was fully characterized by NMR (see below and Figures S17−S24). ESI-MS: calculated mass, 1036.4; observed mass, 1036.8. High resolution MS: calculated mass, 1036.4089; observed mass, 1036.4106. Aba-S_2-DRV8: ^{1}H NMR (800 MHz, DMSO-d_6) δ 7.48 (d, J = 9.4 Hz, 1H), 7.39 (d, J = 8.7 Hz, 1H), 7.21 (dt, J = 15.3, 7.1 Hz, 3H), 7.16−7.13 (m, 1H), 6.61 (d, J = 8.7 Hz, 1H), 6.12 (dt, J = 5.6, 2.1 Hz, 1H), 5.96 (dt, J = 5.6, 2.2 Hz, 1H), 5.48 (d, J = 5.2 Hz, 1H), 5.41 (ddq, J = 8.2, 6.2, 2.1 Hz, 1H), 5.06 (ddd, J = 9.0, 4.5, 2.8 Hz, 1H), 4.84 (dt, J = 8.0, 5.8 Hz, 1H), 4.07 (dd, J = 6.2, 2.1 Hz, 2H), 3.95 (ddd, J = 14.9, 9.1, 4.1 Hz, 1H), 3.85 (dd, J = 9.6, 6.0 Hz, 1H), 3.69 (td, J = 8.2, 1.9 Hz, 1H), 3.56 (ddt, J = 16.4, 8.3, 5.6 Hz, 2H), 3.29 (dd, J = 15.4, 2.9 Hz, 1H), 3.08 (ddp, J = 8.3, 6.2, 2.0 Hz, 1H), 3.04 (dd, J = 15.3, 9.0 Hz, 1H), 2.81 (dt, J = 13.4, 3.8 Hz, 2H), 2.78−2.72 (m, 1H), 2.69 (dt, J = 18.8, 7.1 Hz, 4H), 2.60−2.51 (m, 1H), 2.50−2.47 (m, 3H), 2.42−2.38 (m, 1H), 2.38−2.30 (m, 3H), 2.06 (s, 0H), 1.91−1.85 (m, 2H), 1.83 (q, J = 7.3 Hz, 2H), 1.78 (ddt, J = 13.1, 9.0, 6.5 Hz, 1H), 1.61 (dt, J = 13.8, 5.9 Hz, 1H), 1.39−1.30 (m, 1H), 1.17−1.11 (m, 1H), 0.77 (dd, J = 6.6, 4.5 Hz, 5H). ^{13}C NMR (800 MHz, DMSO-d_6) δ 172.82, 172.35, 155.81, 153.44, 138.77, 137.77, 130.46, 129.56, 129.52, 128.48, 126.54, 123.29, 113.18, 109.22, 109.20, 75.08, 73.07, 70.65, 69.25, 66.72, 59.60, 57.73, 53.72, 49.50, 45.47, 44.45, 40.29, 40.18, 40.08, 39.97, 39.87, 39.77, 39.66, 37.08, 37.05, 35.56, 34.68, 32.51, 32.30, 26.82, 25.89, 24.34, 24.07, 23.56, 20.37, 20.21.

Cell Culture. 12D7-MDR cells were grown in complete RPMI 1640 medium with vincristine (0.5 ng/mL), 50 units/mL of penicillin and 50 μg/mL streptomycin, 5 mM of L-glutamine, and 10% FBS. The growth of cells was maintained at 37 °C in 5% CO_2. hCMEC/D3 cells were cultured according to literature protocols with minor modifications.[41] The medium used for growth consisted of endothelial growth medium-2 (EGM-2) supplemented with 5% fetal bovine serum, 1% penicillin−streptomycin, 0.5% human basic fibroblast growth factor (hbFGF), 1.4 μM hydrocortisone, 5 μg/mL ascorbic acid, 1% (10 mM) HEPES, and 1% lipid concentrate.

Flow Cytometry Assay. Flow cytometry was used to estimate P-gp inhibition using a substrate accumulation assay as described previously with some minor changes.[38] BME medium (with fluorescent P-gp substrate) along with the compound of interest in DMSO (1%) was added to 125 000 cells in suspension and stored in a CO_2 incubator at 37 °C for 30 min. The cells were harvested by centrifugation at 300g at 4 °C for 7 min. The supernatant was carefully removed, and 400 μL of cold, sterile PBS was added to the cell pellet. The accumulation of calcein-AM or NBD-Aba was measured using a FACSCalibur flow cytometer (BD Biosciences) with an excitation wavelength of 488 nm argon laser and an emission 530 nm bandpass filter (FL1). The mean fluorescence value for each concentration corresponded to 10 000 cells. Each sample was run in duplicate, and all the experiments were run in duplicates on two different days. The average fluorescence accumulated in the cells for samples was used to plot the mean fluorescence vs concentration, and the IC_{50} values were estimated using GraphPad Prism.

Cell Viability Assay. The viability of 12D7-MDR cells in the presence of a TH heterodimer (Aba-S_2-NFV1 or Aba-S_2-DRV8) was

DOI: 10.1021/acs.jmedchem.9b00779
J. Med. Chem. XXXX, XXX, XXX−XXX

measured using the standard MTT assay.[44] 20 000 12D7-MDR cells were plated in 96-well plate in 100 μL of cell medium. After 12 h, TH heterodimer in medium was added to each well to give a final concentration of 5, 10, and 20 μM (1% DMSO). After 24 h 20 μL of MTT in PBS (5 mg/mL) was added to all the wells and incubated for 2.5 h. The 96-well plates were centrifuged at 300*g* for 7 min, followed by careful removal of supernatant. 100 μL of DMSO was added to dissolve the formazan. The absorbance of the DMSO solution was read using a plate reader at 590 nm. Cell viability was reported as the ratio of absorbance of cells treated with TH heterodimer relative to cells treated with DMSO.

Stability of TH Heterodimers with DTT. Stability studies with DTT and GSH were adapted from a previously published protocol with some changes.[32] Aba-S_2-NFV1 and Aba-S_2-DRV8 (4 μM) were incubated at 37 °C with 250 mM DTT or 10 mM GSH in degassed 30% methanol/PBS (pH ~ 7.4) containing 5 μM quinine as the internal standard. When monitoring NFV and DRV release, an aliquot of the reaction mixture was taken at different time points and directly analyzed by UPLC−MS. For analysis of Aba release, an aliquot of reaction mixture was taken and stored at −80 °C before analysis. The time points were analyzed using RP-UPLC with a C18 column consisting of solvent A (water and 0.1% formic acid) and solvent B (acetonitrile and 0.1% formic acid), a gradient of 5−95% of solvent B over 10 min, and a flow rate of 0.5 mL/min. The peaks corresponding to *m*/*z* for quinine (325.4), Aba-S_2-NFV1 (1056.4), Aba-S_2-DRV8 (1036.5), Aba-SH (389.4), Aba (287.4), NFV (568.6), and DRV (548.4) were detected and extracted using MassLynx software. The experiments were run in duplicate, and the average percentage of release vs time was fitted using GraphPad Prism 7 to generate $t_{1/2}$ values.

Stability of Aba-S_2-NFV1 and Aba-S_2-DRV8 in Cell Culture Media. The cell media stability studies for the TH heterodimers (Aba-S_2-NFV1 or Aba-S_2-DRV8) were carried out following a previously published protocol with some modifications.[32] Heterodimers (100 μM) were incubated at 37 °C in the cell medium used for 12D7 cells (complete RPMI 1640 medium with 50 units/mL of penicillin and 50 μg/mL streptomycin, 5 mM of L-glutamine, and 10% FBS) with 1% DMSO. Every 24 h ice-cold acetonitrile with 4-methoxybenzyl alcohol (1.0 mM) was added to an aliquot of the reaction mixture (1:1). The resultant solution was vortexed for 1 min, sonicated for 10 min, and centrifuged twice at 10 000*g* for 10 min each. The supernatant was stored at −80 °C. All samples were analyzed using a C8 analytical column (Phenomenex, USA) on RP-HPLC with eluent consisting of solvent A (water and 0.05% TFA) and solvent B (acetonitrile and 0.05% TFA). A gradient of 15−75% solvent B over 30 min with a flow rate of 1.2 mL/min and UV detection at 254 nm was used. The assays were performed in duplicate.

HIV-1 Cell Inhibition Assay. 12D7 cells were grown in the identical medium for the cell culture medium stability studies. The cells in log-phase were pelleted and resuspended at 1 million cells per mL. 500 $TCID_{50}$ HIV-1_{LAI} was used to infect cells for 4 h using a known procedure.[45] These infected cells were plated at a density of 75 000 cells per mL in 48-well plates after three washes with the medium. Different concentrations of the compound of interest were added keeping the DMSO concentration at 0.05%. After 3 days, the medium was replaced with fresh medium containing the same concentration of the compound of interest. On the sixth day, the supernatant was analyzed using ELISA to quantify the amount of HIV-1 p24 (gag) protein generated in each sample.[46] All assays were run in duplicate.

■ ASSOCIATED CONTENT

Supporting Information

The Supporting Information is available free of charge on the ACS Publications website at DOI: 10.1021/acs.jmedchem.9b00779.

Analytical RP-HPLC traces of both TH heterodimers (Aba-S_2-NFV1 and Aba-S_2-DRV8); ^{1}H, ^{13}C, COSY, TOCSY, HMBC, and HMQC NMR spectra for Aba-S_2-NFV1, with ^{1}H and ^{13}C comparison to NFV; ^{1}H, ^{13}C, COSY, TOCSY, and HMQC NMR spectra for Aba-S_2-DRV8, with ^{1}H and ^{13}C comparison to DRV (PDF)

SMILES strings and some data (CSV)

■ AUTHOR INFORMATION

Corresponding Author

*E-mail: chml@purdue.edu.

ORCID

Christine A. Hrycyna: 0000-0001-9881-2063

Jean Chmielewski: 0000-0003-4958-7175

Author Contributions

§N.A. and J.R. contributed equally. The manuscript was written through contributions of all authors. All authors have given approval to the final version of the manuscript.

Notes

The authors declare no competing financial interest.

■ ACKNOWLEDGMENTS

We are grateful to Professor Arun Ghosh for providing the darunavir used in these studies and the NIH AIDS Reagent Program for contributing nelfinavir. This work was supported in part by the Grand Challenges Explorations (GCE) Phase II grant through the Bill & Melinda Gates Foundation (Grant OPP1035237 to Q.Y.), NIH Grant R21MH101020-01 (J.C. and C.A.H.), NIH Grant R21R33AI104268 (Q.Y.), NIH Grant R01AI117835 (Q.Y.), and NIH/NIAAA Grant UH2AA026218 (Q.Y.).

■ ABBREVIATIONS USED

HIV, human immunodeficiency virus; cART, combination antiretroviral therapy; CNS, central nervous system; BBB, blood−brain barrier; P-gp, P-glycoprotein; PR, HIV protease; RT, HIV reverse transcriptase; IN, HIV integrase inhibitor; TH, Trojan horse; RTI, reverse transcriptase inhibitor; PI, protease inhibitor; Aba, abacavir; DRV, darunavir; NFV, nelfinavir; Aba-S_2-NFV1, abacavir-S_2-nelfinavir1; Aba-S_2-DRV8, Abacavir-S_2-darunavir8; PyBOP, benzotriazole-1-yl-oxytripyrrolidinophosphonium hexfluorophosphate; DMAP, 4-dimethylaminopyridine; DIEA, *N*,*N*-diisopropylethylamine; DMF, *N*,*N*-dimethylformamide; DCM, dichloromethane; RP-HPLC, reverse phase high performance liquid chromatography; ESI-MS, electrospray ionization mass spectrometry; NMR, nuclear magnetic resonance; DEPT, distortionless enhancement by polarization transfer; COSY, correlated spectroscopy; HMQC, heteronuclear multiple-quantum correlation; HMBC, heteronuclear multiple bond correlation; TOCSY, total correlated spectroscopy; MTT, 1-(4,5-dimethylthiazol-2-yl)-3,5-diphenylformazan; DTT, dithiothreitol; GSH, glutathione; UPLC-MS, ultraperformance liquid chromatography−mass spectrometry; MALDI-TOF, matrix assisted laser desorption/ionization-time-of-flight

■ REFERENCES

(1) Autran, B.; Carcelain, G.; Li, T. S.; Blanc, C.; Mathez, D.; Tubiana, R.; Katlama, C.; Debré, P.; Leibowitch, J. Positive Effects of Combined Antiretroviral Therapy on CD4+ T Cell Homeostasis and Function in Advanced HIV Disease. *Science* **1997**, *277* (5322), 112−116.

DOI: 10.1021/acs.jmedchem.9b00779
J. Med. Chem. XXXX, XXX, XXX−XXX

(2) Lambotte, O.; Deiva, K.; Tardieu, M. HIV-1 Persistence, Viral Reservoir, and the Central Nervous System in the HAART Era. *Brain Pathol.* **2003**, *13* (1), 95−103.
(3) Pierson, T.; McArthur, J.; Siliciano, R. F. Reservoirs for HIV-1: Mechanisms for Viral Persistence in the Presence of Antiviral Immune Responses and Antiretroviral Therapy. *Annu. Rev. Immunol.* **2000**, *18*, 665−708.
(4) Ivey, N. S.; MacLean, A. G.; Lackner, A. A. Acquired Immunodeficiency Syndrome and the Blood-Brain Barrier. *J. NeuroVirol.* **2009**, *15* (2), 111−122.
(5) Thomas, S. A. Anti-HIV Drug Distribution to the Central Nervous System. *Curr. Pharm. Des.* **2004**, *10* (12), 1313−1324.
(6) Varatharajan, L.; Thomas, S. A. The Transport of Anti-HIV Drugs across Blood-CNS Interfaces: Summary of Current Knowledge and Recommendations for Further Research. *Antiviral Res.* **2009**, *82* (2), A99−109.
(7) Kandanearatchi, A.; Williams, B.; Everall, I. P. Assessing the Efficacy of Highly Active Antiretroviral Therapy in the Brain. *Brain Pathol.* **2003**, *13* (1), 104−110.
(8) Schinkel, A. H. P-Glycoprotein, a Gatekeeper in the Blood-Brain Barrier. *Adv. Drug Delivery Rev.* **1999**, *36* (2−3), 179−194.
(9) Saidijam, M.; Karimi Dermani, F.; Sohrabi, S.; Patching, S. G. Efflux Proteins at the Blood-Brain Barrier: Review and Bioinformatics Analysis. *Xenobiotica* **2018**, *48* (5), 506−532.
(10) Shaik, N.; Giri, N.; Pan, G.; Elmquist, W. F. P-Glycoprotein-Mediated Active Efflux of the Anti-HIV1 Nucleoside Abacavir Limits Cellular Accumulation and Brain Distribution. *Drug Metab. Dispos.* **2007**, *35* (11), 2076−2085.
(11) de Souza, J.; Benet, L. Z.; Huang, Y.; Storpirtis, S. Comparison of Bidirectional Lamivudine and Zidovudine Transport Using MDCK, MDCK-MDR1, and Caco-2 Cell Monolayers. *J. Pharm. Sci.* **2009**, *98* (11), 4413−4419.
(12) Lee, C. G.; Gottesman, M. M.; Cardarelli, C. O.; Ramachandra, M.; Jeang, K. T.; Ambudkar, S. V.; Pastan, I.; Dey, S. HIV-1 Protease Inhibitors Are Substrates for the MDR1 Multidrug Transporter. *Biochemistry* **1998**, *37* (11), 3594−3601.
(13) Bousquet, L.; Roucairol, C.; Hembury, A.; Nevers, M.-C.; Creminon, C.; Farinotti, R.; Mabondzo, A. Comparison of ABC Transporter Modulation by Atazanavir in Lymphocytes and Human Brain Endothelial Cells: ABC Transporters Are Involved in the Atazanavir-Limited Passage across an in Vitro Human Model of the Blood-Brain Barrier. *AIDS Res. Hum. Retroviruses* **2008**, *24* (9), 1147−1154.
(14) Fujimoto, H.; Higuchi, M.; Watanabe, H.; Koh, Y.; Ghosh, A. K.; Mitsuya, H.; Tanoue, N.; Hamada, A.; Saito, H. P-Glycoprotein Mediates Efflux Transport of Darunavir in Human Intestinal Caco-2 and ABCB1 Gene-Transfected Renal LLC-PK1 Cell Lines. *Biol. Pharm. Bull.* **2009**, *32* (9), 1588−1593.
(15) Gimenez, F.; Fernandez, C.; Mabondzo, A. Transport of HIV Protease Inhibitors through the Blood-Brain Barrier and Interactions with the Efflux Proteins, P-Glycoprotein and Multidrug Resistance Proteins. *JAIDS, J. Acquired Immune Defic. Syndr.* **2004**, *36* (2), 649−658.
(16) Hashiguchi, Y.; Hamada, A.; Shinohara, T.; Tsuchiya, K.; Jono, H.; Saito, H. Role of P-Glycoprotein in the Efflux of Raltegravir from Human Intestinal Cells and CD4+ T-Cells as an Interaction Target for Anti-HIV Agents. *Biochem. Biophys. Res. Commun.* **2013**, *439* (2), 221−227.
(17) Kim, R. B.; Fromm, M. F.; Wandel, C.; Leake, B.; Wood, A. J.; Roden, D. M.; Wilkinson, G. R. The Drug Transporter P-Glycoprotein Limits Oral Absorption and Brain Entry of HIV-1 Protease Inhibitors. *J. Clin. Invest.* **1998**, *101* (2), 289−294.
(18) Choo, E. F.; Leake, B.; Wandel, C.; Imamura, H.; Wood, A. J.; Wilkinson, G. R.; Kim, R. B. Pharmacological Inhibition of P-Glycoprotein Transport Enhances the Distribution of HIV-1 Protease Inhibitors into Brain and Testes. *Drug Metab. Dispos.* **2000**, *28* (6), 655−660.
(19) Aller, S. G.; Yu, J.; Ward, A.; Weng, Y.; Chittaboina, S.; Zhuo, R.; Harrell, P. M.; Trinh, Y. T.; Zhang, Q.; Urbatsch, I. L.; Chang, G. Structure of P-Glycoprotein Reveals a Molecular Basis for Poly-Specific Drug Binding. *Science* **2009**, *323* (5922), 1718−1722.
(20) Jin, M. S.; Oldham, M. L.; Zhang, Q.; Chen, J. Crystal Structure of the Multidrug Transporter P-Glycoprotein from Caenorhabditis Elegans. *Nature* **2012**, *490* (7421), 566−569.
(21) Kim, Y.; Chen, J. Molecular Structure of Human P-Glycoprotein in the ATP-Bound, Outward-Facing Conformation. *Science* **2018**, *359* (6378), 915−919.
(22) Bruggemann, E. P.; Currier, S. J.; Gottesman, M. M.; Pastan, I. Characterization of the Azidopine and Vinblastine Binding Site of P-Glycoprotein. *J. Biol. Chem.* **1992**, *267* (29), 21020−21026.
(23) Shapiro, A. B.; Ling, V. Positively Cooperative Sites for Drug Transport by P-Glycoprotein with Distinct Drug Specificities. *Eur. J. Biochem.* **1997**, *250* (1), 130−137.
(24) Dey, S.; Ramachandra, M.; Pastan, I.; Gottesman, M. M.; Ambudkar, S. V. Evidence for Two Nonidentical Drug-Interaction Sites in the Human P-Glycoprotein. *Proc. Natl. Acad. Sci. U. S. A.* **1997**, *94* (20), 10594−10599.
(25) Loo, T. W.; Bartlett, M. C.; Clarke, D. M. Methanethiosulfonate Derivatives of Rhodamine and Verapamil Activate Human P-Glycoprotein at Different Sites. *J. Biol. Chem.* **2003**, *278* (50), 50136−50141.
(26) Chufan, E. E.; Sim, H. M.; Ambudkar, S. V. Molecular Basis of the Polyspecificity of P-Glycoprotein (ABCB1): Recent Biochemical and Structural Studies. *Adv. Cancer Res.* **2015**, *125*, 71−96.
(27) Sauna, Z. E.; Andrus, M. B.; Turner, T. M.; Ambudkar, S. V. Biochemical Basis of Polyvalency as a Strategy for Enhancing the Efficacy of P-Glycoprotein (ABCB1) Modulators: Stipiamide Homodimers Separated with Defined-Length Spacers Reverse Drug Efflux with Greater Efficacy. *Biochemistry* **2004**, *43* (8), 2262−2271.
(28) Pires, M. M.; Hrycyna, C. A.; Chmielewski, J. Bivalent Probes of the Human Multidrug Transporter P-Glycoprotein. *Biochemistry* **2006**, *45* (38), 11695−11702.
(29) Chan, K. F.; Zhao, Y.; Burkett, B. A.; Wong, I. L.; Chow, L. M.; Chan, T. H. Flavonoid Dimers as Bivalent Modulators for P-Glycoprotein-Based Multidrug Resistance: Synthetic Apigenin Homodimers Linked with Defined-Length Poly(Ethylene Glycol) Spacers Increase Drug Retention and Enhance Chemosensitivity in Resistant Cancer Cells. *J. Med. Chem.* **2006**, *49* (23), 6742−6759.
(30) Pires, M. M.; Emmert, D.; Hrycyna, C. A.; Chmielewski, J. Inhibition of P-Glycoprotein-Mediated Paclitaxel Resistance by Reversibly Linked Quinine Homodimers. *Mol. Pharmacol.* **2009**, *75* (1), 92−100.
(31) Kuriakose, J.; Hrycyna, C. A.; Chmielewski, J. Click Chemistry-Derived Bivalent Quinine Inhibitors of P-Glycoprotein-Mediated Cellular Efflux. *Bioorg. Med. Chem. Lett.* **2012**, *22* (13), 4410−4412.
(32) Namanja, H. A.; Emmert, D.; Davis, D. A.; Campos, C.; Miller, D. S.; Hrycyna, C. A.; Chmielewski, J. Toward Eradicating HIV Reservoirs in the Brain: Inhibiting P-Glycoprotein at the Blood−Brain Barrier with Prodrug Abacavir Dimers. *J. Am. Chem. Soc.* **2012**, *134* (6), 2976−2980.
(33) Namanja, H. A.; Emmert, D.; Hrycyna, C. A.; Chmielewski, J. Homodimers of the Antiviral Abacavir as Modulators of P-Glycoprotein Transport in Cell Culture: Probing Tether Length. *MedChemComm* **2013**, *4* (10), 1344−1349.
(34) Emmert, D.; Campos, C. R.; Ward, D.; Lu, P.; Namanja, H. A.; Bohn, K.; Miller, D. S.; Sharom, F. J.; Chmielewski, J.; Hrycyna, C. A. Reversible Dimers of the Atypical Antipsychotic Quetiapine Inhibit P-Glycoprotein-Mediated Efflux in Vitro with Increased Binding Affinity and in Situ at the Blood-Brain Barrier. *ACS Chem. Neurosci.* **2014**, *5* (4), 305−317.
(35) Bohn, K.; Lange, A.; Chmielewski, J.; Hrycyna, C. A. Dual Modulation of Human P-Glycoprotein and ABCG2 with Prodrug Dimers of the Atypical Antipsychotic Agent Paliperidone in a Model of the Blood-Brain Barrierw. *Mol. Pharmaceutics* **2017**, *14* (4), 1107−1119.
(36) Namanja-Magliano, H. A.; Bohn, K.; Agrawal, N.; Willoughby, M. E.; Hrycyna, C. A.; Chmielewski, J. Dual Inhibitors of the Human Blood-Brain Barrier Drug Efflux Transporters P-Glycoprotein and

DOI: 10.1021/acs.jmedchem.9b00779
J. Med. Chem. XXXX, XXX, XXX−XXX

ABCG2 Based on the Antiviral Azidothymidine. *Bioorg. Med. Chem.* **2017**, *25* (19), 5128−5132.
(37) Schuster, I. I. A Carbon-13 NMR Study of Electronic Effects in the Hydrogen Bonding of Trifluoroacetic Acid with Substituted Benzenes, 1- and 2-Substituted Naphthalenes, and 9-Substituted Anthracenes in Chloroform. *J. Org. Chem.* **1985**, *50* (10), 1656−1662.
(38) Hrycyna, C. A.; Ramachandra, M.; Pastan, I.; Gottesman, M. M. Functional Expression of Human P-Glycoprotein from Plasmids Using Vaccinia Virus-Bacteriophage T7 RNA Polymerase System. *Methods Enzymol.* **1998**, *292*, 456−473.
(39) Namanja, H. A. Development of Dimeric Prodrug Inhibitors of P-glycoprotein and ABCG2 To Enhance Brain Penetration of Antiretroviral Agents. Ph.D. Dissertation, Purdue University, 2012.
(40) Lee, C. G.; Pastan, I.; Gottesman, M. M. Retroviral Transfer of Human MDR1 Gene into Human T Lymphocytes. *Methods Enzymol.* **1998**, *292*, 557−572.
(41) Weksler, B. B.; Subileau, E. A.; Perrière, N.; Charneau, P.; Holloway, K.; Leveque, M.; Tricoire-Leignel, H.; Nicotra, A.; Bourdoulous, S.; Turowski, P.; Male, D. K.; Roux, F.; Greenwood, J.; Romero, I. A.; Couraud, P. O. Blood-Brain Barrier-Specific Properties of a Human Adult Brain Endothelial Cell Line. *FASEB J.* **2005**, *19* (13), 1872−1874.
(42) Carl, S. M.; Lindley, D. J.; Das, D.; Couraud, P. O.; Weksler, B. B.; Romero, I.; Mowery, S. A.; Knipp, G. T. ABC and SLC Transporter Expression and Proton Oligopeptide Transporter (POT) Mediated Permeation across the Human Blood–Brain Barrier Cell Line, HCMEC/D3. *Mol. Pharmaceutics* **2010**, *7* (4), 1057−1068.
(43) Poller, B.; Gutmann, H.; Krähenbühl, S.; Weksler, B.; Romero, I.; Couraud, P.-O.; Tuffin, G.; Drewe, J.; Huwyler, J. The Human Brain Endothelial Cell Line HCMEC/D3 as a Human Blood-Brain Barrier Model for Drug Transport Studies. *J. Neurochem.* **2008**, *107* (5), 1358−1368.
(44) Mosmann, T. Rapid Colorimetric Assay for Cellular Growth and Survival: Application to Proliferation and Cytotoxicity Assays. *J. Immunol. Methods* **1983**, *65* (1−2), 55−63.
(45) Richman, D. D.; Kornbluth, R. S.; Carson, D. A. Failure of Dideoxynucleosides to Inhibit Human Immunodeficiency Virus Replication in Cultured Human Macrophages. *J. Exp. Med.* **1987**, *166* (4), 1144−1149.
(46) Davis, D. A.; Brown, C. A.; Singer, K. E.; Wang, V.; Kaufman, J.; Stahl, S. J.; Wingfield, P.; Maeda, K.; Harada, S.; Yoshimura, K.; Kosalaraksa, P.; Mitsuya, H.; Yarchoan, R. Inhibition of HIV-1 Replication by a Peptide Dimerization Inhibitor of HIV-1 Protease. *Antiviral Res.* **2006**, *72* (2), 89−99.
(47) Tang, M. W.; Shafer, R. W. HIV-1 Antiretroviral Resistance: Scientific Principles and Clinical Applications. *Drugs* **2012**, *72* (9), e1−e25.
(48) Pokorná, J.; Machala, L.; Řezáčová, P.; Konvalinka, J. Current and Novel Inhibitors of HIV Protease. *Viruses* **2009**, *1* (3), 1209−1239.

DOI: 10.1021/acs.jmedchem.9b00779
J. Med. Chem. XXXX, XXX, XXX−XXX